# GEOLOGICAL HISTORY AND STRUCTURAL EVOLUTION OF THE WARNER RANGE AND SURPRISE VALLEY, NORTHWESTERN MARGIN OF THE BASIN AND RANGE PROVINCE

A DISSERTATION
SUBMITTED TO THE DEPARTMENT OF GEOLOGICAL AND ENVIRONMENTAL SCIENCES
AND THE COMMITTEE ON GRADUATE STUDIES
OF STANFORD UNIVERSITY
IN PARTIAL FULFILLMENT OF THE REQUIREMENTS
FOR THE DEGREE OF
DOCTOR OF PHILOSOPHY

Anne Elizabeth Egger
March 2010

Includes supplemental files:
1. *(Egger_2010_plate_I.pdf)*

I certify that I have read this dissertation and that, in my opinion, it is fully adequate in scope and quality as a dissertation for the degree of Doctor of Philosophy.

**Elizabeth Miller, Primary Adviser**

I certify that I have read this dissertation and that, in my opinion, it is fully adequate in scope and quality as a dissertation for the degree of Doctor of Philosophy.

**Simon Klemperer**

I certify that I have read this dissertation and that, in my opinion, it is fully adequate in scope and quality as a dissertation for the degree of Doctor of Philosophy.

**Gail Mahood**

Approved for the Stanford University Committee on Graduate Studies.

**Patricia J. Gumport, Vice Provost Graduate Education**

*This signature page was generated electronically upon submission of this dissertation in electronic format. An original signed hard copy of the signature page is on file in University Archives.*

# Abstract

Along the northwestern margin of the Basin and Range province, mid-Miocene to Pliocene volcanic plateaus obscure much of the earlier history of this region. In the northeastern corner of California, however, slip on the relatively isolated Surprise Valley fault has resulted in the uplift of the Warner Range, providing unique insight into the tectonic and magmatic history of this region. In contrast to most of the very active western boundary, the northwestern margin of the Basin and Range remains sparsely mapped and studied. The geologic mapping, cross-sections, geochronology, geochemical analysis, and provenance studies of rock units present in the Warner Range, and geophysical modeling of the Surprise Valley presented here add detail to this understudied region.

A history of subduction-related arc volcanism lasting from ~40 Ma to the mid-Miocene is exposed in the >4 km of volcaniclastic sediments and volcanic rocks of the Warner Range. At the base of the range, ~40 Ma andesite lavas and debris flows mark a return to subduction-related arc volcanism associated with the ancestral Cascade arc. A thick sequence of latest Eocene to Oligocene volcaniclastic rocks thins from 1500 m to 200 m over 35 km of exposure. Predominantly volcanic clast compositions, detrital zircon ages, and paleocurrent indicators suggest that the sequence was deposited in an alluvial plain ~20 km NNE of a volcanic source area. This localized accumulation differs markedly from contemporaneous drainages to the south that transported material westward from central Nevada to the paleoshoreline.

A series of Oligocene volcanic edifices built on this sequence, recording arc volcanism from 28–24 Ma. In the southern part of the range, these Oligocene volcanic rocks are unconformably overlain by mid-Miocene (16–14 Ma) mafic lava flows and tuffs, once thought to be the southern extension of the mid-Miocene flood basalts, but which are now shown to be locally derived and related to arc volcanism. Mid-Miocene rocks were never present in the northern part of the range, however, where Oligocene rocks are directly overlain by late Miocene (10–7 Ma) rhyolite flows. Extension and uplift appears to have occurred in two episodes, the first in the middle Miocene and the second initiating ~3 Ma, which continues to the present day.

The range-bounding Surprise Valley fault currently dips at a moderate angle of ~35° to the east. Seismic velocity and potential field modeling of the basin identified numerous intra-basin faults, but it is not clear if these steeply-dipping faults cut and offset the Surprise Valley fault or sole into it. Geothermal springs occur primarily along intra-basin faults rather than the range-bounding fault, however, which may suggest that this is a system in transition to a new set of more favorably-oriented faults. The total magnitude of extension in the Warner Range region may be as much as 15%, the majority of which is accommodated along the Surprise Valley fault. While this is a relatively minor amount of extension, the Surprise Valley fault appears to have persisted as the westernmost boundary of Basin and Range extension since the mid-Miocene.

# Preface

When I first got involved in field work in the Warner Range, I had no intention of getting a PhD. I was a faculty member at San Juan College, a community college in northwestern New Mexico, when Elizabeth Miller contacted me in the early in 2004 to see if I would be interested in writing a supplement to a ACS-PRF grant that she and Simon Klemperer had; the supplement was specifically intended to involve faculty at non-PhD-granting institutions in research. Despite the fact that I had pursued the community college position because I felt teaching was more my calling than research, I jumped at the chance to get involved in field work again.

We received the supplementary funding, and I started to plan for the summer. Over the following months, I also decided to leave my position at San Juan College and return to Stanford as the Undergraduate Program Coordinator for the GES department. Come May of 2004, I packed up my belongings, drove to California, and headed out to a brand new field area the next day. Two of my students from San Juan College met me and Joe Colgan in the Warner Range, and we worked there for about ten days, until we got snowed out (yes, in late May). Our purpose in conducting new geologic mapping in this area was—in part— to provide surface control for a high-resolution seismic reflection profile that would be collected that fall across the Surprise Valley, adjacent to the Warner Range. The data would be collected with a vibroseis truck in September as part of a much larger crustal refraction seismic experiment headed up by Simon Klemperer. When I started working, that's about the extent of what I knew.

That first summer produced far more questions than answers. We weren't sure how to subdivide the complex sedimentary section—we weren't even sure how to identify exactly what it was we were looking at. I had never spent any time looking at volcanic or volcaniclastic rocks, and though it was easy to see layering, we had a heck of time finding anything to measure bedding on in a pile of what we finally concluded were lahars. What had looked initially like a simple, layer cake stratigraphy was proving a bit more complicated than we had anticipated. There was much to be learned.

Nearly six years later, much has indeed been learned. This project has suited me well for several reasons, primarily because the paucity of previous work in the northwestern Basin and Range made the Warner Range something of a "frontier" for geology. Because so little was known about this region, basic field mapping was a suitable means of developing new understanding. In addition, I have had the opportunity to learn, utilize, and/or see in action a wide variety of techniques well beyond field mapping, including seismic velocity modeling, detrital zircon analysis, potential field mapping and modeling, paleoseismology, paleomagnetic analysis, shallow seismic reflection methods, audio-magneto-telluric methods, and—last, but definitely not least—ATV driving. I've particularly appreciated the opportunity to expand my knowledge and skills in the geophysical techniques that have allowed me to see below the surface, despite my frustration at the limits of what those techniques can actually tell me.

Another component of this project that has made it particularly enjoyable for me is the fact that I've been able to meet and collaborate with an enormous number of scientists. These collaborators are primarily at the U.S. Geological Survey in Menlo Park, including Joe Colgan, Jonathan Glen, Darcy McPhee, Dave Ponce, and Dave John. Trobe Grose, retired from Colorado School of Mines, has become another colleague and friend, and I have greatly appreciated his insight from many years of mapping in northeastern California and his support of my work. I also had the rare opportunity to walk into a trench across the Surprise Valley fault and put my hand on the fault,

thanks to Steve Personius, Mike Machette, and others from the earthquake hazards team at the USGS in Golden, CO. Other collaborators and colleagues included John Louie and his students at the University of Nevada-Reno and Don Prothero and his students at Occidental College.

Finally, the Warner Range and Surprise Valley have been an ideal classroom, and I've brought several groups of students out into the field with me. In fact, it was only after bringing three years' worth of students into the field that I realized that, if I didn't put all of this information together into a coherent story, no one else would, and that's when I decided to pursue this PhD. As a result, this thesis includes several years of data collected by students in field research courses taught by Elizabeth Miller and myself in addition to the results of my own mapping, analysis, and collaborative work with other scientists, primarily Joe Colgan and Jonathan Glen at the U.S. Geological Survey in Menlo Park.

# Acknowledgements

I have an enormous number of people to thank for helping to make this happen. First and foremost, this PhD would simply not have been possible without Elizabeth Miller's openness to a rather non-traditional arrangement – I wanted to keep my job while I finished the research. Elizabeth was ready to go to bat for me the moment I brought up the idea with her, and I cannot thank her enough for that. Steve Graham and Jerry Harris, who both have served as Assistant Dean for Academic Affairs (and my bosses) during this process were also tremendously supportive and understanding.

Similarly, I have greatly appreciated each of my committee member's ability to work with me as a colleague in my job as Undergraduate Program Coordinator and as a scientific mentor and advisor. They put enormous trust in my ability to wear several hats while juggling lots of balls, and I can only hope that I have merited that trust.

Every time I look at a geologic map or cross-section, some part of my brain says, "What would Elizabeth think?" She has an astounding ability to see relationships in the field and map them beautifully, and she quickly picks out geometric inconsistencies and impossibilities in others' maps. I try to channel her three- and four-dimensional thinking when looking at maps critically. In working with Elizabeth as Undergraduate Program Coordinator, I have also come to greatly respect and admire her commitment to field education. She is a rigorous instructor in the field, but she also really knows how to have fun, and makes it a hard, rewarding, and enjoyable experience for everyone—a model I hope to emulate.

After that first field season in May 2004, I returned to the Warners in September to help out with the seismic experiment. Though I had known Simon Klemperer before, I got to know him (and his work style) much better that fall, despite the fact that I was stationed in Cedarville and he was miles away in Winnemucca. I marvel at Simon's ability to process information quickly and thoughtfully, and to make rapid-fire

decisions when necessary. He has been incredibly patient with my learning geophysics pretty much on a "need-to-know" basis, and I have benefited a great deal from participating in his crustal group seminar. I have also thoroughly enjoyed working with Simon on our SES undergraduate research program, to which he has been devoted; I have learned a great deal from his approach to this program and to undergraduate students, teaching, and research in general.

Gail Mahood became so entranced with my field area herself that she bought a house there. And she graciously opened her door to students and colleagues. The last two years of field work would not have been the same without my regular conversations with Gail, where I could bring back a rock or tell her something I'd seen during the day and get her feedback. She also unhesitatingly shared her insights (often along with Wes Hildreth's) as they drove around exploring; I felt privileged to be privy to the insights of two such experienced volcanologists. I continue to walk away from every conversation with her having learned something new.

Marty Grove is newer to my committee and to my field area, but he still was more than willing to help me run samples through the night in the SHRIMP lab—on Christmas Eve. He willingly jumped into my committee feet first.

Beyond my committee, I have particularly benefited from interactions with several people. George Thompson is always delighted to talk about anything to do with the Basin and Range, and always interested in new information and new ideas. He has been an invaluable resource for me to bounce ideas off of to find out if they are completely unrealistic or maybe not quite so crazy after all. Joe Wooden has been a great support to me in the SHRIMP lab and beyond, willing to put in extra time and effort to help me prepare my samples and interpret the results. Jonathan Glen, a co-author on Chapter 3, introduced me to a number of new techniques that opened my eyes to ways of thinking about the Earth in general and the Basin and Range in particular. He has also provided invaluable support over the past three years, despite his constant efforts to get me involved in new projects.

Throughout this entire process, the person who has contributed the most to my understanding of the northern Basin and Range and kept me within the bounds of reality is Joe Colgan, a co-author on two of the chapters. Joe has been a great companion in the field, a prompt and helpful reviewer, and, above all, an excellent friend and colleague.

I feel compelled to list and acknowledge the entirety of undergraduate and graduate students that have participated in field work in the Warner Range, because this thesis includes much of their hard work. Undergraduate students since 2004 include: Sarah Aarons, Noah Athens, Lee Chang, Christina Contreras, James Dudley, Katy Elsbury, Valentina Fontiveros, Pablo Garcia del Real, Julia James, Hari Mix, Ilana Lohr-Schmidt, Christina Munoz, Annie Scofield, Silas Stafford, Tom Stilson, Carly York. Those first two students from San Juan College were Brad Christensen and Patrick Ostrye. Graduate students include: Matt Coble, Steve Davis, Julie Fosdick, Gwyneth Hughes, Emily Pope, Shauna Reidel-Bash, Ariel Strickland, Nick Van Buer. Still others who joined us in the field: Dwight Harbaugh, Sergei Katkov, Constanze Stuebner, and Ben Surpless.

Several other people have helped keep me sane throughout this process, particularly Katie Keranen, Jim Metcalf, Julie Fosdick, Derek Lerch, Jen Wilcox and the Coastside Runners Club, Robyn Dunbar, Elaine Andersen. While I cannot unequivocally recommend the path of having a full-time job while finishing a PhD, all of these people have helped to make it possible, often even enjoyable.

# Table of Contents

# List of tables

# List of figures

# Introduction

Along the northwestern margin of the Basin and Range province, mid-Miocene to Pliocene volcanic plateaus obscure much of the earlier history of this region. In the northeastern corner of California, however, slip on the relatively isolated Surprise Valley fault has resulted in the uplift of the Warner Range. The Surprise Valley fault is the westernmost large-offset normal fault at this latitude, making it also the western boundary of the Basin and Range extensional province. In contrast to most of the very active western boundary, the northwestern margin of the Basin and Range—the portion of the western boundary that lies north of the Sierra Nevada mountain range and includes the Surprise Valley fault—remains sparsely mapped and studied.

The work presented here addresses that deficit, building on and complementing the work of several other recent PhD theses and ongoing work. Joe Colgan described the history of extension in much of northwestern Nevada, including the Pine Forest and Santa Rosa ranges (Colgan, 2005). Derek Lerch described the volcanic history of the Black Rock Range in addition to providing a geophysical picture of the crust across the transition from extended to unextended terrain (Lerch, 2007). Matt Coble is currently working on the earliest calderas and volcanic products associated with the Yellowstone hot spot (Coble and Mahood, 2008). The geologic mapping, provenance

studies, and geophysical modeling of the Warner Range and surrounding region presented in this thesis help constrain the tectonic evolution and current structural setting of the northwestern margin.

This thesis consists of three chapters in addition to this introduction.

Chapter 1, *Evolution of the northwestern margin of the Basin and Range: Insights from the volcanic and extensional history of the Warner Range and environs, NE California*, addresses the geologic history of this region during the Cenozoic through geologic mapping, geochronology, and geochemical and geophysical data. From at least the late Eocene through the middle Miocene, the Warner Range region experienced arc-related volcanism and sedimentation, resulting in the accumulation of a thick sequence of volcaniclastic sediments and volcanic rocks. Extension and uplift appears to have occurred in two episodes, the first in the middle Miocene and the second initiating ~3 Ma, which resulted in flexural uplift of the Warner Range, and continuing to the present day. The total magnitude of extension in the Warner Range region may be as much as 15%, the majority of which is accommodated along the Surprise Valley fault. Supporting geochronological data was provided largely by Joe Colgan at the U.S. Geological Survey, in conjunction with his colleagues David John and Robert Fleck, also of the USGS, and Chris Henry, from the Nevada Bureau of Mines and Geology. Joe and Elizabeth Miller are co-authors on this chapter, which will be submitted to *Geosphere*, as they both initiated the mapping project and provided key support and analysis of the data.

Chapter 2, *Provenance and paleogeographic implications of Eocene-Oligocene sedimentary rocks in the northwestern Basin and Range*, focuses on the oldest unit exposed in the Warner Range. Late Eocene and Oligocene sedimentary rocks are only rarely exposed in the northwestern Basin and Range, so their mere presence here provides insight that is available nowhere else. The chapter combines detrital zircon analysis with sedimentology to determine the provenance of this unit. Detrital zircon analysis on coarse sandstones and dating of individual granite cobbles show a range of

ages consistent with a local, volcanic source area primarily from the SSW with some far-traveled input from northern Nevada; the far-traveled component increases in influence as the unit thins to the north. Comparison with other sedimentary sequences of Eocene age and integration with paleofloral and geophysical data help define drainage divides, and suggest that this sequence accumulated in a relatively isolated, intra-arc basin. This localized accumulation differs markedly from contemporaneous drainages to the south that transported material westward from central Nevada to the paleoshoreline, and suggests that ongoing volcanism had a strong influence on paleogeography in this region during the Eocene and Oligocene. This chapter is published in *International Geology Review* (Egger et al., 2009a) with co-authors by Joe Colgan, U.S. Geological Survey, and Carly York, both of whom aided primarily in the field work. Carly conducted the SHRIMP work on the granitic cobbles from the Flume Canyon for her senior thesis while an undergraduate at Stanford.

Chapter 3, *The northwestern margin of the Basin and Range Province: Structural setting of a developing basin from seismic and potential field data*, moves from the range into the basin and from the geologic past into the present. We use seismic velocity and potential field modeling help determine the nature of basin fill and identify intra-basin faults. Based on a detailed gravity and magnetic profile, we identify shallow subsurface basalt flows and several faults within the valley that may accommodate hundreds of meters of vertical offset, possibly cutting and offsetting the ~30° east-dipping Surprise Valley fault that rotated during footwall tilting of the adjacent Warner Mountains. Some of these intra-basin faults correspond with mapped Quaternary fault scarps, but others have no surface expression. These faults may represent the currently active fault system within the basin. This chapter is published in *Tectonophysics* (Egger et al., 2009b), and is co-authored by Jonathan M.G. Glen and David A. Ponce, both of the U.S. Geological Survey. All three of us participated in the collection of field data. David Ponce produced and compiled most of the rock property measurements that facilitated the potential field modeling. Jonathan Glen created the potential field models. I created the seismic velocity model, the basis for the potential field model, and provided the geological mapping to constrain all of the

modeling. Jonathan and I worked together to match the potential field model to the surface features and to develop the interpretation.

The appendices consist of detailed map unit descriptions, major and trace element geochemistry data tables, geochronological data, detrital zircon analysis methods, and data from the detrital zircon analysis.

## References

Coble, M.A., and Mahood, G.A., 2008, New geologic evidence for additional 16.5-15.5 Ma silicic calderas in northwest Nevada related to initial impingement of the Yellowstone hot spot: IOP Conference Series: Earth and Environmental Science, v. 3, p. 012002.

Colgan, J.P., 2005, Timing and magnitude of Basin and Range extension in northwestern Nevada [PhD thesis]: Stanford, CA, Stanford University.

Egger, A.E., Colgan, J.P., and York, C., 2009a, Provenance and palaeogeographic implications of Eocene-Oligocene sedimentary rocks in the northwestern Basin and Range: International Geology Review, v. 51, p. 900 - 919.

Egger, A.E., Glen, J.M.G., and Ponce, D.A., 2009b, The northwestern margin of the Basin and Range province: Part 2: Structural setting of a developing basin from seismic and potential field data: Tectonophysics, v. In Press, Corrected Proof.

Lerch, D., 2007, Geophysical and geological characterization of Cenozoic tectonism and magmatism across the northwestern margin of the Basin and Range province [PhD thesis]: Stanford, CA, Stanford University.

# Chapter 1

## Evolution of the northwestern margin of the Basin and Range: The geology of the Warner Range and environs, NE California

**ABSTRACT**

Along the northwestern margin of the Basin and Range province, mid-Miocene to Pliocene volcanic rocks cover and obscure much of the earlier history of the region. In the northeastern corner of California, however, slip on the relatively isolated Surprise Valley fault has resulted in the uplift of the Warner Range, exposing rocks as old as late Eocene. Geologic mapping, cross-sections, geochronology, and geochemical analysis of rocks in the Warner Range and surrounding region document a long history of volcanism and extension from the Eocene to the present that provides unique insight into the evolution of this margin.

A history of subduction-related arc volcanism lasting from ~40 Ma to the mid-Miocene is exposed in the >4 km of volcaniclastic sediments and volcanic rocks of the Warner Range. At the base of the range, ~40 Ma andesite lavas and debris flows mark a return to subduction-related arc volcanism associated with the ancestral Cascade arc to the region. A thick, late Eocene to early Oligocene (34-28 Ma) volcaniclastic sequence records ongoing, proximal volcanic activity. A series of Oligocene volcanic edifices were built on this sequence. Geochemical analysis suggests these were the product of subduction-related arc volcanism, and geochronology limits the period of volcanic activity between ~28–24 Ma. The arc volcanism that occurred in the Warner

Range in the Oligocene was the result of subduction of the Juan de Fuca plate, distinguishing this northwestern corner of the Basin and Range from the rest of the province further east and south, which experienced magmatism that swept southward through time. Thus, the Warner Range region can be considered part of the "ancestral" Cascades.

In the southern part of the range, Oligocene volcanic rocks are unconformably overlain by locally-derived, subduction-related mid-Miocene mafic lava flows and tuffs, once thought to be the southern extension of the Steens basalt. Thus, arc-related magmatism continued in region into the mid-Miocene, despite the nearby impingement of the Yellowstone hotspot and voluminous eruptions of continental flood basalts that blanketed much of the surrounding region.

Extensional normal faulting began in the mid- to late Miocene, sometime after 14 Ma, in relative isolation from other Basin and Range normal faults. Later Miocene and Pliocene (8-3 Ma) volcanic rocks flowed into low-lying areas produced by initial mid-Miocene extension. These younger basalts are also cut by normal faults, requiring a second episode of extension that began after 3 Ma and resulted in most of the accumulated 8 km of dip-slip motion slip along the Surprise Valley fault. Since the mid-Miocene, 12-15% extension has been accommodated across the Warner Range region, primarily along the Surprise Valley fault.

A protracted or two-part history of extension, such as that seen in the Warner Range, has been noted elsewhere in the western Basin and Range. While relatively little extension has been accommodated in the Warner Range region, it continues to the present day, and the Surprise Valley fault appears to have thus persisted as the westernmost boundary of Basin and Range extension since the mid-Miocene.

## INTRODUCTION

Modern deformation and seismic activity across the actively extending Basin and Range province of the western U.S. is concentrated along its borders, where it is bounded by the unextended Sierra Nevada and Colorado Plateau, respectively (Fig. 1). Geodetic surveys have shown that the western margin of the province also accommodates 15-25% of Pacific-North American plate motion, primarily within the Walker Lane, a 100-150 km-wide zone of distributed dextral shear (e.g. Bennett et al., 2003; Thatcher et al., 1999) (Fig. 1), highlighting the importance of the western margin of the Basin and Range to our overall understanding of plate boundary processes and deformation in western North America. A significant amount of recent work has focused on the structural evolution of the western margin of the province along the eastern side of the Sierra Nevada and the relationship between extensional and strike-slip faulting (e.g. Cashman et al., 2009; Henry et al., 2007; Oldow, 2003; Surpless et al., 2002; Trexler et al., 2000). In contrast, there have been few detailed investigations of the geologic and structural history of the northern continuation of the western margin of the Basin and Range—the portion of the boundary that lies north of the Sierra Nevada and east of the Cascades (dashed line, Fig. 1).

Several features set the northwestern margin of the Basin and Range apart from its better-studied southern counterpart. First, its tectonic setting differs in that it lies north of the Mendocino triple junction and thus inboard of a modern subduction zone rather than the San Andreas strike-slip plate boundary (Fig. 1). South of the triple junction, the Walker Lane lies within the Basin and Range and WNW-ESE-directed extension occurs both to the east and west of the zone of dextral shear (Cashman et al., 2009; Surpless, 2008). North of the triple junction, dextral strike-slip faulting interpreted as northward propagation of the Walker Lane dies out to the west of significant extension in the Basin and Range (Fig. 1) (Faulds et al., 2005; Unruh et al., 2003). Second, the amount of extension that has occurred in the northwestern portion of the Basin and Range is significantly less than that farther south in the province. Here, normal faults associated with Miocene and younger extension decrease in offset and die out

northwards, transitioning to the relatively unextended High Lava Plains of southern Oregon (Fig. 1) (Jordan et al., 2004; Lerch et al., 2008; Scarberry et al., 2009). In comparison, the western margin of the Basin and Range further south has undergone high magnitude extension (>100%) such as in the Singatse-Wassuk region (Proffett and Dilles, 1984; Surpless et al., 2002) (Fig. 1). As a result of relatively little extension, pre-Tertiary basement is rarely exposed along the northwestern margin.

Finally, the northwestern margin of the Basin and Range has experienced a different Tertiary magmatic history than much of the rest of the province. Based on this study, andesitic magmatism related to subduction was re-established in the region as early as ~40 Ma, as opposed to only ~16 Ma further south (e.g. Busby et al., 2008), but this earlier evolution of the region is largely buried by voluminous mid-Miocene and younger volcanic cover. Yellowstone hot spot volcanism began in the region ca. 16 Ma with a massive outpouring of flood basalts (the Steens and Columbia River basalts) (e.g. Hooper et al., 2002) and was followed closely by the development of rhyolitic calderas, now exposed on the Sheldon Plateau (Figs. 1, 2) (Coble and Mahood, 2008; Greene, 1984). A significantly younger episode of widespread volcanism occurred in the Modoc Plateau region (Fig. 1) and lasted from ~8-2 Ma; this later episode is dominated by smaller volume, more mafic eruptions of distinctive low-potassium, high-alumina olivine tholeiites that filled low-lying topography and remain mostly undissected (Carmichael et al., 2006; McKee et al., 1983).

The Warner Range in northeastern California provides an opportunity to learn more about both the pre-Miocene tectonic and magmatic history of the northwestern Basin and Range and the evolution of the margin since extension began, most likely in the mid- to late Miocene. The Surprise Valley normal fault, which bounds the range, is the largest-offset fault along the northwestern margin of the Basin and Range (Figs. 1, 2). The Warner Range exposes a thick section of volcanic, volcaniclastic, and sedimentary rocks that record a semi-continuous history of magmatism and sedimentation dating back to the late Eocene. The mountain range thus provides a critical window into the earlier magmatic and structural evolution of the region. The

Surprise Valley fault, approximately 85 km long with about 8 km of total dip slip motion, is similar in extent and offset to other large Basin and Range faults but developed in relative isolation from faults in the rest of the province (Fig. 2). The slip history of the fault can thus reveal the nature of extension along this margin since its inception. The geologic mapping, cross-sections, geochronology, and geochemical analyses presented here provide new details about the geology, volcanic history, and structural evolution of the Warner Range and surrounding region that help elucidate the history of the less studied and more enigmatic northwestern margin of the Basin and Range.

**PREVIOUS WORK**

In comparison to most of the western margin of the Basin and Range, the region encompassing the Warner Range has been sparsely mapped and studied. Russell (1928) pursued reconnaissance mapping in the Warner Mountains because he believed that, unlike much of the rest of the "Basin ranges", no previous episode of folding had disturbed the layers of sedimentary and volcanic rocks, and the faulting event that produced the modern topography could be studied in isolation. Numerous subsequent investigators focused on a single aspect of the stratigraphy of the range, primarily the well-preserved Eocene and Oligocene flora in the sedimentary sequence at the base of the range (Axelrod, 1966; MacGinitie, 1941; Myers, 1998; 2003; 2006). The spectacular eruption of a mud volcano at Lake City Hot Springs (Fig. 3) in 1951 (White, 1955) inspired additional work in the region focused on groundwater (Ford et al., 1963) and geothermal exploration (see Plate I for locations of geothermal drill holes) (U.S. Geological Survey, 1981).

Martz (1970) mapped the central portion of the range, adding detail to Russell's earlier reconnaissance mapping, particularly in the lower sedimentary sequence (Fig. 3). Geological mapping in the southern portion of the Warner Range was undertaken for the purposes of assessing potential mineral resources prior to the designation of the South Warner Wilderness Area (Fig. 3) (Duffield et al., 1976). As part of that study,

Duffield and McKee (1986) dated several volcanic units exposed in the range, establishing the Oligocene age of the sedimentary section and mid-Miocene age of rocks at the crest of the range. Carmichael et al. (2006) added significantly to the geochronological and geochemical database for the region in their study of the nature and extent of late Miocene and Pliocene lava flows, previously described farther west on the Devil's Garden Plateau by McKee et al. (1983).

Hedel (1980; 1981; 1984) mapped Quaternary fault scarps in the Surprise Valley; these were more closely studied and verified in the field and with photogeologic methods by Bryant (1990), and these revised scarps are shown in Figure 3 and Plate I. A seismic reflection profile was collected across the Surprise Valley (Lerch et al., 2009) and the data were modeled using both seismic velocity and potential field methods (Egger et al., 2009b). Numerous intra-basin faults were identified by this last study, and additional seismic, audio-magneto-telluric, and potential field data are being used to constrain those structures (Athens et al., 2009; McPhee et al., 2009; Stilson et al., 2008). A trench was dug across the Surprise Valley fault for paleoseismic studies to determine earthquake recurrence intervals in this region (Personius et al., 2009). Geothermal exploration continues in the region today, resulting in the drilling of a core north of Lake City (Fig. 3) (Benoit et al., 2005; Egger et al., 2009a).

On a regional scale, geophysical studies have shown that the crust beneath the northwestern margin of the Basin and Range thins homogeneously from ~37 km thick beneath the Modoc Plateau (and the Warner Range) to ~31 km beneath northwestern Nevada (Fig. 2b) (Lerch et al., 2007). Potential field modeling shows that the velocity and density of upper crustal units also changes across this transition: the Warner Range lies west of a 15-km-thick low-velocity, low-density ($V_p \approx 6.0$ km/s), and low $V_p/V_s$ zone in the upper crust (Fig. 2b) interpreted as the northward continuation of the Sierra Nevada batholith (Fig. 1) (Gashawbeza et al., 2008; Lerch et al., 2007; Van Buer et al., 2009). The results of all of these studies are incorporated into the geologic history of the Warner Range as described below.

## GEOLOGIC HISTORY OF THE WARNER RANGE AND SURROUNDING REGION

An approximately 4.5 km thick, west-dipping sequence of Eocene to upper Miocene sedimentary and volcanic rocks is exposed in the Warner Range. In his reconnaissance mapping, Russell (1928) noted that "the volcanic rocks of this region are for the most part extensive sheets lying concordantly, one above the other, bent or broken only in relation to comparatively recent Basin Range faulting." In contrast to Russell's description and that of others (e.g. Duffield et al., 1976) that suggest units are conformable and laterally continuous throughout the range, geologic mapping associated with this study reveals that units are not uniformly distributed and that unit thicknesses change rapidly and dramatically along strike (Fig. 4) with multiple unconformities within the section. The section has been cut by at least two sets of normal faults. The unit descriptions, map relations, and geologic history we detail in this section refer extensively to Plate I, a geologic map; and Figure 4, a series of stratigraphic columns and a N-S cross-section along the length of the range. All geochronologic data referred to in the text are listed and fully referenced in Table 1. Detailed map unit descriptions, geochemical data, and geochronological data are included in Appendix A.

### *Pre-Oligocene (40 Ma) geologic setting*

No rocks older than ~40 Ma are exposed within ~100 km of the study area (Fig. 2), therefore little is known about the pre-late Eocene history of this region. The nearest exposures of pre-Tertiary rocks occur in the Black Rock Range, approximately 100 km to the east, where late Eocene (ca. 35 Ma) volcanic rocks were erupted across eroded Paleozoic metasedimentary rocks intruded by Cretaceous granite (Fig. 2) (Lerch et al., 2008). On the basis of seismic velocity and potential field modeling, Fuis et al. (1987) interpret plutonic basement (with a modeled $\rho = 2.73$ g/cm$^3$) to be shallow beneath the Warner Range—as little as 1 km below the exposed base of the section at Cedarville. Potential field modeling along a transect in Surprise Valley (Fig. 3) suggests that rocks of densities characteristic of continental basement (with a

modeled $\rho = 2.67$ g/cm$^3$) are encountered ~1.5 km below the base of the rock sequence exposed in the Warner Range (Egger et al., 2009b).

On the basis of apatite fission-track and (U-Th)/He dating of Cretaceous granites in northwestern Nevada, Colgan et al. (2006) concluded that 5 ± 2 km of material was eroded off the pre-Tertiary basement prior to deposition of Tertiary rocks, mostly during the late Cretaceous. By constructing an early Tertiary paleogeologic map from regional analysis of the basal Tertiary unconformity, Van Buer et al. (2009) inferred a similar history for the western Basin and Range and Sierra Nevada, where an erosional period lasting from about 85 to 45 Ma stripped as much as 5 km of material off the pre-Tertiary basement. We assume a similar history for basement rocks beneath the Warner Range region, such that, by the early Eocene, batholithic and/or metamorphic basement was exposed across a low-relief region of moderate elevation. This assumption is supported by the presence of granite cobbles in conglomerates near the base of the exposed section in the Warner Range (Egger et al., 2009a). Based on these considerations, we show the depositional base of the stratified section of the Warner Range in our cross-sections at a minimum depth of 0.5 km below the lowest exposed strata, and we infer that basement to be largely plutonic rocks of the Sierra Nevada batholith and the country rocks it intruded.

*Late Eocene-Oligocene (~40-27.5 Ma) volcaniclastic sedimentation*

Based on the above considerations, it is likely that volcanism and deposition began in the region in the late Eocene. The oldest rocks exposed in the Warner Range consist of deeply weathered andesitic breccias, lahars, and debris flows with minor pyroxene- and hornblende-andesite lava flows (Fig. 4). This unit, called the McCulley Ranch Formation (Tmrv) by Martz (1970), is only exposed in the central portion of the range near Cedarville (Plate I). Axelrod (1966) reported a K-Ar age on feldspar from a flow near the top of this unit that yielded an age of 40.8 ± 3.0 Ma (corrected age). This unit may correlate with a similar andesitic sequence exposed ~90 km to the north at Drake Peak (Fig. 2), dated at 40.2 ± 4.0 Ma (K-Ar) (Wells, 1980). The mineralogy and stratigraphy of these andesitic sequences suggest a subduction-related arc origin

(Martz, 1970; Wells, 1980). Thus the latest Eocene in the Warner Range marks the return of arc magmatism to the general region after a hiatus of perhaps as much as 40 my (represented by the time gap between the youngest intrusive rocks of the Sierra Nevada batholith ages of ~80 Ma and the earliest documented Tertiary andesitic lavas), although the predominance of debris flows and lahars over lava flows suggests these deposits were distal with respect to their volcanic sources. Similarly, volcanic rocks associated with arc magmatism in the western Cascades are as old as 45 Ma (du Bray et al., 2006).

Along the length of most of the Warner Range, a thick section of sedimentary and volcaniclastic rocks is exposed and was originally called the Lower Cedarville Formation by Russell (1928) (Plate I). Based on detailed mapping in a portion of the range between Cedarville and Lake City (Fig. 3), Martz (1970) subdivided the Lower Cedarville Formation into three units; from oldest to youngest, these are the Steamboat Formation, the Deep Creek Formation, and the Lost Woods Formation (see Egger et al., 2009a for a complete discussion of formation names). Our mapping confirms the formation boundaries suggested by Martz (1970) and extends these subdivisions south of Cedar Pass (Fig. 3, Plate I), where we use his same formation names.

The Steamboat Formation (Tsbn, Tscc, and Tsu) is a cliff-forming, coarse-grained alluvial sandstone and conglomeratic sequence that ranges from ~1500 m thick in its southernmost exposures to 200 m thick where it is encountered in a drill core (Figs. 3,4) (Egger et al., 2009a). In addition to this change in thickness, paleocurrent indicators and detrital zircon ages indicate a proximal volcanic source to the SSW, most likely within 20 km (Egger et al., 2009a). Several dates on thin tuffs and reworked tuffs within the Steamboat Formation (Table 1) all suggest it was deposited between ~33 Ma and ~30 Ma (Duffield and McKee, 1986; Myers, 1998). Thin lake deposits contain abundant leaf fossils and paleofloral analysis suggests paleoelevations of 1-2 km (Myers, 1998; Myers, 2003).

The Deep Creek Formation (Tdc) consists primarily of tuffs and reworked tuffaceous sediments, and generally forms a tree-covered slope above the conglomeratic cliffs of the Steamboat Formation. Martz (1970) described these tuffs as "welded", but more often they are silicified and slightly hydrothermally altered to a greenish tint. Duffield and McKee (1986) dated an andesitic ash at 28.8 ± 1.1 Ma (K-Ar, hornblende) that may be from unit Tdc (Table 1).

The Lost Woods Formation (Tlw) consists of conspicuously red-weathering volcanic breccias, volcaniclastic sandstones and conglomerates, minor mafic tuff, and autobrecciated lava flows. This unit contains more basalt than the underlying volcaniclastic sequence, and many of the breccias consist of homogeneous vesicular basalt clasts. In finer-grained sedimentary layers, Tlw includes petrified logs up to 1 m in diameter (Fig. 5a). On the ridge south of Cedar Pass, where the Lost Woods Formation is most extensively exposed, we measured orientations of the long axes of 13 of these logs (Fig. 5b), which are reliable indicators of paleofluvial transport direction (Fritz and Harrison, 1985). Though the number of samples is fewer than ideal, the nearly N-S trend of the majority of logs is apparent, indicating a roughly similar source direction as that of the underlying Steamboat Formation, though it is unclear, based on the logs alone, if the flow direction would have been to the north or the south. No units within the Lost Woods Formation have been dated but its age is fairly well constrained between ~29 and 27.5 Ma based on ages from rocks in units above and below (Fig. 4).

This entire sequence of ~40-27.5 Ma volcaniclastic and sedimentary rocks was deposited in a continental basin within a system of active volcanoes—an intra-arc basin, as suggested by the presence of numerous ash layers, coarse volcanic breccias, highly variable thickness of units, and the presence of occasional lava flows throughout the sequence (Duffield and McKee, 1986; Egger et al., 2009a; Martz, 1970). The spatial extent of this intra-arc basin is unknown, but a similar (although much thinner) sequence is exposed near Drake Peak (Fig. 2) approximately 100 km

north of the study area (Wells, 1980), suggesting it could be at least 100 km long in its north-south dimension.

*Oligocene (~27.5-24 Ma) arc volcanism*

The Warner Range and adjacent Hays Canyon Range to the east expose remnants of three late Oligocene volcanic edifices: the Lake City basalts (called the Soldier Creek volcanics by Martz, 1970), the Cedar Pass complex (our name), and the Hays Volcano (name given by Carmichael et al., 2006). These three edifices and additional, more distal volcanic deposits (Tovu) are very closely related in space and time, as is typical of volcanic edifices within the modern Cascade arc (Hildreth, 2007).

The Lake City basalts (Tovl) are exposed in the northern Warner Range where they reach a thickness of more than 2 km (Fig. 4). The unit consists of interlayered basalt, basaltic andesite and andesite flows, and mafic tuff and tuff breccia (Fig. 6). Basalts have a dark aphanitic matrix with mm-sized plagioclase laths and variable but large (up to 2 cm) phenocrysts of plagioclase and pyroxene in varying amounts. The entire sequence thins to the south, pinching out completely just north of Cedar Pass, indicating the flows likely represent part of a basaltic shield volcano (Fig. 4, Plate I). The sequence ranges in age from 27.83 ± 0.21 Ma at the base of the sequence, and 25.70 ± 0.94 Ma at the top (Table 1, Appendix A) (Colgan et al., in prep). The cinder-rich mafic tuffs are thickest ~10 km north of Cedar Pass, suggesting a vent area in this general area (Fig. 3, Fig. 4, Plate I). The Lake City basalts are similar in composition to the basaltic andesite of Twelvemile Peak, described by Wells (1980) and exposed ~80 km to the north; it is likely the two units are of similar age.

The Cedar Pass complex (Tovc) consists primarily of volcanic breccias, andesite and basaltic andesite flows, and minor shallow dacite intrusions (Fig. 6). Commonly, breccias consist of hornblende-rich andesite block-and-ash flows. Dikes of hornblende andesite radiate out from a center ~5 km southwest of Cedar Pass in Dry Creek Basin; breccias also dip radially away from Dry Creek Basin, suggesting a possible vent location in this area (Plate I, Fig. 3). Numerous dates within the complex all fall

within 26.6-27.0 Ma (Table 1, Appendix A) (Colgan et al., in prep), suggesting the rapid development of an andesitic composite volcano or dome complex on the flank of the slightly older basaltic shield volcano (Tovl) to the north.

Farther south of the vent area, breccias disappear and contemporaneous Oligocene volcanics (Tovu) consist mostly of more distal andesite flows and ignimbrites (Plate I) (Duffield and McKee, 1986). Duffield et al. (1976) mapped Tovu as part of a "composite volcanic" unit, or Tvc. Geochronologic data (Table 1, Appendix A) (Colgan et al., in prep) have determined that the Tvc unit of Duffield et al. (1976) contains a significant unconformity bracketed by the ~26-27 Ma Oligocene volcanic unit and the overlying early Miocene (~19-17 Ma) welded tuffs, described below. We have therefore separated Duffield et al.'s (1976) Tvc into two units: Tovu (Oligocene) and Trt (early Miocene) (Plate I). Tovu is also exposed in the Hays Canyon Range to the east (Fig. 2, Plate I). Carmichael et al. (2006) report an age of 26.26 ± 0.13 Ma on what they refer to as the Fortynine Tuff, which we include in Tovu (Plate I). The Hays volcano (Tovh), exposed in the southern portion of the Hays Canyon Range, is a basaltic to basaltic andesite shield volcano dated at 23.8-24.5 Ma (Table 1, Appendix A) (Colgan et al., in prep).

Major and trace element geochemistry of this sequence of 24-28 Ma volcanic rocks reveals that they are similar to rocks of both the modern and ancestral Cascade arc (Fig. 7). In contrast, coeval Oligocene volcanic rocks in the Black Rock Range and Pine Forest Range to the east (Fig. 2) comprise a bimodal sequence of basalt to basaltic trachyandesite and rhyolite tuffs (Colgan et al., 2006; Lerch et al., 2008). Although no rocks older than mid-Miocene are exposed on the Sheldon Plateau between the Warner and Black Rock Ranges, the volcanic edifices exposed in the Warner and Hays Canyon Ranges may mark the easternmost extent of subduction-related arc volcanism during the Eocene and Oligocene (e.g. Cousens et al., 2008).

*Early Miocene (~19-17) tuffs and sediments*

Few rocks of early Miocene age are preserved in the Warner Range, suggesting a near cessation of proximal volcanic activity ~24 Ma. A thin unit of rhyolitic tuffs and sediments (Trt) crops out between Parker Creek and Emerson Peak (Fig. 4; Plate I), which Duffield et al. (1976) included in their unit Tvc. A new date of 19.22 ± 0.27 Ma on a reworked tuff at the base of this unit (Table 1) (Colgan et al., in prep) suggests a 4-6 my hiatus in deposition, followed by minor deposition of sediments and tuffs derived from distal, rhyolitic volcanic activity during the early Miocene. Scarberry et al. (2009) report arc volcanic activity ~21-23 Ma in the Coleman Hills, near the Abert Rim in Oregon (Fig. 2), possibly representing the migration of arc volcanic activity north, away from the Warner Range region in the early Miocene.

*Mid-Miocene (16-14 Ma) basaltic volcanism*

Despite the decrease in volcanic activity, it appears that relatively little erosion took place during this time, as Oligocene features still acted as topographic barriers to subsequent, younger volcanic flows and breccias. In the southern Warner Range, more than 1 km of basalts and basaltic andesites (Tmbl and Tmbu), and tuffs (Tmt) were deposited from ~16-14 Ma (Duffield and McKee, 1986), but these lavas were blocked from flowing north because of the topographic high formed by the Cedar Pass complex (Fig. 4, Plate I). A similar relationship is observed in the Hays Canyon Range, where mid-Miocene basalt flows bank into the flanks of the Hays Volcano (Carmichael et al., 2006) (Plate I), as well in farther north in Oregon (Fig. 2) (Scarberry et al., 2009; Wells, 1980).

The mid-Miocene age of these basalt flows initially led to their interpretation as part of the extensive Steens Basalt (e.g. Brueseke et al., 2007). However, the mid-Miocene volcanic rocks in the Warner and Hays Canyon ranges are geochemically distinct from the Steens basalt (Fig. 8) and instead are more similar to arc volcanic rocks of the Cascade Range (Fig. 7). In addition, the flows exposed in the Warner Range were erupted from mafic shield volcanoes such as those seen to the southwest of the Warner

Range (Fig. 2), whereas the Steens basalts were erupted from a more diffuse network of dikes (e.g. Camp et al., 2003).

Beginning ~15 Ma and continuing to ~7 Ma, the Warner Range and surrounding region experienced pulses of local rhyolitic magmatism (for locations mentioned below, see Figure 3), including the eruption of extensive ~15 Ma rhyolites south of Eagleville (Duffield and McKee, 1986), 12-14 Ma rhyolite magmatism coincident with gold mineralization in the High Grade District (Keats, 1985), and numerous rhyolite and obsidian domes erupted 7-9 Ma south of Fandango Pass, where they lie directly above Oligocene basalts (Fig. 4; Plate I) (Duffield and McKee, 1986).

*Late Miocene to Pliocene (~8-3 Ma) volcanism*

Latest Miocene and Pliocene volcanic rocks in the region consist primarily of a distinctive series of low-potassium, high-alumina olivine tholeiites (Tlb) erupted between 8 and 3 Ma; these rocks are described in detail elsewhere (Carmichael et al., 2006; McKee et al., 1983), along with interbedded rhyolite domes (Tmr) and tuffs and tuffaceous sediments (Tts). Geochemically, the compositions of the basalt flows show little variability (Figs. 6, 7). Individual flows are thin, reaching only a few meters in thickness at most, but are interbedded with tuffs, tuffaceous sediments, and lacustrine deposits (Tts where mapped separately). The flows crop out extensively throughout the region, on both the west and east sides of the Warner Range and Surprise Valley fault (Plate I). Despite their broad distribution, our mapping suggests that these flows were limited by pre-existing topography of both the Hays Canyon and Warner ranges, in contrast to the interpretation of Carmichael et al. (2006) that they were once continuous across the southern Warner Range. While the middle Miocene basalts now comprise the highest peaks in the modern Warner Range, the younger lava flows are not present in the higher parts of the range and are confined to the modern valleys on the east and west sides. On the east side of the Surprise Valley, a 3 Ma flow banks into the Oligocene tuffs of the Hays Canyon Range; on the west side, horizontal flows directly overlie Oligocene rocks west of the range (Plate I). On the southwest side of

the Warner Range, they appear to have flowed across pre-existing normal faults, which may have also controlled the vent location (Plate I).

These flows were never, therefore, continuous across the region, and instead erupted simultaneously at several locations, covering the low-lying areas with a thin veneer of basalt. Unlike the earlier Oligocene and Miocene volcanism, this magmatic event did not generate significant volcanic edifices, and what are likely volcanic vents appear as small, low-relief shields (Fig. 3) and plugs. Vents are located just north of the road between Vya and Cedarville, on the Devil's Garden Plateau, and on the west flank of the Warner Range (Fig. 3, Plate I).

*Pleistocene lake deposits*

Pleistocene and younger deposits are dominated by sedimentary deposits from pluvial Lake Surprise, which reached a high stand of 1533.6 m (Zimbelman et al., 2008), filling the valley with water to a depth of ~156 m (~512 feet). Along the western side of the valley, the remains of several Gilbert-type fan deltas stand up to 30 m above the surrounding valley floor (Plate I). Numerous shorelines are visible, particularly at the southern end of the valley, where tufa deposits have cemented Pleistocene beach gravels (Zimbelman et al., 2008).

## FAULTING AND EXTENSION

*Faults in the Warner Range region*

The rock units described above are cut and variably offset and tilted by a series of normal faults (Plate I). The most significant of these trend approximately north-south and include the range-bounding Surprise Valley and Hays Canyon faults (Fig. 3), of which the Surprise Valley fault has accommodated the most slip. Another set of faults and fractures trends NW-SE, paralleling a pervasive regional fracture system that becomes more prominent farther north in Oregon (Fig. 2). In the Warner Range region, the most significant NW-trending structure is the fault that forms Fandango Valley (Fig. 2, Plate I). In the southern portion of the Warner Range, a set of four normal faults near Emerson Creek includes curved faults whose trends vary from NE-

SW to N-S. These Emerson Creek faults are all down-to-the-E and -SE (similar to the Surprise Valley fault), accommodate up to a several hundred meters of offset, and are cut by the Surprise Valley fault (Plate I). Finally, in the central portion of the Warner Range, a set of E-W-oriented normal faults accommodate a few hundred meters of offset, at most, and appear to be entirely within the Oligocene sedimentary section (Plate I).

The majority of the uplift and tilt of units in the Warner Range is linked to motion along the Surprise Valley fault (SVF), an 86-km long down-to-the-east normal fault that bounds the eastern flank of the range (Fig. 3, Plate I). The SVF includes several major segments connected by step-overs that primarily step to the left (Fig. 3), likely reflecting the growth and connection of a system of en echelon fault segments (e.g. Ferrill et al., 1999; Peacock, 2002). The most significant of these step-overs coincides with minor topographic highs in the Surprise Valley, dividing the valley into a series of three sub-basins that host the upper, middle, and lower lakes (Fig. 3, Plate I).

Several Quaternary fault scarps occur as far as 2 km from the main range-front fault (Fig. 3, Plate I), cutting and displacing basin sediments by as much as 15 m (Hedel, 1980). A number of fault scarps initially mapped throughout the valley by Hedel (1984) were field- and photo-checked by Bryant (1990), who reclassified some as paleoshorelines and eliminated others. The remaining scarps are concentrated at the step-overs of the range-front fault, propagating into the basin (Fig. 3, Plate I) and may be fault splays that initiate at the juncture of en echelon segment boundaries (e.g. Anders and Schlische, 1994).

A high-resolution seismic reflection profile reveals that the SVF now dips moderately (28° ± 6°) to the east (Lerch et al., 2009). The location of this profile (Fig. 3) is within one of the complex step-over zones along the range-bounding fault, and therefore the reflector imaged at this location may represent an anomalously shallow dip of the fault with respect to its average dip. Lerch et al. (2009) also model a 30-40° east-dipping reflector at the latitude of Cedarville, which we believe to be more representative of

the dip of the fault as a whole. Assuming a modern eastward dip of 35° (the average of 30-40°) for the SVF and restoring the 25° of rotation for the most tilted units exposed in the range, the Surprise Valley fault may have initiated at an angle of ~60°, an angle that is well within the range expected for normal fault initiation (54-69°) (e.g. Friedrich et al., 2004; Twiss and Moores, 1992). Based on the reasoning above, we assume a present-day angle for the SVF of 35° in our cross-sections and utilize an initial 60° dip in our restored cross sections (Fig. 9).

Colgan et al. (2008) proposed two phases of slip and exhumation along the Surprise Valley fault on the basis of thermochronometry of apatite from a single granite cobble from the base of the exposed sedimentary section in the Warner Range (see Fig. 3 for location). Modeling of apatite fission track ages and track lengths in this sample suggest a poorly-constrained phase of exhumation and cooling between about 14 and 8 Ma that may account for about one-third of the total exhumation of the sample. (U-Th)/He-dating of apatites from the same sample suggests a period of rapid cooling and exhumation between about 3 Ma and 1 Ma that could account for most of the remaining two-thirds of the exhumation, though additional slip (on the order of 500-700 m, assuming a geothermal gradient of 35-40° C) is required since 1 Ma to exhume the sample to its present exposure elevation (Colgan et al., 2008). As described below, our mapping confirms the presence of two episodes of extension and lends additional insight to the total amount of extension and how it has been accommodated.

*The onset of extension*

Prior to the onset of extensional faulting in the mid-Miocene, the site of the modern Warner Range was characterized by significant topographic relief. The mid-Miocene volcanic edifices southwest of Eagleville (Fig. 2) rose as much as 500 m above the landscape, and the eroded remnants of the Oligocene volcanic centers rose at least some distance above the surrounding area (Fig. 9). In fact, mid-Miocene relief is still locally present in this part of the Basin and Range: for instance, the mid-Miocene volcanic edifices south of the Warner Range are still barely eroded today (Fig. 2). Late Oligocene and early Miocene volcanic edifices produced long-lived topographic relief

as evidenced by map relationships in both the Warner Range and farther north at Drake Peak (Wells, 1980) and near the Abert Rim in Oregon (Fig. 2) (Scarberry et al., 2009) where younger volcanic units have been shown to abut or thin towards older volcanic edifices.

In the southern portion of the Warner Range, the youngest rocks exposed at the crest are 14.1 ± 0.4 Ma (Duffield and McKee, 1986). Because the SVF and the Emerson Creek faults cut these rock units, the displacement associated with these faults must be younger than 14 Ma. It is not clear how much younger, however, and the geological constraints on their inception and timing of displacement are few. In the southern Warner and the Hays Canyon ranges, numerous 14-14.5 Ma basalt dikes that appear to be feeder dikes for the overlying Mid-Miocene basalt flows trend N10-35°W, averaging N25°W (Duffield and McKee, 1986). Several segments of the SVF roughly parallel the dike orientations (Plate I), perhaps indicating that the fault initiated in the same stress regime and at about the same time. The Emerson Creek faults like initiated at the same time, possibly acting as splay faults of the SVF near its southern termination (e.g. Anders and Schlische, 1994); eventually, however, motion on these splay faults ceased and the SVF became a single, dominant fault. In the northern Warner Range, in contrast to the southern portion, rhyolite domes as young as 7.3 ± 0.3 Ma (Duffield and McKee, 1986) cap the range. Late Miocene volcanic rocks occur on both sides of the SVF at this latitude (Plate I), but it has not proven possible to definitively tie a particular unit across the fault.

These geologic relationships suggest three possibilities for initiation of extensional faulting in the region: (1) motion along the entire Surprise Valley fault (and Emerson Creek faults) initiated at or shortly after 14 Ma and younger volcanic units in the northern part of the range were erupted at a later time on both sides of the SVF, (2) motion along the SVF initiated only after 7 Ma, or (3) motion along the SVF initiated in the south shortly after 14 Ma and migrated northward over the next 5-10 my, a phenomenon observed along the Abert Rim in Oregon (Scarberry et al., 2009). The existing thermochronology, though minimal, indicates that some exhumation or

cooling may have occurred between 14 and 8 Ma, which suggests that the Surprise Valley fault initiated during that time frame and that (2) is therefore not likely. It is not possible to distinguish between (1) and (3) with our existing mapping, geo- and thermo-chronology, but based on the presence of late Miocene rocks in the north (but not in the south), we suggest that motion along the SVF began in the south around 14 Ma and propagated northward, reaching the northern Warner Range after ~7 Ma.

*Late Miocene to Pliocene extension*

By 4 Ma, there was enough relief generated by slip on both the Warner and Hays Canyon range-bounding faults that basalt flows flowing down the Surprise Valley banked unconformably into Oligocene and mid-Miocene volcanic rocks along the valley margins. On the western flank of the Warner Range, a basalt flow dated at 2.76 ± 0.20 Ma (Carmichael et al., 2006) covers a pre-existing normal fault, which may have also controlled the vent location for these flows (Plate I). These late Miocene and Pliocene basalt flows that range in age from ~8-3 Ma (Carmichael et al., 2006) are clearly cut by normal faults on both the west and east side of the Warner Range (Fig. 9, Plate I), indicating a second episode of extension and uplift after the deposition of these units. The dip direction of these faults, as well as the amount of offset and tilt they accommodate varies considerably along the length of the range, creating several tilt domains, shown schematically in Figure 3. On the eastern margin of the Upper Lake basin (Fig. 3), offset along east-dipping normal faults reaches several hundred meters, and fault-bound blocks are tilted and rotated up to 15° to the west (Fig. 9a, Plate I). The faults die out and dips on the flows flatten to the north (Fig. 3, Plate I). Within a given tilt domain, all basalt flows share similar dips, regardless of age, suggesting that faulting and tilting began after ~3 Ma.

These faults are most numerous and have the greatest offset just north of the road between Cedarville and Vya (Fig. 3, Plate I), where several conjugate (west-dipping) faults have also developed, resulting in a series of interfingering horsts and grabens. This zone of more intense faulting likely represents a transverse antithetic accommodation zone (Fig. 3), as defined by Faulds and Varga (1998), which

accommodates the transition from a half-graben in the upper lake basin (Fig. 9a) to a full graben in the middle and lower lake basins (Fig. 9b, c).

This younger episode of extension continues to the present, although the SVF has not been seismically active in historical times and even small earthquakes are relatively infrequent in this region compared with the rest of northern California (Uhrhammer, 1991) (Figs. 1,2). Potential for major (> magnitude 6) earthquakes is significant, however. A recent paleoseismology study of the Surprise Valley fault revealed evidence for 5 surface-rupturing earthquakes in the last 18 ka, the most recent of which occurred 1.2 ± 0.1 ka (Personius et al., 2009). A geodetic survey across the northern and western Basin and Range calculated an E-W extension rate of 1.6 ± 0.3 mm/yr across the SVF based on measurements of the differential horizontal velocity between two stations, one near the crest of the Warner Range (CEDR) and another on the east side of the valley (ALKA) (Fig. 3) (Hammond and Thatcher, 2007), although the authors have recently revised their estimate of extension rate down to 1.0 mm/yr (W. Thatcher, written communication, 2009).

As a result of extension and uplift since the mid-Miocene, rock units near the crest of the Warner Range that we infer were subhorizontal prior to slip on the Surprise Valley fault now dip as much as 20-25° to the west and flatten to horizontal westward over a distance of about 10 km (Plate I, Fig. 9c). Footwall flexure is an expected result of footwall unloading and isostatic compensation produced by motion along steeply dipping normal faults (Buck, 2007 and references therein; Thompson and Parsons, 2009). In the case of the Surprise Valley fault, the imaged Moho shows no evidence for rise or truncation related to the Surprise Valley fault at depth (Fig. 2) (Lerch et al., 2007). Because of the lack of Moho offset or pull-up, it is reasonable to conclude that the tilting and flexure seen in the upper crust are accommodated in the mid- to lower crust by flow. Mid- and lower-crustal flow has been well-documented in the Basin and Range, where the Moho remains flat despite variable upper crustal extension (Gans, 1987; Klemperer et al., 1986). Heat flow in the region, as measured in numerous wells (Raines et al., 1996), reaches 90-100 $mW/m^2$, higher even than the average for the

Basin and Range (Blackwell et al., 1991). Surface heat flow of this magnitude suggests a geothermal gradient as high as 40-45° C/km, and thus a local brittle-ductile transition zone (assumed to occur at 350° C) at less than 8 km depth, facilitating the accommodation of flexure by flow in the mid-crust (e.g. Lerch et al., 2009).

*Magnitude of extension*

Utilizing the top of Tovu as a marker and the minimum depth to bedrock in Surprise Valley based on a drill hole log (Plate I), we calculate a minimum of 8 km of dip-slip motion along the Surprise Valley fault near Warren Peak at cross-section D-D', resulting in a stratigraphic throw of ~4.5 km (vertical component of dip-slip motion) and a horizontal component of slip of ~6.5 km as measured with respect to the present-day fault angle (Fig. 9c). Comparison of the distance between the eastern and western extents of cross-section D-D' before and after restoration yields a total horizontal extension of 7.3 km across a distance of 50 km (~15% strain) since the mid-Miocene (Fig. 9c). A similar restoration of cross-section C-C' yields a total horizontal extension of 6.1 km over ~51 km (~12% strain) across the same region since the mid-Miocene (Fig. 9b). The lack of units that can tied across the fault further north precludes our ability to restore cross-section B-B'.

## DISCUSSION

*Magmatic history and its implications*

From the late Eocene to the mid-Miocene, the Warner Range region was a site of arc volcanism, along with the western Cascades (du Bray et al., 2006). In the Oligocene (28-24 Ma) in particular, volcanoes within the active arc were located at the site of the modern Warner Range (Fig. 10), where volcanic centers have the geomorphic expression of arc-related volcanoes, share geochemical features with contemporaneous volcanism in the western Cascades, and are in the geographic position behind the subduction zone at the time. Oligocene volcanic centers are also present near the modern Cascades, approximately 150 km to the west, indicating either that the arc was very wide at the time or that it has been subsequently extended (Fig. 10). A velocity profile of the crust beneath the Modoc Plateau more closely resembles velocities seen

beneath the Sierra Nevada than velocities in rifts such as the Salton Trough (Fuis et al., 1987), and thus significant extension in this area is unlikely. Modern volcanic arcs with widths >100 km are not common, but the Kurile-Kamchatka arc is one example (Volynets, 1994).

The arc volcanism that occurred in the Warner Range in the Oligocene was the result of subduction of the Juan de Fuca plate, distinguishing this northwestern corner of the Basin and Range from the rest of the province further east and south, which experienced magmatism that swept southward through time (Fig. 10) (Armstrong and Ward, 1991; Christiansen and Yeats, 1992). This regional pattern of magmatism is believed to have developed as the consequence of the peeling away of the shallow Laramide slab (Humphreys, 1995). Thus, the Warner Range region can be considered part of the "ancestral" Cascades. While the presence of an Oligocene ancestral arc farther south has been both supported (e.g. Busby et al., 2008; Cousens et al., 2008) and dismissed (e.g. Glazner and Farmer, 2008), the case is clearer at the latitude of the Warner Range. In addition, subduction-related arc volcanism not only began here as early as in the western Cascades, but it continued sporadically in the Warner region through the mid-Miocene, becoming more mafic and generating smaller eruptive centers than during the earlier, Oligocene episode. This continued arc magmatism contrasts with the widespread flood basalts of similar age that blanketed the region further north and east (e.g. Hooper et al., 2002) (Fig. 1).

*Extensional faulting history in the context of Basin and Range evolution*

When extension began in the mid-Miocene, the Surprise Valley fault moved in isolation from other major Basin and Range faults, which currently lie nearly 100 km away in the extension direction across the Sheldon Plateau (Fig. 2). Why might extension have localized here, while the typical spacing of Basin and Range normal faults is closer to 20-30 km across the rest of the province (Stewart, 1971)? Temperature, composition, magmatism, and pre-existing crustal weaknesses are all factors that can cause localization of extensional strain (e.g. Buck, 2007). One possibility is that Yellowstone hot spot volcanism, which began in the region 16-17

Ma (prior to extension) resulted in strengthening of the crust through the addition of mafic material to the lower crust, if boundary conditions that would allow extension weren't present at that time. The spatial distribution of the oldest Yellowstone-related calderas seems to correlate geographically with the region currently lacking normal faults (Fig. 2) (Coble and Mahood, 2008) and may help explain the wider-than-average spacing of normal faults in this region. Once the Surprise Valley fault was established, additional strain would have preferentially been accommodated along this existing structure, resulting in the accumulation of a minimum of 8 km of dip-slip—an amount comparable to some of the largest faults in the Basin and Range like the Schell Creek fault (Gans and Miller, 1983) and the White Mountain fault zone (Stockli et al., 2003).

The Warner Range and surrounding region has experienced only limited, 12-15% extension since the mid-Miocene. The sequence of events by which this may have occurred and their relationship to the region's magmatic history is represented schematically in Figure 11. Rejuvenated arc-related magmatism erupted from basaltic volcanoes in the middle Miocene, primarily 16-14 Ma (Fig. 11a), filling pre-existing, erosional topography with up to 1 km of basalts, basaltic andesites, and mafic tuffs. Arc-related volcanism ceased and horst-and-graben-style normal faulting began sometime after 14, propagating northward after 7 Ma and resulting in a limited amount of extension, perhaps 3-5% (approximately 1/3$^{rd}$ of the total extension to correlate with thermochronologic modeling that suggests that 1/3$^{rd}$ of the exhumation occurred between about 14 and 8 Ma) (Fig. 11b). Mafic volcanism resumed ~8 Ma; these melts may have been channeled through fractures and crustal weaknesses, as they reached the surface from a hot, shallow aesthenospheric mantle source and show very little crustal contamination (Fig. 11c) (Carmichael et al., 2006; McKee et al., 1983). The addition of these melts to the base of the crust was likely accompanied by a temperature increase in the crust that would have raised the brittle-ductile transition zone (Fig. 11c). When extension began again ~3 Ma, renewed slip along the Surprise Valley fault resulted in footwall flexure that was accommodated by flow in the mid-

crust (Fig. 11d). This second episode of extension and slip on the fault resulted in most of the uplift, tilting, and exhumation of the Warner Range.

A protracted or two-part history of extension, such as that seen in the Warner Range, has been noted elsewhere in the western Basin and Range. Faulting began ~12 Ma in the Black Rock Range (Lerch et al., 2008) and Pine Forest Range (Fig. 2) (Colgan et al., 2006), as well as in the Verdi-Boca basin near Reno (Fig. 1) (Henry and Perkins, 2001). Somewhat earlier extension is documented in the Shawave Range (Fig. 2), where apatite fission track ages across the exhumed Shawave pluton suggest an episode of exhumation that lasted from 14.5 ± 1.4 Ma until 12.9 ± 0.7 Ma (Whitehill, 2009). The timing of earlier fault slip and extension in the Warner Range is not well constrained, but one possibility is that the Shawave and Warner ranges represented the western boundary of extension ca. 14 Ma. While extension subsequently migrated westward at the latitude of the Shawave Range—possibly due to the northwestward propagation of dextral shear in the Walker Lane (e.g. Faulds et al., 2005)—the boundary of significant extension at the latitude of the Warner Range has remained where it was in the Miocene.

The second phase of extension in the Warner Range, beginning ~3 Ma, appears to be a widespread phenomenon along the western margin of the Basin and Range, and possibly in the interior of the province as well. The 3 Ma extensional episode is coeval with rejuvenation of extension in the Carson Range (Surpless et al., 2002), Wassuk Range (Stockli et al., 2002), and the Verdi-Boca basin (Henry and Perkins, 2001; Mass et al., 2009) (Fig. 1). Extension may have continued to 3 Ma or less in the Black Rock Range (Lerch et al., 2008) and Pine Forest Range (Colgan et al., 2006) (see Fig. 2 for locations), but is lesser in magnitude than the extension that has been documented along much of today's western boundary of the province. Mass et al. (2009) suggest that this young episode of extension may be a consequence of accelerated rollback of the Juan de Fuca slab, but the ranges affected by young faulting extend south beyond the projected southern limit of the Juan de Fuca plate at ~3 Ma (Fig. 1), thus suggesting a different driving mechanism.

## CONCLUSIONS

The Warner Range and surrounding region provide key insight into the development of the northwestern margin of the Basin and Range. The long history of subduction-related arc volcanism recorded in the >4 km thick succession of volcaniclastic sediments and volcanic rocks represents a unique exposure at this latitude and marks the easternmost extent of and the return to normal subduction following the Laramide flat-slab subduction of the early Tertiary. In addition, arc-related magmatism continued in region into the mid-Miocene, despite the nearby impingement of the Yellowstone hotspot and voluminous eruptions of continental flood basalts that blanketed much of the surrounding region.

The extensional history of the Surprise Valley fault shares some similarities with other portions of the western margin of the Basin and Range, despite its unique tectonic setting. Cross-cutting relationships seen in the Warner Range region suggest two episodes of extension—the first in the mid- to late-Miocene, the second starting after ~3 Ma—that appear to be widespread events, though the timing of these two events still needs to be better constrained. In contrast to much of the Basin and Range, however, the Surprise Valley fault has been relatively isolated throughout its existence, perhaps due to its location immediately west of a series of hotspot-related silicic calderas.

Although the total amount of extension from the Modoc Plateau into north central Nevada may be as little as 5% since the middle Miocene (e.g. Wells and Heller, 1988), the majority of that extension was accommodated along the Surprise Valley fault, resulting locally in ~15% extension. While this is relatively minor, the Warner Range and Surprise Valley fault appears to have persisted as the westernmost boundary of Basin and Range extension since its initiation in the mid- to late Miocene. In contrast, extension has stepped westward over the past 15 Ma further south (e.g. Surpless et al., 2002). Today, the Surprise Valley fault remains the actively deforming western boundary of the Basin and Range.

## References

Anders, M.H., and Schlische, R.W., 1994, Overlapping faults, intrabasin highs, and the growth of normal faults: Journal of Geology, v. 102, p. 165-180.

Armstrong, R.L., and Ward, P.L., 1991, Evolving geographic patterns of Cenozoic magmatism in the North American Cordillera; the temporal and spatial association of magmatism and metamorphic core complexes: Journal of Geophysical Research, v. 96, p. 13,201-13,224.

Athens, N., Fontiveros, V.C., Glen, J.M.G., Klemperer, S., Egger, A.E., and Morin, R.L., 2009, Potential-field modeling and high-resolution seismic imaging to characterize subsurface structure in Surprise Valley, California: EOS Transactions, v. 90, p. Abstract T21D-1846.

Atwater, T., and Stock, J., 1998, Pacific-North America plate tectonics of the Neogene southwestern United States; an update: International Geology Review, v. 40, p. 375-402.

Axelrod, D.I., 1966, Potassium-argon ages of some western Tertiary floras: American Journal of Science, v. 264, p. 497-506.

Bennett, R.A., Wernicke, B., Niemi, N.A., Friedrich, A.M., and Davis, J.L., 2003, Contemporary strain rates in the northern Basin and Range province from GPS data: Tectonics, v. 22, p. 1008-1038.

Benoit, D., Moore, J., Goranson, C., and Blackwell, D.D., 2005, Core Hole Drilling and Testing at the Lake City, California geothermal field: Geothermal Resources Council Transactions, v. 29, p. 203-208.

Blackwell, D.D., Steele, J.L., and Carter, L.S., 1991, Heat-flow patterns of the North American continent; a discussion of the geothermal map of North America: Boulder, CO, Geol. Soc. Am., p. 423-436.

Brueseke, M.E., Heizler, M.T., Hart, W.K., and Mertzman, S.A., 2007, Distribution and geochronology of Oregon Plateau (U.S.A.) flood basalt volcanism: The Steens Basalt revisited: Journal of Volcanology and Geothermal Research, v. 161, p. 187-214.

Bryant, W.A., 1990, Surprise Valley and related faults, Lassen and Modoc counties, *in* CDMG Fault Evaluation Report, Volume 217: Sacramento, 17 p.

Buck, W.R., 2007, Dynamic Processes in Extensional and Compressional Settings: The Dynamics of Continental Breakup and Extension, *in* Schubert, G., ed., Treatise on Geophysics: Amsterdam, Elsevier, p. 335-376.

Busby, C.J., Hagan, J.C., Putirka, K., Pluhar, C.J., Gans, P.B., Wagner, D.L., Rood, D., DeOreo, S.B., and Skilling, I., 2008, The ancestral Cascades Arc; Cenozoic evolution of the central Sierra Nevada (California) and the birth of the new plate boundary: Special Paper - Geological Society of America, v. 438, p. 331-378.

Camp, V.E., Ross, M.E., and Hanson, W.E., 2003, Genesis of flood basalts and Basin and Range volcanic rocks from Steens Mountain to the Malheur River Gorge, Oregon: Geological Society of America Bulletin, v. 115, p. 105-128.

Carmichael, I.S.E., Lange, R.A., Hall, C.M., and Renne, P.R., 2006, Faulted and tilted Pliocene olivine-tholeiite lavas near Alturas, NE California, and their bearing on the uplift of the Warner Range: Geological Society of America Bulletin, v. 118, p. 1196-1211.

Cashman, P.H., Trexler, J.H., Muntean, T.W., Faulds, J.E., Louie, J.N., and Oppliger, G.L., 2009, Neogene tectonic evolution of the Sierra Nevada-Basin and Range transition zone at the latitude of Carson City, Nevada: Special Paper - Geological Society of America, v. 447, p. 171-188.

Christiansen, R.L., and Yeats, R.S., 1992, Post-Laramide geology of the U.S. Cordilleran region, *in* Burchfiel, B.C., Lipman, P.W., and Zoback, M.L., eds., The Cordilleran Orogen—Conterminous U.S., Volume G-3: Decade of North America Geology: Boulder, CO, Geological Society of America, p. 261-406.

Coble, M.A., and Mahood, G.A., 2008, New geologic evidence for additional 16.5-15.5 Ma silicic calderas in northwest Nevada related to initial impingement of the Yellowstone hot spot: IOP Conference Series: Earth and Environmental Science, v. 3, p. 012002.

Colgan, J.P., Dumitru, T.A., McWilliams, M., and Miller, E.L., 2006, Timing of Cenozoic volcanism and Basin and Range extension in northwestern Nevada: New constraints from the northern Pine Forest Range: Geological Society of America Bulletin, v. 118, p. 126-139.

Colgan, J.P., Shuster, D.L., and Reiners, P.W., 2008, Two-phase Neogene extension in the northwestern Basin and Range recorded in a single thermochronology sample: Geology, v. 36, p. 631-634.

Cousens, B., Prytulak, J., Henry, C., Alcazar, A., and Brownrigg, T., 2008, Geology, geochronology, and geochemistry of the Miocene-Pliocene Ancestral Cascades arc, northern Sierra Nevada, California and Nevada: The roles of the upper mantle, subducting slab, and the Sierra Nevada lithosphere: Geosphere, v. 4, p. 829-853.

du Bray, E.A., John, D.A., Putirka, K., and Cousens, B.L., 2009, Geochemical database for igneous rocks of the ancestral Cascades Arc; southern segment, California and Nevada: U. S. Geological Survey Data Series DS-0439.

du Bray, E.A., John, D.A., Sherrod, D.R., Evarts, R.C., Conrey, R.M., and Lexa, J., 2006, Geochemical database for volcanic rocks of the western Cascades, Washington, Oregon, and California: U. S. Geological Survey Data Series DS-0155, 49 p.

Duffield, W.A., and McKee, E.H., 1986, Geochronology, structure, and basin-range tectonism of the Warner Range, northeastern California: Geological Society of America Bulletin, v. 97, p. 142-146.

Duffield, W.A., Weldin, R.D., and Davis, W.E., 1976, Mineral resources of the South Warner Wilderness, Modoc County, California: U. S. Geological Survey Bulletin, v. B1385, 31 p.

Egger, A.E., Colgan, J.P., and York, C., 2009a, Provenance and palaeogeographic implications of Eocene-Oligocene sedimentary rocks in the northwestern Basin and Range: International Geology Review, v. 51, p. 900-919.

Egger, A.E., Glen, J.M.G., and Ponce, D.A., 2009b, The northwestern margin of the Basin and Range province: Part 2: Structural setting of a developing basin from seismic and potential field data: Tectonophysics, In Press, Corrected Proof.

Faulds, J.E., Henry, C.D., Hinz, N.H., Hammond, W.C., Kreemer, C., and Blewitt, G., 2005, Kinematics of the northern Walker Lane: An incipient transform fault along the Pacific-North American plate boundary: Geology, v. 33, p. 505-508.

Faulds, J.E., and Varga, R.J., 1998, The role of accommodation zones and transfer zones in the regional segmentation of extended terranes, Special Paper - Geological Society of America, v. 323, p. 1-45.

Ferrill, D.A., Stamatakos, J.A., and Sims, D., 1999, Normal fault corrugation: implications for growth and seismicity of active normal faults: Journal of Structural Geology, v. 21, p. 1027-1038.

Ford, R.S., Soderstrand, J.N., Franson, R.E., Beach, F.H., Feingold, S.A., Hail, W.R., Iwamura, T.I., and Swanson, A.A., 1963, Northeastern counties ground-water investigation: Calif. Department of Water Resources Bulletin, v. 98, 224 p.

Friedrich, A.M., Lee, J., Wernicke, B.P., and Sieh, K., 2004, Geologic context of geodetic data across a Basin and Range normal fault, Crescent Valley, Nevada: Tectonics, v. 23, 24 p.

Fritz, W.J., and Harrison, S., 1985, Transported trees from the 1982 Mount St. Helens sediment flows: Their use as paleocurrent indicators: Sedimentary Geology, v. 42, p. 49-64.

Fuis, G.S., Zucca, J.J., Mooney, W.D., and Milkereit, B., 1987, A geologic interpretation of seismic-refraction results in northeastern California: Geological Society of America Bulletin, v. 98, p. 53-65.

Gans, P.B., 1987, An open-system, two-layer crustal stretching model for the eastern Great Basin: Tectonics, v. 6, p. 1-12.

Gans, P.B., and Miller, E.L., 1983, Field trip 6; Style of mid-Tertiary extension in east-central Nevada: Special Studies - Utah Geological and Mineral Survey, v. 59, p. 107-160.

Gashawbeza, E.M., Klemperer, S.L., Wilson, C.K., and Miller, E.L., 2008, Nature of the crust beneath northwest Basin and Range province from teleseismic receiver function data: Journal of Geophysical Research, v. 113, 14 p.

Glazner, A.F., and Farmer, G.L., 2008, Ancestral Cascades = modern Cascades: Abstracts with Programs - Geological Society of America, v. 40, p. 98.

Greene, R.C., 1984, Geologic appraisal of the Charles Sheldon Wilderness Study Area, Nevada and Oregon: U. S. Geological Survey Bulletin, p. 13-34.

Hammond, W.C., and Thatcher, W., 2004, Contemporary tectonic deformation of the Basin and Range Province, Western United States; 10 years of observation with the Global Positioning System: Journal of Geophysical Research, v. 109, p. 403-423.

—, 2005, Northwest Basin and Range tectonic deformation observed with the Global Positioning System, 1999-2003: Journal of Geophysical Research, v. 110, p. 405-416.

—, 2007, Crustal deformation across the Sierra Nevada, northern Walker Lane, Basin and Range transition, western United States measured with GPS, 2000–2004: Journal of Geophysical Research, v. 112, 26 p.

Hedel, C.W., 1980, Late Quaternary faulting in western Surprise Valley, Modoc County, California [Master's thesis]: San Jose, CA, San Jose State University.

—, 1981, Map showing geothermal resources of the Lake City-Surprise Valley known geothermal resource area, Modoc County, California: Miscellaneous Field Studies Map, MF-1299.

—, 1984, Maps showing geomorphic and geologic evidence for late Quaternary displacement along the Surprise Valley and associated faults, Modoc County, California: Miscellaneous Field Studies Map, MF-1429.

Henry, C.D., Faulds, J.E., and dePolo, C.M., 2007, Geometry and timing of strike-slip and normal faults in the northern Walker Lane, northwestern Nevada and northeastern California; strain partitioning or sequential extensional and strike-

slip deformation?: Special Paper - Geological Society of America, v. 434, p. 59-79.

Henry, C.D., and Perkins, M.E., 2001, Sierra Nevada-Basin and Range transition near Reno, Nevada: Two-stage development at 12 and 3 Ma: Geology, v. 29, p. 719-722.

Hildreth, W., 2007, Quaternary magmatism in the Cascades; geologic perspectives: U. S. Geological Survey Professional Paper, v. P 1744, 125 p.

Hooper, P.R., 2000, Chemical discrimination of Columbia River basalt flows: Geochemistry, Geophysics, Geosystems, v. 1, 16 p.

Hooper, P.R., Binger, G.B., and Lees, K.R., 2002, Ages of the Steens and Columbia River flood basalts and their relationship to extension-related calc-alkalic volcanism in eastern Oregon: Geological Society of America Bulletin, v. 114, p. 43-50.

Humphreys, E.D., 1995, Post-Laramide removal of the Farallon slab, western United States: Geology, v. 23, p. 987-990.

Johnson, J.A., Hawkesworth, C.J., Hooper, P.R., and Ben Binger, G., 1998, Major- and trace-element analyses of Steens Basalt, southeastern Oregon: Open-File Report - U. S. Geological Survey, v. OF 98-0482, 30 p.

Jordan, B.T., Grunder, A.L., Duncan, R.A., and Deino, A.L., 2004, Geochronology of age-progressive volcanism of the Oregon High Lava Plains: Implications for the plume interpretation of Yellowstone: Journal of Geophysical Research, v. 109, p. 19.

Keats, D.G., 1985, Geology and Mineralization of the high Grade District, Modoc County, California [MS thesis]: Corvallis, OR, Oregon State University.

Klemperer, S.L., Hauge, T.A., Hauser, E.C., Oliver, J.E., and Potter, C.J., 1986, The Moho in the northern Basin and Range province, Nevada, along the COCORP 40° N seismic-reflection transect: Geological Society of America Bulletin, v. 97, p. 603-618.

Le Bas, M.J., Le Maitre, R.W., Streckeisen, A., and Zanettin, B.A., 1986, Chemical classification of volcanic rocks based on the total alkali-silica diagram: Journal of Petrology, v. 27, p. 745-750.

Lerch, D.W., Klemperer, S.L., Egger, A.E., Colgan, J.P., and Miller, E.L., 2009, The northwestern margin of the Basin-and-Range Province, part 1: Reflection profiling of the moderate-angle (~30°) Surprise Valley Fault: Tectonophysics, In Press, Corrected Proof.

Lerch, D.W., Klemperer, S.L., Glen, J.M.G., Ponce, D.A., Miller, E., and Colgan, J., 2007, Crustal structure of the northwestern Basin and Range Province and its transition to unextended volcanic plateaus: Geochemistry Geophysics Geosystems, v. 8, p. 1-21.

Lerch, D.W., Miller, E., McWilliams, M., and Colgan, J., 2008, Tectonic and magmatic evolution of the northwestern Basin and Range and its transition to unextended volcanic plateaus: Black Rock Range, Nevada: Geological Society of America Bulletin, v. 120, p. 300-311.

MacGinitie, H.D., 1941, A middle Eocene flora from the central Sierra Nevada: Carnegie Institution of Washington Publication, p. 178.

Martz, P.W., 1970, The geology of a portion of the northern Warner mountains, Modoc County, California [MS thesis]: Davis, CA, University of California at Davis.

Mass, K.B., Cashman, P.H., and Trexler, J.H., 2009, Stratigraphy and structure of the Neogene Boca Basin, northeastern California; implications for late Cenozoic tectonic evolution of the northern Sierra Nevada: Special Paper - Geological Society of America, v. 447, p. 147-170.

McKee, E.H., Duffield, W.A., and Stern, R.J., 1983, Late Miocene and early Pliocene basaltic rocks and their implications for crustal structure, northeastern California and South-central Oregon: GSA Bulletin, v. 94, p. 292-304.

McPhee, D.K., Glen, J.M.G., Egger, A.E., and Chuchel, B.A., 2009, Geophysical Investigation of the Lake City Fault Zone, Surprise Valley, California, and Implications for Geothermal Circulation EOS Transactions, v. 90, p. Abstract H53F-1005.

Myers, J.A., 1998, Paleovegetational heterogeneity and the record of Eocene-Oligocene climate change in the interior Pacific Northwest [PhD thesis]: Santa Barbara, CA, University of California at Santa Barbara.

—, 2003, Terrestrial Eocene-Oligocene vegetation and climate in the Pacific Northwest: New York, NY, Columbia University Press, p. 171-185.

—, 2006, The latest Eocene Badger's Nose flora of the Warner Mountains northeast California; the "in between" flora: PaleoBios, v. 26, p. 11-29.

Oldow, J.S., 2003, Active transtensional boundary zone between the western Great Basin and Sierra Nevada block, western U.S. Cordillera: Geology, v. 31, p. 1033-1036.

Peacock, D.C.P., 2002, Propagation, interaction and linkage in normal fault systems: Earth-Science Reviews, v. 58, p. 121-142.

Personius, S.F., Crone, A.J., Machette, M.N., Mahan, S.A., and Lidke, D.J., 2009, Moderate rates of late Quaternary slip along the northwestern margin of the Basin and Range Province, Surprise Valley fault, northeastern California: Journal of Geophysical Research, v. 114, 17 p.

Pierce, K.L., and Morgan, L.A., 1992, The track of the Yellowstone hot spot; volcanism, faulting, and uplift: Memoir - Geological Society of America, v. 179, p. 1-53.

Proffett, J.M., and Dilles, J.H., 1984, Geologic map of the Yerington District, Nevada, Volume 77: Reno, NV, Nevada Bureau of Mines and Geology.

Raines, G.L., Sawatsky, D.L., and Connors, K.A., 1996, Great Basin Geoscience Database, Volume DDS-41, U.S. Geological Survey.

Reed, J.C., Wheeler, J.O., and Tucholke, B.E., 2005, Geologic Map of North America, Continent-Scale Map-001: Boulder, CO, Geological Society of America.

Russell, R.J., 1928, Basin Range structure and stratigraphy of the Warner Range, northeastern California: University of California Publications in Geological Sciences, v. 17, p. 387-496.

Scarberry, K.C., Meigs, A.J., and Grunder, A.L., 2009, Faulting in a propagating continental rift: Insight from the late Miocene structural development of the Abert Rim fault, southern Oregon, USA: Tectonophysics, In Press, Corrected Proof.

Stewart, J.H., 1971, Basin and Range Structure: A System of Horsts and Grabens Produced by Deep-Seated Extension: Geological Society of America Bulletin, v. 82, p. 1019-1044.

Stilson, T., Garcia del Real, P., Munoz, C., Egger, A.E., Glen, J.M., Aaron, S., Athens, N., Bouligand, C., Dudley, J., Fontiveros, V., Pope, E.C., and Stafford, S.N., 2008, The faults and hot springs of Surprise Valley; perspectives from detailed gravity and magnetic data: Eos, Transactions, American Geophysical Union, v. 89, p. T21B-1969.

Stockli, D.F., Dumitru, T.A., McWilliams, M.O., and Farley, K.A., 2003, Cenozoic tectonic evolution of the White Mountains, California and Nevada: Geological Society of America Bulletin, v. 115, p. 788-816.

Stockli, D.F., Surpless, B.E., Dumitru, T.A., and Farley, K.A., 2002, Thermochronological constraints on the timing and magnitude of Miocene and Pliocene extension in the central Wassuk Range, western Nevada: Tectonics, v. 21, p. 10-28.

Surpless, B., 2008, Modern strain localization in the central Walker Lane, Western United States; implications for the evolution of intraplate deformation in transtensional settings: Tectonophysics, v. 457, p. 239-253.

Surpless, B., Stockli, D.F., Dumitru, T.A., and Miller, E.L., 2002, Two-phase westward encroachment of Basin and Range extension into the northern Sierra Nevada: Tectonics, v. 21, p. 1002-1014.

Thatcher, W., Foulger, G.R., Julian, B.R., Svarc, J., Quilty, E., and Bawden, G.W., 1999, Present-Day Deformation Across the Basin and Range Province, Western United States: Science, v. 283, p. 1714-1718.

Thompson, G.A., and Parsons, T., 2009, Can footwall unloading explain late Cenozoic uplift of the Sierra Nevada crest?: International Geology Review, v. 51, p. 986-993.

Trexler, J.H., Cashman, P.H., Muntean, T., Schwartz, K., Ten Brink, A., Faulds, J.E., Perkins, M., and Kelly, T., 2000, Neogene basins in western Nevada document the tectonic history of the Sierra Nevada-Basin and Range transition zone for the last 12 Ma: GSA Field Guide, v. 2, p. 97-116.

Twiss, R.J., and Moores, E.M., 1992, Structural geology: New York, NY, W.H. Freeman and Company, 532 p.

U.S. Geological Survey, 1981, Total field aeromagnetic anomaly map, Surprise valley known geothermal resource area, California, U.S. Geological Survey Open-File Report, Volume 81-0997.

Uhrhammer, R.A., 1991, Northern California seismicity, *in* Slemmons, D.B., Engdahl, E.R., Zoback, M.D., and Blackwell, D.D., eds., Neotectonics of North America, Volume 1: Decade of North American Geology: Boulder, CO, Geological Society of America, p. 99-106.

Unruh, J., Humphrey, J., and Barron, A., 2003, Transtensional model for the Sierra Nevada frontal fault system, eastern California: Geology, v. 31, p. 327-330.

Van Buer, N.J., Miller, E.L., and Dumitru, T.A., 2009, Early Tertiary paleogeologic map of the northern Sierra Nevada batholith and the northwestern Basin and Range: Geology, v. 37, p. 371-374.

Volynets, O.N., 1994, Geochemical types, petrology, and genesis of late Cenozoic volcanic rocks from the Kurile-Kamchatka island-arc system: International Geology Review, v. 36, p. 373-405.

Wells, R.E., 1980, Drake Peak; a structurally complex rhyolite center in southeastern Oregon: U. S. Geological Survey Professional Paper, v. 1124-E, p. E1-E16.

Wells, R.E., and Heller, P.L., 1988, The relative contribution of accretion, shear, and extension to Cenozoic tectonic rotation in the Pacific Northwest: Geological Society of America Bulletin, v. 100, p. 325-338.

Wesnousky, S.G., 2005, Active faulting in the Walker Lane: Tectonics, v. 24, 35 p.

White, D.E., 1955, Violent mud-volcano eruption of Lake City Hot Springs, northeastern California: Geological Society of America Bulletin, v. 66, p. 1109-1130.

Whitehill, C., 2009, Cenozoic evolution of the Shawave-Nightingale horst block, Northwestern Basin and Range, Nevada, U.S.A [PhD thesis]: Stanford, CA, Stanford University.

Zimbelman, J.R., Garry, B., and Irwin, R.P., 2008, Field investigation of pluvial features in Surprise Valley as analogs for pluvial landforms on Mars: Abstracts with Programs - Geological Society of America, v. 40, p. 294.

## Figures

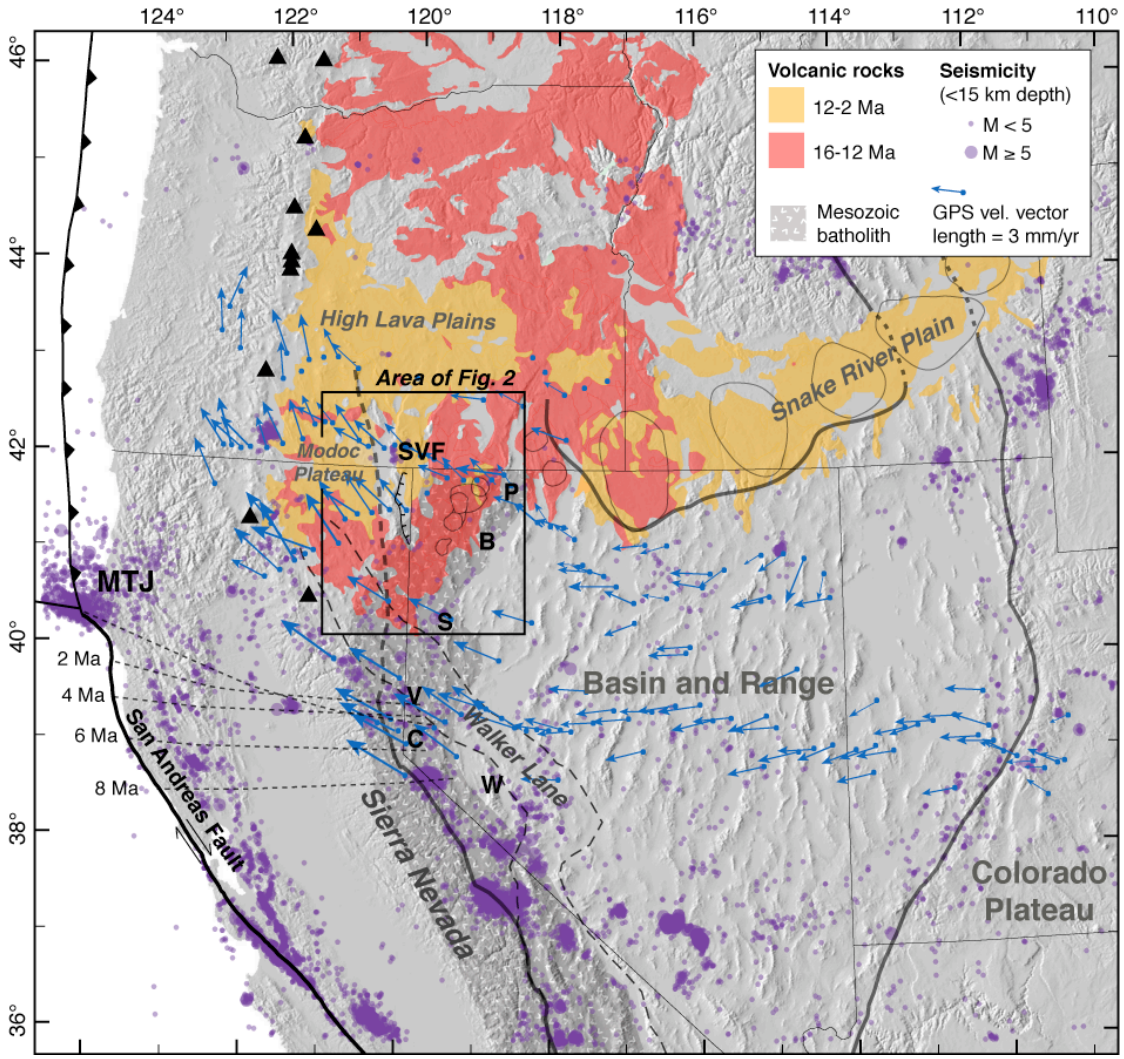


**Figure 1.** Selected tectonic features in the western U.S. and main region of Neogene volcanic rocks along the northern and western boundary of the Basin and Range province from (Reed et al., 2005). Thick gray lines show approximate boundary of the Basin and Range province. Black triangles—active volcanoes of the Cascades. Inferred Yellowstone hot spot calderas outlined with thin gray lines after Pierce and Morgan (1992) in the Snake River Plain and Coble and Mahood (2008) in northwest Nevada. Main region underlain by Mesozoic batholithic rocks after Van Buer et al. (2009). Northern Walker Lane extent after Faulds et al. (2005); southern after Wesnousky (2005). Short dashed lines—location of Mendocino edge of subducting Juan de Fuca slab over the last 8 Ma (Atwater and Stock, 1998). GPS velocity vectors from Hammond and Thatcher (2004, 2005). Earthquake data from the Northern California Earthquake Catalog and ANSS Worldwide Earthquake Catalog. Localities referred to in text: B—Black Rock Range; C—Carson Range; P—Pine Forest Range; S—Shawave Range; SVF— Surprise Valley fault; V—Verdi-Boca Basin; W—Wassuk Range.

Figure 2

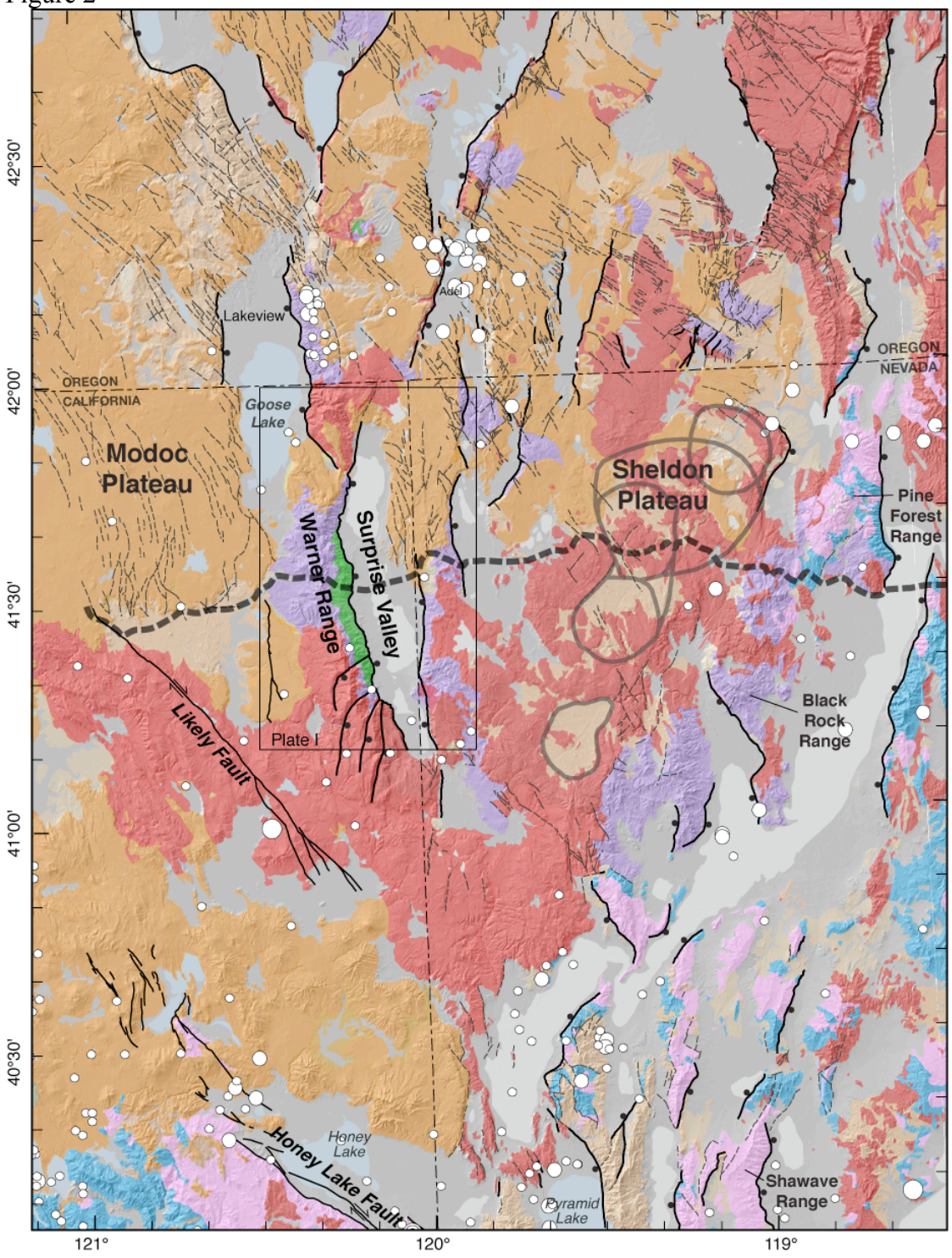
42°30'
42°00'
41°30'
41°00'
40°30'
121°
120°
119°
Lakeview
OREGON
CALIFORNIA
OREGON
NEVADA
Goose Lake
Modoc Plateau
Sheldon Plateau
Warner Range
Surprise Valley
Pine Forest Range
Black Rock Range
Likely Fault
Plate I
Honey Lake
Honey Lake Fault
Pyramid Lake
Shawave Range

(a)

Figure 2 (cont.)

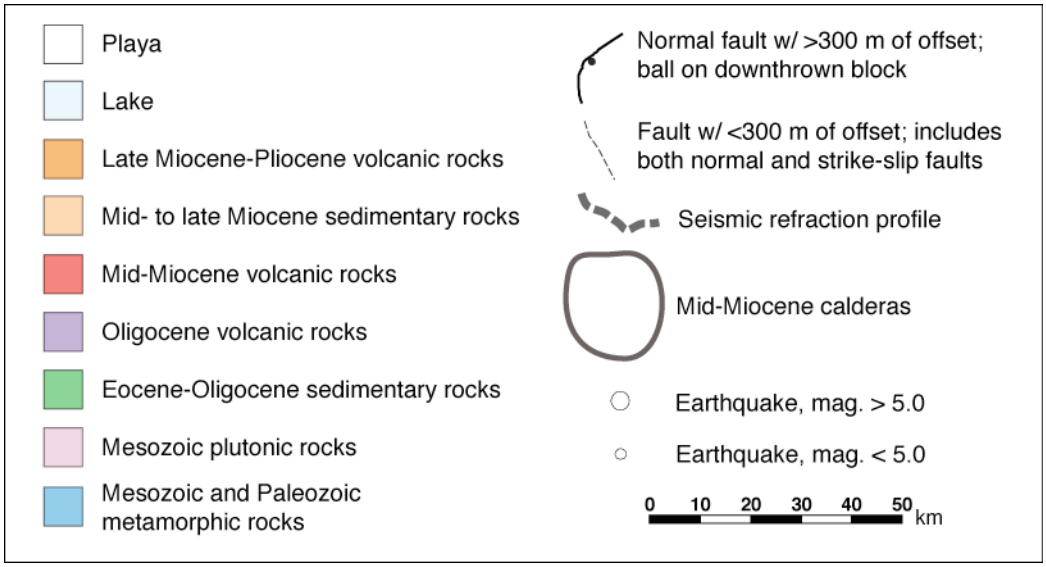


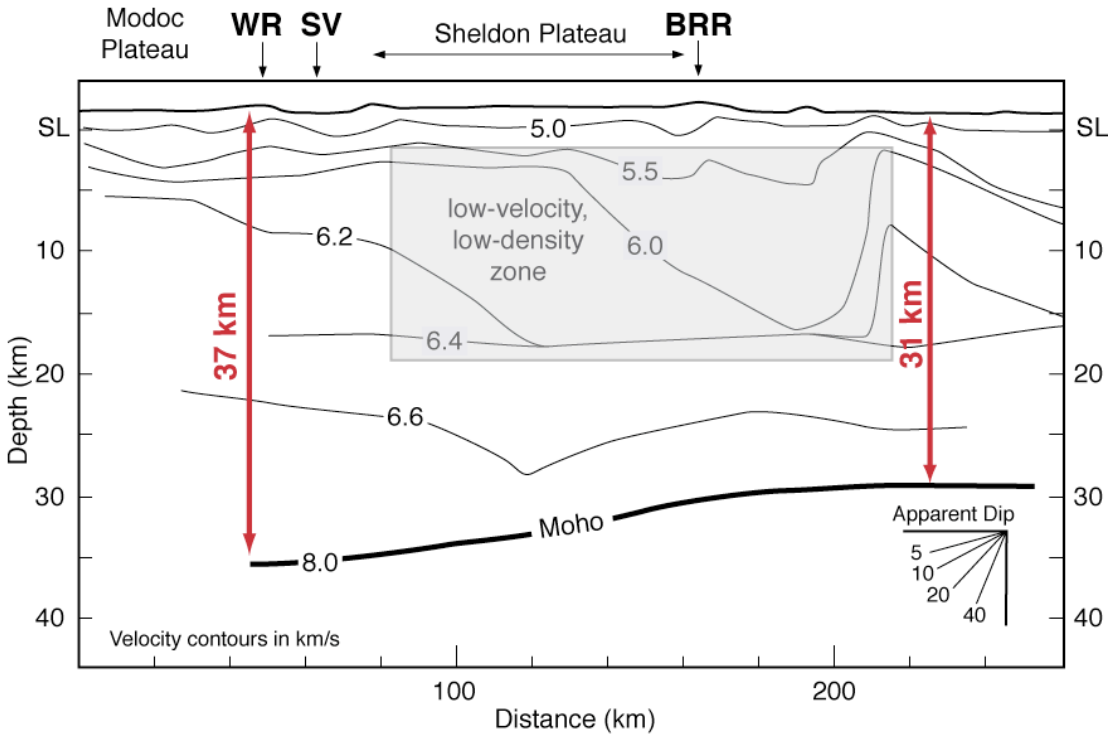


(b)

**Figure 2.** (a) Simplified geologic map, from state geologic maps, and index to Plate I. Outlines of mid-Miocene calderas from Coble and Mahood (2008). Dashed line shows location of seismic refraction profile (Lerch et al., 2007). (b) Crustal velocity profile, modified from Lerch et al. (2007). WR—Warner Range, SV—Surprise Valley, BRR—Black Rock Range. Box encloses low-velocity zone interpreted as the northward continuation of the Sierra Nevada batholith in the subsurface.

Figure 3 *(explanation next page)*

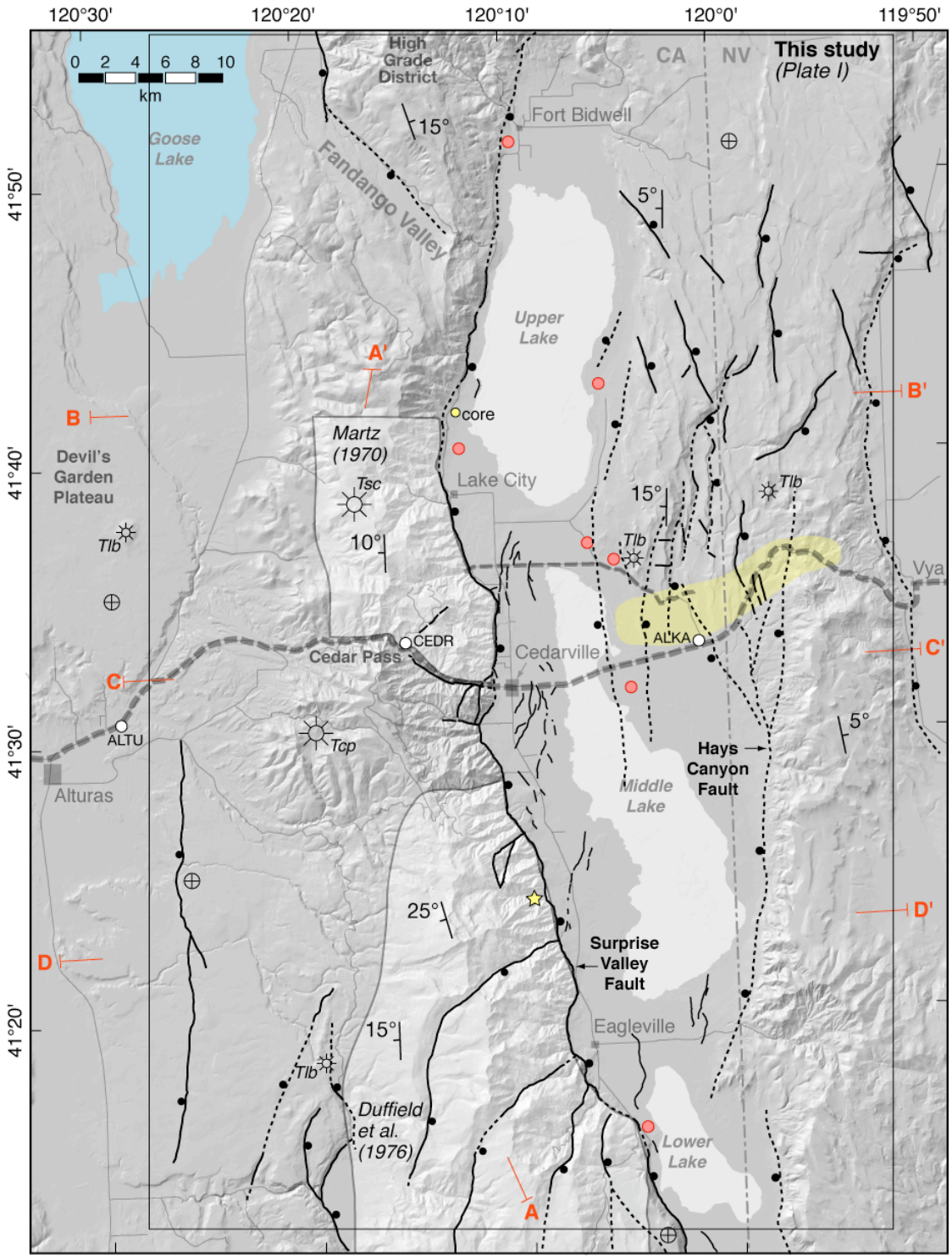

**Figure 3.** Cenozoic fault map (ball on downthrown block) and index of previous work in the Warner Range region. Black stars are approximate volcanic vent locations and their map unit labels as described in text and Plate I. Thin dashed gray line is the seismic reflection line (Lerch et al., 2009) along which seismic velocity and potential field models were constructed (Egger et al., 2009b). Thicker dashed gray line is the location of the seismic refraction profile also shown in Figure 2 (Lerch et al., 2007). Red lines—cross-section lines (Plate I, Fig. 9). Yellow star—loction of thermochronology sample studied by Colgan et al. (2008). Red circles—hot spring locations. White circles—GPS stations (Hammond and Thatcher, 2007). Yellow shaded region is the accommodation zone described in the text. Cross-section A-A' shown in Figure 4; others shown in Figure 6.

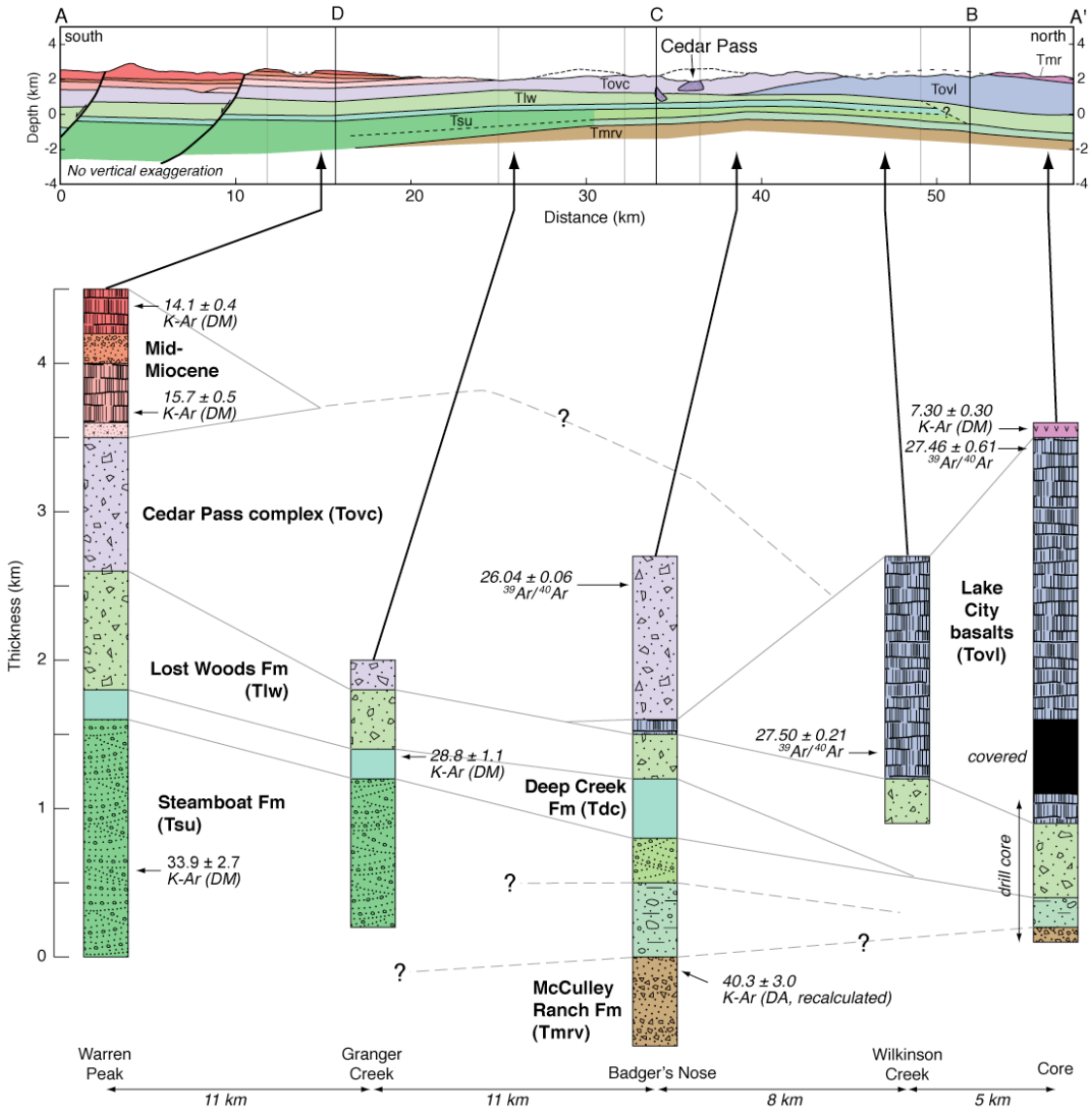


**Figure 4.** Stratigraphic columns of units exposed in the Warner Range and cross-section A-A', showing likely correlations and age relationships of units. On cross-section, gray lines correspond to bends in section (Plate I); lettered black lines indicate crossing lines with perpendicular cross-sections (Figure 9). Selected geochronologic ages are from Duffield and McKee (1986)—DM, Axelrod (1966)—DA, and all others are from Colgan et al., in prep (Table 1, Appendix A).

(a)

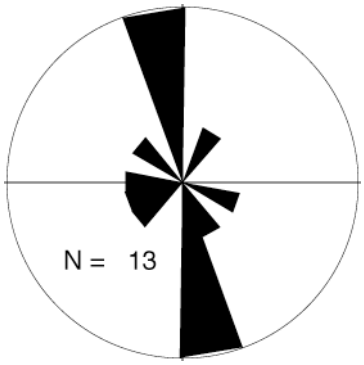


(b)

**Figure 5.** (a) Photograph of petrified logs in Lost Woods Formation (b) Rose diagram showing orientation of petrified logs in Lost Woods Formation.

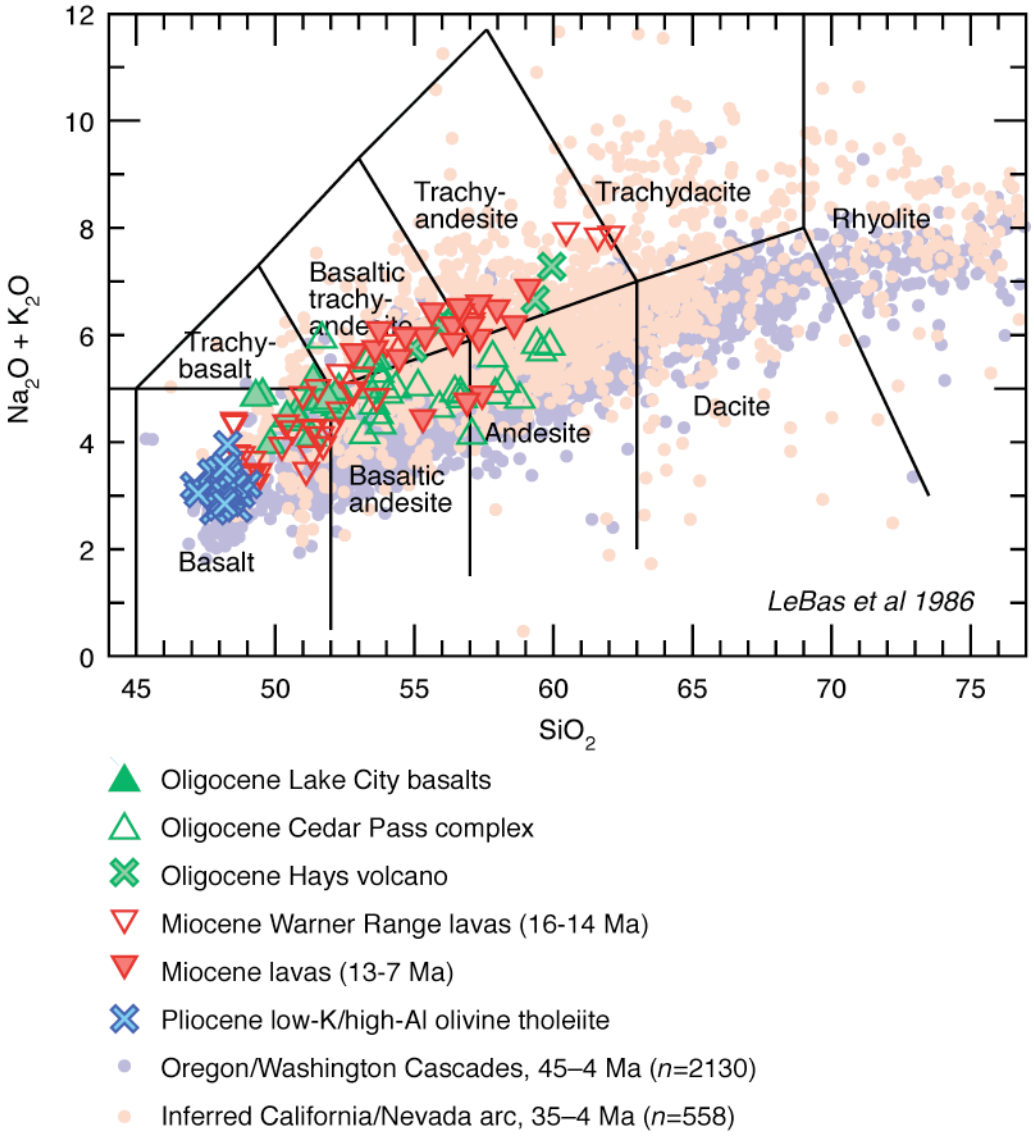


**Figure 6.** Total alkali-silica discrimination diagram for igneous rocks (Le Bas et al., 1986) comparing volcanic rocks in the Warner Range to rocks from the western Cascade arc and the inferred ancestral Cascade arc in California and Nevada (see Figure 10 for locations). Samples from the Warner Range were analyzed at the Washington State University GeoAnalytical Lab using x-ray fluorescence. See appendix for data tables. Additional data from Carmichael et al. (2006). Oregon/Washington Cascades data is from du Bray et al. (2006); California/Nevada data from du Bray et al. (2009).

Figure 7 *(explanation next page)*

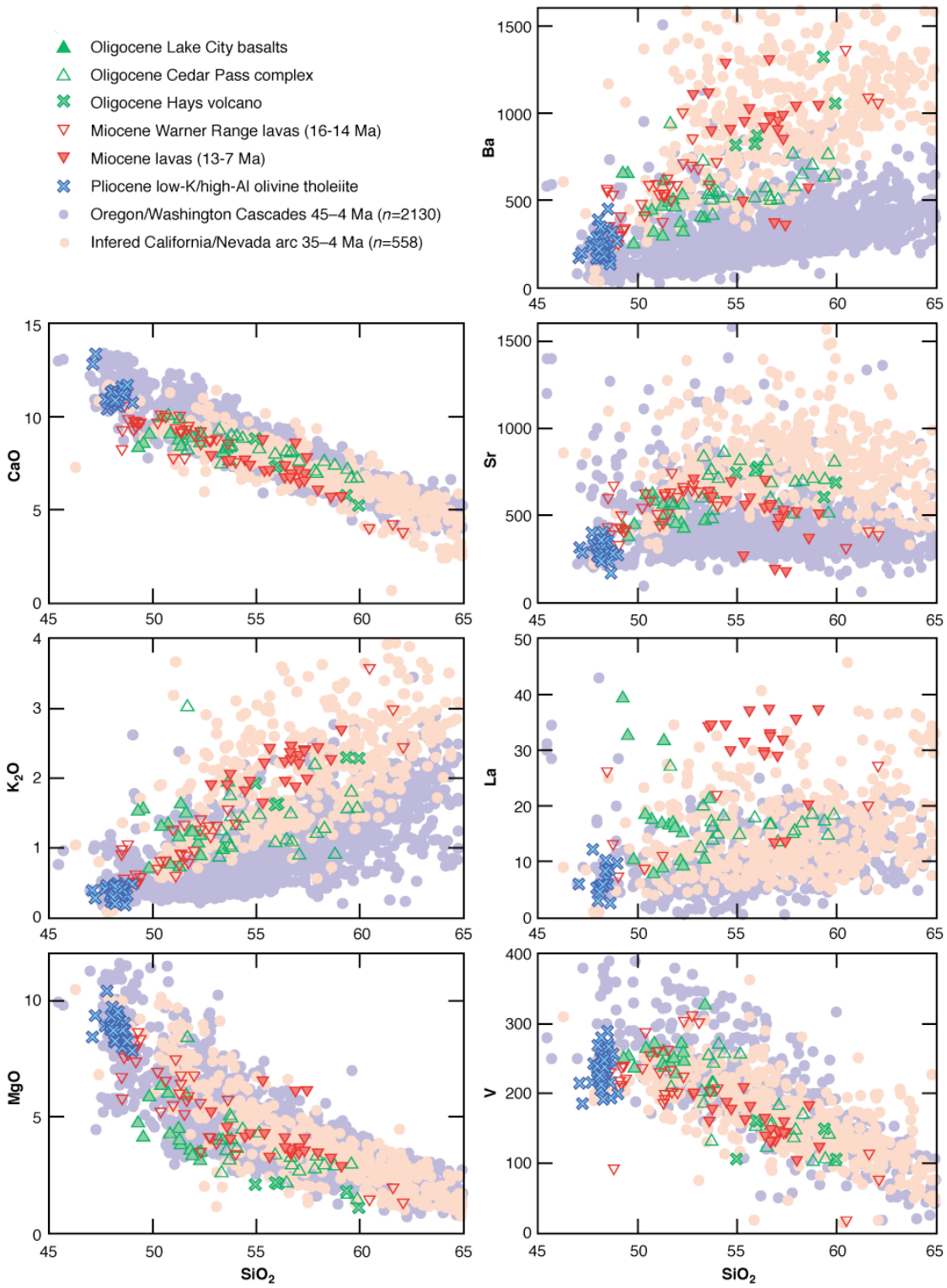

**Figure 7.** Harker diagrams comparing volcanic rocks in the Warner Range to rocks from the western Cascade arc and the inferred ancestral Cascade arc. Samples from the Warner Range were analyzed at the Washington State University GeoAnalytical Lab using x-ray fluorescence. See Appendix A for data tables. Additional data from Carmichael et al. (2006). Oregon/Washington Cascades data is from du Bray et al. (2006); California/Nevada data from du Bray et al. (2009), see Figure 10 for locations.

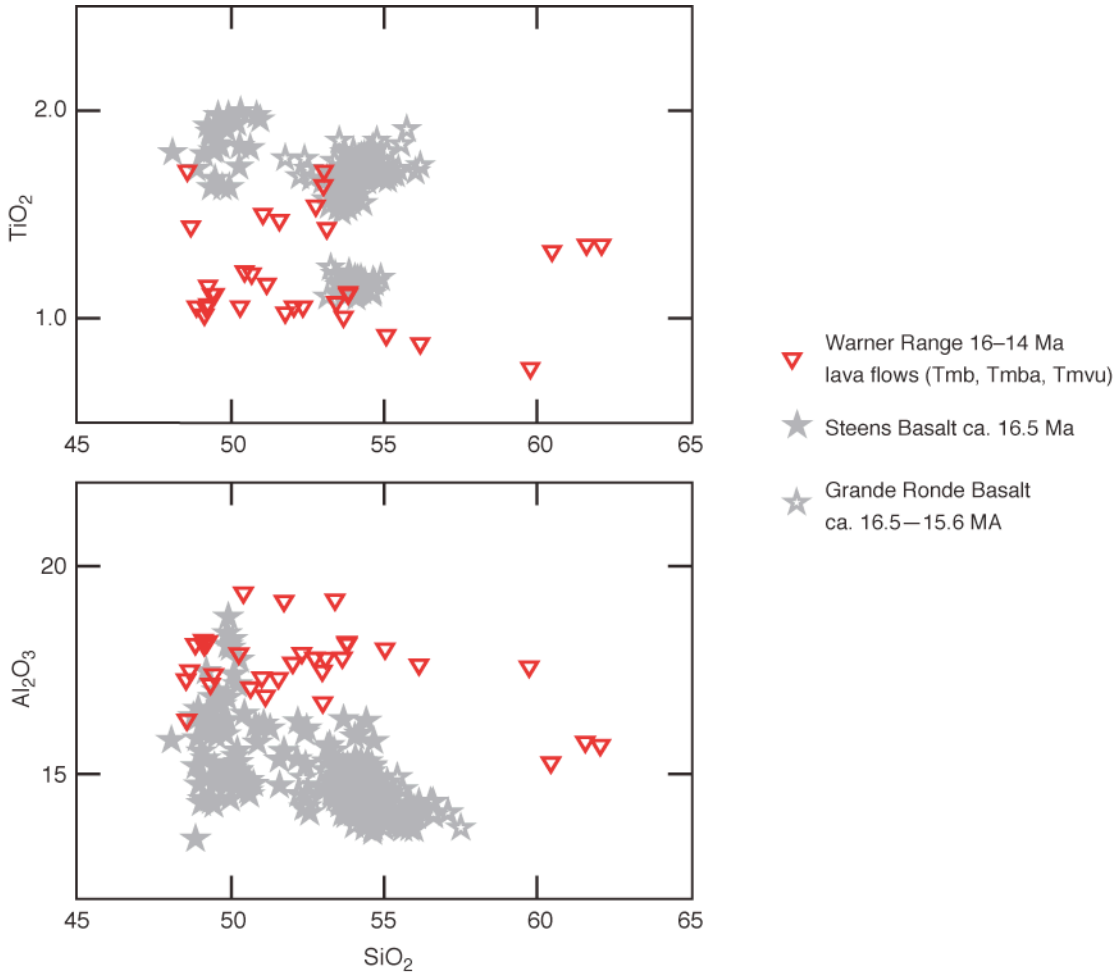


**Figure 8.** Harker diagrams comparing mid-Miocene volcanic rocks in the Warner Range to Steens and Columbia River flood basalts. Samples from the Warner Range were analyzed at the Washington State University GeoAnalytical Lab using x-ray fluorescence. See appendix for data tables. Columbia River basalts data from Hooper (2000); Steens data from Johnson et al., (1998)

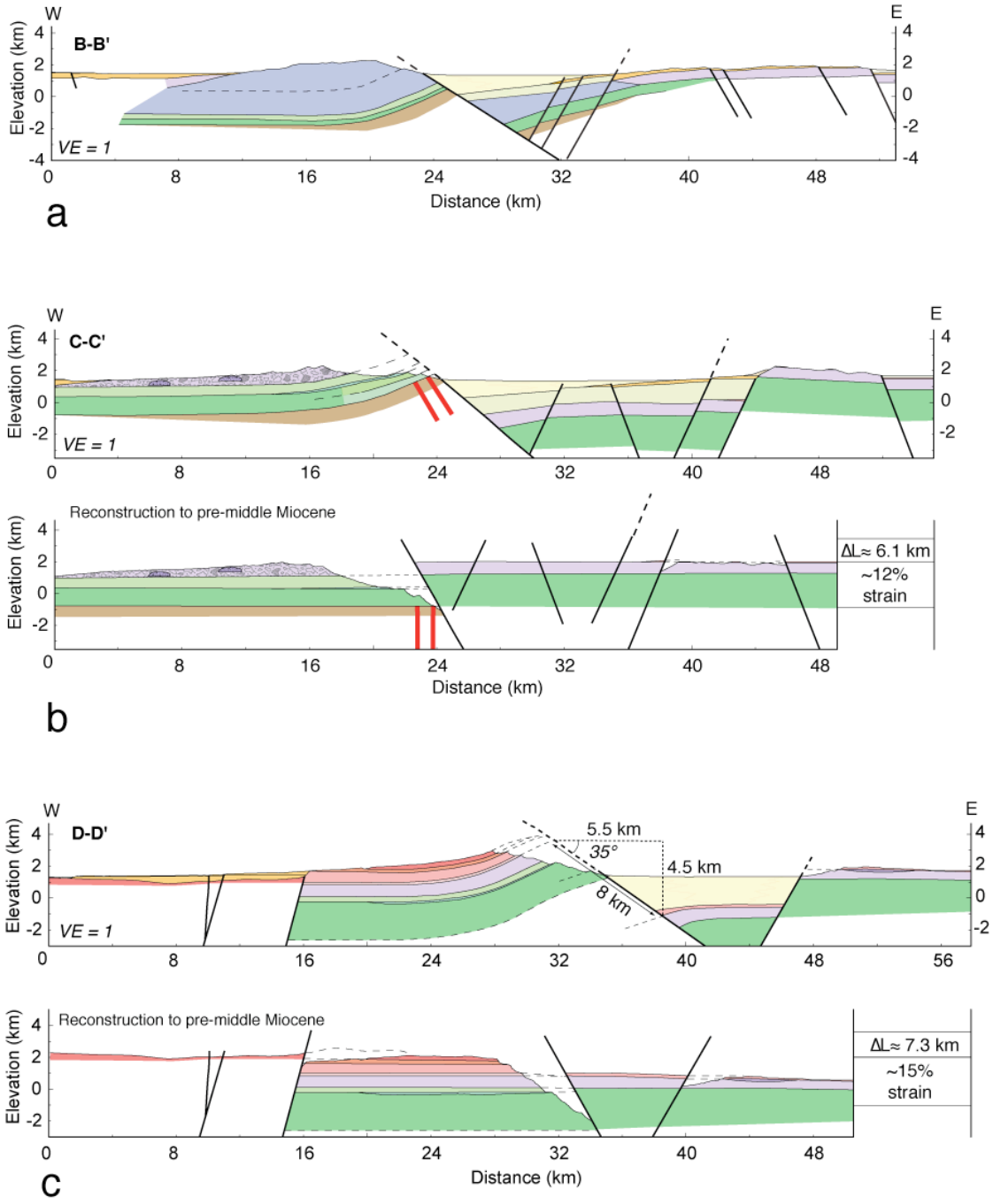


**Figure 9.** E-W cross-sections, restored to pre-extensional configurations. No vertical exaggeration (VE). See Figure 4 for color key and Plate I (and Figure 3) for location of cross-section lines.

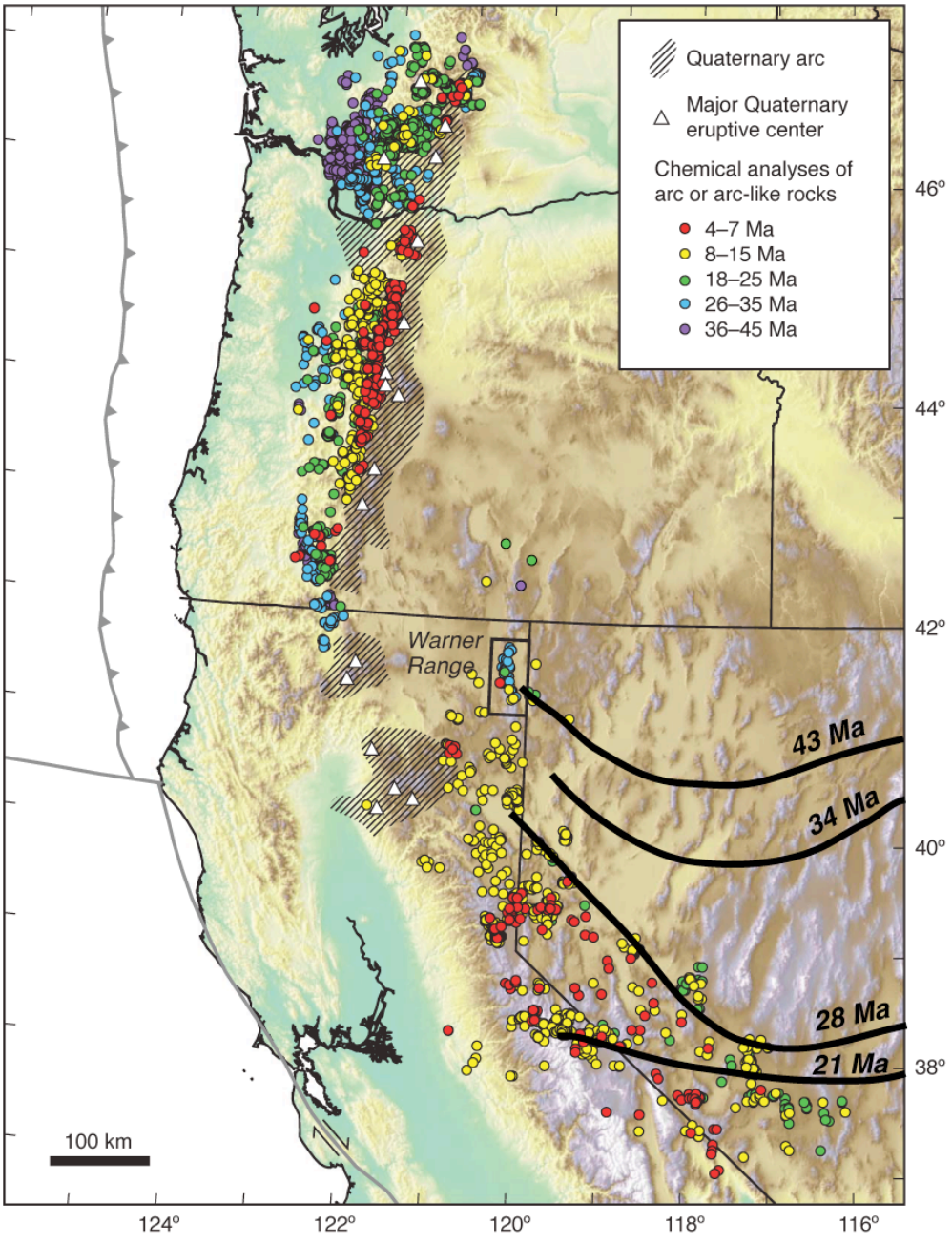


**Figure 10.** Map of western United States showing Quaternary Cascade volcanic arc (Hildreth, 2007), Eocene to Pliocene "western" Cascade arc (du Bray et al., 2007), and inferred "ancestral Cascades" in California and Nevada (du Bray et al., 2009). Thick lines indicate the timing of the southward sweep of magmatism inferred to be related to the removal of the Laramide slab (Humphreys, 1995).

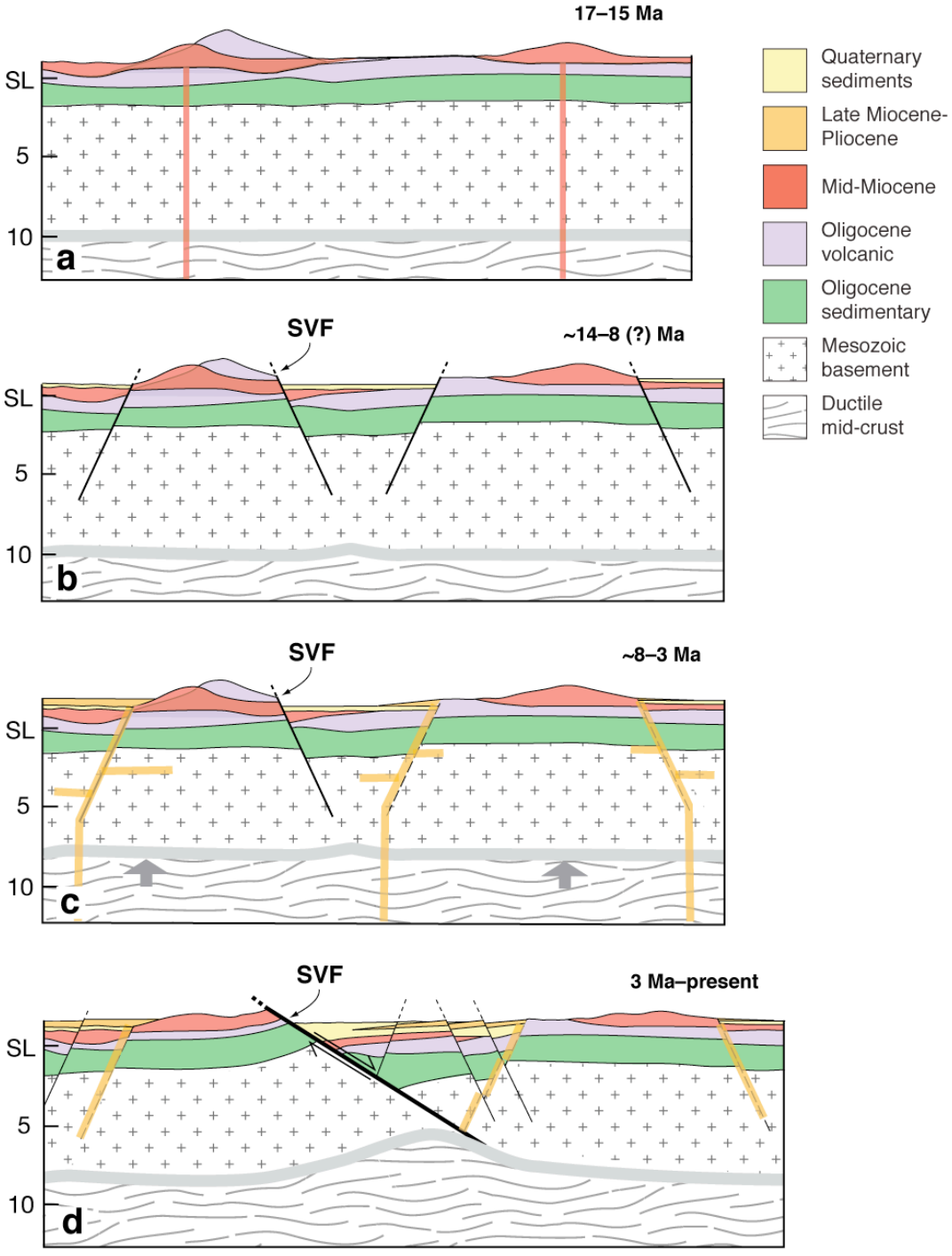


**Figure 11.** Schematic series of cross-sections depicting the extensional history of the Warner Range region: (a) Mid-Miocene volcanism, (b) onset of extension, (c) Late Miocene-Pliocene volcanism, which raises the brittle-ductile transition zone (gray line) (d) Pliocene-present extension. Long dashed lines indicate faults that are no longer active. Thickness of line indicating fault represents relative offset—thicker lines indicate more offset.

# Tables

| Sample | Longitude[1] | Latitiude[1] | Unit | Rock Type | Method | Mineral | Age (±1σ)[2] | Source[3] |
|---|---|---|---|---|---|---|---|---|
| *Eocene volcanic rocks* | | | | | | | | |
| F0457 | -120.19123 | 41.57976 | Tmrv | Andesite lava | K-Ar | feldspar | 40.8 ± 3.0[4] | A |
| *Oligocene sedimentary sequence* | | | | | | | | |
| D63B | -120.15444 | 41.38333 | Tsu | Andesitic ash | K-Ar | hornblende | 33.9 ± 2.7 | D |
| unreported | Granger Canyon | | Tsu | Reworked tuff | $^{40}Ar/^{39}Ar$ | unknown | 31.56 ± 0.42 | M |
| D113B | -120.16833 | 41.42083 | Tsu | Andesitic ash | K-Ar | hornblende | 31.1 ± 1.3 | D |
| unreported | Badger's Nose | | Tsu | Andesitic ash | $^{40}Ar/^{39}Ar$ | unknown | 30.19 ± 0.48 | M |
| 699_15A | -120.22167 | 41.50000 | Tdc | Andesitic ash | K-Ar | hornblende | 28.8 ± 1.1 | D |
| *Lake City basalts* | | | | | | | | |
| JC08WR405 | -120.23168 | 41.60900 | Tovl | Basalt | $^{40}Ar/^{39}Ar$ | groundmass | 27.83 ± 0.21 | Co |
| WR07AE40 | -120.25011 | 41.70415 | Tovl | Basalt | $^{40}Ar/^{39}Ar$ | plagioclase | 25.70 ± 0.94 | Co |
| AE05WR03 | -120.22406 | 41.57833 | Tovl | Basalt | $^{40}Ar/^{39}Ar$ | plagioclase | 27.49 ± 0.33 | Co |
| 07-C-6 | -120.24034 | 41.60912 | Tovl | Olivine basalt | $^{40}Ar/^{39}Ar$ | plagioclase | 27.14 ± 0.08 | Co |
| *Cedar Pass complex and comparable age Oligocene rocks* | | | | | | | | |
| SV70a | -120.2612 | 41.4920 | Tovc | Basaltic andesite | $^{40}Ar/^{39}Ar$ | groundmass | 30.02 ± 0.52[5] | Ca |
| 966_15 | -120.2717 | 41.5883 | Tovc | Andesite | K-Ar | hornblende | 28.7 ± 1.1 | D |
| SV96 | -120.2583 | 41.5090 | Tovc | Basaltic andesite | $^{40}Ar/^{39}Ar$ | groundmass | 27.07 ± 0.22[5] | Ca |
| H08-57 | -120.24623 | 41.60567 | Tovc | Ashflow tuff | $^{40}Ar/^{39}Ar$ | sanidine | 26.642 ± 0.077 | Co |
| 433 | -120.3222 | 41.5083 | Tovc | Andesite | K-Ar | hornblende | 26.6 ± 1.1 | D |
| WR07-AE49 | -120.22595 | 41.48698 | Tovu | Basalt | $^{40}Ar/^{39}Ar$ | plagioclase | 26.86 ± 0.08 | Co |
| 07-C-19 | -120.27277 | 41.58808 | Tovc | Andesite lava | $^{40}Ar/^{39}Ar$ | plagioclase | 26.736 ± 0.045 | Co |
| D27B | -120.2164 | 41.4389 | Tovu | Ashflow tuff | K-Ar | biotite | 26.3 ± 1.0 | D |
| SV163 | -119.89567 | 41.60400 | Tovc[6] | Dacite ashflow | $^{40}Ar/^{39}Ar$ | dacite glass | 26.26 ± 0.13 | Ca |
| JC07WR303 | -120.26150 | 41.61350 | Tovu | Ashflow tuff | $^{40}Ar/^{39}Ar$ | sanidine | 26.35 ± 0.11 | Co |
| JC08WR412 | -120.21734 | 41.43877 | Tovu | Ashflow tuff | $^{40}Ar/^{39}Ar$ | sanidine | 25.765 ± 0.061 | Co |
| JC08WR411 | -120.21417 | 41.44050 | Tovu | Ashflow tuff | $^{40}Ar/^{39}Ar$ | sanidine | 25.526 ± 0.058 | Co |
| *Later Oligocene volcanic rocks* | | | | | | | | |
| SV130 | -119.89133 | 41.32767 | Tovh | Basaltic andesite | $^{40}Ar/^{39}Ar$ | groundmass | 24.55 ± 0.16 | Ca |
| 07-C-10 | -120.21695 | 41.43917 | Tovb | Andesite lava | $^{40}Ar/^{39}Ar$ | groundmass | 24.47 ± 0.34 | Co |
| SV25 | -119.97900 | 41.35317 | Tovh | Basaltic andesite | $^{40}Ar/^{39}Ar$ | groundmass | 23.91 ± 0.13 | Ca |
| *Early Miocene volcanic rocks* | | | | | | | | |
| JC08WR410 | -120.22570 | 41.43801 | Trt | Reworked tuff | $^{40}Ar/^{39}Ar$ | sanidine | 19.22 ± 0.27 | Co |
| 1011 | -120.2433 | 41.4606 | Trt | Ashflow tuff | K-Ar | biotite | 17.3 ± 0.6 | D |
| *Middle Miocene volcanic rocks* | | | | | | | | |
| BT1 | -120.2644 | 41.2053 | Tmvu | Rhyolite | K-Ar | biotite | 16.0 ± 0.5 | D |
| R54B | -120.1106 | 41.2383 | Tmvu | Rhyolite | K-Ar | biotite | 15.9 ± 0.5 | D |
| D302B | -120.1578 | 41.2811 | Tmbl | Basalt | K-Ar | whole-rock | 15.8 ± 0.5 | D |
| D144B | -120.1506 | 41.2861 | Tmbl | Basalt | K-Ar | whole-rock | 15.7 ± 0.5 | D |
| D474B | -120.1822 | 41.2117 | Tmbl | Basalt | K-Ar | whole-rock | 15.7 ± 0.4 | D |
| SV19 | -119.9335 | 41.2755 | Tmbl | Basalt | $^{40}Ar/^{39}Ar$ | groundmass | 15.53 ± 0.11 | Ca |
| R38B | -120.0983 | 41.2433 | Tmvu | Rhyolite | K-Ar | biotite | 15.5 ± 0.5 | D |
| SV49 | -119.9685 | 41.3223 | Tmvu | Basalt | $^{40}Ar/^{39}Ar$ | groundmass | 15.44 ± 0.17 | Ca |
| SV126 | -120.0645 | 41.1997 | Tmvu | Basalt | $^{40}Ar/^{39}Ar$ | groundmass | 15.36 ± 0.08 | Ca |
| SV153 | -119.8990 | 41.6062 | Tmvu | Basalt | $^{40}Ar/^{39}Ar$ | groundmass | 15.15 ± 0.55 | Ca |
| SV142 | -120.3415 | 41.3795 | Tmbu | Basalt | $^{40}Ar/^{39}Ar$ | groundmass | 14.57 ± 0.08 | Ca |
| D398B | -120.2939 | 41.2817 | Tmvu | Rhyolite | K-Ar | biotite | 14.5 ± 0.4 | D |
| D418B | -120.2150 | 41.2633 | Tmbu | Basalt | K-Ar | whole-rock | 14.1 ± 0.4 | D |
| D235B | -120.1933 | 41.3111 | Tmbu | Basalt | K-Ar | whole-rock | 14.1 ± 0.4 | D |
| SV31 | -120.4140 | 41.2315 | Tmvu | Pumice | $^{40}Ar/^{39}Ar$ | plagioclase | 14.09 ± 0.05 | Ca |

**Table 1, cont.**

| Sample | Longitude[1] | Latitiude[1] | Unit | Rock Type | Method | Mineral | Age (±1σ)[2] | Source[3] |
|---|---|---|---|---|---|---|---|---|
| D173B | -120.2200 | 41.4039 | Tmbu | Basalt | K-Ar | whole-rock | 14.0 ± 0.4 | D |
| SV59 | -120.4403 | 41.2295 | Tmvu | Pumice from tuff | $^{40}Ar/^{39}Ar$ | plagioclase | 13.52 ± 0.06 | Ca |
| SV136 | -120.4148 | 41.2305 | Tmvu | Basaltic andesite | $^{40}Ar/^{39}Ar$ | groundmass | 12.12 ± 0.05 | Ca |
| SV52-1 | -120.5498 | 41.4593 | Tts | Andesite glass | $^{40}Ar/^{39}Ar$ | whole-rock | 12.02 ± 0.06 | Ca |
| SV52-2 | -120.5498 | 41.4593 | Tts | Andesite glass | $^{40}Ar/^{39}Ar$ | whole-rock | 11.90 ± 0.08 | Ca |
| SV52-3 | -120.5498 | 41.4593 | Tts | Andesite glass | $^{40}Ar/^{39}Ar$ | whole-rock | 11.83 ± -.10 | Ca |
| *Late Miocene silicic rocks* | | | | | | | | |
| OH1 | -120.3250 | 41.8500 | Tmr | Obsidian | K-Ar | whole-rock | 9.2 ± 0.3 | D |
| SH1 | -120.3233 | 41.7967 | Tmr | Obsidian | K-Ar | whole-rock | 7.9 ± 0.2 | D |
| BC1 | -120.2533 | 41.7081 | Tmr | Obsidian | K-Ar | whole-rock | 7.3 ± 0.3 | D |
| *Late Miocene-Pliocene basalts* | | | | | | | | |
| SV154 | -119.9985 | 41.6792 | Tlb | Basaltic andesite | $^{40}Ar/^{39}Ar$ | groundmass | 8.08 ± 0.09 | Ca |
| SV161 | -119.8750 | 41.8312 | Tlb | Basalt | $^{40}Ar/^{39}Ar$ | groundmass | 8.03 ± 0.08 | Ca |
| SV6 | -119.8547 | 41.8623 | Tlb | Basalt | $^{40}Ar/^{39}Ar$ | groundmass | 7.69 ± 0.07 | Ca |
| SV24 | -120.0745 | 41.8403 | Tlb | Basaltic andesite | $^{40}Ar/^{39}Ar$ | groundmass | 7.33 ± 0.06 | Ca |
| SV134 | -120.0505 | 41.6585 | Tlb | Basalt | $^{40}Ar/^{39}Ar$ | groundmass | 5.95 ± 0.08 | Ca |
| SV13 | -119.9582 | 41.9065 | Tlb | Basalt | $^{40}Ar/^{39}Ar$ | groundmass | 4.91 ± 0.10 | Ca |
| SV35 | -120.5028 | 41.2615 | Tlb | Basalt | $^{40}Ar/^{39}Ar$ | groundmass | 4.61 ± 0.15 | Ca |
| SV132 | -120.0468 | 41.5987 | Tlb | Basalt | $^{40}Ar/^{39}Ar$ | groundmass | 4.36 ± 0.13 | Ca |
| SV150 | -119.9603 | 41.6425 | Tlb | Basalt | $^{40}Ar/^{39}Ar$ | groundmass | 4.33 ± 0.08 | Ca |
| SV92 | -120.6320 | 41.5011 | Tlb | Basalt | $^{40}Ar/^{39}Ar$ | groundmass | 4.31 ± 0.18 | Ca |
| SV4 | -120.0307 | 41.5845 | Tlb | Basalt | $^{40}Ar/^{39}Ar$ | groundmass | 4.28 ± 0.16 | Ca |
| SV27 | -120.4400 | 41.4283 | Tlb | Basalt | $^{40}Ar/^{39}Ar$ | groundmass | 3.98 ± 0.06 | Ca |
| SV18 | -119.9843 | 41.5593 | Tlb | Basalt | $^{40}Ar/^{39}Ar$ | groundmass | 3.84 ± 0.06 | Ca |
| SV162 | -119.9615 | 41.9947 | Tlb | Basalt | $^{40}Ar/^{39}Ar$ | groundmass | 3.81 ± 0.15 | Ca |
| SV137 | -120.5157 | 41.3765 | Tlb | Basalt | $^{40}Ar/^{39}Ar$ | groundmass | 2.94 ± 0.10 | Ca |
| SV139 | -120.3263 | 41.3142 | Tlb | Basalt | $^{40}Ar/^{39}Ar$ | groundmass | 2.76 ± 0.20 | Ca |

[1]Precision of Lat/Long as originally reported. Locations in this study are NAD27 coordinates. Coordinate systems used by Carmichael et al. (2007) and Duffield & McKee (1986) are not specified and assumed to be NAD27. Coordinates for Axelrod (1966) given in township, section, range; lat/long were determined approximately.

[2]Precison of ages as originally reported. All $^{40}Ar/^{39}Ar$ dates calculated relative to Fish Canyon Tuff sanidine = 28.02 Ma.

[3]A=Axelrod (1966), Ca=Carmichael et al. (2006); Co=Colgan et al. (in prep); D=Duffield and McKee (1986); M=Myers (1998). See references for complete source information.

[4]Corrected age—published age of 40.0 ± 3.0 used $4.72 \times 10^{-30}$/yr as the decay constant for K.

[5]We do not use these two ages in our determination of the age of the Cedar Pass complex, as the MSWD values are >100.

[6]Carmichael et al. (2006) refer to this unit as the Fortynine Tuff

**Table 1.** Summary of geochronology from the Warner Range and surrounding area. Location, rock type, method used, and the source publication are given for all age dates shown in Plate I and referred to in the text. Complete data shown in Appendix A.

# Chapter 2

## Provenance and paleogeographic implications of Eocene-Oligocene sedimentary rocks in the northwestern Basin and Range

**ABSTRACT**

A thick sequence of uppermost Eocene to lower Oligocene volcaniclastic and sedimentary rocks is exposed at the base of the Warner Range in northeastern California. This isolated exposure provides insight into the paleogeographic setting of the northwestern Basin and Range during this time period. Significant thinning of the unit over 35 km of lateral exposure and predominantly volcanic clast compositions suggest that the sequence was deposited in an alluvial plain adjacent to a volcanic arc. Paleocurrent indicators in the conglomerates define a NNE transport direction. Detrital zircon analysis on coarse sandstones and dating of individual granite cobbles show a range of ages consistent with a local, volcanic source area primarily from the SSW with some far-traveled input from northern Nevada; the far-traveled component increases in influence as the unit thins to the north. Comparison with other sedimentary sequences of Eocene age and integration with paleofloral and geophysical data help define drainage divides, and suggest that this sequence accumulated in a relatively isolated, intra-arc basin. This localized accumulation differs markedly from contemporaneous drainages to the south that transported material westward from central Nevada to the paleoshoreline, and suggests that ongoing volcanism had a strong influence on paleogeography in this region during the Eocene and Oligocene.

## INTRODUCTION

Few rocks of late Eocene and early Oligocene age are exposed in the northwestern Basin and Range (Fig. 1). Across most of northwestern Nevada, upper Oligocene and Miocene volcanic sedimentary rocks are generally deposited unconformably on Mesozoic plutonic and metamorphic rocks (Bonham, 1969; Colgan et al., 2006; Lerch et al., 2008). Older Tertiary rocks are demonstrably absent with the exception of a few upper Eocene lava flows (Lerch et al., 2007), consistent with a low-relief, externally drained plateau in this part of the Basin and Range during the mid-Tertiary. Along most of the northwestern margin of the Basin and Range, the only exposures are flat-lying, middle Miocene and younger volcanic rocks of the High Lava Plains and Modoc Plateau (Fig. 1) almost entirely obscure the earlier Tertiary history of this region.

The Warner Range in northeastern California (Fig. 1) opens a narrow window into the units that lie below this young volcanic cover, exposing a thick section of sedimentary, volcaniclastic, and volcanic rocks that spans the latest Eocene to Pliocene time interval (Carmichael et al., 2006; Duffield and McKee, 1986; Russell, 1928). Near the base of this sequence, a coarse-grained alluvial sandstone and conglomeratic sequence of latest Eocene and early Oligocene age is exposed over a distance of approximately 25 km along strike (approximately N-S). Here, we present a description of this sequence and its depositional environment together with paleocurrent, clast-composition, and detrital zircon data that offer insight into its source. These data have implications for the otherwise poorly-understood paleogeography of northwestern Nevada and northeastern California during the latest Eocene and into the Oligocene.

## EOCENE AND OLIGOCENE SEDIMENTARY SEQUENCE

The Warner Range exposes a thick sequence of Eocene to upper Miocene sedimentary and volcanic rocks that have been uplifted, tilted, and exposed by late Miocene and younger slip along the Surprise Valley fault (Fig. 2). The base of this sequence is primarily sedimentary and volcaniclastic; it was originally called the Lower Cedarville

Formation by Russell (1928). Based on detailed field mapping in a portion of the range between Cedarville and Lake City (Fig. 2), Martz (1970) subdivided the Lower Cedarville Formation into five unit and mapped at least one unconformity within it (Table 1). In their mapping of the South Warner Wilderness area between Granger Canyon and Eagleville (Fig. 2), Duffield et al. (1976) did not subdivide the sedimentary sequence, though they alluded to the presence of at least three recognizable units based on composition, color, and vegetation. Myers (1998) and (2006) retained the nomenclature of Martz (1970) in paleofloral analyses of fossil assemblages in this sequence (Myers, 1998; 2006). Our new mapping in 2004 and 2005 confirmed the formation boundaries suggested by Martz (1970) and extended these subdivisions to the south between Cedar Pass and the South Warner Wilderness (Fig. 2), and thus here we use those formation names (Table 1).

In this study, we focus on the provenance and paleogeographic implications of the Steamboat Formation, near the base of the exposed sedimentary sequence with a depositional age of 34-31 Ma (Duffield and McKee, 1986; Myers, 2006). This unit is of interest because it is one of the few exposed sequences of sedimentary rocks of this age in the region, offering insight into the paleotopography and drainage system of northwestern Nevada and northeastern California during the early Oligocene.

*Thickness and extent of the Steamboat Formation*

Near Warren Peak in the South Warner Wilderness (Fig. 2), the Steamboat Formation reaches a thickness of approximately 1500 m, but the base is not exposed (Fig. 3). Near Badger's Nose north of Cedarville (Fig. 2), it sits unconformably on older Eocene lava flows and breccias and has a thickness of approximately 800 m. Correlative rocks encountered at depth in a drill core north of Lake City (Fig. 2) are approximately 200 m thick (Fig. 3). Thus, despite the lack of consistent exposure of the base of the unit, it appears to thin from at least 1500 m to 200 m from south to north over a distance of approximately 35 km. The east-west extent of the formation is unknown, as the surrounding area is covered by middle Miocene and younger volcanic rocks.

*Lithology of the Steamboat Formation*

The unit consists of interbedded cobble- to boulder-conglomerate, coarse sandstone, debris-flow deposits, tuff, and shale (Fig. 4a). The vast majority of clasts in the conglomerate sections are sub-angular to sub-rounded and consist of volcanic material, primarily porphyritic andesite with phenocrysts of plagioclase and hornblende. Clasts are up to 1 m in size with an average size of ~10 cm. In a few localities, a small number of granitic and metamorphic basements clasts are present, perhaps as much as 5%. The very coarse-grained sandstones are volcaniclastic, containing both abundant volcanic lithic fragments and primary ash fall crystals (Fig. 4b). The coarse sandstones and conglomerates make up the majority of the section east of Warren Peak (Fig. 2), becoming thinner and interfingering with finer-grained sediments and lacustrine sequences to the north. In Granger Canyon, debris-flow conglomerates clearly infill channels cut down into finer-grained sediments (Fig. 4c).

The presumably equivalent sedimentary sequence encountered in the core, ~11 km north of the last exposure in the range (Fig. 2), differs significantly in lithology (Fig. 5). Conglomerate sequences contain abundant, well-rounded clasts of granitic and metamorphic rocks ~3-4 cm in diameter, and volcanic clasts are rare. In thin section, sandstone sequences are arkosic and well-sorted, with significantly more quartz and fewer lithics than the exposures in the range (Fig. 6). Despite the difference in lithology with the exposed Steamboat Formation, the overall sedimentary character of both units – predominantly sandstone and conglomerate – is similar. In addition, both the exposed Steamboat Formation and the sedimentary sequence in the core contrast significantly with an overlying matrix-supported debris flow unit, called the Lost Woods Formation, which is easily recognizable in outcrop and in the core by its distinct reddish color (Fig. 5). It is possible that the volcanic unit at the base of the core correlates with the McCulley Ranch Formation (Table 1, Fig. 3), but this potential correlation has not been systematically addressed.

*Fossils*

The Steamboat Formation includes two fossiliferous layers at different stratigraphic levels. At its base north of Cedarville, a well-documented floral assemblage marks the transition from the latest Eocene to Oligocene (Myers, 2006). The fossils occur in a 1 m-thick lacustrine siltstone that extends laterally (mainly to the south) approximately 7 km (Fig. 3) (Myers, 2006). The same floral assemblage is exposed at Steamboat Canyon (Fig. 2). Both assemblages include ferns and conifers that occur throughout the sequence, but also in dense mats at ~10 cm intervals, which Myers (2006) interpreted as seasonal changes and winter leaf fall. The repeated sequence indicates that the lake persisted through several seasons, though the minimal thickness of the entire layer suggests an ephemeral feature. Based on the assemblages and analysis of leaf physiognomy, Myers (2003) estimated that paleoelevation at the time of deposit was >1000 m, not significantly different than today.

*Paleocurrent indicators*

We measured the orientation of imbricated cobbles at three localities in the range (Fig. 2). Imbrication directions were largely consistent within a single conglomeratic channel, but varied as much as 180 degrees between different channels. Data from Cottonwood Canyon exemplify this relationship: 17 measurements in a channel near the base of the exposure show a strong paleocurrent direction towards the NW, while 16 measurements in a bed approximately 30 m stratigraphically higher in the sequence show a bit more variability with an average paleocurrent to the ESE (Fig. 2). While braided rivers tend to display more consistency in their paleocurrent directions, a spread in paleocurrent directions of 180° is expected in a coarse alluvial fan or alluvial plain (e.g. Miall, 1977).

*Depositional environment*

The spread of paleocurrent indicators, abundance of very coarse volcanic detritus, immaturity of the sandstones, and the presence of intermittent lakes all suggest that this unit was deposited on an alluvial plain proximal to a volcanic source. Given the decrease in thickness from ~1500 m in the furthest south exposures to ~200 m 35 km

to the north and the direction of the paleocurrent indicators, it is also like that the main source area – presumably the Eocene volcanic arc – lay to the south and/or southwest. At least once during deposition of this sequence, however, a lake of at least 7 km in diameter formed and persisted through several seasons (Myers, 2006). This suggests an intermittently closed basin, but perhaps only ephemerally so as is typical in active volcanic regions where debris flows, landslides, and lava flows can create sudden changes in topography that block drainage (Costa and Schuster, 1988). Such natural dams typically occur within river valleys, however, as opposed to broad alluvial plains, and the large majority of modern examples are eroded within one year of formation (Costa and Schuster, 1988). It is possible that accumulation of these sediments and intermittent lake formation was influenced by intra-arc extension and normal faults. This has been documented in the Eocene Clarno Formation of northern Oregon (Fig. 1) (White and Robinson, 1992) although no such faults have been found thus far in the Warner Range.

Duffield and McKee (1986) report two K-Ar ages on hornblende from andesitic tuffs within the Steamboat Formation: 33.9 ± 2.7 Ma and 31.1 ± 1.3 Ma (Fig. 2). Myers (1998) reports two additional $^{40}Ar/^{39}Ar$ ages: 30.19 ± 0.48 Ma on a tuff near the base of the Cougar Cliffs member near Badger's Nose and 31.56 ± 0.42 Ma on a tuffaceous sandstone in Granger Canyon. The narrow timespan of these ages either means that they are from the same unit, or that deposition of the entire sequence was quite rapid during the early Oligocene. Despite the significant thickness of this unit, especially at its southern extent, rapid deposition is common in intra-arc basins and generally closely related to individual explosive eruptive events (e.g. Smith, 1988).

A detailed stratigraphic study of this unit has yet to be undertaken, but the lithologies present and the relationships between them strongly resemble the Eocene Clarno Formation, exposed in northwestern Oregon (White and Robinson, 1992).

## GRANITIC COBBLE AND DETRITAL ZIRCON ANALYSIS

*Methods*

Three samples of coarse sandstones were collected from exposures in Granger Canyon and an unnamed canyon 1.8 km south of Cottonwood Canyon (see Fig. 2 for sample locations) and from five depth intervals in the LCHS-5 core: 3755' (two samples), 3763', 3990', 4145', and 4147' (Fig. 5; note that sample numbers correspond with depth in the core in feet rather than stratigraphic thickness). Core samples consisted of 10-20 cm-long pieces of 3.6 cm diameter core. Granite cobbles were collected from Granger Canyon, Cottonwood Canyon, and the same unnamed canyon south of Cottonwood Canyon, as well as from two depth intervals in the core (Fig. 5). Zircons were separated from all samples using standard mineral separation techniques and analyzed as described in the appendix.

Zircons are rare in sandstone outcrop samples from the Warner Range, and heavy mineral concentrates contained a significant proportion of other non-magnetic minerals. Hand-picking of these three samples still only produced 4 zircon grains from WR07AE58 and 8 grains from WR08AE26 (both from Granger Canyon) and 15 grains from WR07AE59 (from the unnamed canyon). Given the very small sample size, data from these samples are interpreted together, although they were analyzed separately.

In contrast, sandstone samples from the LCSH-5 core were relatively abundant in zircon, especially considering the much smaller sample size. In general, these sandstones are finer grained (though still coarse), better sorted, and have a higher proportion of quartz than the sandstone sampled in the range. The relative abundance of quartz and zircon is consistent with the much higher proportion of crystalline basement cobbles in the core section than in the range. The core samples also contained abundant pyrite, likely a result of hydrothermal alteration (the LCHS-5 core was drilled for geothermal exploration). Hand-picking still resulted in a smaller than ideal number of grains for detrital analysis, generally 15-30 per sample.

One of two samples from core depth interval 3755' was analyzed using laser ablation-inductively coupled mass spectrometry (LA-ICP MS) at the University of Arizona in 2006. The remaining samples were analyzed using the SHRIMP-RG (sensitive high-resolution ion microprobe with reverse geometry) at the Stanford–U.S. Geological Survey Microisotopic Analytical Center in 2008 and 2009. Because the results were similar from both techniques, the data were combined in the following analysis.

*Results*

The combined detrital zircon data from all nine sandstone samples are shown in Figure 7. The age data are plotted as histograms, which show only the age measurement, with superimposed relative probability curves that incorporate the uncertainty associated with the analyses. Each age measurement plots as a normal distribution with 2σ uncertainty; these individual normal distributions are summed to create the relative probability curve. The combined histogram with a total of 152 grains shows three peaks: a sharp bimodal peak in the middle Eocene (ca. 35-45 Ma), a broad bimodal peak in the early Cretaceous (ca. 100-130), and a smaller unimodal peak in the middle Jurassic at ca. 170 Ma (Fig. 5, inset). A small number of Paleozoic and Precambrian grains are present.

Cobble ages are shown in Table 2 in order of increasing age. Thirteen out of sixteen cobbles are between 100 and 115 Ma. It is worth noting that the four youngest cobbles all come from one location, Granger Canyon, and the two Jurassic cobbles both come from the core sample 4145' (Table 2). In general, it appears that cobbles of similar age tend to occur in the same location, rather than being spread throughout the range.

Detrital zircon data show a somewhat similar distribution when broken down by stratigraphic level in the core and outcrop sample location (Fig. 8), though the small sample size for each of these subdivisions limits the statistical significance of the age distributions. In this analysis, core samples from 4145' and 4147' are combined, as are samples from 3755' and 3763'. The middle Jurassic peak is most prominent in the deepest core sample, and absent in the outcrop samples. The bimodal Cretaceous peak

in the combined data (Fig. 7) appears to consist of two unimodal peaks – a younger one centered on 100-110 Ma in the range, and an older one centered on 115-120 in core sample 4145', while samples from the shallower core depths have a broad distribution of ages in the Cretaceous and no clear peak (Fig. 8). Although the grains older than 250 Ma are not shown in Figure 5, similar patterns emerge: Proterozoic grains occur only in the shallower core samples and in one outcrop sample from the unnamed canyon, WR08AE26 (see appendix for all age data).

All samples contain grains from the middle Eocene and maintain some amount of bimodality, but several additional details warrant noting. The Eocene grains make up a much larger proportion of core sample 3755' - 28 of 57 grains between 30 and 50 Ma – than they do in any of the other samples. The youngest grains are in outcrop samples (the two youngest grains ages from core sample 3755' are younger than the overlying Oligocene lava flows, and thus are disregarded). The youngest grain from outcrop samples is 31.2 ± 0.6 Ma, which overlaps with dated ash layers in this unit and probably represents primary ash fall.

**INTERPRETATION OF DETRITAL ZIRCON DATA**

The three age peaks in the detrital zircon data – mid-Jurassic, mid-Cretaceous, and Eocene – have significant implications for the provenance and paleogeography of this region during the early Oligocene. We discuss the two Mesozoic peaks first, then the Eocene peak.

Sierran magmatism is generally agreed to have occurred in three pulses during the Mesozoic: a Triassic, Jurassic, and Cretaceous pulse (Chen and Moore, 1982; Stern et al., 1981). Batholithic rocks from the three pulses are systematically distributed throughout California and Nevada: in the central and southern portion of the Sierra Nevada, Cretaceous plutons form the core of the range and are flanked on both the east and west by Jurassic plutons, with Triassic plutons exposed only on the eastern side of the batholith (Stern et al., 1981). This pattern breaks down farther north, however, beyond the northern extent of the modern Sierra Nevada mountain range. At

this latitude, the batholith is distributed throughout northwestern Nevada, where it is broken up by a series of Basin and Range normal faults (Fig. 1). Triassic plutons are less abundant here than farther south and the main belt of Jurassic plutons swings west to the Klamath Moutains, though scattered Jurassic plutons occur throughout northern Nevada (Colgan et al., 2006; Wyld and Wright, 1997). The Cretaceous pulse, initially divided into two different intrusive episodes by Evernden and Kistler (1970) and subsequently recognized as a single, long-lived magmatic period by Stern et al. (1981), comprises the bulk of the exposure of the batholith in northwestern Nevada. The distribution of Cretaceous plutons is not uniform by age, however: primarily, plutons north of the Granite Range near Gerlach, Nevada, range in age from 98-115 Ma, and younger ones are apparently absent (Colgan et al., 2006; Wyld and Wright, 2001).

Given this distribution of plutonic ages, it is not surprising that the Triassic magmatic pulse is not represented in the detrital zircons in the Steamboat Formation. The Jurassic pulse is only minimally represented and only significantly in the deepest core sample (Fig. 8), but this relatively small peak of Jurassic ages is consistent with dated plutons throughout northern Nevada and thus is not particularly diagnostic in determining a potential source area for this unit.

The distribution of Cretaceous ages is more informative. As noted earlier, the Cretaceous magmatic pulse was long-lived, lasting about 45 million years from ca. 125 Ma to ca. 80 Ma. In the Warner Range samples, there is a notable lack of zircons from the late Cretaceous, about 80-100 Ma (Fig. 7). This is true for all stratigraphic levels in the core as well as the samples from the range (Fig. 8), and only one of the 16 dated cobbles comes from this time period (Table 2). The closest exposures of Cretaceous granite within this age range lie in the Selenite Range, only 100 km to the southeast of the southern Warner Range (Fig. 1) (Nick van Buer, unpublished data). Farther south and west of the Selenite Range, 80-100 Ma plutons are abundant (Nick van Buer, personal communication). The virtual absence of 80-100 Ma zircons in the Steamboat Formation therefore seems to require the presence of a drainage divide not

far south of the its exposure that limited input from this region with abundant late Cretaceous plutons.

The closest exposures of the most common ages in both the detrital samples and the cobbles (100-120 Ma) are plutons exposed in the Santa Rosa Range, Slumbering Hills, and Pine Forest Range (Colgan et al., 2006; Wyld and Wright, 2001), suggesting a source region at least 100 km to the east. Paleovalleys cut into Cretaceous plutons and their wall rocks are locally preserved beneath Late Oligocene and early Miocene volcanic rocks in the Pine Forest and Pueblo Mountains (Colgan et al., 2006), and may be remnants of west-flowing drainages that transported granitic detritus from this area to reach the modern Warner Range. The intervening Sheldon Plateau (Fig. 1) exposes only flat-lying late Oligocene to middle Miocene volcanic rocks, however, so the presence of west-flowing Oligocene rivers in this region cannot be directly verified.

The Tertiary age peak in the detrital data is much narrower than the Mesozoic peaks. The most common age of Tertiary zircons in all of our samples is 40-41 Ma, an age characteristic of volcanic rocks of northeastern Nevada (Brooks et al., 1995; Haynes, 2003; Henry and Ressel, 2000; Ressel and Henry, 2006). An alternative possibility is that these zircons were derived from nearby volcanoes that were subsequently eroded away and/or covered with younger volcanic and sedimentary rocks.

In fact, it is possible that both hypothesized sources are represented in the Steamboat Formation. As noted earlier, the Tertiary ages display a bimodal distribution in the cumulative probability plots in both the summarized data (Fig. 7) and the stratigraphically separated data (Fig. 8). The two modes are approximately 38 Ma and 40 Ma. Hafnium concentrations, measured routinely during analysis on the SHRIMP-RG, display a wide range of values from <6000 ppm to >12,000 ppm (Fig. 9). While concentrations alone cannot indicate a specific source, the wide range of values alone suggests multiple sources. In fact, some of the highest hafnium concentrations (>12,000 ppm) also correspond with the most rounded zircons with ages ca. 42 Ma (Fig. 9), all within the sample from core depth 3990'. The rounding suggests that these

zircons are far-traveled. In contrast, the youngest grains present in the range (whose ages overlap with dated tuffs within the section and thus are presumably proximal, primary ash fall deposits) are euhedral, with hafnium concentrations ~7800 ppm. A tight cluster of three zircons with ages ca. 40 Ma and hafnium concentrations ~9000 ppm (Fig. 9) all occur within one sample from core depth 3755' and may represent a product of a single eruption; the large size and lack of rounding of these three zircons may indicate a proximal source. The conclusions that can be drawn from these associations are preliminary, at best, but they do suggest multiple source regions for the suite of Tertiary zircons present in this unit.

## DISCUSSION: PROVENANCE OF LATEST EOCENE TO OLIGOCENE SEDIMENTS

The lithology and detrital zircon analysis of the Steamboat Formation suggest both a main, proximal source with minor, more distant input from the east, increasing in influence towards the north.

### *Proximal source*

The immature sandstones of the Steamboat Formation and the predominantly volcanic clasts suggest a nearby volcanic source area, possibly as close as 20 km based on the presence of massive conglomerates (Smith, 1988), and most likely to the SSW based on paleocurrent indicators and thinning of the unit to the north. Currently, there are no rocks of Oligocene age exposed within 20-30 km of the southern Warner Mountains that might provide the volcanic source of this unit. Based purely on the age relationship and lithologic similarity of clasts, however, the South Willow Formation in the Granite Range approximately 50 km to the SE (Fig. 1) could be a source for this sedimentary sequence. The South Willow Formation is a volcanic unit consisting of mafic to intermediate flows and breccias that vary in composition from olivine basalt to dacite, with pyroxene andesite and hornblende andesite as the dominant rock types (Bonham, 1969). A K-Ar date of 32.3 ± 1.2 Ma on biotite from a dacite dike (recalculated from Bonham, 1969) overlaps the ages of dated tuffs in the Steamboat Formation. The South Willow Formation unconformably overlies a granitic pluton

dated using U-Pb geochronology on zircon at 102.7 ± 1.3 Ma (Nick van Buer, unpublished data). Seven zircons in all of the detrital samples and three cobbles – all from Granger Canyon – fall within error of this Cretaceous age, providing some support for the correlation between the South Willow and Steamboat Formations. Overall, however, the majority of volcanic detritus in the Steamboat Formation does not resemble the most common lithology in the South Willow Formation.

It is also a strong possibility that the original source volcano for this volcaniclastic deposit was either eroded away, buried under the mid-Miocene and younger volcanic rocks (Fig. 2), or some combination of both. If so, it is possible that this and the volcano associated with the South Willow Formation formed part of a roughly linear belt trending SW-NE, which shed sediments to the north and blocked input from farther south. One possible line of evidence supporting this claim is the presence of an enigmatic regional gravity low with a SW-NE trend that has proven challenging to model based on surface geology and seismic data (Fig. 1) (Blakely et al., 1997). It could be that this low reflects the extent of an extensional sedimentary basin formed during the Oligocene. Though speculative, an episode of N-S or NW-SE-directed extension during this time is also supported by the presence of E-W-oriented dikes in the Warner Range (Duffield et al., 1976). Though the dikes themselves are undated, they appear only in the lowermost Oligocene exposures and do not cut the younger late Oligocene or Mid-Miocene units at the top of the range, suggesting they were emplaced prior to ca. 26 Ma.

*Distal source*

This proximal source cannot account for all of the features in the data, however. The much larger Jurassic and Tertiary signals in the samples from the core suggest that this portion of the formation received more input from a different, more distant source. The ages of the Tertiary zircons suggest that this source may have been as far away as the modern Independence Mountains (Fig. 1). By removing 20-25% extension across most of the northern Basin and Range and 5% across the Sheldon Plateau, this suggests a drainage as long as 300 km.

Unfortunately, few rocks of the appropriate age remain in the intervening region to test this hypothesis. Instead, late Oligocene to middle Miocene volcanic rocks lie unconformably on Mesozoic basement throughout the region (Colgan et al., 2006; Van Buer et al., in press). It is possible that an Oligocene-age river system was incised into an elevated plateau, resulting in little deposition in the intervening region, or that these rivers flowed north around a topographic high, possibly generated by the southward sweep of magmatism in Nevada during the Tertiary (Dickinson, 2006).

## REGIONAL AND TECTONIC IMPLICATIONS

Despite the limited exposure of the Steamboat Formation, it does allow us to draw some tentative conclusions about the paleogeography of northeastern California and northwestern Nevada during the early Oligocene. Most fundamentally, this unit highlights the differences between the paleogeography at this latitude and the areas farther south and north at this time.

### *Late Eocene paleogeography (ca. 40-38 Ma, Fig. 10a)*

By the late Eocene, a river system that drained central Nevada directly west to the paleoshoreline (near the modern eastern edge of the Central Valley) had been established as far north as the northern Sierra Nevada (Cassel et al., this volume; Henry, 2008) and arc volcanism had long since ceased. In the northernmost Central Valley, the late Eocene-aged Montgomery Creek Formation records southward-directed paleocurrent indicators (Aalto, 1988) and contains detrital micas from the Idaho batholith (Renne et al., 1990). The lack of exposed Eocene sedimentary rocks in the intervening region limits our ability to further define the drainage system during this time, but there were clearly no significant topographic barriers to transport. In northwestern Nevada, 35-40 Ma lava flows fill erosional topography cut into Cretaceous granitic basement (Brueseke and Hart, 2008; Colgan et al., 2006; Lerch et al., 2008).

Farther north at this time, the deposition of the Clarno Formation in northern Oregon (Fig. 1) has been interpreted as an intra-arc alluvial deposit in a normal-fault-bounded basin developed in response to extension and rotation in a back-arc setting (White and Robinson, 1992). In the Warner Range, the minimally exposed McCulley Ranch Formation is presumed to be late Eocene in age (Axelrod, 1966; Myers, 2006), and records andesitic volcanism (Martz, 1970), consistent with an intra-arc setting.

*Latest Eocene to Early Oligocene (ca. 34-31 Ma, Fig. 10b)*

An erosional unconformity overlies the McCulley Ranch Formation in the Warner Range, indicating a hiatus in sedimentary deposition from 38-34 Ma. Based on fossil evidence, deposition of the overlying Steamboat Formation began ca. 34 Ma and continued until ca. 31 Ma, based on the ages of interbedded tuffs (Myers, 2006).

By the latest Eocene, it appears that an isolated, intra-arc basin had developed in the northeastern California. Unlike the Eocene Montgomery Creek Formation in the Central Valley, the Steamboat Formation received no input from the Idaho batholith to the north, and instead received sediment from the east, possibly via a system of drainages incised into a low-relief plateau. The southern margin of the basin was likely less than 50 km south of the current exposure, and was bordered on the southern margin by andesitic volcanoes that provided a source area for the majority of sediments to the basin. This basin occasionally was closed, forming a lake surrounded by ferns and *Metasequoia* (Myers, 2006), typical species of the warm, wet Eocene. Despite the evidence for basin formation, it is likely that the elevation of this region during the Oligocene was not too different from the modern elevation of 1.5 km, based on paleofloral analysis (Myers, 2003).

The most conservative interpretation is that the basin into which the Steamboat Formation was deposited was 50-60 km from south to north, and an unknown width that could be as little as 10-15 km from east to west – a size comparable to the modern Surprise Valley east of the Warner Range. It is possible, however that the exposure of the sedimentary sequence in the Warner Range is just a glimpse into a much larger

basin that trended SW-NE from just south of the Warner Range across northwestern Nevada, similar to the depositional environment of the Eocene Clarno Formation in Oregon (White and Robinson, 1992).

Regardless of the absolute extent of the basin, the paleogeography of this region during the latest Eocene and early Oligocene was clearly strongly influenced by the ongoing presence of arc volcanism and cannot be explained simply by drainage off of a high plateau, as appears to have been the case farther to the south.

**Acknowledgements**

The authors thank Marty Grove and Jim Wright for running one detrital sample on the LA-ICPMS at University of Arizona and Kathy Surpless for dating three cobbles from the core on the SHRIMP-RG. Marty Grove, Ariel Strickland, and Joe Wooden provided invaluable help running the remaining samples and reducing the data. Chris Henry and Joe Wooden provided timely reviews and discussions that greatly improved the manuscript.

## References

Aalto, K.R., 1988, Sedimentology of the Montgomery Creek Formation, Shasta County, California: California Geology, v. 41, p. 254-260.

Axelrod, D.I., 1966, Potassium-argon ages of some western Tertiary floras: American Journal of Science, v. 264, p. 497-506.

Black, L.P., Kamo, S.L., Allen, C.M., Davis, D.W., Aleinikoff, J.N., Valley, J.W., Mundil, R., Campbell, I.H., Korsch, R.J., Williams, I.S., and Foudoulis, C., 2004, Improved $^{206}Pb/^{238}U$ microprobe geochronology by the monitoring of a trace-element-related matrix effect; SHRIMP, ID-TIMS, ELA-ICP-MS and oxygen isotope documentation for a series of zircon standards: Chemical Geology, v. 205, p. 115-140.

Blakely, R.J., Christiansen, R.L., Guffanti, M.C., Wells, R.E., Donnelly-Nolan, J.M., Muffler, L.J.P., Clynne, M.A., and Smith, J.G., 1997, Gravity anomalies, Quaternary vents, and Quaternary faults in the southern Cascade Range, Oregon and California; implications for arc and backarc evolution: Journal of Geophysical Research, v. 102, p. 22,513-22,527.

Blakey, R.C., 1997, Paleogeographic evolution of the passive-margin to active-margin transition, early Mesozoic, western North America: Abstracts with Programs - Geological Society of America, v. 29, p. 202.

Bonham, H.F., 1969, Geology and mineral deposits of Washoe and Storey counties, Nevada, with a section on Industrial rock and mineral deposits by Keith G. Papke: Nevada Bureau of Mines, Bulletin, v. 70, p. 140.

Brooks, W.E., Thorman, C.H., and Snee, L.W., 1995, The $^{40}Ar/^{39}Ar$ ages and tectonic setting of the middle Eocene Northeast Nevada volcanic field: Journal of Geophysical Research, v. 100, p. 10,403-10,416.

Brueseke, M.E., and Hart, W.K., 2008, Geology and petrology of the mid-Miocene Santa Rosa-Calico volcanic field, northern Nevada: Bulletin - Nevada Bureau of Mines and Geology, v. 113, p. 83.

Carmichael, I.S.E., Lange, R.A., Hall, C.M., and Renne, P.R., 2006, Faulted and tilted Pliocene olivine-tholeiite lavas near Alturas, NE California, and their bearing on the uplift of the Warner Range: Geological Society of America Bulletin, v. 118, p. 1196-1211.

Cassel, E.J., Calvert, A.T., and Graham, S.A., 2009, Age, geochemical composition and distribution of Oligocene ignimbrites in the Northern Sierra Nevada, California: Implications for landscape morphology, elevation and drainage divide geography of the Nevada Plano: International Geology Review, this volume.

Chen, J.H., and Moore, J.G., 1982, Uranium-Lead Isotopic Ages from the Sierra Nevada Batholith, California: Journal of Geophysical Research, v. 87.

Colgan, J.P., Dumitru, T.A., Reiners, P.W., Wooden, J.L., and Miller, E.L., 2006, Cenozoic tectonic evolution of the Basin and Range Province in northwestern Nevada: American Journal of Science, v. 306, p. 616-654.

Costa, J.E., and Schuster, R.L., 1988, The formation and failure of natural dams: Geological Society of America Bulletin, v. 100, p. 1054-1068.

Dickinson, W.R., 2006, Geotectonic evolution of the Great Basin: Geosphere, v. 2, p. 353-368.

Duffield, W.A., and McKee, E.H., 1986, Geochronology, structure, and basin-range tectonism of the Warner Range, northeastern California: Geological Society of America Bulletin, v. 97, p. 142-146.

Duffield, W.A., Weldin, R.D., and Davis, W.E., 1976, Mineral resources of the South Warner Wilderness, Modoc County, California: U. S. Geological Survey Bulletin, v. B1385, p. 31.

Evernden, J.F., and Kistler, R.W., 1970, Chronology of emplacement of Mesozoic batholithic complexes in California and western Nevada: U. S. Geological Survey Professional Paper, v. P 0623, p. 42.

Haynes, S.R., 2003, Development of the Eocene Elko basin, northeastern Nevada: Implications for paleogeography and regional tectonism [M.S. thesis], The University of British Columbia.

Henry, C.D., 2008, Ash-flow tuffs and paleovalleys in northeastern Nevada: Implications for Eocene paleogeography and extension in the Sevier hinterland, northern Great Basin: Geosphere, v. 4, p. 1-35.

Henry, C.D., and Ressel, M.W., 2000, Interrelation of Eocene magmatism, extension, and carlin-type gold deposits in northeastern Nevada: GSA Field Guide, v. 2, p. 165-187.

Ireland, T.R., and Williams, I.S., 2003, Considerations in zircon geochronology by SIMS, *in* Hanchar, J.M., and Hoskin, P.W.O., eds., Zircon, Volume 53: Reviews in Mineralogy and Geochemistry, Mineralogical Society of America and Geochemical Society, p. 215-241.

Lerch, D.W., Klemperer, S.L., Glen, J.M.G., Ponce, D.A., Miller, E., and Colgan, J., 2007, Crustal structure of the northwestern Basin and Range Province and its transition to unextended volcanic plateaus: Geochemistry Geophysics Geosystems, v. 8, p. 1-21.

Lerch, D.W., Miller, E., McWilliams, M., and Colgan, J., 2008, Tectonic and magmatic evolution of the northwestern Basin and Range and its transition to unextended volcanic plateaus: Black Rock Range, Nevada: Geological Society of America Bulletin, v. 120, p. 300-311.

Ludwig, K.R., 2001, Squid: A users' manual: Berkeley Geochronology Center Special Publication, v. 2, p. 19.

—, 2003, Isoplot 3.00, a Geochronological Tool-kit for Excel: Berkeley Geochronology Center Special Publication, v. 4, p. 67.

Martz, P.W., 1970, The geology of a portion of the northern Warner mountains, Modoc County, California [MS thesis]: Davis, CA, University of California at Davis.

Miall, A.D., 1977, A review of the braided-river depositional environment: Earth-Science Reviews, v. 13, p. 1-62.

Myers, J.A., 1998, Paleovegetational heterogeneity and the record of Eocene-Oligocene climate change in the interior Pacific Northwest [PhD thesis]: Santa Barbara, CA, University of California at Santa Barbara

—, 2003, Terrestrial Eocene-Oligocene vegetation and climate in the Pacific Northwest: New York, NY, Columbia University Press, 171-185 p.

—, 2006, The latest Eocene Badger's Nose flora of the Warner Mountains northeast California; the "in between" flora: PaleoBios, v. 26, p. 11-29.

Renne, P.R., Becker, T.A., Swapp, S.M., and Higinbotham, L., 1990, $^{40}Ar/^{39}Ar$ laser-probe dating of detrital micas from the Montgomery Creek Formation, northern California:Clues to provenance, tectonics, and weathering processes: Geology, v. 18, p. 563-566.

Ressel, M.W., and Henry, C.D., 2006, Igneous Geology of the Carlin Trend, Nevada: Development of the Eocene Plutonic Complex and Significance for Carlin-Type Gold Deposits: Economic Geology, v. 101, p. 347-383.

Russell, R.J., 1928, Basin Range structure and stratigraphy of the Warner Range, northeastern California: University of California Publications in Geological Sciences, v. 17, p. 387-496.

Smith, G.A., 1988, Sedimentology of proximal to distal volcaniclastics dispersed across an active foldbelt: Ellensburg Formation (late Miocene), central Washington: Sedimentology, v. 35, p. 953-977.

Stacey, J.S., and Kramers, J.D., 1975, Approximation of terrestrial lead isotope evolution by a two-stage model: Earth and Planetary Science Letters, v. 26, p. 207-221.

Stern, T.W., Bateman, P.C., Morgan, B.A., Newell, M.F., and Peck, D.L., 1981, Isotopic U-Pb ages of zircon from the granitoids of the central Sierra Nevada, California: U. S. Geological Survey Professional Paper, v. P 1185, p. 17.

Van Buer, N.J., Miller, E.L., and Dumitru, T.A., 2009, Early Tertiary paleogeologic map of the northern Sierra Nevada Batholith and the northwestern Basin and Range: Geology.

White, J.D.L., and Robinson, P.T., 1992, Intra-arc sedimentation in a low-lying marginal arc, Eocene Clarno Formation, central Oregon: Sedimentary Geology, v. 80, p. 89-114.

Wyld, S.J., and Wright, J.E., 1997, Triassic-Jurassic tectonism and magmatism in the Mesozoic continental arc of Nevada: Classic relations and new developments, *in* Link, P.K., and Kowallis, B.J., eds., Proterozoic to Recent Stratigraphy, Tectonics, and Volcanology, Utah, Nevada, Southern Idaho and Central Mexico: Geological Society of America Field Trip Guide Book, Volume 42, Brigham Young University Geology Studies, p. 197-224.

—, 2001, New evidence for Cretaceous strike-slip faulting in the United States Cordillera and implications for terrane-displacement, deformation patterns, and plutonism: American Journal of Science, v. 301, p. 150-181.

# Figures

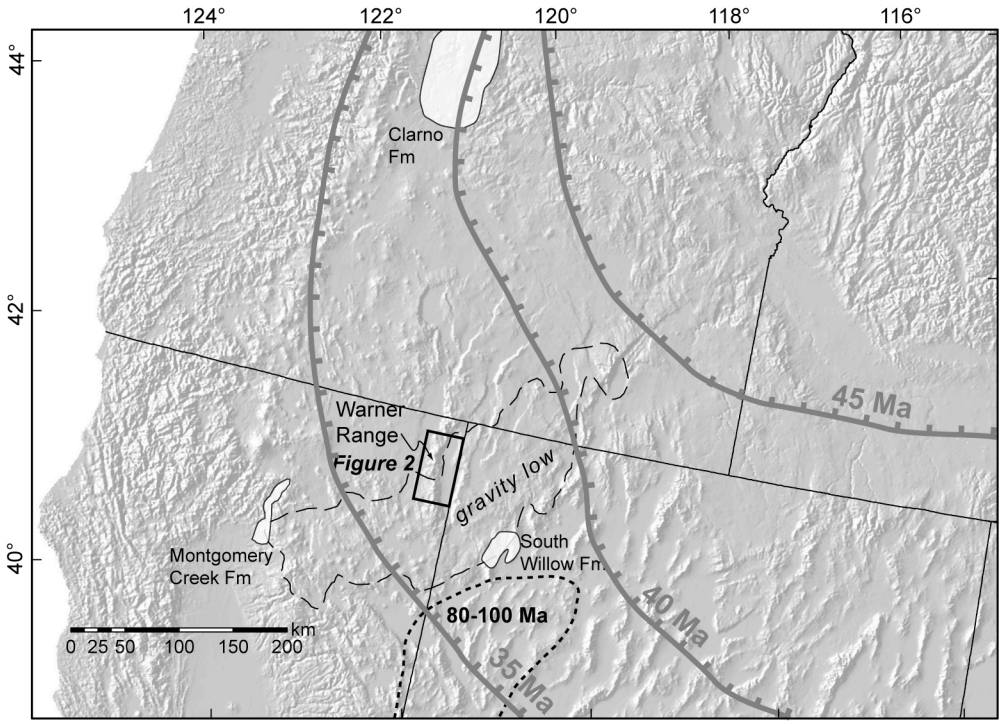


**Figure 1.** Shaded relief map of the northwestern Basin and Range and Pacific Northwest, showing locations of the study area with respect to exposures of Eocene and Oligocene sedimentary rocks and 80-100 Ma plutonic rocks. Tertiary magmatic sweeps from Dickinson (2006). Outline of gravity low from Blakely et al. (1997). See text for explanation.

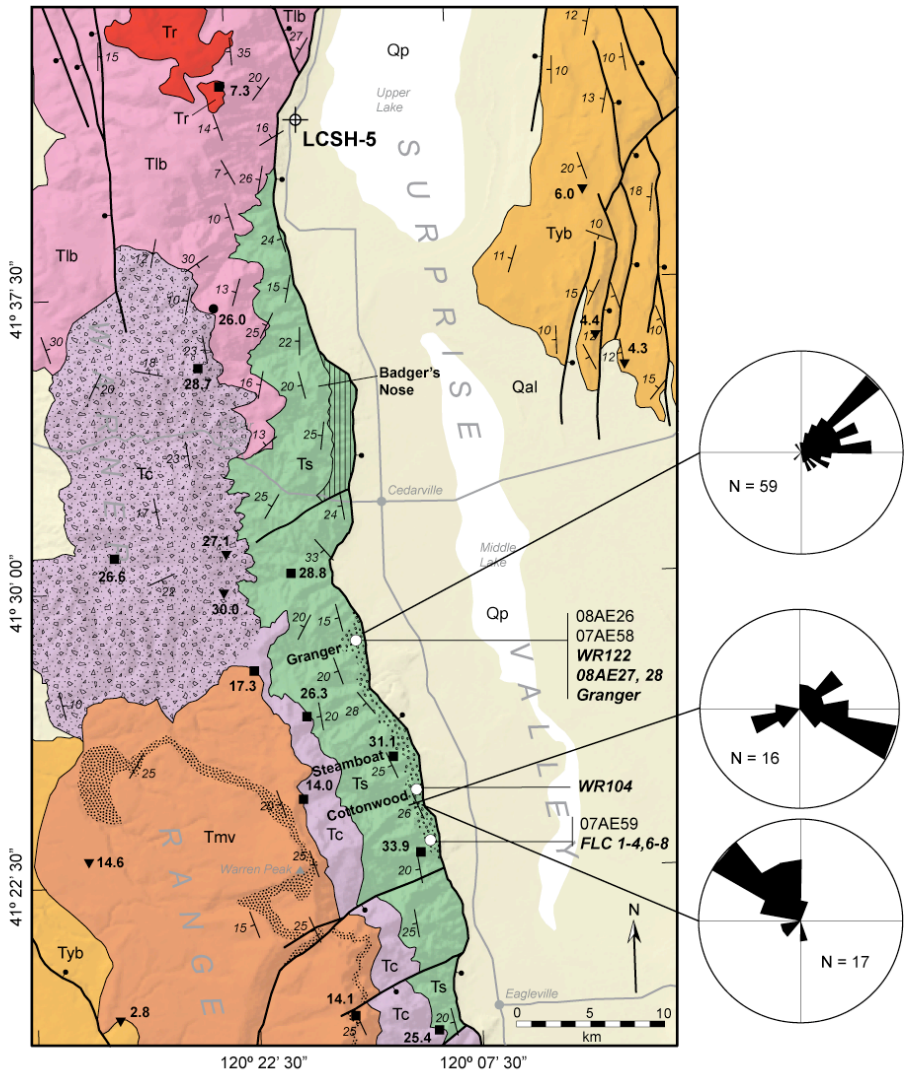


**Figure 2.** Geologic map of the study area, including sample localities and paleocurrent measurements.

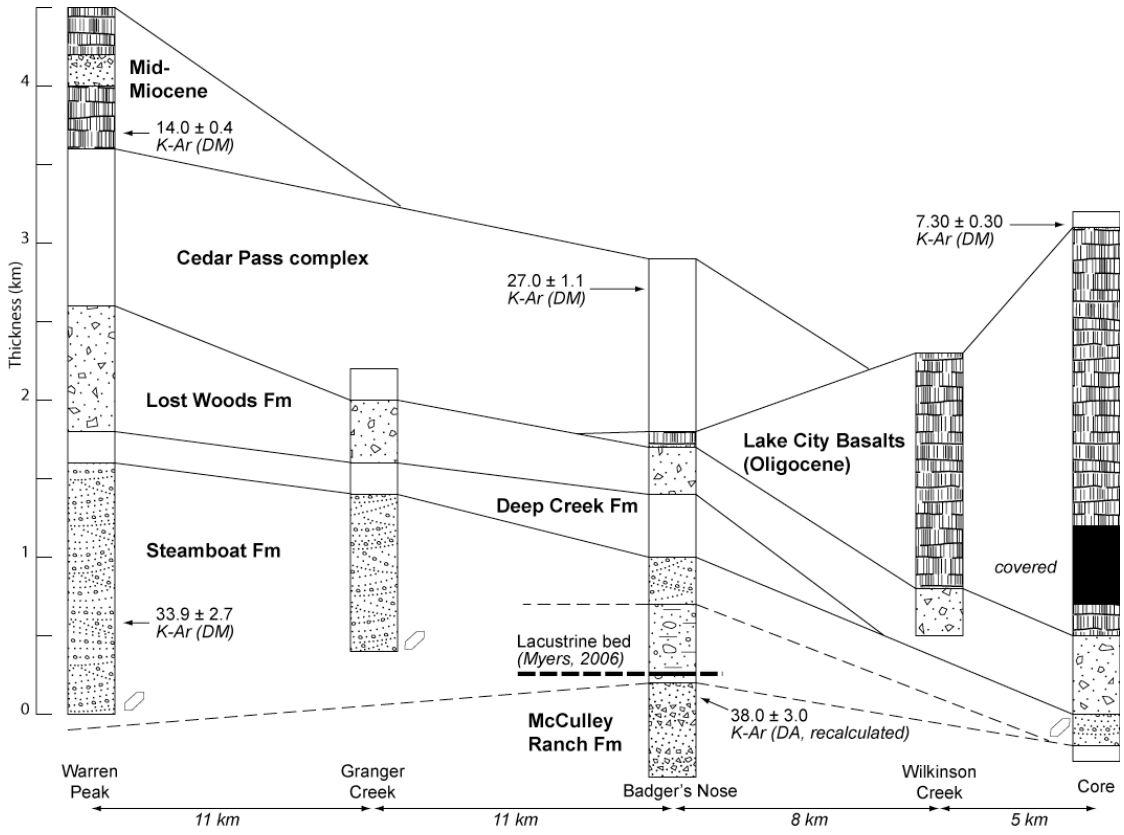


**Figure 3.** Correlated stratigraphic columns from four sections that correspond with three exposed sequences in the range and finally in the core. Age data from DM (Duffield and McKee, 1986) and DA (Axelrod, 1966). Locations shown on Figure 2. Sections span ca. 35 km, show decrease in thickness from ~900 m in south to ~200 m in core. Relative stratigraphic location of detrital samples and cobbles shown. See Figure 5 for detailed lithology of the core.

**Figure 4.** (explanation follows)

**(a)**

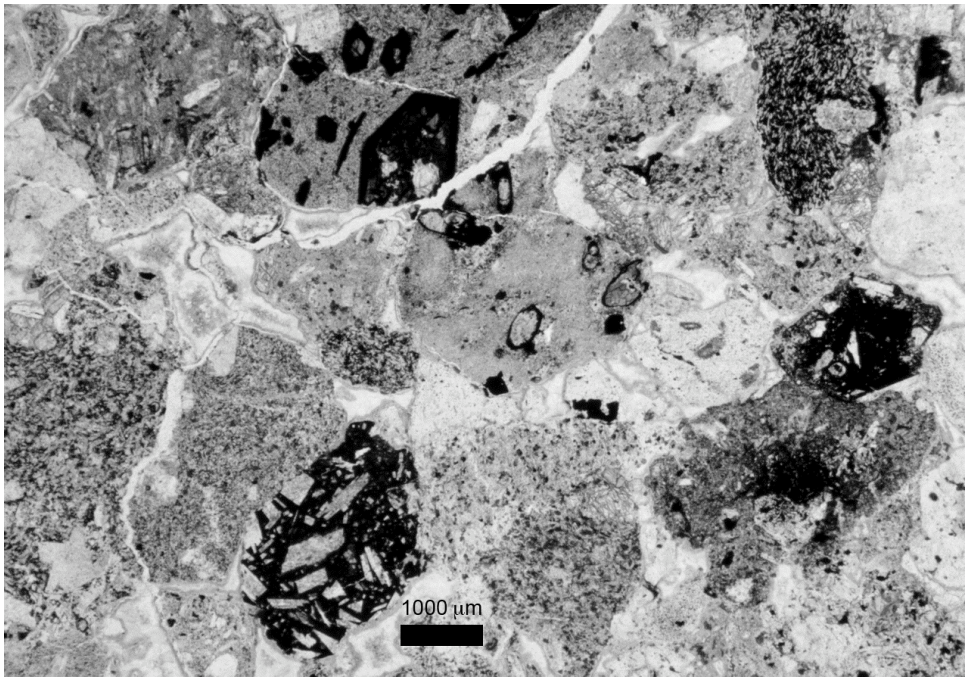


**(b)**

**(c)**

**Figure 4.** Outcrop photos and photomicrographs of the Steamboat Formation. (a) Typical outcrop showing interbedded coarse sandstone and conglomerate near the mouth of Granger Creek. (b) Photomicrograph of coarse sandstone shown in 4a, from sample WR07AE59. Scale bar is 1000 microns. (c) Debris flow filling channel cut into then-flat-lying tuffs and fine-grained sandstones.

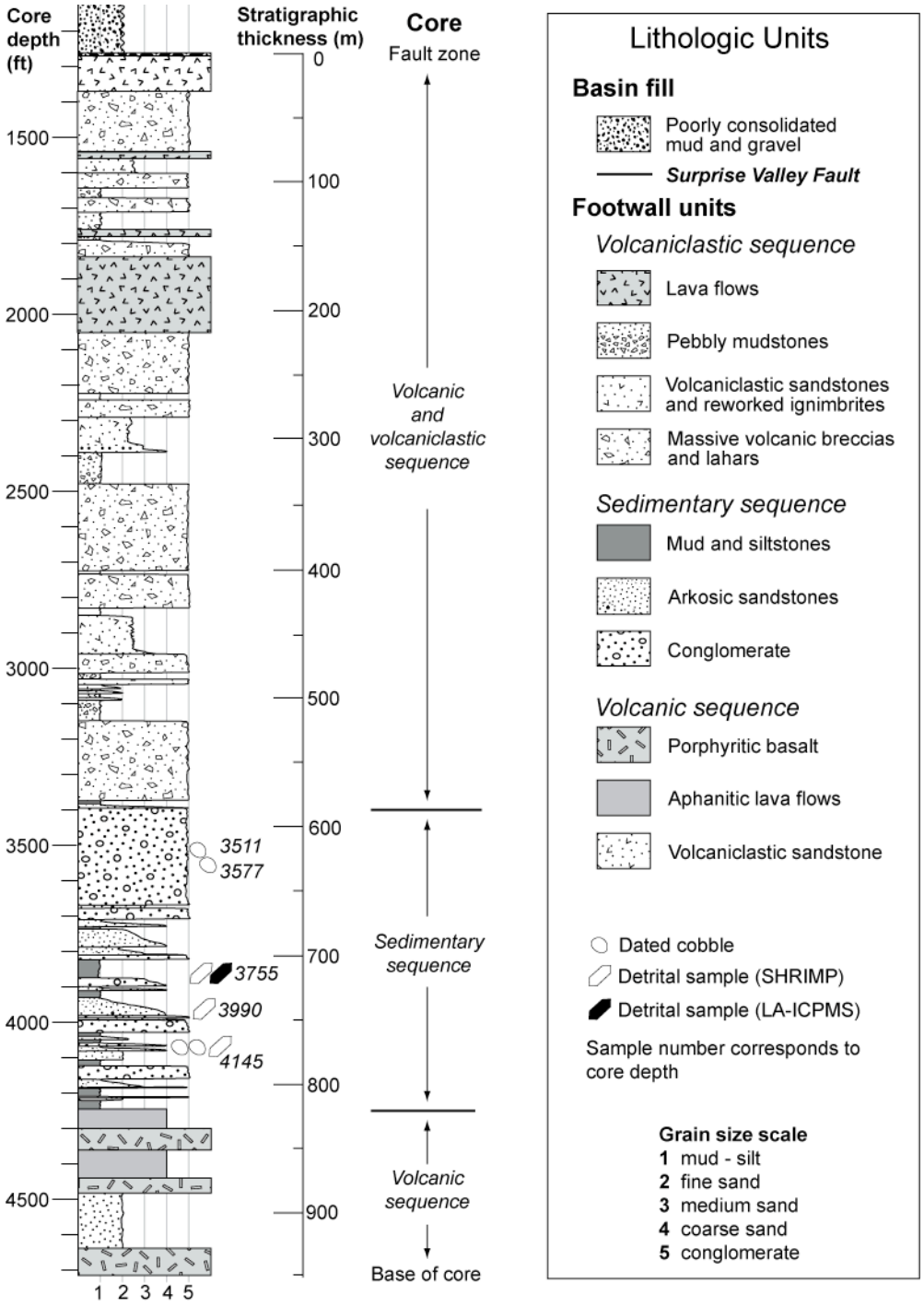


**Figure 5.** Detailed lithologic log of the LCHS-5 core (see Figure 2 for location). The scale on the left indicates drill depth of the core in feet, which corresponds with our sample numbers. The scale on the right indicates stratigraphic depth in meters, corrected for an average 25° dip measured on several bedding planes visible in the core samples.

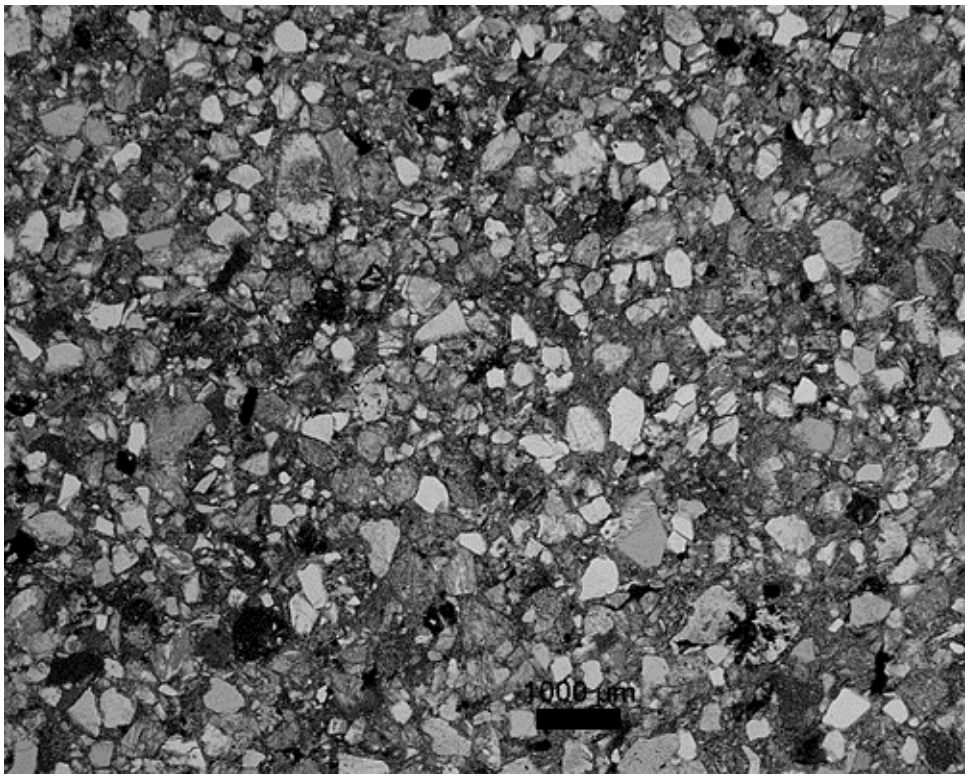


**Figure 6.** Photomicrograph of sandstone in the core at depth 3990'. Scale bar is 1000 microns.

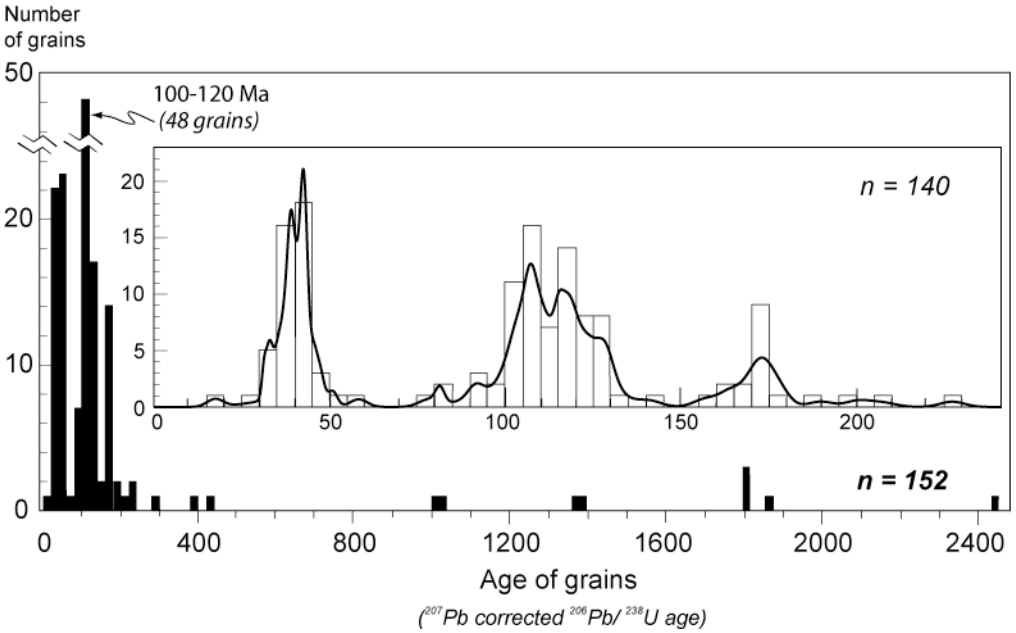


**Figure 7.** All detrital zircon data. Large graph shows all data in 20 million year bins, inset graph only includes grains younger than 250 Ma in 5 million year bins. See Figure 2 for location of samples in the range and Figure 5 for depth in core.

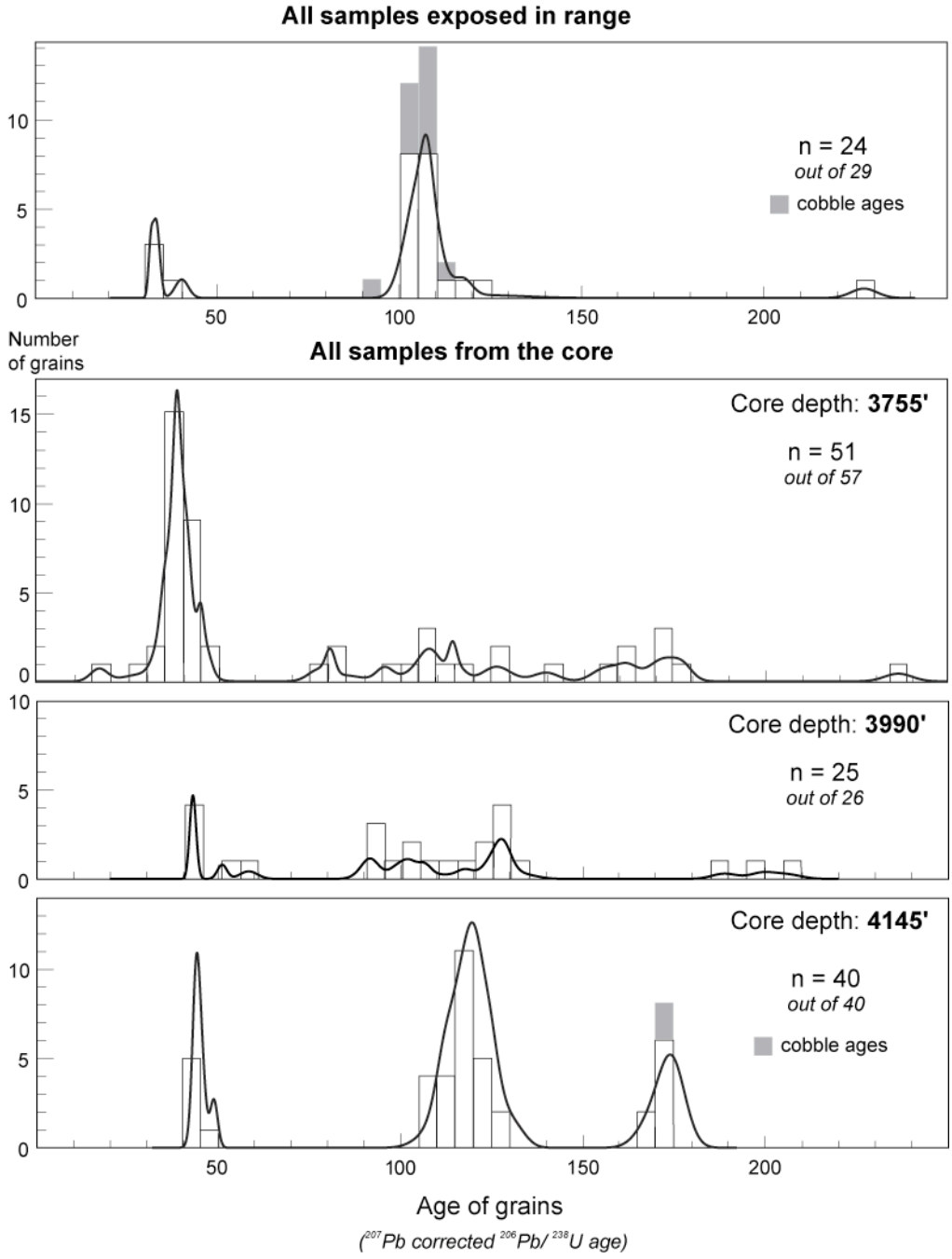


**Figure 8.** Detrital zircon data by location and stratigraphic level in core, limited to 0-250 Ma age range and shown in 5 Ma bins. Cobble ages are shown in gray in appropriate bins. See text for interpretation.

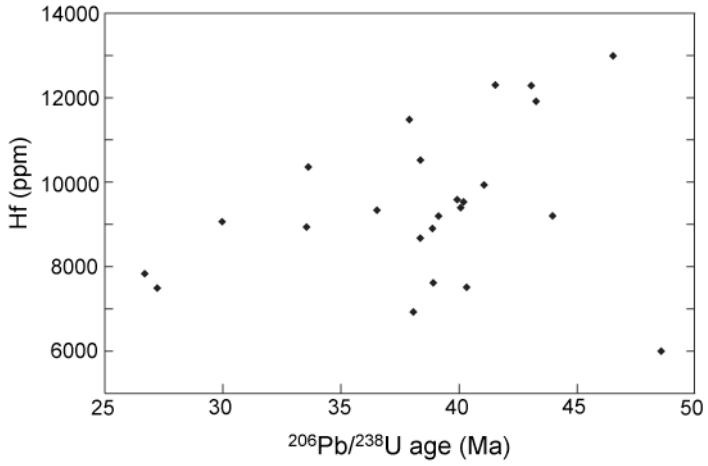


**Figure 9.** Hafnium concentration plotted vs. age for all Tertiary zircons dated using the SHRIMP-RG.

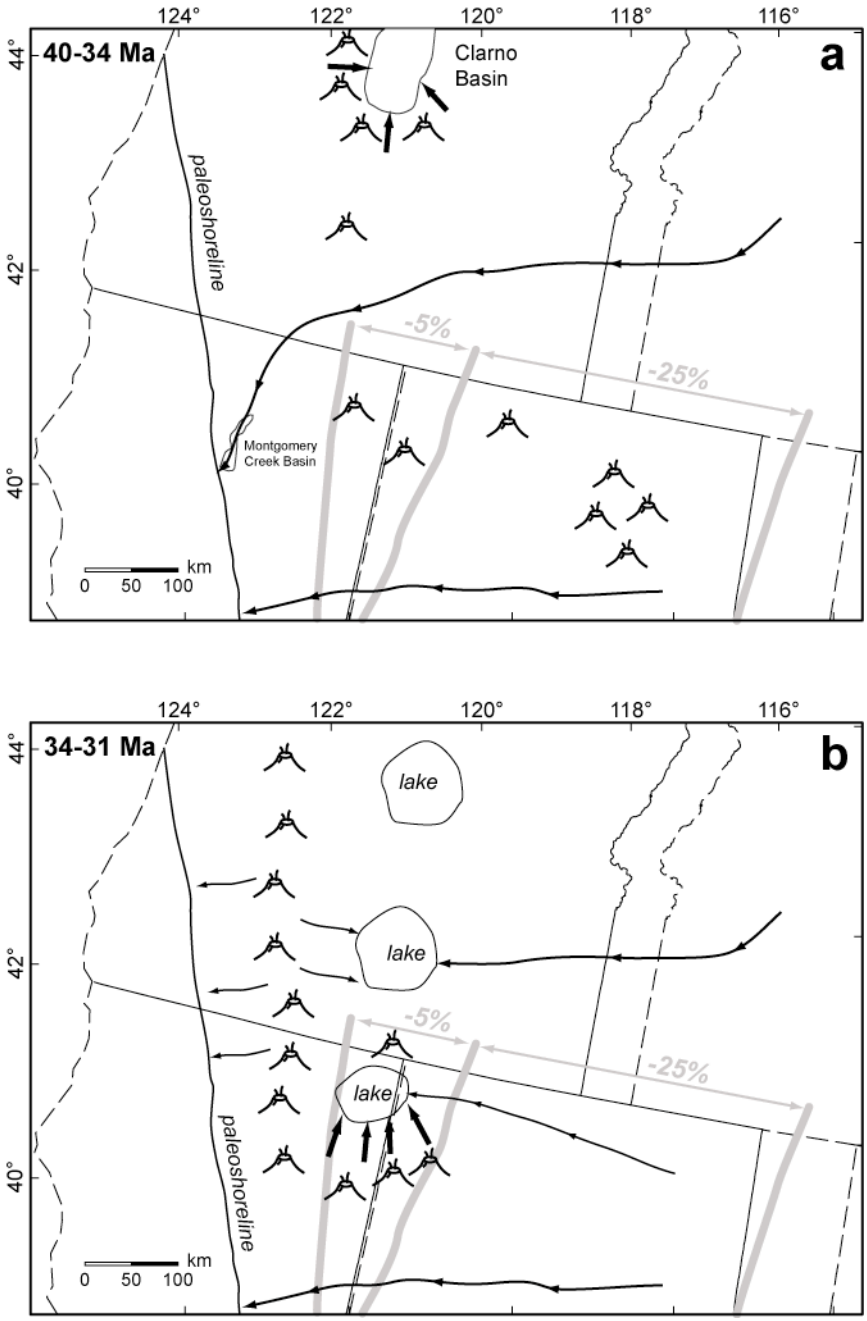


**Figure 10.** Paleogeographic reconstructions of the region based on detrital zircon data and paleocurrent indicators from this study combined with regional data as discussed in the text. Area shown is the same as in Figure 1; approximate locations of correlative formations and Cretaceous batholith discussed in text are shown. The area of Figure 2 (study area) is indicated by small box for reference. Dashed lines indicate location of modern shoreline and state boundaries; solid lines indicate paleoshoreline (based on Blakey, 1997) and approximate location of state boundaries with Miocene and younger extension removed; the percentage of extension removed is shown in gray (Lerch et al., 2007). Arrows indicate drainage direction. (a) Paleogeographic setting of the region during the late Eocene, ca. 40-38 Ma. (2) Paleogeographic setting of the region during the latest Eocene – early Oligocene, ca. 34-31 Ma.

## Tables

<table>
<tr><th>Russell (1928)</th><th>Martz (1970)</th><th>Duffield and Weldin (1976)</th><th>Myers (1998)</th><th>This study, Fig. 2</th></tr>
<tr><td rowspan="6">Lower Cedarville Formation</td><td>Lost Woods Fm</td><td rowspan="4">Ts (Oligocene sedimentary rocks)</td><td>Lost Woods Fm</td><td>Ts</td></tr>
<tr><td>Deep Creek Fm</td><td>Deep Creek Fm</td><td>Ts</td></tr>
<tr><td>Steamboat Fm - Cougar Cliffs</td><td>Badger's Nose 3</td><td rowspan="3">Ts - Steamboat Formation</td></tr>
<tr><td rowspan="2">Steamboat Fm - Badger Nose</td><td>Badger's Nose 2</td></tr>
<tr><td>Badger's Nose 1</td></tr>
<tr><td>unconformity</td><td rowspan="2">not exposed</td><td>unconformity</td><td>unconformity</td></tr>
<tr><td>McCulley Ranch</td><td>McCulley Ranch</td><td>McCulley Ranch</td></tr>
</table>

**Table 1.** Names of formations used by different authors in the Warner Range.

| Sample number | Location | n[1] | Mean age ($^{206}Pb/^{238}U$)[2] | Error (95% conf) | MSWD[3] | Probability |
|---|---|---|---|---|---|---|
| Granger | Granger | 5 (7) | **93.8** | ± 2.2 | 1.18 | 0.32 |
| WR122 | Granger | 6 | **103.7** | ± 1.5 | 0.89 | 0.49 |
| WR08AE28 | Granger | 6 | **103.9** | ± 2.4 | 1.00 | 0.42 |
| WR08AE27 | Granger | 6 | **104.4** | ± 3.8 | 3.42 | 0.00 |
| FLC 6 | unnamed canyon | 6 | **105.3** | ± 1.2 | 1.02 | 0.41 |
| FLC 7 | unnamed canyon | 6 | **106.5** | ± 1.1 | 1.00 | 0.42 |
| FLC 1 | unnamed canyon | 5 (6) | **107.3** | ± 1.1 | 1.88 | 0.11 |
| FLC 8 | unnamed canyon | 5 (6) | **107.7** | ± 1.2 | 0.61 | 0.66 |
| FLC 2 | unnamed canyon | 4 (6) | **108.6** | ± 1.5 | 0.96 | 0.41 |
| FLC 4 | unnamed canyon | 4 (6) | **108.7** | ± 1.9 | 0.75 | 0.52 |
| WR104 | Cottonwood | 6 | **109.5** | ± 1.0 | 1.18 | 0.31 |
| FLC 3 (NN) | unnamed canyon | 4 (6) | **110.2** | ± 1.7 | 0.07 | 0.98 |
| 3511 | core | 8 (9) | **111.7** | ± 1.1 | 0.78 | 0.61 |
| 3577 | core | 9 | **113.7** | ± 1.1 | 1.31 | 0.23 |
| 4145gc | core | 5 | **168.0** | ± 1.8 | 0.05 | 0.99 |
| 4145 | core | 8 (9) | **170.7** | ± 2.0 | 1.74 | 0.89 |

[1] n is number of grains used to calculate age, the total number of grains analyzed is in parentheses
[2] $^{207}Pb$ corrected
[3] Mean square weighted deviate

**Table 2.** Zircon U-Pb ages of granite cobbles. Cobbles are listed by age. See Figure 2 for location of samples in the range and Figure 5 for depth in core.

# Chapter 3

## The northwestern margin of the Basin and Range Province: Structural setting of a developing basin from seismic and potential field data

**ABSTRACT**

Surprise Valley in northeastern California offers an ideal opportunity to examine the structural setting of a developing extensional basin due to its late Miocene to recent activity in isolation from other major normal fault-bound basins. Seismic velocity and potential field modeling help determine the nature of basin fill and identify intra-basin faults. Based on a detailed gravity and magnetic profile, we identify shallow subsurface basalt flows and several faults within the valley that may accommodate hundreds of meters of vertical offset, possibly cutting and offsetting the ~30° east-dipping Surprise Valley fault that rotated during footwall tilting of the adjacent Warner Mountains. Some of these intra-basin faults correspond with mapped Quaternary fault scarps, but others have no surface expression. These faults may represent the currently active fault system within the basin. If so, they would indicate that basin development is transitioning away from the main range front normal fault to a new set of steep intra-basin faults that are more favorable for accommodating regional transtensional strain.

## INTRODUCTION

Along the northwestern margin of the Basin and Range province, normal faulting is encroaching on the largely unextended Modoc Plateau (Fig. 1). The Surprise Valley fault (SVF) is the westernmost large-offset normal fault in the northwestern Basin and Range, and it is isolated from other large-offset faults to the east by the ~90 km-wide Sheldon Plateau (Fig. 1). The SVF may have been active as early as 12 Ma (Colgan et al., 2008b), and the presence of Quaternary fault scarps and an active geothermal system suggest that it is still active today. Thus, the Surprise Valley fault and associated structures provide an excellent opportunity to study the evolution of continental extension and normal faulting.

Like many faults in the Basin and Range province that are considered active, however, the SVF has not experienced historical seismicity. Detailed geodetic data can provide some constraints on fault motion in seismically inactive regions (e.g. Friedrich et al., 2004), but the data available for the Surprise Valley are widely spaced (Hammond and Thatcher, 2005). Such data have also proven misleading in other parts of the Basin and Range when compared with geological measures of extension (e.g. Oskin et al., 2008). Paleoseismic trenching has discerned earthquake recurrence intervals along nearby Basin and Range normal faults such as the Southern Steens fault zone in northern Nevada (Personius et al., 2007b), allowing calculation of a slip rate, but similar trenching along the Santa Rosa Range fault zone yielded ambiguous results due in part to the presence of multiple fault strands (Personius and Mahan, 2005). Recent activity and slip histories can also be inferred from calculations of diffusion erosion rates of degraded fault scarps (e.g. Lee et al., 2001), but in Surprise Valley, some recent fault scarps may be buried under lake sediments or heavily modified by wave action of the long-lived pluvial lake (Reheis, 1999). Given these constraints, geophysical mapping and modeling of seismic, gravity, and magnetic data lend critical insight into the nature of structures at depth, revealing structures that do not have surface expression, and may also help resolve likely fault interactions, constraining the nature of faults and their sense of slip. These techniques have proved useful in illuminating subsurface

structures and rock units in other valleys of the Basin and Range, including the Crater flat region (Brocher et al., 1998) and Dixie Valley (Blackwell et al., 2002).

The comparison with Dixie Valley is particularly apt given the presence of a geothermal system: in Surprise Valley, subsurface structures appear to play a particularly important role in the location of hot springs. In the present study, seismic velocity and potential field modeling are used to resolve the subsurface geometry of major basin-bounding faults, to identify and describe the nature of intra-basin faults, and ultimately to compare different scenarios of basin evolution. Our geophysical modeling, combined with geologic mapping, seismic reflection data, and potential field mapping suggest that the Surprise Valley fault may currently be in transition from a single, large-offset normal fault to a more intra-basinal system consisting of an array of smaller-offset normal faults.

## GEOLOGIC SETTING

Surprise Valley straddles the California-Nevada border, stretching about 100 km south from the Oregon border (Fig. 1). The Surprise Valley fault (SVF) separates the valley from the Warner Range to the west, which exposes a thick series of Eocene (?) to late Miocene sedimentary and volcanic rocks (Fig. 2) (Colgan et al., 2008a; Duffield and McKee, 1986; Fosdick et al., 2005). These rock units display significant variability in thickness along strike. For example, the Oligocene Lake City basalt (Tlb in Figure 2) pinches out completely from an exposed thickness of >1 km over a distance of approximately 10 km. Near the study area, these rocks have been tilted approximately 20° westward by motion along the SVF (Fig. 2). On the eastern side of the valley, low-lying ridges of 4-8 Ma basalts (Carmichael et al., 2006) dip more gently (10-15°) westward into the basin. These younger basalts are not present at the crest of the Warner Range. The lateral discontinuity of units in this region make determination of fault offset difficult, but estimates range from 3.6 km of vertical offset (Duffield and McKee, 1986) to as much as 8 km (Fosdick et al., 2005).

Like many normal faults, the SVF has a corrugated, curvilinear trace and the range front makes several abrupt steps along its length (Fig. 2). A particularly prominent step occurs at the boundary between the Cedarville and Lake City segments where the SVF changes strike abruptly by ~45° and the number of Quaternary fault scarps increases (Fig. 2). This region resembles a segment boundary (as defined by Zhang et al., 1991) or accommodation zone (e.g., Faulds and Varga, 1998), as it coincides with an abrupt widening of the valley to the south, a large number of small-offset faults that cut the young basalts (Fig. 2), and a topographic high separating the upper and middle playa lakes in the valley, remnants of a Pleistocene pluvial lake that reached a depth of ~500' (Reheis, 1999). Within the topographic high, a wide zone of faults and fractures that has been previously mapped by Hedel (1984) as the Lake City Fault Zone (LCFZ) cuts northwestward across the valley (Fig. 2). The nature and origin of the LCFZ are enigmatic, though geophysical studies suggest that it accommodates little vertical offset (Glen et al., 2008; Griscom and Conradi, 1976; Hedel, 1984). Regionally, the LCFZ shares a NW-SE trend with Fandango Valley (Fig. 2) and the Brothers and Eugene-Denio Fault Zones in Oregon (Fig. 1), both of which have been shown to accommodate oblique right-lateral slip (Crider, 2001).

The LCFZ is closely associated with the Surprise Valley geothermal system, the object of periodic exploration since a spectacular mud-volcano eruption near the Lake City hot springs in 1951 (LC in Figure 2) (White, 1955). While this association of structures and geothermal activity has long been recognized (Benoit et al., 2004; Hedel, 1981), the details of the interactions between the LCFZ, the Surprise Valley fault, and other N-S-trending structures have proven difficult to incorporate into a geothermal and hydrological model. In fact, the majority of springs in Surprise Valley do not occur along either the LCFZ or the SVF, and instead are offset basinward from faults on both the east and west margins of the valley (Fig. 2). Some springs occur along mapped Quaternary fault scarps, but many do not – particularly the geothermal springs (Fig. 2). Renewed exploration, including drilling near Lake City in 2005 conducted by Amp Resources (Benoit et al., 2005; Miller et al., 2005), a magneto-telluric survey of the same region by Enel-North America (Andrew Rael, pers. comm.,

2008), and investigation into He-isotopes in spring waters (Barker et al., 2005) have all sought to better characterize this geothermal system and its relation to surface and subsurface structures. Measured $^{3}He/^{4}He$ ratios also provide insight into the basin-scale interactions between structures. In general, higher values represent a larger mantle component to the fluids, while lower values represent greater crustal contribution and/or residence time in the crust (Kennedy and van Soest, 2006). The ratios measured in geothermal waters near Fort Bidwell are markedly higher than those seen in springs that fall along the LCFZ (Barker et al., 2005), suggesting that the LCFZ may provide lateral permeability that does not occur along the range-front fault, allowing waters to circulate and mix in the crust for longer periods of time.

A seismic reflection profile was collected across the valley in 2004 (Fig. 2) (Lerch et al., 2008). In the reflection profile, the most prominent reflector is a gently-dipping feature on the western side of the valley, presumed to be the Surprise Valley fault (see Lerch et al., 2009). When corrected for apparent dip related to crossing the fault at an oblique angle, this reflector indicates a fault dipping approximately 30° to the east – a relatively shallow dip for an active range-bounding normal fault. In contrast, a paleoseismic trench located 3.8 km south of the seismic reflection profile (Fig. 2) revealed a normal fault dipping 68° to the east, cutting and offsetting fine-grained lake sediments (Personius et al., 2007a). No single unit could be tied across the fault, but an ash that correlates with the 7630-year-old ash from the Mt. Mazama eruption in the Oregon Cascades was exposed in the hangingwall, providing a minimum offset and displacement of ~1 mm/yr. It is possible that the 68° fault observed in the trench is a listric splay of the Cedarville segment of the SVF, which shallows to ~30° at depth (e.g. Axen et al., 1999). Another possible interpretation is that the steeper fault exposed in the trench cuts the gently dipping fault imaged in the seismic profile. These two possible interpretations lead to different conclusions about both the geothermal system and the seismic hazard potential for the valley. The geophysical methods applied here may help distinguish between these two interpretations where detailed surface mapping cannot.

## DATA COLLECTION METHODS

We used a combination of seismic velocity and potential field modeling to better constrain the present geometry of the range-bounding fault system and to define the offsets and significance of the faults mapped within Surprise Valley. Seismic velocity modeling can constrain the depth of a basin and identify abrupt changes in velocity that create reflections indicative of lithologic contacts. Variations in gravity and magnetics occur due to lateral contrasts in rock density and magnetic properties (induced and remanent magnetizations), respectively. The shape, depth, and rock properties associated with a source all determine the character of its potential field anomaly. As a result, the combination of seismic and potential field data can be used to resolve the geometry of known or concealed features, particularly when combined with other geologic constraints provided by the regional tectonic setting and surface geologic mapping. A series of detailed transects of ground-based magnetometer data and closely-spaced gravity data were collected (Glen et al., 2008) and digitized (from Griscom and Conradi, 1976) in order to perform joint gravity and magnetic modeling and interpretation. One of these transects was along the high-resolution seismic reflection line described by Lerch et al. (2009) (Figs. 2, 3). These detailed transects were combined with regional gravity and magnetic field data (Ponce et al., 2009).

### *Gravity data*

Gravity data were compiled from a variety of sources (Griscom and Conradi, 1976; Snyder et al., 1981; Ponce, 1997; Tilden, 2005; Plouff, 1977; PACES gravity data at http://paces.geo.utep.edu/, 2008; Ponce et al., 2009). In addition, we collected 793 new gravity stations to provide roughly 1 km regional station-spacing in the valley, 1-2 km spacing in the ranges, and 100-500 m spacing along several detailed transects that cross the valley (Fig. 3b). All gravity data collected for this study were tied to a primary base station in Alturas, California (Jablonski, 1974).

New data were reduced using standard gravity methods that include: earth-tide, instrument drift, latitude, free-air, simple Bouguer, curvature, terrain, and isostatic corrections (Blakely, 1995) to yield isostatic anomalies. Regional data were corrected

from observed gravity values to the same datum and using the same reduction parameters as our new data. The gravity map and profile derived from these data (Figs. 3a, 4) reflects anomalies produced by lateral variations in crustal density. Maximum horizontal gradients (MHG) in gravity were calculated, following the technique of Blakely (1995), to aid in identification of these contrasts (Fig. 3a). Because MHG tend to lie over near-vertical boundaries representing prominent rock-property contrasts, they are useful in estimating the extent of rock units and locating faults with vertical offset.

*Magnetic data*

Sources of magnetic data employed in this study include a high-resolution aeromagnetic survey of the LCFZ-area and a truck-towed magnetometer profile (USGS, 1981; Kucks et al., 2006; Ponce et al., 2009). The high-resolution survey (see Fig. 3b for area covered) was flown at an elevation of 122 m above ground with flight lines oriented north-northeast and spaced 1/4 mile apart (survey 81-997; USGS, 1981). Data from this survey were derived from digitized contours of the original survey maps. Ground-magnetic measurements were collected using a truck-towed cesium-vapor magnetometer across the valley (Fig. 3). A centrally located portable proton-precession base-station magnetometer was used to record diurnal variations of the Earth's magnetic field during the survey. The data were corrected for the diurnal variations, and filtered to remove cultural noise such as passing cars, culverts, fences, and power lines. The map and profile derived from these data (Figs. 3b, 4) therefore reflect variations in the magnetic field that arise largely from contrasts in rock magnetic properties attributable to a number of different causes including depths to the magnetic sources, crustal structures juxtaposing different rock types, metamorphism and alteration, variations in remanent magnetization, and variations in the concentration and type of magnetic minerals within rock units.

## FEATURES OF POTENTIAL FIELD DATA

The focus of this work is on features identified in profiles along the model transect (Fig. 4), but regional and high-resolution gravity and magnetic maps were useful in

identifying the lateral extent and character of anomalies away from the transect, an important component of interpreting the nature of sources from which anomalies arise, and critical to modeling features off-axis to the transect. The most prominent features in the gravity map (Fig. 3a) include a broad gravity low occupying the valley, reflecting low-density alluvial and volcanic basin-fill deposits, and a broad gravity high over exposed or inferred mafic volcanic units in the Warner Mountains and along the western margin of the valley floor. Situated between these two features is a moderate-to-steep gravity gradient that occurs along the Surprise Valley Fault. The most prominent feature in the magnetic field map is a low that occurs within the central part of the valley (Fig. 3b). Magnetic highs flanking this low along the margins of the basin (a, b, and c in Fig. 3b) do not correspond with surficial features, and thus are inferred to represent the presence of highly magnetic mafic rocks in the underlying volcanic basement and thin basalt flows interbedded with the basin sediments. Smaller magnetic lows may represent mafic igneous units that are reversely magnetized or rocks that have undergone hydrothermal alteration that has destroyed or alter magnetic minerals (d in Fig. 3b).

The prominent gravity and magnetic highs on the west side of the valley are also, not surprisingly, the most conspicuous features along the model transect (Fig. 4). These appear as broad, eastward-decreasing ramps, largely coincident with each other, that drop from highs in the west to lows in the central portion of the valley. The gravity profile drops over 6 km to the lowest values observed along the profile, marking what is interpreted to be the deepest part of the basin (Fig. 4). The amplitude and frequency content of this feature suggest that it is caused in large degree by rocks at depth, typical of the gradients seen at other large-offset normal faults in the Basin and Range (e.g. Okaya and Thompson, 1985; Pakiser and Kane, 1965). Not even the most prominent fault scarp (Fig. 4, black triangle) is represented by any significant change in the gravity profile. In contrast, a series of small amplitude, high-frequency magnetic anomalies, superimposed on the magnetic ramp, do suggest the presence of some shallow magnetic sources. The most prominent of these occurs at the eastern terminus of the ramp where the field gradient changes abruptly (Fig. 4, feature 1). This feature

lies within the basin, east of the surface trace of the SVF, and, corresponds with a zone of fault scarps and springs (Fig. 2).

A second feature of interest is a coincident minor gravity high and magnetic low at 8.5 km (Fig. 4, feature 2). This feature is proximal to several major hot springs on the east side of the valley as well as the inferred southeastern extension of the Lake City Fault Zone (Figs. 3a and b). The low in the magnetic profile is part of a narrow, elongate E-W-trending magnetic low that can be seen in map view (Fig. 3b). At the eastern extent of this low, basalt flows are exposed at the surface. Results from our preliminary paleomagnetic study of samples taken from these flows in the vicinity of the magnetic low indicate that they are reversely magnetized – a fact that appears to account for the low in the potential field model (see discussion below). The corresponding minor gravity high is associated with a series of MHGs in the gravity data (Fig. 3a) that trend N-S, nearly perpendicular to the negative magnetic anomaly and roughly parallel with the range front.

These two features proved most challenging to replicate with potential field modeling based solely on mapped geology and reflection seismic data. Thus, we began with a seismic velocity model to help constrain the geometry of the potential field model.

## MODELING

### *Seismic velocity modeling*

The 16-km high-resolution seismic reflection/refraction profile modeled in this study was collected in September 2004 with the Network for Earthquake Engineering Simulation (NEES) tri-axial (T-Rex) vibrator. The details of this survey technique are given in Lerch et al. (2008) and the results are described by Lerch et al. (2009). Data processing for velocity modeling consisted of standard techniques: picking first arrivals in selected sweeps, forward modeling, and inversion. Fifteen sweeps located within the western 9 km of the line were selected based on roughly even spacing and data quality (Fig. 2). A sweep from the western end of the line shows fast first arrivals (low slope of first arrivals on consecutive traces) within 2 km east of the sweep (Fig.

5a). In contrast, a sweep closer to the center of the basin (Fig. 5b) shows much slower first arrivals (steeper slope in arrivals on consecutive traces). The first reflection hyperbola appears at approximately 600 ms, likely reflecting off a dense basalt flow within the lake sediments visible in the reflection profile (see Figure 2 in Lerch et al, 2009). Both east and west of source point 13971, the first arrivals flatten out, most noticeably to the west, showing the presence of higher seismic velocities at depth.

We used RayGUI 2.3 for our forward and inverse modeling, a GUI by Song and ten Brink based on Colin Zelt's RayInvr code (Song and ten Brink, 2004; Zelt and Smith, 1992). The velocity model is constrained by 1580 picks with an uncertainty of < 100 ms on all picks except those from the westernmost six receivers, for which we accepted a larger uncertainty of 200 ms during modeling to accommodate their location up to 500 m south of the profile and west of the Surprise Valley fault. Given constraints from geological mapping, published Quaternary fault scarps (Hedel, 1984), and seismic reflection data (Lerch et al., 2009), we used forward modeling to achieve a working model consisting of three phases of arrivals that correspond to three discontinuous layers within the valley reaching a depth of approximately 1.5 km (Fig. 6). Iterative inversion produced only minor velocity changes and little improvement in travel time residuals ($T_{RMS}$), shown in Table 1. The uppermost layer (phase 1 in Table 1) is best defined with 948 picks and a $T_{RMS}$ of 0.033 s; phases 2 and 3 are based on far fewer picks and have greater travel time residuals associated with them.

The velocity model is shown in Figure 6 overlain on the seismic reflection profile (see Lerch et al., 2009 for more detail on the reflection profile), along with the modeled arrivals for the two sweeps shown in Figure 5. A notable feature of the model is the marked asymmetry across the basin, both in velocities and in the dips of modeled units. This suggests a westward dip to the main part of the basin and faster velocities on the west. Although it was developed independently of the reflection profile, the velocity model has several features that match aspects of the reflection section. The moderately dipping feature at the base of the model matches well with the reflector assumed to be the Surprise Valley Fault; this feature cannot be directly constrained in

the model given the limit of reversed ray coverage (shown by the thick dashed line in Figure 6b), but was introduced to provide a suitable gradient to create turning rays. In addition, the transparent region labeled “zone e” and interpreted as fan deposits by Lerch et al. (2009) corresponds to higher velocities than those seen in the main depocenter. The dashed unit in the model with a velocity gradient of 2.0-2.5 km/s created some problems: although it improved the travel time residuals for sweeps coming from the west, it decreased the fit for sweeps coming from the east. We included it in the final model, however, because it matches well with a zone with prominent reflectors in the reflection profile. The modeled geometry of this feature suggests it may be bounded to the east by a steeply dipping normal fault.

This velocity model, along with the constraints provided by surface geology and seismic reflection data, was used as a starting point for potential field modeling.

*Two-dimensional potential field modeling*

Using the seismic velocity model as a starting point to constrain basin structures and densities, we developed a two-dimensional (2D) potential field model using a 2D forward modeling package (GMSYS®) (Fig. 7, Fig. 3 for location**)**. The focus of our modeling efforts was a 9-km profile for which we had detailed gravity and magnetic data. In addition to modeled velocities for units in the basin, the model incorporates information from our mapping, wells and drill-cores (Fig. 2; Benoit et al., 2005), seismic reflection (Lerch et al, 2009), and measured rock property data (Ponce et al., 2009). Rock units consist of horizontal tabular prisms or blocks aligned with their longest axes perpendicular to the profile. Their surface extents are consistent in size, shape, and orientation with exposed rock units and with features observed in the seismic reflection profile (Lerch et al., 2009) and velocity modeling. Although the profile is roughly perpendicular to the strike of the primary basin bounding faults, it crosses the range-front fault near a significant left step, creating an asymmetry in the crust to the north and south of the profile. We initially attempted to model the effects of this asymmetry but found its influence to be minimal and thus did not incorporate it into the final model.

To begin, we determined P-wave velocity-derived densities for subsurface units in the basin using the Brocher (2008) modification of the Nafe-Drake relationship (Ludwig et al., 1970) that provides a best-average velocity-to-density conversion based on a broad range of common rock types, including a simple density-depth function to account for compaction. For exposed units, we used magnetic susceptibility and density values measured on hand samples collected in the field area (Ponce et al., 2009). Induced components of magnetization were calculated assuming an ambient field of 51,850 nT with an inclination of 65º and declination of 15º. Remanent magnetization directions of the model source bodies were assumed to be parallel to a time-averaged geocentric axial dipole field direction with an inclination of 65 º, and declination of 0º (or declination of 180 º, inclination of -65 º, in the case of one reversely magnetized unit). Magnetizations were assumed for units based on values consistent with published values for appropriate rock types. Well logs from two exploratory geothermal wells beyond the extent of the velocity model (Fig. 2) were used to estimate sediment depths.

Rock property values assigned to unexposed shallow-to-mid-upper crustal units (particularly on the west side of the valley) are poorly constrained. The only information on crustal lithology at these levels comes from the core LCSH-5 where mafic volcanic units occur near the base of the drill-core at a depth of 4200’ (Fig. 2) (Miller et al., 2005). Extrapolating these units to the lower part of the model appears to be reasonable, since relatively high densities and magnetic susceptibilities, consistent with the basal-core samples, are required to match the observed gravity and magnetic profiles. Because metamorphic or crystalline basement rocks are not exposed anywhere in the study area, nor were they penetrated in the core or any drill holes, densities for crust comprising the deepest parts of the model are also poorly constrained so we use average values for continental crust.

**MODEL FEATURES**

Initial development of the model based on the seismic reflection section and velocity modeling within the valley (described above) produced a reasonably good fit with the observed gravity profile, particularly on the west side of the basin. Several modifications, however, were required to achieve a best-fit model (Fig. 7) that also accounted for features observed in the magnetic profile. These modifications consist of (1) making significant lateral changes in the thickness of units in the subsurface, (2) adding several faults with vertical offset which are not expressed on the surface, (3) assigning a reverse magnetization and confined extent (perpendicular to the plane of the transect) to mafic flows on the east side of the valley, and (4) adding a shallow, mafic basalt flow on the western side of the basin.

The most significant changes in thickness are in the subsurface units on the eastern side of the profile. These units correspond with Oligocene volcanic rocks exposed in the Warner Range, where they are observed to vary widely in thickness (Fig. 2). The nature of the exposure in the Warner Range, the geologic interpretation of these two units as a progression from more mafic to intermediate arc volcanism (Colgan et al., 2008a), and the thick exposure of Oligocene tuff in the Hays Canyon Range immediately southwest of the study area (Carmichael et al., 2006) support this modification to the model. By increasing the thickness of tuff (Fig. 7, Tc, light purple) at the expense of basalts and andesites (Fig. 7, Tlb, light red), we were able to better fit the relatively low gravity values at the eastern end of the profile.

We also modified the initial model by adding several steeply-dipping faults with relatively minor (but measuarable) vertical offsets. Some of these inferred faults correspond to both mapped Quaternary fault scarps and maximum horizontal gradients (MHG) in the gravity data (Fig. 7), validating the correlation between MHG and structural features and suggesting that these relatively minor topographic scarps may accommodate significant offset at depth. Other inferred faults match MHG and gradient changes in the magnetic profile but do not correspond to surface features (Fig. 7). In map view, these MHG form continuous, parallel lines within the basin,

variably 1-3 km inboard from the range-front faults (Fig. 3a). They roughly parallel the main range-front fault but do not exhibit the same corrugation. These features may indicate a nested graben in the interior basin, similar to those observed in Dixie Valley (Smith et al., 2001) and Verdi Valley (Ramelli et al., 1999). The size of the anomalies marked by the MHG differs considerably, however, from 1-2 mGal on the west side to 3-4 mGal on the east (Fig. 7). The eastern MHG and associated anomaly is proximal to two of the major geothermal springs: Leonards Hot Spring and Seyferth Hot Spring (Fig. 2). The hydrothermal alteration associated with these springs could lead to enhancement of the positive gravity anomaly through cementation and densification of surrounding rocks.

The lack of surface expression of these inferred intra-basin faults may indicate that they are no longer active. However, the faults inferred solely from the gravity and magnetic profiles all lie well within the youngest alluvium deposits of the Pleistocene Lake Surprise, and any surface ruptures within the last 10 ka (or perhaps even much younger, given the modern presence of seasonal lakes) could have been removed through wave action and slumping. It is worth noting that, although this profile does not cross the LCFZ, elsewhere, Griscom and Conradi (1976) mapped the LCFZ on the basis of discrete change in frequency and amplitude of noise in several magnetic profiles that cross the zone, in contrast with the changes in gradient seen across faults with vertical offset.

Interestingly, there is no significant feature in either the gravity or magnetic profile that correlates with the largest topographic fault scarp within the basin, the northward projection of the Cedarville segment of the fault (indicated by the black triangles on the model in Fig. 7 and in Fig. 3). Typically, a complex faulting geometry exists at depth at these segment boundaries early in the extensional history of a region (Anders and Schlische, 1994; Crider, 2001; Marchal et al., 2003), but it appears that the presence of a segment boundary is no longer a significant influence on the fault geometry in this region.

The dashed calculated model fit line in Figure 7 includes these first two modifications, but the model still shows significant misfits. The following two modifications were made to account for these misfits; the solid calculated model fit line in Figure 7 includes them. In order to model the magnetic low on the east end of the profile, we assigned a reverse magnetization to Tyb (outlined in red in Fig. 7) that crop out along an east-trending magnetic low observed in the high-resolution magnetic map (dotted line in Fig. 3b). This modification is based on paleomagnetic results from samples taken from near the low (white triangles, Fig. 3b) that indicate these flows are reversely magnetized. As noted above, the declination of this unit was changed to 180º and inclination to -65º. Although the lateral extent of these reversed flows is not yet known, assuming that they are confined to the region of the low (i.e., limiting their extent perpendicular to the plane of the model to the extent of the low observed in Figure 3b) largely helps to account for the low in the potential field model.

The final modification to the model is the most significant and also the most speculative: in order to account for a significant deficiency in the calculated magnetic profile on the western end of the model, we added a thin, faulted mafic lava flow interbedded with the alluvial deposits (Fig. 7, red body in the shallow subsurface on the west side of the valley). Steps in the flow, resulting from faulting, proved an effective means of reproducing sharp gradients in both potential field profiles and in accounting for the magnitude and shape of the ramps, particularly in the magnetic profile.

The presence of flows interbedded with the alluvium is speculative because there is no surficial evidence for any flows sourced or localized along the range front on the western side of the valley. Their inclusion in the model, however, can account for the sharp changes in potential field gradients that require shallow sources, and they provide a convenient explanation for the higher-than-expected densities and susceptibilities inferred for the fan deposits. Our mapping has shown that localized flows are common in the young basalt-dominated hills to the NE of the study area (Fig. 2), and their lack of surface exposure here could reflect a short-lived episode of

volcanism that has been subsequently buried by sedimentation. Regardless, it is clear that the magnetic profile is influenced by sources both at depth and in the upper few hundred meters of the profile, and a shallow basalt flow interbedded with and overlying the fan deposits can account for the high frequency features in the magnetic profile.

**IMPLICATIONS FOR BASIN DEVELOPMENT**

Our model suggests two possibilities for the tectonic setting and structural development of Surprise Valley, each of which offers different implications for ongoing evolution of the basin. The first possibility is that extension is occurring along a single significant range-front fault. In this case, the multiple intra-basin faults, particularly those observed along the west side of the profile, represent listric steepening of strands of the main, active SVF imaged at a shallow angle at depth, as described by Lerch et al. (2009). This relationship between surface expressions of faults and their equivalents at depth has been demonstrated in many other places, including large systems such as the Gulf of Mexico (e.g. Bradshaw and Zoback, 1988) and Gulf of Corinth (Goldsworthy and Jackson, 2001) as well as within other portions of the Basin and Range, including Dixie Valley (Caskey et al., 1996) and the Sierra El Mayor of Baja California (Axen et al., 1999)

Another possibility is that the intra-basin faults represent the nascent and currently active fault system that is inferred to cut the SVF at depth, which may have become too shallow, given frictional resistance, to continue to slip (e.g. Proffett, 1977; Surpless et al., 2002) or may no longer be oriented favorably to accommodate regional stresses. The imaged angle of the fault of ~30° is not shallow enough in and of itself to inhibit slip, especially given the presence of an active hydrothermal system. As described next, however, the regional strain may be influencing the ongoing slip along the Surprise Valley Fault.

GPS velocity vectors indicate that the Modoc Plateau is moving away from the Basin and Range at a highly oblique, NNW-angle, at ~2 mm/year (Fig. 1) (Hammond and

Thatcher, 2005). Hammond and Thatcher (2007) postulate that this motion is accommodated along the Surprise Valley Fault, but the highly corrugated nature of the fault (Fig. 2) makes this unlikely. In the Eastern California Shear Zone, strain is commonly partitioned between range-front normal faults and strike-slip faults within the valley (Surpless et al., 2005; Wesnousky and Jones, 1994). A similar process could be at work in Surprise Valley: if dextral strike-slip motion is being accommodated within Surprise Valley, it must be occurring along a different fault system than the main SVF. Our models suggest that intra-basin faults in Surprise Valley are relatively steep (~65-70°) and that there is vertical offset of units up to hundreds of meters along them, but the lateral variations in thickness of units would make it difficult to distinguish vertical offset from lateral displacement of a unit of variable thickness. While it is likely that the majority of motion on these faults is vertical to produce the observed anomalies, it is possible that some right-lateral strike-slip motion could be accommodated along the N-trending intra-basin faults.

Given these constraints, it is possible that Surprise Valley is undergoing a transition to a new system of faults that are developing as the old one has become unfavorably oriented – either to accommodate dextral motion or to overcome frictional resistance, or a combination of the two. These transitions are difficult to resolve with geological and geophysical data, but have critical consequences for seismic hazard evaluation and geothermal prospecting. The offsets along the faults within Surprise Valley implied by the geophysical modeling suggest that these could now be accommodating the majority of extensional strain in the region; the fact that there are so many of them may suggest that strain accommodation has not yet localized along a single fault, as would occur over time. They already appear to localize springs and hydrothermal activity, and some of their surface offset may have been overprinted by the recent presence of Lake Surprise combined with a low earthquake recurrence rate. The younger faults may also act to localize small-scale volcanic activity as indicated in our model that includes a shallow, subsurface basalt flow. While these features are well-constrained within the study area, they are less constrained to the north and south, and our ongoing work focuses on better constraining these apparently significant features.

## CONCLUSIONS

Seismic velocity modeling confirms the presence of a shallowly east-dipping fault on the west side of Surprise Valley that puts basin fill against the bedrock of the Warner Mountains. The question remains, however, whether or not this fault is currently active.

The potential field maps and models described in this study highlight the importance of faults without significant surface expression in determining the structural setting of a basin-range system. Our data cannot be explained solely by the location of the profile in a segment boundary zone, nor by a single, shallowly-dipping normal fault bounding a basin filled with unconsolidated lake sediments. Instead, we suggest that the presence of faults within the valley may represent a transition to a new set of steeply dipping faults to accommodate extension – possibly transtension – and uplift along this margin of the Basin and Range.

**Acknowledgments**

The authors thank Derek Lerch, Katie Keranen and Claudia Flores for help with velocity modeling. Joe Colgan, Simon Klemperer, and Elizabeth Miller provided very helpful conversations and reviews during the preparation of this paper. Seismic data utilized in this paper were acquired with funding from NSF grant 0444696 to Klemperer. We also thank Dave John, Gary Axen, and two anonymous reviewers for thorough and thoughtful reviews that greatly improved the organization and structure of this manuscript.

## References

Anders, M.H. and Schlische, R.W., 1994. Overlapping faults, intrabasin highs, and the growth of normal faults. Journal of Geology, 102: 165-180.

Axen, G.J. et al., 1999. Range-front fault scarps of the Sierra El Mayor, Baja California: Formed above an active low-angle normal fault? Geology, 27(3): 247-250.

Barker, B., Kennedy, M., Hoversten, M., van Soest, M.C. and WIllams, K., 2005. Geothermal Exploration at Fort Bidwell, California. Proceedings, Thirtieth Workshop on Geothermal Reservoir Engineering, January 31-February 2, 2005, SGP-TR-176, 5pp.

Bennett, R.A., Wernicke, B., Niemi, N.A., Friedrich, A.M. and Davis, J.L., 2003. Contemporary strain rates in the northern Basin and Range province from GPS data. Tectonics, 22(2), 3:1-3:22.

Benoit, D., Goranson, C., Blackwell, D.D. and Wesnousky, S.G., 2004. Overview of the Lake City, California geothermal system. Geothermal Resources Council Transactions, 28: 311-315.

Benoit, D., Moore, J., Goranson, C. and Blackwell, D.D., 2005. Core Hole Drilling and Testing at the Lake City, California geothermal field. Geothermal Resources Council Transactions, 29: 203-208.

Blackwell, D.D., Leidig, M., Smith, R.P., Johnson, S.D. and Wisian, K.W., 2002. Exploration and Development Techniques for Basin and Range Geothermal Systems: Examples from Dixie Valley, Nevada. Geothermal Resources Council Transactions, 26: 6.

Blakely, R.J., 1995. Potential theory in gravity and magnetic applications. Cambridge University Press, New York, 441 pp.

Bradshaw, G.A. and Zoback, M.D., 1988. Listric normal faulting, stress refraction, and the state of stress in the Gulf Coastal Basin. Geology, 16(3): 271-274.

Brocher, T.M., 2008. Compressional and Shear-Wave Velocity versus Depth Relations for Common Rock Types in Northern California. Bulletin of the Seismological Society of America, 98(2): 950-968.

Brocher, T.M., Hunter, W.C. and Langenheim, V.E., 1998. Implications of seismic reflection and potential field geophysical data on the structural framework of the Yucca Mountain-Crater Flat region, Nevada. Geological Society of America Bulletin, 110(8): 947-971.

Buck, W.R., 1988. Flexural rotation of normal faults. Tectonics, 7(5): 959-973.

California Division of Mines and Geology, 1978. Aeromagnetic map of the Modoc area, California. California Division of Mines and Geology Open File Report. OFR 78-13A.

Carmichael, I.S.E., Lange, R.A., Hall, C.M. and Renne, P.R., 2006. Faulted and tilted Pliocene olivine-tholeiite lavas near Alturas, NE California, and their bearing on the uplift of the Warner Range. Geological Society of America Bulletin, 118(9-10): 1196-1211.

Caskey, S.J., Wesnousky, S.G., Zhang, P., Slemmons., D.B., Louie, J.N., and Abbott, R.E., 1996. Surface faulting of the 1954 Fairview Peak (MS 7.2) and Dixie Valley (MS 6.8) earthquakes, central Nevada. Bulletin of the Seismological Society of America, 86(3): 761-787.

Colgan, J.P., Egger, A.E. and John, D.A., 2008a. Oligocene and Miocene arc volcanism in northeastern California. EOS Transactions AGU, Fall Meeting Supplement, 89(53): V31B-2131.

Colgan, J.P., Shuster, D.L. and Reiners, P.W., 2008b. Two-phase Neogene extension in the northwestern Basin and Range recorded in a single thermochronology sample. Geology, 36(8): 631-634.

Crider, J.G., 2001. Oblique slip and the geometry of normal-fault linkage: mechanics and a case study from the Basin and Range in Oregon. Journal of Structural Geology, 23(12): 1997-2009.

Duffield, W.A. and McKee, E.H., 1986. Geochronology, structure, and basin-range tectonism of the Warner Range, northeastern California. Geological Society of America Bulletin, 97(2): 142-146.

Faulds, J.E. and Varga, R.J., 1998. The role of accommodation zones and transfer zones in the regional segmentation of extended terranes. In: J.E. Faulds and R.J. Varga (Editors), Accommodation Zones and Transfer Zones: The Regional Segmentation of the Basin and Range Province. Geological Society of America Special Paper, 323: 1-45.

Fosdick, J., Egger, A.E., Colgan, J.P., Surpless, B.E., Miller, E.L., and Lerch, D.W., 2005. Cenozoic evolution of the northwestern boundary of the Basin and Range; geologic constraints from the Warner Range and Surprise Valley region. Abstracts with Programs - Geological Society of America, 37(7): 70.

Friedrich, A.M., Lee, J., Wernicke, B.P. and Sieh, K., 2004. Geologic context of geodetic data across a Basin and Range normal fault, Crescent Valley, Nevada. Tectonics, 23(2): 24 pp.

Glen, J.M.G., Egger, A.E. and Ponce, D.A., 2008. Structural control of hot springs in a developing basin-and-range setting, Surprise Valley, California, northwestern Great Basin. Geothermal Resources Council Transactions, 32: 8 pp.

Goldsworthy, M. and Jackson, J., 2001. Migration of activity within normal fault systems: examples from the Quaternary of mainland Greece. Journal of Structural Geology, 23: 489-506.

Griscom, A. and Conradi, A., 1976. Principal facts and preliminary interpretation for gravity profiles and continuous magnetometer profiles in Surprise Valley, California. U. S. Geological Survey Open-File Report, 76-0260: 21 pp.

Hammond, W.C. and Thatcher, W., 2005. Northwest Basin and Range tectonic deformation observed with the Global Positioning System, 1999-2003. Journal of Geophysical Research, 110(B10405): 12 pp.

Hammond, W.C. and Thatcher, W., 2007. Crustal deformation across the Sierra Nevada, northern Walker Lane, Basin and Range transition, western United States measured with GPS, 2000–2004. Journal of Geophysical Research, 112(B05411): 26 pp.

Hedel, C.W., 1981. Map showing geothermal resources of the Lake City-Surprise Valley known geothermal resource area, Modoc County, California. U. S. Geological Survey Miscellaneous Field Studies Map, MF-1299.

Hedel, C.W., 1984. Maps showing geomorphic and geologic evidence for late Quaternary displacement along the Surprise Valley and associated faults, Modoc County, California, U. S. Geological Survey Miscellaneous Field Studies Map, MF-1299.

Jablonski, H.M., 1974. World relative gravity reference network North America. 25, U.S. Defense Mapping Agency Aerospace Center, Reference Publication 25, 1261 pp.

Kennedy, B.M. and van Soest, M.C., 2006. A helium isotope perspective on the Dixie Valley, Nevada, hydrothermal system. Geothermics, 35(1): 26-43.

Kucks, R.P., Hill, P.L. and Ponce, D.A., 2006. Nevada magnetic and gravity maps and data: A website for the distribution of data, U.S. Geological Survey Digital Data Series, 234.

Lawrence, R.D., 1976. Strike-slip faulting terminates the Basin and Range province in Oregon. Geological Society of America Bulletin, 87(6): 846-850.

Lee, J., Rubin, C.M. and Calvert, A., 2001. Quaternary faulting history along the Deep Springs fault, California. Geological Society of America Bulletin, 113(7): 855-869.

Lerch, D.W., Klemperer, S.L., Stokoe, K.H. and Menq, F.-Y., 2008. Integration of the NEES T-Rex Vibrator and PASSCAL Texan Recorders for Seismic Profiling of Shallow and Deep Crustal Targets. Seismological Research Letters 79(1): 41-46.

Lerch, D.W., Klemperer, S.L., Egger, A.E., Colgan, J.P., and Miller, E.L., (2009). The northwestern margin of the Basin and Range Province, Part 1: Reflection profiling of the moderate-angle (~30°) Surprise Valley Fault. Tectonophysics doi:10.1016/j.tecto.2009.05.028

Ludwig, W.J., Nafe, J.E. and Drake, C.L., 1970. Seismic refraction. The Sea, Vol. 4, Part 1. Wiley-Intersci., New York, 53-84 pp.

Marchal, D., Guiraud, M. and Rives, T., 2003. Geometric and morphologic evolution of normal fault planes and traces from 2D to 4D data. Journal of Structural Geology, 25: 135-158.

Miller, E.L., Colgan, J.P., Surpless, B.E., Riedel-Bash, S., Strickland, A., Egger, A.E., and Benoit, D., 2005. Drill core data from the Warner Range and Surprise Valley. Abstracts with Programs - Geological Society of America, 37(7): 203-204.

Okaya, D.A. and Thompson, G.A., 1985. Geometry of Cenozoic Extensional Faulting: Dixie Valley, Nevada. Tectonics, 4(1): 107-125.

Oskin, M. et al., 2008. Elevated shear zone loading rate during an earthquake cluster in eastern California. Geology, 36(6): 507-510.

Pakiser, L.C. and Kane, M.F., 1965. Gravity study of Owens Valley. U. S. Geological Survey Professional Paper, 0470: 191-195.

Personius, S.F., Crone, A.J., Machette, M.N., Lidke, D.J., Mahan, and Bradley, L.,, 2007a. Logs and scarp data from a paloseismic investigation of the Surprise Valley fault zone, Modoc County, California. U.S. Geological Survey Scientific Investigations 2983: 2 sheets.

Personius, S.F., Crone, A.J., Machette, M.N., Mahan, S.A., Kyung, J.B., Cisneros, H., and Lidke, D.J. 2007b. Late Quaternary Paleoseismology of the Southern Steens Fault Zone, Northern Nevada. Bulletin of the Seismological Society of America, 97(5): 1662-1678.

Personius, S.F. and Mahan, S.A., 2005. Unusually Low Rates of Slip on the Santa Rosa Range Fault Zone, Northern Nevada. Bulletin of the Seismological Society of America, 95(1): 319-333.

Plouff, D., 1977. List of principal facts and gravity anomalies for an area between Orovada, Nevada, and Adel, Oregon. U.S. Geological Survey Open-File Report, OF 77-0683, 45 pp.

Ponce, D.A., 1997. Gravity data of Nevada. U.S. Geological Survey Digital Data Series, Report DDS-0042.

Ponce, D.A., Glen, J.M.G., Egger, A.E. and Bouligand, C., 2009. Geophysical studies in the vicinity of Warner Mountains and Surprise Valley, Northeast California, Northwest Nevada, and Southern Oregon. U.S. Geological Survey Open-File Report OF 2009-1157, 19 pp.

Proffett, J.M., 1977. Cenozoic geology of the Yerington District, Nevada, and implications for the nature and origin of Basin and Range faulting. Geol Soc Am Bull, 88(2): 247-266.

Ramelli, A.R., Bell, J.W., dePolo, C.M. and Yount, J.C., 1999. Large-magnitude, late Holocene earthquakes on the Genoa fault, west-central Nevada and eastern California. Bulletin of the Seismological Society of America, 89(6): 1458-1472.

Reheis, M., 1999. Extent of Pleistocene Lakes in the Western Great Basin, U.S. Geological Survey Miscellaneous Field Studies Map, MF-2323.

Smith, R.P., Wisian, K.W. and Blackwell, D.D., 2001. Geologic and Geophysical Evidence for Intra-Basin and Footwall Faulting at Dixie Valley, Nevada. Geothermal Resources Council Transactions, 25: 8 pp.

Snyder, D.B., Roberts, C.W., Saltus, R.W. and Sikora, R.F., 1981. Magnetic tape containing the principal facts of 64,402 gravity stations in the State of California. U.S. Geological Survey Report, 2,161, PB82-168287, 30 pp., Natl. Tech. Inf. Serv., U.S. Dept. of Commer., Springfield,VA.

Song, J.L. and ten Brink, U.S., 2004. RayGUI 2.0 - A Graphical User Interface for Interactive Forward and Inversion Ray-Tracing,. U.S. Geological Survey Open-File Report, 2004-1426.

Surpless, B., Stockli, D.F., Dumitru, T.A. and Miller, E.L., 2002. Two-phase westward encroachment of Basin and Range extension into the northern Sierra Nevada. Tectonics, 21(1): 13 pp.

Surpless, B.E., and Miller, E.L., 2005. Strain partitioning across the central Walker Lane; geodetic and geologic constraints. Abstracts with Programs - Geological Society of America, 37(7): 203.

Tilden, J.E., Ponce, D.A; Glen, J.M.G.; and Gans, K.D, 2005. Gravity and magnetic data along a seismic refraction-reflection line in northwest Nevada and northeast California. U.S. Geological Survey Open-File Report, OF 2005-1446: 12 pp.

United States Geological Survey, 1981. Total field aeromagnetic anomaly map, Surprise Valley Known Geothermal Resource Area, California, U. S. Geological Survey Open-File Report, 81-0997.

Wesnousky, S.G. and Jones, C.H., 1994. Oblique slip, slip partitioning, spatial and temporal changes in the regional stress field, and the relative strength of active faults in the Basin and Range, Western United States. Geology (Boulder), 22(11): 1031-1034.

White, D.E., 1955. Violent mud-volcano eruption of Lake City Hot Springs, northeastern California. Geological Society of America Bulletin, 66: 1109-1130.

Zelt, C.A. and Smith, R.B., 1992. Seismic traveltime inversion for 2-D crustal velocity structure. Geophysical Journal International, 108(1): 16-34.

Zhang, P., Mao, F. and Slemmons, D.B., 1999. Rupture terminations and size of segment boundaries from historical earthquake ruptures in the Basin and Range Province. Tectonophysics, 308(1-2): 37-52.

## Figures

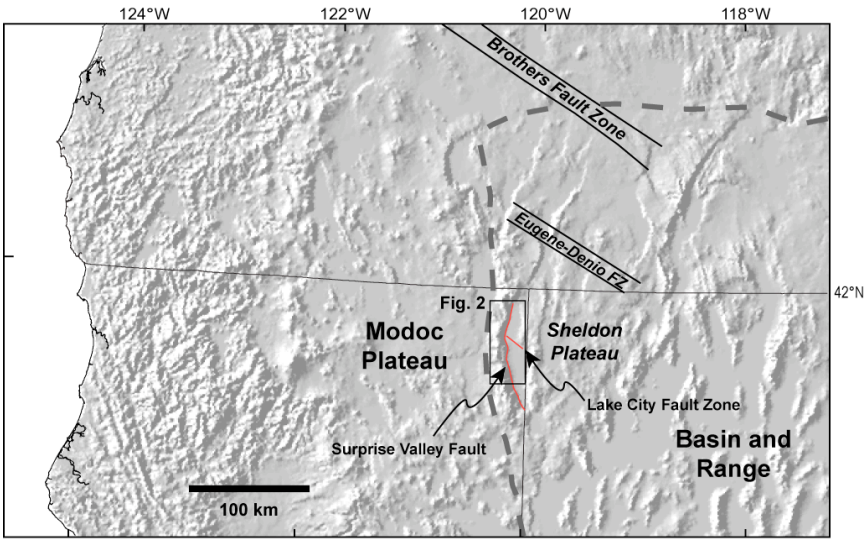


**Figure 1.** Shaded relief map of the northwestern margin of the Basin and Range province. Major NW-SE-trending fracture zones are labeled. Inset box shows the study area of the Warner Range and Surprise Valley lying between the Sheldon and Modoc plateaus, which have experienced very little extension.

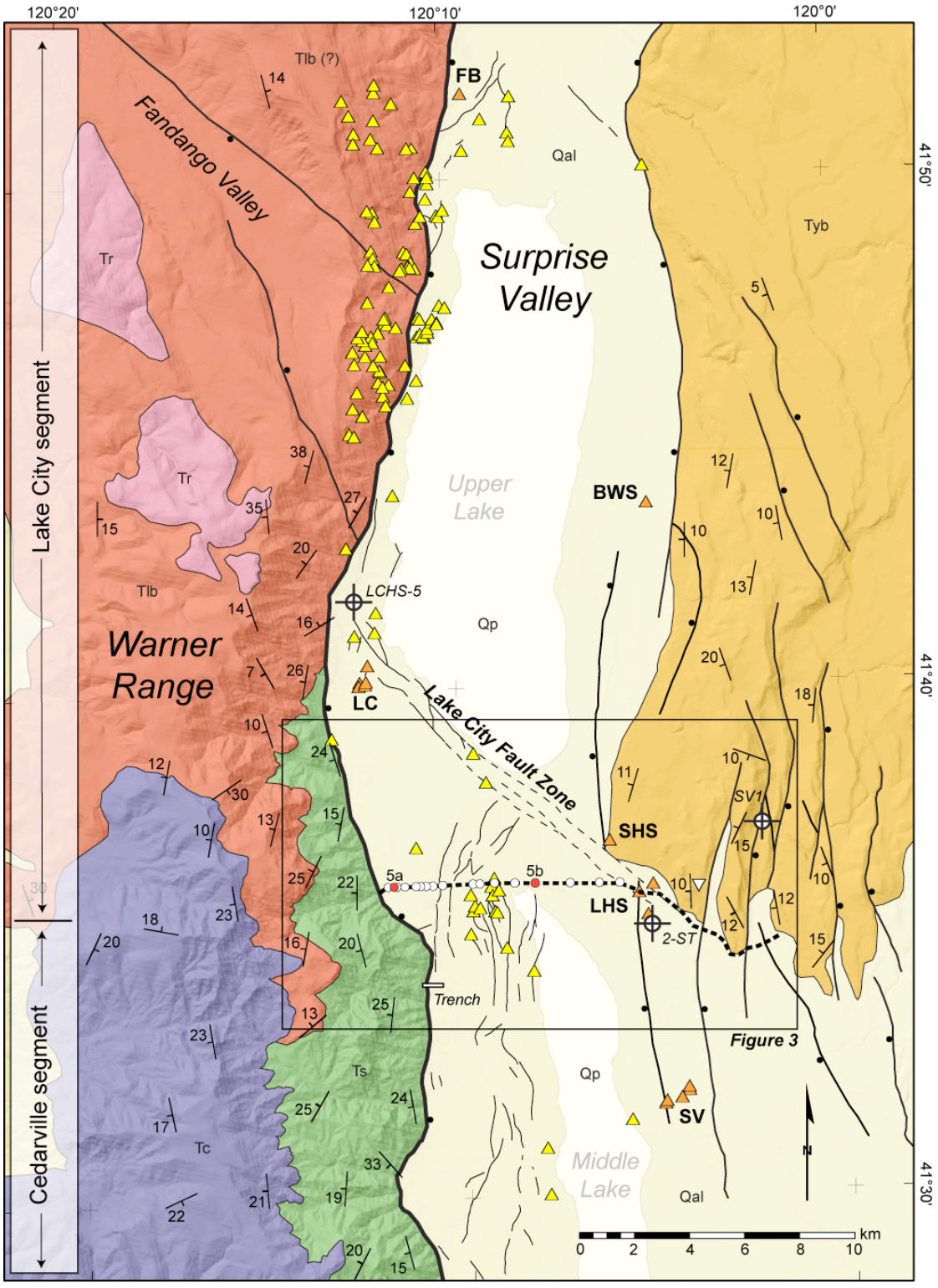


**Figure 2.** Simplified geologic map of the northern Warner Range and Surprise Valley, draped over a shaded relief map. See legend (next page) for description of units and symbols. Location of seismic line and Vibroseis sweeps selected for velocity modeling shown.

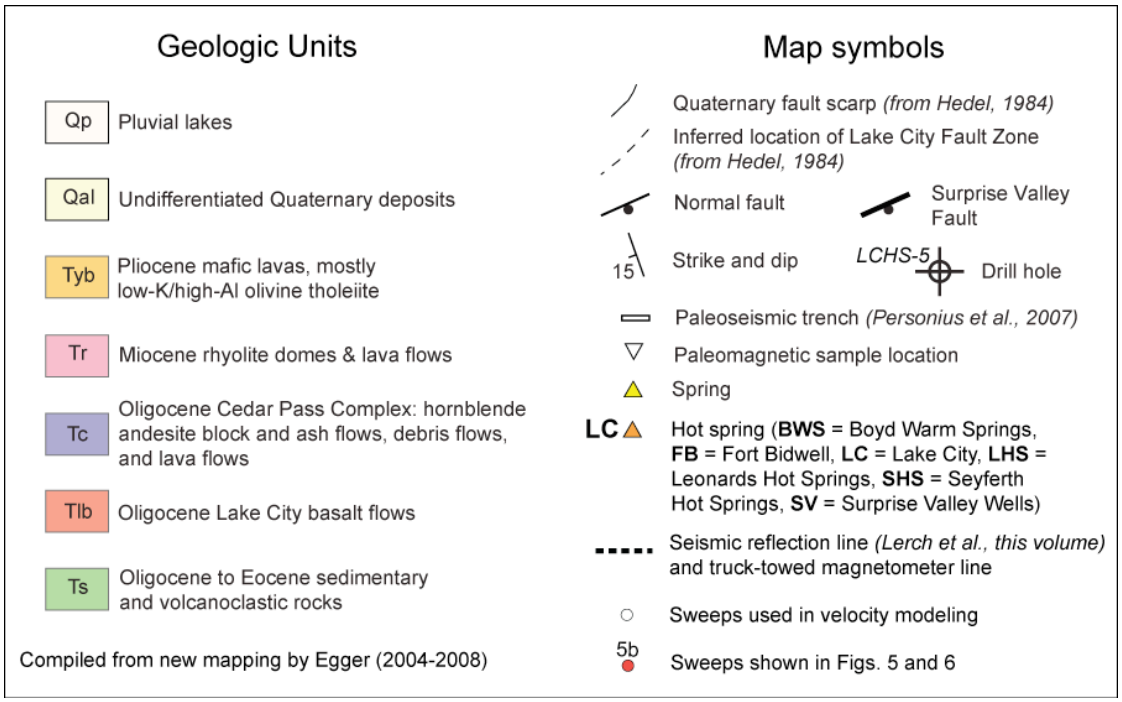


**Figure 2, cont.** Legend for geologic map.

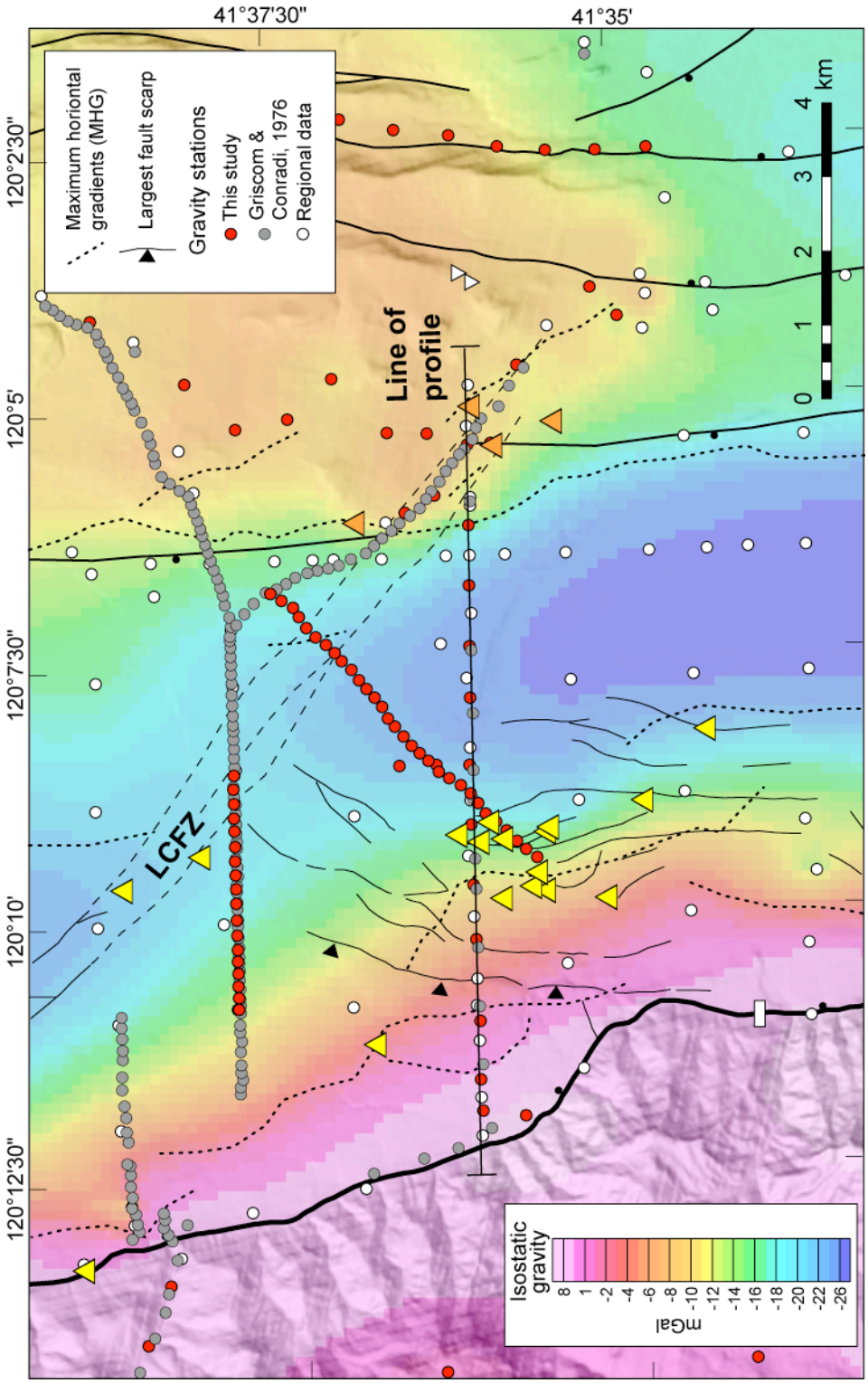


**Figure 3a.** Isostatic gravity map of study area including all gravity stations used to derive the grid. Symbols used here are the same as in Figure 2; refer to Figure 2 legend for complete description.

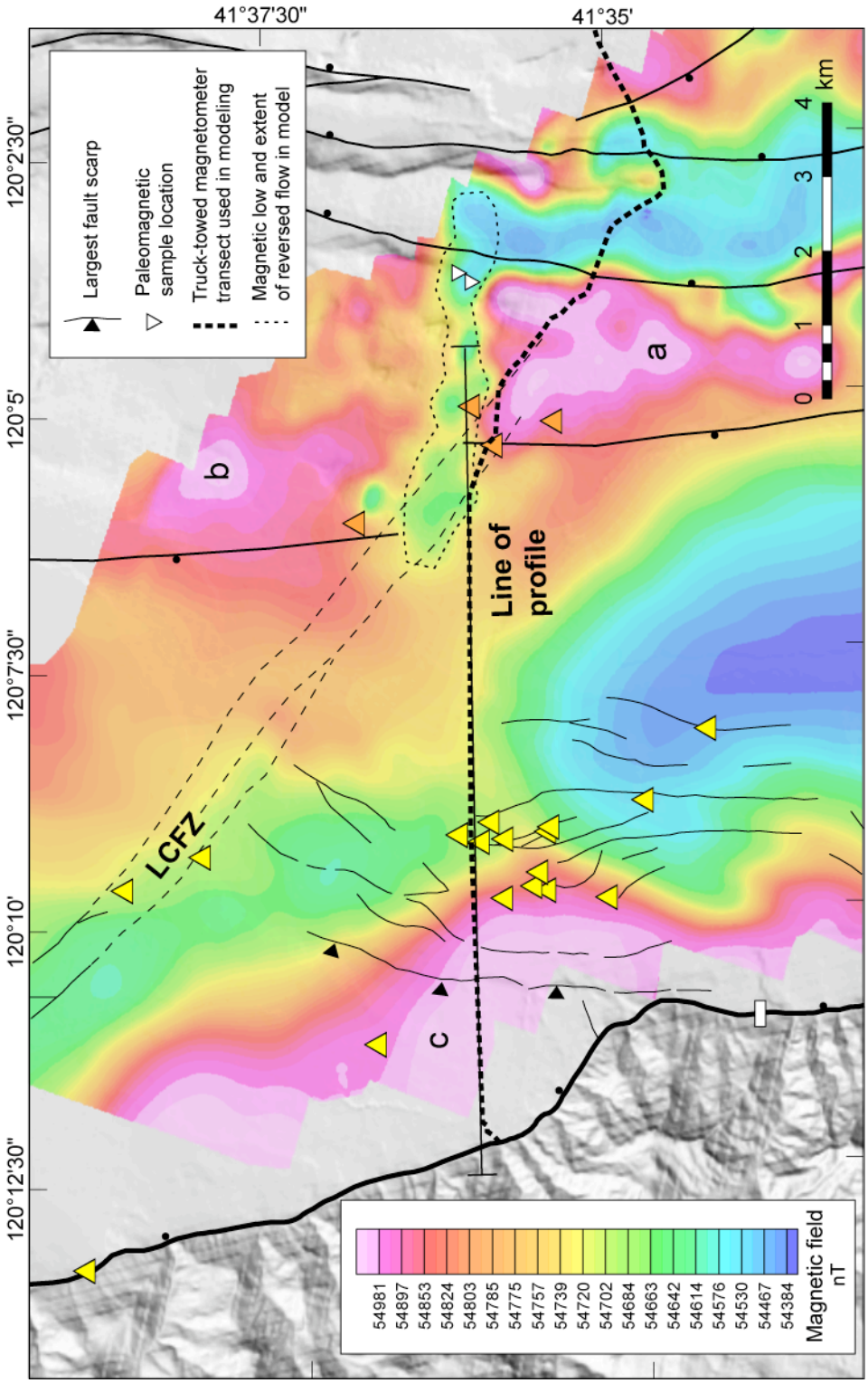


**Figure 3b.** High-resolution aeromagnetic map of study area (from U.S. Geological Survey OF 81-997-4077). Note numerous features with high magnetic susceptibility (bright pink areas) but no surface expression in the topography. Symbols used here are the same as in Figure 2; refer to Figure 2 legend for complete description.

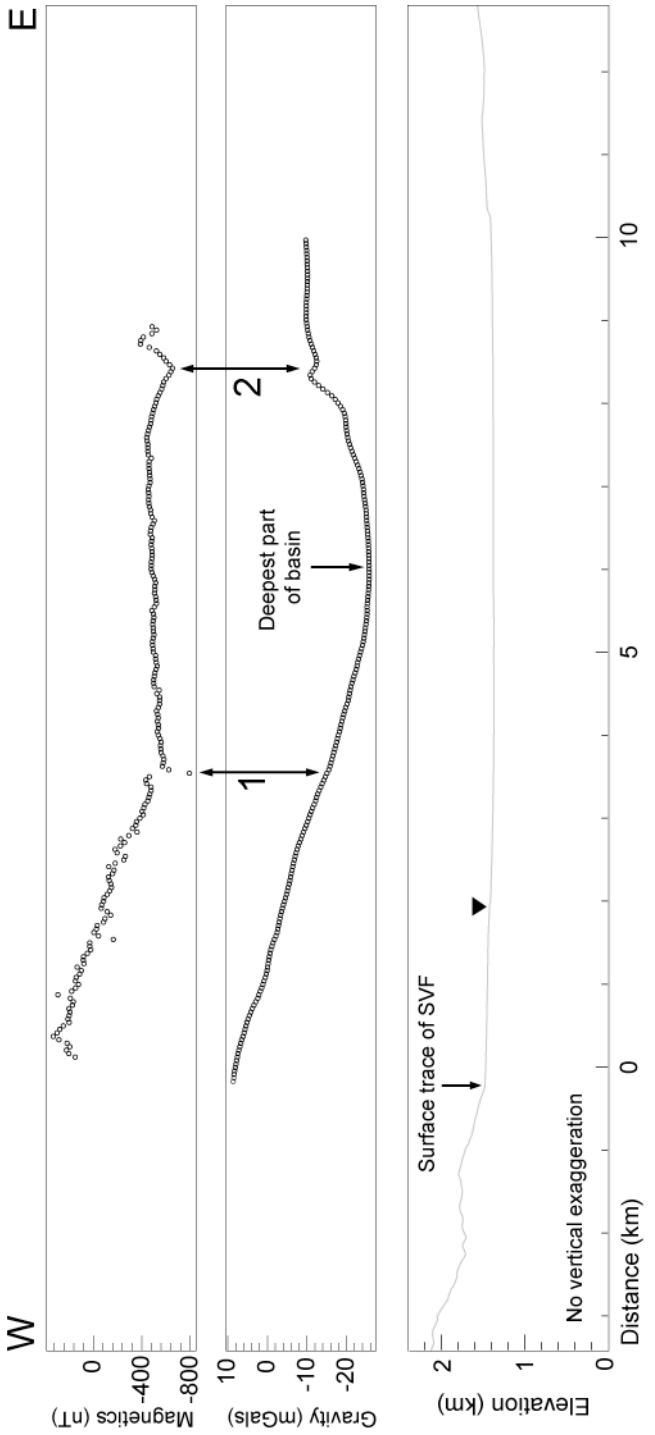


**Figure 4.** Potential field data and topographic profile used in the model. Line of profile is shown in Figure 3. Gravity profile is extracted from gridded, detailed data; magnetic data is from a truck-towed magnetometer transect. Both are limited to the extent of detailed data along a straight-line transect. Black triangle indicates location of topographically most significant Quaternary fault scarp.

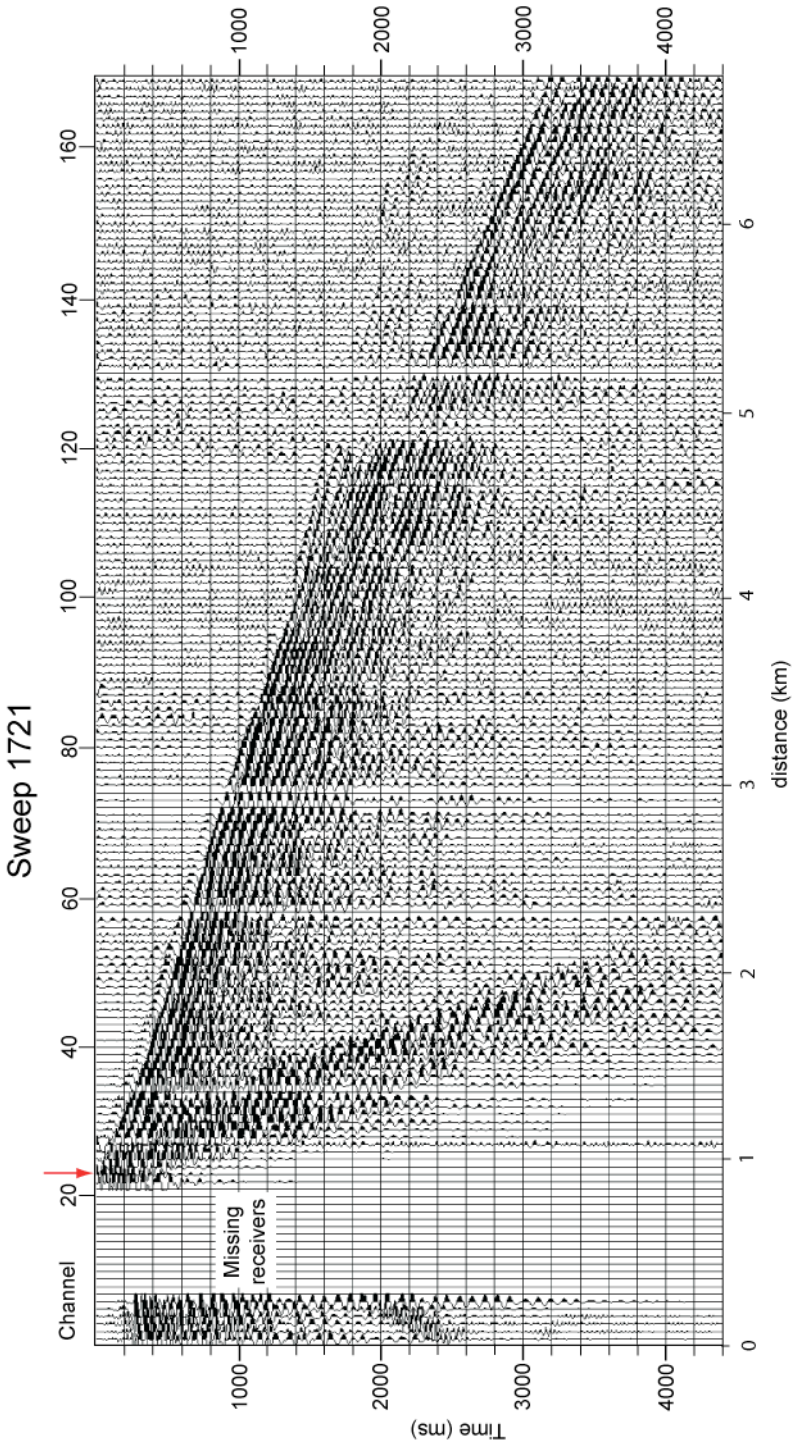


**Figure 5a.** Sweep 01721 from west end of line; location of Vibroseis truck marked by red arrow here and in Figure 6 and by a red circle in Fig. 2.

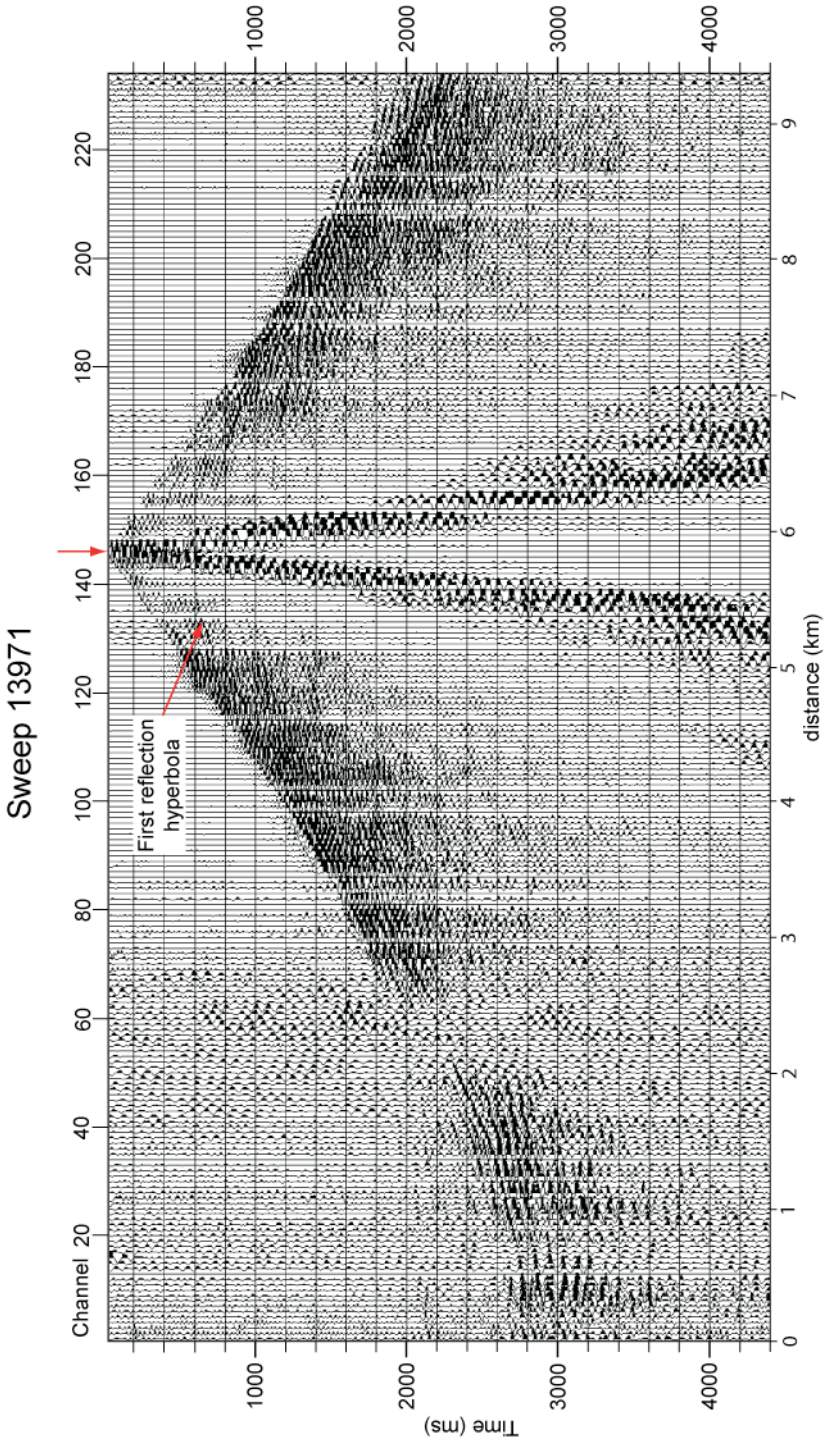


**Figure 5b.** Sweep 13971 from central portion of the basin; location of Vibroseis truck marked by red arrow here and in Figure 6 and by a red circle in Fig. 2.

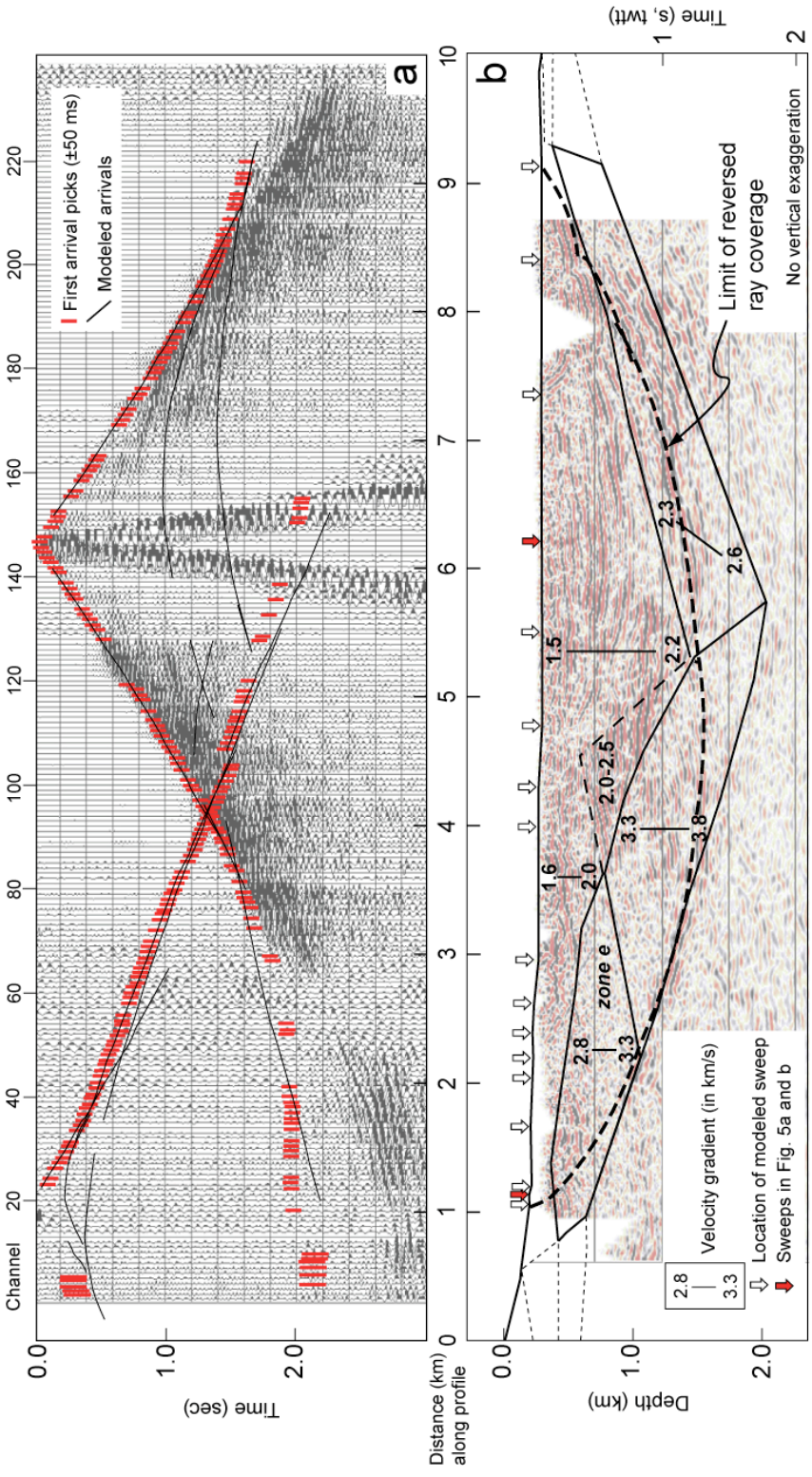


**Figure 6** *(see next page for explanation)*

**Figure 6.** (a) Observed first arrivals (red lines) with 100 ms errors and modeled results (black lines) from the two example sweeps shown in Figs. 5a and 5b. (b) Velocity model (see Table 1 for number of picks used and travel time residuals) overlain on a seismic reflection profile. Depth on left axis, two-way travel time (ttwt) on right axis. Wide dashed line in shows the deepest limit of ray coverage. The highest velocities at the base of the basin were introduced into the model to provide suitable gradients to create turning rays, but are not directly observed from the data. “Zone e” is the relatively transparent zone in the reflection profile noted and described in Lerch et al. (2009). See text for further explanation of features.

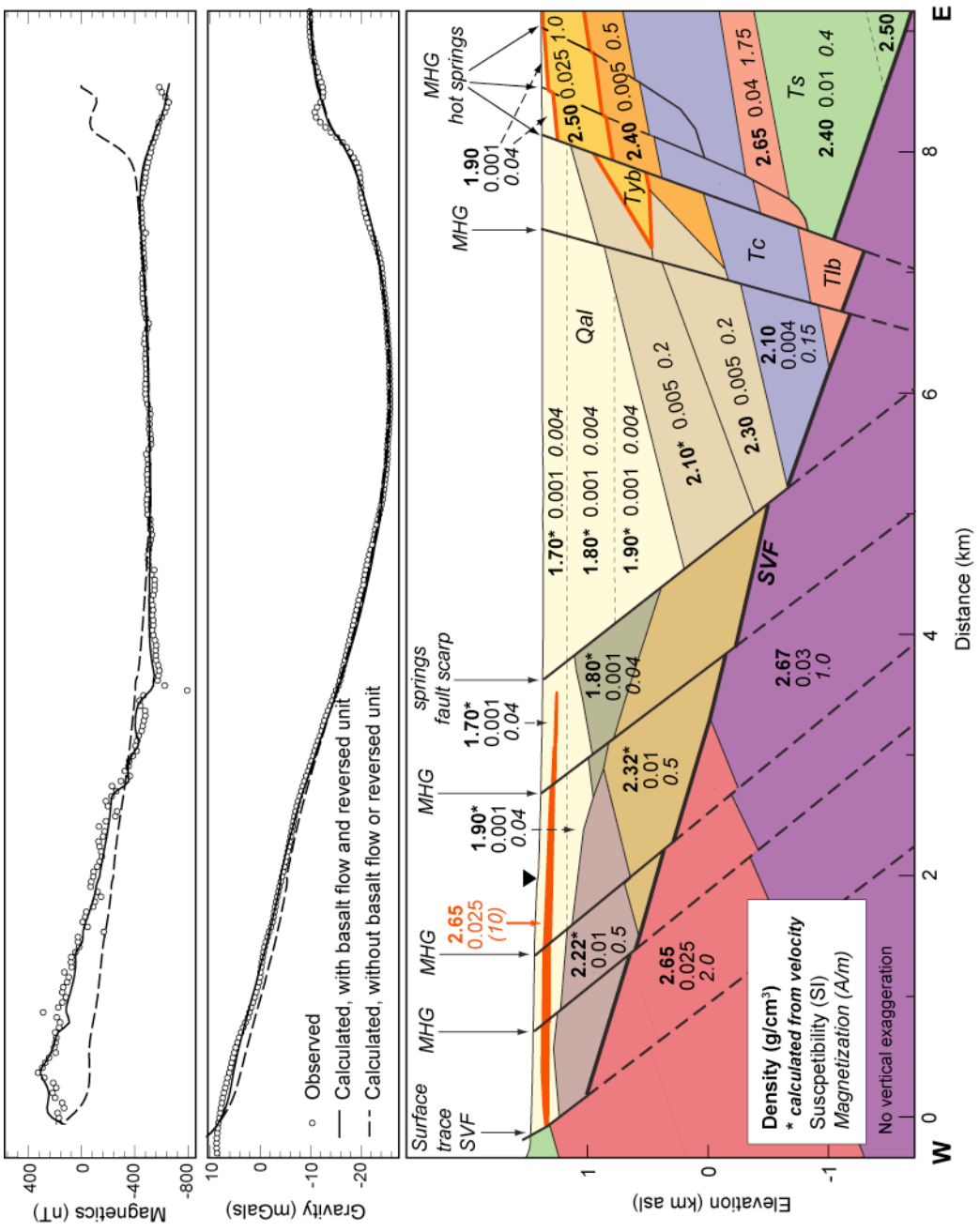


**Figure 7.** Potential field model. Units labeled Qal, Tyb, Ts, Tc, and Tlb correspond with geologic units shown in Figure 2. Properties of other units are inferred based on seismic velocity modeling and achieving the best-fit potential field model as described in the text. Inferred steeply-dipping faults are shown in solid lines through the basin and dashed into the basement to indicate that modeling cannot determine if these faults sole into the Surprise Valley Fault (SVF on figure) or cut it at depth as we show here. Annotation on these faults indicates correlations with features shown in Figure 3. Black triangle indicates location of topographically most significant Quaternary fault scarp. Features in red are not included in the dashed line model calculations; they are included in the solid line calculations.

## Tables

| Phase | Points used | TRMS (s) | $chi^2$ |
|---|---|---|---|
| **all** | 1247/1580 | 0.052 | 0.26 |
| **1** | 948 | 0.033 | 0.112 |
| **2** | 199 | 0.096 | 0.92 |
| **3** | 100 | 0.068 | 0.358 |

**Table 1.** Errors associated with seismic velocity model shown in Figure 6. The phase refers to the number of layers that modeled rays pass through. "Points used" refers to the number of picked first arrivals used in the model. $T_{RMS}$ is the square root of the sum of the square of the travel time residuals (in seconds), a measure of the difference between the observed and modeled travel times. Normalized chi-square values in the final column are an indication of goodness of fit.

**Appendix A**

# Major and Trace Element Geochemical Data
# Geochronological Data
# Map Unit Descriptions

**On the following pages:**

**Table A1.** Major and trace element geochemical data on samples from the Warner Range. All analyses were performed at the Washington State University GeoAnalytical Lab using X-ray fluorescence.

**Tables A2-A9.** Geochronology data for samples in the Warner Range and analyzed at the U.S. Geological Survey in Menlo Park, CA, by Joseph P. Colgan and Robert Fleck.

**Figure A1.** Plateau diagrams for samples in Tables A2-A9.

**Tables A10-A13.** Geochronology data for samples in the Warner Range and analyzed at the New Mexico Geochronology Research Laboratory in Socorro, NM, by Chris Henry.

**Table A14.** Map unit descriptions

## Table A1.

| Sample | 05BS1 | 05BS2 | 06WC0101 | 06WC0202 | 07-C-10 | 07-C-12 | 07-C-13 |
|---|---|---|---|---|---|---|---|
| **Unit** | **Tlb** | **Tlb** | **Tovl** | **Tovl** | **Tovu** | **Tovu** | **Tovu** |
| **Description** | basalt | basalt | basalt | basalt | basalt | andesite | andesite |
| **Latitude**[1] | 41.51598 | 41.51598 | 41.67611 | 41.67811 | 41.60999 | 41.58488 | 41.58488 |
| **Longitude**[1] | -120.48062 | -120.48062 | -120.25994 | -120.25894 | -120.26893 | -120.2605 | -120.2605 |
| **$SiO_2$** | 48.35 | 48.67 | 50.94 | 51.31 | 51.68 | 56.66 | 56.72 |
| **$TiO_2$** | 0.889 | 0.882 | 1.38 | 1.257 | 1.23 | 0.63 | 0.64 |
| **$Al_2O_3$** | 17.62 | 17.69 | 18.38 | 18.36 | 15.85 | 18.61 | 18.78 |
| **FeO** | 9.57 | 9.45 | 10.27 | 9.79 | 8.05 | 7.42 | 7.5 |
| **MnO** | 0.164 | 0.167 | 0.196 | 0.193 | 0.14 | 0.18 | 0.15 |
| **MgO** | 10.37 | 8.73 | 3.46 | 3.35 | 8.39 | 3.25 | 2.93 |
| **CaO** | 10.42 | 11.53 | 7.76 | 7.79 | 8.2 | 8.04 | 8.14 |
| **$Na_2O$** | 2.31 | 2.58 | 3.55 | 3.72 | 2.9 | 3.4 | 3.72 |
| **$K_2O$** | 0.19 | 0.19 | 1.51 | 1.3 | 3.02 | 1.49 | 1.09 |
| **$P_2O_5$** | 0.115 | 0.122 | 0.493 | 0.434 | 0.52 | 0.31 | 0.33 |
| **Volume sum** | 97.58 | 99.88 | 97.93 | 97.5 | 98.25 | 98.33 | 98.2 |
| **Ba** | 168 | 216 | 611 | 595 | 938 | 521 | 499 |
| **La** | 3 | 6 | 24 | 22 | 29 | 15 | 17 |
| **Ce** | 7 | 11 | 49 | 38 | 57 | 29 | 31 |
| **Rb** | 3 | 1 | 34 | 27 | 133 | 23 | 22 |
| **Sr** | 214 | 249 | 569 | 587 | 654 | 675 | 684 |
| **Y** | 21 | 22 | 34 | 32 | 20 | 18 | 17 |
| **Zr** | 46 | 47 | 164 | 142 | 225 | 78 | 77 |
| **Nb** | 1.3 | 1.9 | 5.8 | 5 | 14.5 | 2.7 | 2.3 |
| **Co** | | | | | | | |
| **Cr** | 219 | 237 | 6 | 5 | 376 | 7 | 7 |
| **Ni** | 173 | 170 | 14 | 11 | 164 | 1 | 2 |
| **Sc** | 39 | 42 | 28 | 24 | 25 | 15 | 15 |
| **V** | 237 | 253 | 223 | 221 | 208 | 153 | 156 |
| **Cu** | 114 | 115 | 141 | 143 | 52 | 40 | 55 |
| **Mo** | | | | | | | |
| **Pb** | 1 | 2 | 12 | 10 | 5 | 6 | 7 |
| **Zn** | 66 | 64 | 115 | 112 | 78 | 92 | 86 |
| **Ga** | 15 | 16 | | | 18 | 19 | 20 |
| **Th** | 0 | 0 | 4 | 3 | 5 | 1.9 | 2.7 |
| **U** | | | 3 | 2 | | | |
| **Nd** | 6 | 9 | 28 | 24 | 32 | 16 | 16 |

[1] Latitude and longitude in WGS 84 coordinates.
* Sample data from Victor Camp, personal communication, 2008. Location is approximate based on field notes.

## Table A1, cont.

| Sample | 07-C-14 | 07-C-15 | 07-C-16 | 07-C-19 | 07-C-2 | 07-C-20 | 07-C-3 |
|---|---|---|---|---|---|---|---|
| **Unit** | **Tovu** | **Tovu** | **Tovu** | **Tovu** | **Tovu** | **Tovu** | **Tovu** |
| **Description** | andesite | andesite | andesite | andesite lava | basalt flow | andesite | andesite lava |
| **Latitude**[1] | 41.58488 | 41.58539 | 41.58816 | 41.58819 | 41.54073 | 41.58826 | 41.50745 |
| **Longitude**[1] | -120.2605 | -120.26017 | -120.2634 | -120.27171 | -120.28651 | -120.27425 | -120.28935 |
| **$SiO_2$** | 53.21 | 53.8 | 58.79 | 58.28 | 59.4 | 59.58 | 54.06 |
| **$TiO_2$** | 0.75 | 0.78 | 0.53 | 0.63 | 0.56 | 0.6 | 0.81 |
| **$Al_2O_3$** | 19.09 | 18.59 | 18.58 | 18.18 | 18.89 | 17.91 | 18.88 |
| **FeO** | 9.05 | 9.02 | 6.43 | 6.92 | 6.01 | 6.21 | 8.41 |
| **MnO** | 0.2 | 0.17 | 0.24 | 0.17 | 0.17 | 0.14 | 0.15 |
| **MgO** | 3.99 | 4.01 | 2.89 | 2.93 | 1.67 | 2.96 | 3.64 |
| **CaO** | 9.26 | 8.98 | 7.38 | 7.58 | 7.16 | 6.67 | 8.94 |
| **$Na_2O$** | 3.27 | 3.31 | 3.89 | 3.81 | 4.26 | 3.88 | 3.57 |
| **$K_2O$** | 0.87 | 1.01 | 0.91 | 1.28 | 1.56 | 1.8 | 1.32 |
| **$P_2O_5$** | 0.32 | 0.33 | 0.35 | 0.23 | 0.32 | 0.24 | 0.23 |
| **Volume sum** | 98.6 | 97.56 | 97.19 | 98.93 | 98.53 | 97.94 | 98.47 |
| **Ba** | 404 | 414 | 702 | 648 | 632 | 761 | 544 |
| **La** | 13 | 14 | 20 | 17 | 19 | 20 | 15 |
| **Ce** | 28 | 29 | 38 | 33 | 41 | 34 | 26 |
| **Rb** | 21 | 23 | 15 | 26 | 30 | 32 | 24 |
| **Sr** | 676 | 618 | 848 | 693 | 823 | 650 | 709 |
| **Y** | 18 | 18 | 19 | 18 | 21 | 17 | 17 |
| **Zr** | 61 | 64 | 94 | 88 | 94 | 108 | 77 |
| **Nb** | 2 | 1.5 | 2.9 | 2.3 | 2.6 | 3.1 | 2.9 |
| **Co** | | | | | | | |
| **Cr** | 6 | 17 | 12 | 16 | 2 | 26 | 5 |
| **Ni** | 2 | 9 | 2 | 3 | 0 | 6 | 1 |
| **Sc** | 20 | 22 | 11 | 19 | 9 | 15 | 25 |
| **V** | 202 | 213 | 102 | 169 | 106 | 141 | 269 |
| **Cu** | 51 | 70 | 33 | 43 | 26 | 37 | 51 |
| **Mo** | | | | | | | |
| **Pb** | 5 | 5 | 14 | 6 | 6 | 8 | 7 |
| **Zn** | 103 | 95 | 102 | 81 | 88 | 80 | 77 |
| **Ga** | 19 | 18 | 20 | 18 | 20 | 18 | 20 |
| **Th** | 1.7 | 1.3 | 3.2 | 3.7 | 4.4 | 3.4 | 2.8 |
| **U** | | | | | | | |
| **Nd** | 17 | 16 | 21 | 16 | 21 | 18 | 15 |

[1] Latitude and longitude in WGS 84 coordinates.
* Sample data from Victor Camp, personal communication, 2008. Location is approximate based on field notes.

## Table A1, cont.

| Sample | 07-C-5 | 07-C-6 | 07-C-7 | 07-C-8 | 07-C-9 | AE04WR117 | AE05WR01 |
|---|---|---|---|---|---|---|---|
| **Unit** | **Tovu** | **Tovu** | **Tovu** | **Tovu** | **Tovu** | **Tovu** | **Tovc** |
| **Description** | andesite plug | basalt flow | basalt flow | basalt flow | basalt flow | andesite | andesite |
| **Latitude**[1] | 41.55702 | 41.60923 | 41.61213 | 41.6093 | 41.61356 | 41.50322 | 41.54 |
| **Longitude**[1] | -120.26344 | -120.23928 | -120.24778 | -120.24514 | -120.26045 | -120.25042 | -120.28 |
| **$SiO_2$** | 57.82 | 51.26 | 53.64 | 51.61 | 57.07 | 56.74 | 59.87 |
| **$TiO_2$** | 0.6 | 1.3 | 1.39 | 1.47 | 0.77 | 0.49 | 0.558 |
| **$Al_2O_3$** | 18.65 | 18.57 | 17.37 | 17.26 | 19.87 | 20.94 | 19.07 |
| **FeO** | 7.02 | 10.31 | 8.52 | 9.39 | 7.55 | 6.09 | 6.09 |
| **MnO** | 0.27 | 0.2 | 0.58 | 0.15 | 0.14 | 0.17 | 0.146 |
| **MgO** | 2.76 | 4.49 | 4.01 | 5.92 | 2.67 | 2.33 | 1.45 |
| **CaO** | 7.07 | 8.73 | 8.62 | 9.09 | 7.6 | 8.19 | 6.69 |
| **$Na_2O$** | 3.38 | 3.6 | 3.58 | 3.27 | 3.23 | 3.91 | 4.22 |
| **$K_2O$** | 2.19 | 1.16 | 1.94 | 1.5 | 0.9 | 0.85 | 1.57 |
| **$P_2O_5$** | 0.24 | 0.39 | 0.35 | 0.34 | 0.2 | 0.28 | 0.32 |
| **Volume sum** | 96.62 | 96.86 | 96.27 | 97.23 | 98.37 | 97.33 | 98.94 |
| **Ba** | 765 | 465 | 610 | 489 | 504 | 560 | 645 |
| **La** | 15 | 16 | 21 | 19 | 15 | 16 | 18 |
| **Ce** | 29 | 35 | 47 | 42 | 30 | 34 | 40 |
| **Rb** | 33 | 22 | 43 | 34 | 20 | 16 | 29 |
| **Sr** | 589 | 540 | 622 | 598 | 637 | 795 | 804 |
| **Y** | 17 | 28 | 24 | 23 | 21 | 15 | 20 |
| **Zr** | 82 | 104 | 191 | 147 | 82 | 79 | 93 |
| **Nb** | 2.6 | 2.8 | 11.1 | 8.7 | 2.6 | 2.3 | 2.3 |
| **Co** | | | | | | | |
| **Cr** | 8 | 22 | 63 | 93 | 9 | 2 | 1 |
| **Ni** | 0 | 19 | 44 | 51 | 2 | 0 | 3 |
| **Sc** | 13 | 29 | 21 | 27 | 21 | 11 | 10 |
| **V** | 136 | 242 | 201 | 243 | 182 | 101 | 102 |
| **Cu** | 55 | 132 | 60 | 87 | 69 | 46 | 21 |
| **Mo** | | | | | | | |
| **Pb** | 7 | 9 | 10 | 9 | 8 | 7 | 7 |
| **Zn** | 99 | 102 | 89 | 90 | 91 | 80 | 80 |
| **Ga** | 20 | 20 | 20 | 20 | 21 | 20 | 21 |
| **Th** | 2.6 | 2 | 7.5 | 4.6 | 2.6 | 3 | 5 |
| **U** | | | | | | | |
| **Nd** | 16 | 24 | 27 | 25 | 15 | 17 | 23 |

[1] Latitude and longitude in WGS 84 coordinates.
* Sample data from Victor Camp, personal communication, 2008. Location is approximate based on field notes.

## Table A1, cont.

| Sample | AE05WR03 | CR-637* | CR-638* | CR-639* | CR04-528* | CR04-529* | CR04-530* |
|---|---|---|---|---|---|---|---|
| Unit | Tovl | Tovu | Tovu | Tovu | | | |
| Description | basalt | | | | | | |
| Latitude[1] | 41.5783 | 41.66109 | 41.66109 | 41.66109 | 41.26307 | 41.26307 | 41.26307 |
| Longitude[1] | -120.2241 | -120.27659 | -120.27659 | -120.27659 | -120.14126 | -120.14126 | -120.14126 |
| $SiO_2$ | 50.84 | 50.14 | 49.85 | 50.11 | 50.61 | 51.78 | 54.36 |
| $TiO_2$ | 0.989 | 1.043 | 1.039 | 1.037 | 1.016 | 1.674 | 0.84 |
| $Al_2O_3$ | 20.25 | 20.8 | 20.71 | 21.03 | 18.21 | 16.33 | 17.07 |
| FeO | 9.92 | 8.81 | 8.74 | 8.32 | 6.88 | 9.97 | 7.29 |
| MnO | 0.159 | 0.154 | 0.154 | 0.127 | 0.168 | 0.174 | 0.117 |
| MgO | 4.26 | 3.47 | 3.35 | 3.22 | 3.24 | 4.07 | 4.28 |
| CaO | 9.06 | 10.19 | 10.2 | 10.32 | 9.37 | 8.22 | 8.01 |
| $Na_2O$ | 3.61 | 3.3 | 3.28 | 3.26 | 3.45 | 3.67 | 3.27 |
| $K_2O$ | 0.77 | 0.75 | 0.72 | 0.74 | 1.53 | 1.34 | 1.36 |
| $P_2O_5$ | 0.149 | 0.202 | 0.2 | 0.197 | 0.315 | 0.48 | 0.226 |
| Volume sum | 99.76 | | | | | | |
| Ba | 317 | 287.6 | 280 | 278.6 | 719.8 | 713.6 | 606.5 |
| La | 8 | 9.6 | 1.6 | 14.2 | 20.2 | 19.4 | 16 |
| Ce | 23 | 21.6 | 28.5 | 25.2 | 34.4 | 45.1 | 31.4 |
| Rb | 13 | 11.6 | 11 | 11 | 19.1 | 20.8 | 28.1 |
| Sr | 580 | 591.5 | 595.4 | 609 | 670.8 | 576.6 | 569.7 |
| Y | 21 | 20.6 | 20.8 | 21.4 | 22 | 31.7 | 17.4 |
| Zr | 59 | 72.4 | 73 | 72.8 | 131.9 | 140.2 | 111 |
| Nb | 1.9 | 1.6 | 1.3 | 2 | 4.6 | 6.4 | 4.5 |
| Co | | 15.1 | 13.6 | 13.4 | 93.6 | 41.6 | 140.5 |
| Cr | 18 | 15.1 | 13.6 | 13.4 | 93.6 | 41.6 | 140.5 |
| Ni | 24 | 16.2 | 17 | 16.5 | 47.7 | 38.9 | 61.4 |
| Sc | 27 | 30.9 | 28.2 | 29.6 | 29.7 | 29.9 | 25.3 |
| V | 270 | 243.9 | 229.8 | 228 | 219.4 | 328 | 193 |
| Cu | 125 | 109.4 | 122.1 | 119 | 80.5 | 142.5 | 58.6 |
| Mo | | 2.3 | 1.8 | 2.2 | 0.2 | 1 | 0.8 |
| Pb | 6 | 2.4 | 1.3 | 1.2 | 0.7 | 2.5 | 0.4 |
| Zn | 78 | 67.7 | 69.2 | 69.3 | 69.7 | 95.6 | 74.5 |
| Ga | 20 | | | | | | |
| Th | 0 | 2 | 1.7 | 1.8 | 6 | 6.2 | 8 |
| U | | 1.3 | 1.5 | 1.4 | 2.3 | 0.5 | 0.9 |
| Nd | 14 | 9.9 | 14.4 | 12 | 21.2 | 26.8 | 15.5 |

[1] Latitude and longitude in WGS 84 coordinates.
* Sample data from Victor Camp, personal communication, 2008. Location is approximate based on field notes.

## Table A1, cont.

| Sample | CR04-531* | CR04-532* | CR04-533* | CR04-534* | CR04-535* | CR04-536* | CR04-537* |
|---|---|---|---|---|---|---|---|
| Unit | | | | | Tmvu | Tmvu | Tmvu |
| Description | | | | | | | |
| Latitude[1] | 41.26307 | 41.26307 | 41.26307 | 41.26307 | 41.26232 | 41.26232 | 41.26232 |
| Longitude[1] | -120.14126 | -120.14126 | -120.14126 | -120.14126 | -120.15395 | -120.15395 | -120.15395 |
| $SiO_2$ | 51.54 | 51.24 | 58.31 | 53.83 | 48.71 | 51.59 | 47.8 |
| $TiO_2$ | 1.077 | 1.054 | 0.731 | 0.887 | 1.093 | 1.502 | 1.079 |
| $Al_2O_3$ | 17.42 | 17.28 | 17.16 | 17.63 | 17.15 | 17.42 | 16.64 |
| FeO | 7.22 | 7.62 | 6.15 | 7.05 | 10.01 | 9.27 | 10.1 |
| MnO | 0.105 | 0.103 | 0.109 | 0.12 | 0.163 | 0.152 | 0.163 |
| MgO | 4.17 | 4.25 | 2.94 | 5.62 | 8.23 | 4.06 | 8.39 |
| CaO | 9.16 | 8.75 | 6.4 | 7.51 | 9.56 | 8.56 | 9.36 |
| $Na_2O$ | 3.4 | 3.33 | 3.51 | 3.72 | 2.82 | 3.58 | 2.66 |
| $K_2O$ | 1.4 | 1.32 | 2.08 | 1.16 | 0.58 | 1.29 | 0.5 |
| $P_2O_5$ | 0.341 | 0.334 | 0.2 | 0.294 | 0.259 | 0.424 | 0.252 |
| Volume sum | | | | | | | |
| Ba | 736.9 | 795.6 | 778.6 | | 343.8 | 701.1 | 335.5 |
| La | 13.3 | 13.9 | 20 | | 5.9 | 16 | 6.8 |
| Ce | 35.7 | 39 | 31.9 | | 20.3 | 47.9 | 21.3 |
| Rb | 26.6 | 15.9 | 46.9 | | 6.7 | 10.1 | 4.6 |
| Sr | 728.5 | 729.4 | 543 | | 417.9 | 645.5 | 406.5 |
| Y | 18.2 | 17.7 | 18.1 | | 22.3 | 28.2 | 22.3 |
| Zr | 121.1 | 123.7 | 140.4 | | 64.8 | 128 | 59.4 |
| Nb | 5.5 | 5.3 | 5.9 | | 3 | 6.3 | 2.9 |
| Co | 113.6 | 115.4 | 21.5 | | 165.7 | 41.1 | 180.2 |
| Cr | 113.6 | 115.4 | 21.5 | | 165.7 | 41.1 | 180.2 |
| Ni | 74.4 | 66.1 | 15.8 | | 156.6 | 41.9 | 172.1 |
| Sc | 26.7 | 28.3 | 21.3 | | 26.1 | 27 | 27.7 |
| V | 213.1 | 231 | 160.7 | | 221.1 | 310.6 | 238.9 |
| Cu | 61.7 | 67.8 | 29.1 | | 110.7 | 132.9 | 78.4 |
| Mo | 0.7 | 0.5 | 1.3 | | 1 | 0.9 | 0.1 |
| Pb | -2.3 | -1.2 | 2 | | -0.1 | 1.2 | -1 |
| Zn | 65 | 80.3 | 58.7 | | 87.2 | 91.3 | 88.8 |
| Ga | | | | | | | |
| Th | 7.1 | 7.1 | 7.8 | | 1.2 | 3.8 | 1 |
| U | 1.1 | 0.7 | 2 | | 0.3 | 1.2 | 0.8 |
| Nd | 18.8 | 22 | 17.1 | | 12.2 | 24.5 | 11.2 |

[1] Latitude and longitude in WGS 84 coordinates.
* Sample data from Victor Camp, personal communication, 2008. Location is approximate based on field notes.

## Table A1, cont.

| Sample | CR04-538* | CR04-539* | CR04-540* | CR04-541* | CR04-542* | CR04-543* | CR04-544* |
|---|---|---|---|---|---|---|---|
| Unit | Tmvu | Tmvu | Tmvu | Tmvu | Tmvu | Tmvu | Tmvu |
| Description | | | | | | | |
| Latitude[1] | 41.26232 | 41.26232 | 41.26232 | 41.26232 | 41.26232 | 41.26232 | 41.26232 |
| Longitude[1] | -120.15395 | -120.15395 | -120.15395 | -120.15395 | -120.15395 | -120.15395 | -120.15395 |
| $SiO_2$ | 49.43 | 47.24 | 47.19 | 47.1 | 50.25 | 49.53 | 58.53 |
| $TiO_2$ | 1.125 | 1.015 | 1.005 | 1.099 | 1.437 | 1.459 | 1.28 |
| $Al_2O_3$ | 16.31 | 17.46 | 17.39 | 17.43 | 16.87 | 16.82 | 14.76 |
| FeO | 9.7 | 9.92 | 9.85 | 9.72 | 10.89 | 11.09 | 8.48 |
| MnO | 0.154 | 0.159 | 0.155 | 0.148 | 0.179 | 0.168 | 0.203 |
| MgO | 7.23 | 7.65 | 7.59 | 7.08 | 5 | 5.36 | 1.42 |
| CaO | 9.09 | 9.09 | 9.41 | 9.35 | 7.6 | 7.58 | 3.9 |
| $Na_2O$ | 2.78 | 2.78 | 2.76 | 2.92 | 3.59 | 3.52 | 4.23 |
| $K_2O$ | 0.59 | 0.48 | 0.51 | 0.6 | 1.31 | 1.23 | 3.47 |
| $P_2O_5$ | 0.295 | 0.232 | 0.23 | 0.306 | 0.381 | 0.381 | 0.542 |
| Volume sum | | | | | | | |
| Ba | 536.6 | 304.1 | 299.2 | 411.4 | 627.3 | 595.3 | 1363.3 |
| La | 12.3 | 9.4 | 10.6 | 11 | 14.1 | 12.4 | 49.6 |
| Ce | 30.7 | 27 | 22.9 | 31.1 | 36.9 | 39.1 | 98.5 |
| Rb | 3.8 | 5.5 | 5.6 | 5.2 | 22.3 | 20 | 81.1 |
| Sr | 444.5 | 424.5 | 433.2 | 501 | 512.5 | 508.7 | 313.7 |
| Y | 24.6 | 22.2 | 21.5 | 22.4 | 27.7 | 27.9 | 63 |
| Zr | 84.3 | 68.7 | 69.6 | 71.2 | 112.7 | 111.2 | 339.4 |
| Nb | 3.7 | 2.7 | 2.6 | 3.6 | 4.6 | 4.7 | 14.7 |
| Co | 149.9 | 48.1 | 58.1 | 37.6 | 15.3 | 14.6 | -5.3 |
| Cr | 149.9 | 48.1 | 58.1 | 37.6 | 15.3 | 14.6 | -5.3 |
| Ni | 148.7 | 145.7 | 149.7 | 142 | 71.8 | 75.6 | 4 |
| Sc | 24.8 | 25.7 | 26 | 28.1 | 22 | 24.1 | 20 |
| V | 230.4 | 212 | 217.6 | 236.5 | 262.1 | 259.8 | 18.8 |
| Cu | 112.2 | 83.1 | 89.8 | 67.3 | 122.3 | 68 | 90.8 |
| Mo | 0.2 | -0.1 | 0.3 | -0.2 | 0.4 | 0.4 | 1.2 |
| Pb | 0.7 | -0.6 | -1.4 | -1.7 | 0.7 | -0.6 | 12.9 |
| Zn | 84.4 | 92.3 | 87.7 | 83.9 | 96.7 | 98.7 | 129.4 |
| Ga | | | | | | | |
| Th | 1.7 | 0.6 | 0.2 | 1.3 | 3.6 | 2.4 | 5.1 |
| U | 0.4 | 0.5 | -0.3 | 0.1 | 1.3 | 0 | 2.3 |
| Nd | 15.3 | 13 | 12.1 | 16 | 18.3 | 19.2 | 50.5 |

[1] Latitude and longitude in WGS 84 coordinates.
* Sample data from Victor Camp, personal communication, 2008. Location is approximate based on field notes.

## Table A1, cont.

| Sample | CR04-545* | CR04-575* | CR04-576* | CR04-577* | CR04-578* | ELM05 WR10 | ELM05WR13 |
|---|---|---|---|---|---|---|---|
| **Unit** | **Tmvu** | **Tmvu** | **Tmvu** | **Tmvu** | **Tmvu** | **Tovl** | **Tdc** |
| **Description** | | | | | | basaltic andesite | rhyolite tuff |
| **Latitude**[1] | 41.26232 | 41.23686 | 41.23686 | 41.23686 | 41.23686 | 41.62 | 41.6186 |
| **Longitude**[1] | -120.15395 | -120.07983 | -120.07983 | -120.07983 | -120.07983 | -120.25 | -120.2237 |
| **$SiO_2$** | 50.52 | 51.12 | 51.3 | 50.99 | 51.76 | 54.2 | 60.67 |
| **$TiO_2$** | 0.997 | 1.045 | 1.05 | 1.057 | 1.197 | 1.389 | 0.506 |
| **$Al_2O_3$** | 18.73 | 17.99 | 17.81 | 18.16 | 18.04 | 17.59 | 19.37 |
| **FeO** | 8.09 | 8.94 | 8.98 | 9.04 | 8.96 | 8.48 | 4.01 |
| **MnO** | 0.132 | 0.145 | 0.147 | 0.147 | 0.15 | 0.17 | 0.076 |
| **MgO** | 5.77 | 6.41 | 6.78 | 5.65 | 4.05 | 4.16 | 1.24 |
| **CaO** | 9.3 | 9.24 | 9.15 | 9.21 | 8.56 | 8.01 | 4.09 |
| **$Na_2O$** | 3.09 | 3.34 | 3.33 | 3.2 | 3.73 | 3.65 | 4.45 |
| **$K_2O$** | 0.78 | 0.92 | 0.93 | 0.89 | 1.15 | 2 | 5.28 |
| **$P_2O_5$** | 0.269 | 0.381 | 0.383 | 0.386 | 0.435 | 0.358 | 0.312 |
| **Volume sum** | | | | | | 98.36 | 99.57 |
| **Ba** | 504.4 | 541.1 | 525.8 | 586.5 | 856.5 | 635 | 1247 |
| **La** | 14.6 | 15.8 | 16.4 | 13.6 | 24 | 19 | 27 |
| **Ce** | 34.4 | 33.2 | 40.1 | 40 | 42.4 | 53 | 52 |
| **Rb** | 18.9 | 11.5 | 12.6 | 11.1 | 11.2 | 40 | 85 |
| **Sr** | 745 | 627.3 | 614.3 | 631.9 | 676.5 | 622 | 672 |
| **Y** | 18.2 | 21.7 | 22.3 | 21.5 | 25 | 26 | 13 |
| **Zr** | 90.1 | 110.3 | 109.1 | 112 | 133.3 | 195 | 170 |
| **Nb** | 3.7 | 5.4 | 5.1 | 5.4 | 6.1 | 10.4 | 5.2 |
| **Co** | 106.5 | 152.6 | 157.9 | 176.4 | 128.5 | | |
| **Cr** | 106.5 | 152.6 | 157.9 | 176.4 | 128.5 | 45 | 5 |
| **Ni** | 86.7 | 120.5 | 125 | 125.6 | 73.8 | 43 | 6 |
| **Sc** | 23.7 | 25.6 | 25 | 29.4 | 24.1 | 23 | 6 |
| **V** | 202.1 | 191.5 | 198.7 | 232.7 | 198.5 | 205 | 62 |
| **Cu** | 74.9 | 84.9 | 71.9 | 67.6 | 65.7 | 74 | 14 |
| **Mo** | 0.3 | 0.7 | 0.8 | 0.5 | 0 | | |
| **Pb** | -2.4 | -1.2 | -0.7 | -0.6 | -0.5 | 11 | 17 |
| **Zn** | 77.1 | 86 | 82.7 | 95.4 | 93.4 | 87 | 70 |
| **Ga** | | | | | | 21 | 17 |
| **Th** | 4.7 | 6.5 | 5.4 | 6.4 | 4.9 | 7 | 7 |
| **U** | 2 | 0.4 | 0.1 | 0.8 | 0.3 | | |
| **Nd** | 14.3 | 21.8 | 22.5 | 23.2 | 26.9 | 28 | 23 |

[1] Latitude and longitude in WGS 84 coordinates.

* Sample data from Victor Camp, personal communication, 2008. Location is approximate based on field notes.

## Table A1, cont.

| Sample | ELM05WR17 | ELM05WR19 | ELM05WR7 | JC05WR01 | JC07WR301 | JCF05WR10 | JCF05WR13 |
|---|---|---|---|---|---|---|---|
| **Unit** | **Tovc** | **Tovc** | **Tmrv** | | | **Tlw** | **Tovu** |
| **Description** | hbl dacite | ignimbrite | basalt | rhyolite tuff | basalt flow | basaltic andedsite | andesite |
| **Latitude**[1] | 41.542 | 41.5423 | 41.58 | 41.61 | 41.61264 | 41.563 | 41.5787 |
| **Longitude**[1] | -120.2635 | -120.2681 | -120.19 | -120.24 | -120.24755 | -120.2197 | -120.244 |
| **$SiO_2$** | 55.8 | 57.31 | 49.4 | 71.09 | 50.75 | 53.07 | 57.65 |
| **$TiO_2$** | 0.774 | 0.558 | 0.837 | 0.453 | 1.47 | 0.698 | 0.597 |
| **$Al_2O_3$** | 18.36 | 19.23 | 16.93 | 16.25 | 17.26 | 19.35 | 18.62 |
| **FeO** | 7.56 | 6.7 | 9.31 | 0.8 | 9.45 | 6.19 | 7.06 |
| **MnO** | 0.126 | 0.151 | 0.166 | 0.014 | 0.17 | 0.245 | 0.205 |
| **MgO** | 4.15 | 2.74 | 10.17 | 0.13 | 6.01 | 1.13 | 3.3 |
| **CaO** | 8.03 | 8.12 | 10.4 | 0.58 | 10.05 | 11.42 | 7.3 |
| **$Na_2O$** | 3.59 | 3.58 | 2.37 | 5.32 | 3.18 | 4.91 | 3.78 |
| **$K_2O$** | 1.39 | 1.33 | 0.31 | 5.32 | 1.34 | 2.64 | 1.14 |
| **$P_2O_5$** | 0.224 | 0.274 | 0.116 | 0.04 | 0.34 | 0.339 | 0.345 |
| **Volume sum** | 99.15 | 97.67 | 97.47 | 98.54 | 98.38 | 93.76 | 97.28 |
| **Ba** | 584 | 570 | 208 | 1371 | 442 | 1160 | 499 |
| **La** | 13 | 12 | 5 | 34 | 18 | 26 | 17 |
| **Ce** | 30 | 33 | 18 | 52 | 37 | 44 | 34 |
| **Rb** | 25 | 22 | 4 | 144 | 30 | 49 | 26 |
| **Sr** | 630 | 780 | 277 | 101 | 621 | 775 | 706 |
| **Y** | 18 | 15 | 18.8 | 28 | 23 | 13 | 18 |
| **Zr** | 81 | 73 | 49 | 410 | 131 | 124 | 87 |
| **Nb** | 2.7 | 1.2 | 1.6 | 21.6 | 7.7 | 4.6 | 2.2 |
| **Co** | | | | | | | |
| **Cr** | 29 | 10 | 374 | 3 | 77 | 3 | 13 |
| **Ni** | 15 | 8 | 164 | 3 | 55 | 5 | 9 |
| **Sc** | 24 | 16 | 40 | 8 | 31 | 10 | 14 |
| **V** | 217 | 137 | 246 | 11 | 257 | 75 | 124 |
| **Cu** | 65 | 31 | 102 | 3 | 93 | 20 | 49 |
| **Mo** | | | | | | | |
| **Pb** | 8 | 9 | 3 | 21 | 6 | 14 | 6 |
| **Zn** | 75 | 80 | 67 | 70 | 91 | 84 | 92 |
| **Ga** | 18 | 19 | 16 | 20 | 18 | 18 | 18 |
| **Th** | 3 | 3 | 0 | 18 | 2.7 | 7 | 2 |
| **U** | | | | | | | |
| **Nd** | 17 | 18 | 11 | 31 | 22 | 20 | 20 |

[1] Latitude and longitude in WGS 84 coordinates.
* Sample data from Victor Camp, personal communication, 2008. Location is approximate based on field notes.

## Table A1, cont.

| Sample | KEWR2 | KEWR3 | KSWR06 | LCHS5-422 | LCHS5-443 | NVBWR7 | WR06AE10 |
|---|---|---|---|---|---|---|---|
| **Unit** | **Tovu** | **Tovu** | **Tlw** | **?** | **?** | **Tovc** | **Tovu** |
| **Description** | basaltic andesite | andesite | tuff | basalt from core | basalt from core | andesite | basaltic andesite |
| **Latitude**[1] | 41.5807 | 41.588 | 41.61 | 41.6967 | 41.6967 | 41.5794 | 41.51042 |
| **Longitude**[1] | -120.2611 | -120.2724 | -120.23 | -120.21082 | -120.21082 | -120.2537 | -120.25932 |
| **$SiO_2$** | 55 | 59.84 | 76.5 | 48.55 | 51.42 | 56.82 | 55.91 |
| **$TiO_2$** | 0.685 | 0.506 | 0.143 | 1.148 | 1.184 | 0.629 | 0.653 |
| **$Al_2O_3$** | 19.15 | 18.54 | 12.98 | 18.42 | 18.77 | 18.58 | 19.08 |
| **FeO** | 7.96 | 6.29 | 1.2 | 10.66 | 9.23 | 7.45 | 7.87 |
| **MnO** | 0.139 | 0.141 | 0.013 | 0.197 | 0.171 | 0.159 | 0.199 |
| **MgO** | 3.94 | 2.5 | 1.34 | 5.78 | 2.99 | 3.23 | 3.36 |
| **CaO** | 8.03 | 6.38 | 2.4 | 8.85 | 8.62 | 8.06 | 7.97 |
| **$Na_2O$** | 3.59 | 4.11 | 0.74 | 3.26 | 3.83 | 3.67 | 3.55 |
| **$K_2O$** | 1.23 | 1.44 | 4.66 | 0.69 | 1.16 | 1.07 | 1.08 |
| **$P_2O_5$** | 0.277 | 0.258 | 0.022 | 0.308 | 0.374 | 0.321 | 0.33 |
| **Volume sum** | 98.18 | 98.43 | 89.72 | 97.85 | 97.75 | 98.9 | |
| **Ba** | 459 | 628 | 1412 | 299 | 491 | 479 | 513 |
| **La** | 12 | 17 | 18 | 14 | 15 | 13 | 18 |
| **Ce** | 25 | 29 | 38 | 22 | 34 | 30 | 33 |
| **Rb** | 22 | 26 | 155 | 12 | 24 | 22 | 22 |
| **Sr** | 669 | 776 | 574 | 538 | 548 | 664 | 746 |
| **Y** | 17 | 14 | 14 | 23 | 28 | 18 | 20 |
| **Zr** | 63 | 74 | 92 | 72 | 101 | 73 | 66 |
| **Nb** | 2.3 | 2.1 | 11.2 | 2.9 | 3.8 | 2.1 | 2.7 |
| **Co** | | | | | | | |
| **Cr** | 8 | 7 | 2 | 33 | 4 | 19 | 5 |
| **Ni** | 9 | 8 | 4 | 33 | 8 | 9 | 0 |
| **Sc** | 20 | 13 | 4 | 30 | 31 | 17 | 16 |
| **V** | 181 | 95 | 12 | 261 | 239 | 152 | 152 |
| **Cu** | 38 | 33 | 7 | 138 | 155 | 48 | 55 |
| **Mo** | | | | | | | |
| **Pb** | 6 | 6 | 23 | 5 | 7 | 6 | 6 |
| **Zn** | 85 | 80 | 39 | 89 | 100 | 90 | 96 |
| **Ga** | 19 | 18 | 14 | | | 20 | 20 |
| **Th** | 2 | 3 | 21 | 1 | 2 | 2 | 4 |
| **U** | | | | 1 | 1 | | 1 |
| **Nd** | 14 | 14 | 17 | 15 | 21 | 16 | 23 |

[1] Latitude and longitude in WGS 84 coordinates.
* Sample data from Victor Camp, personal communication, 2008. Location is approximate based on field notes.

## Table A1, cont.

| Sample | WR07AE02 | WR07AE04 | WR07AE06 | WR07AE07 | WR07AE08 | WR07AE100 | WR07AE102 |
|---|---|---|---|---|---|---|---|
| **Unit** | **Tovl** | **Tovl** | **Tovl** | **Tovl** | **Tlb** | **Tlb** | **Tlb** |
| **Description** | andesite | basalt | basalt | rhyolite | andesite | basalt | basalt |
| **Latitude**[1] | 41.72294 | 41.73073 | 41.72433 | 41.73605 | 41.74173 | 41.53729 | 41.62456 |
| **Longitude**[1] | -120.20685 | -120.20375 | -120.20966 | -120.21937 | -120.22739 | -119.98094 | -119.93138 |
| **$SiO_2$** | 57.91 | 49.55 | 49.3 | 73.03 | 59.1 | 48.43 | 48.31 |
| **$TiO_2$** | 0.94 | 1.95 | 1.919 | 0.15 | 0.92 | 0.949 | 0.917 |
| **$Al_2O_3$** | 18.13 | 16.45 | 16.25 | 15.28 | 17.15 | 17.62 | 17.73 |
| **FeO** | 8.7 | 13.19 | 13.31 | 1.38 | 6.63 | 9.25 | 9.32 |
| **MnO** | 0.07 | 0.23 | 0.245 | 0.05 | 0.12 | 0.169 | 0.172 |
| **MgO** | 2.18 | 4.12 | 4.73 | 0.05 | 2.91 | 9.14 | 9.53 |
| **CaO** | 5.75 | 8.55 | 8.33 | 0.66 | 5.75 | 11.19 | 10.93 |
| **$Na_2O$** | 3.74 | 3.31 | 3.31 | 5.32 | 4.19 | 2.7 | 2.52 |
| **$K_2O$** | 2.27 | 1.56 | 1.53 | 4.02 | 2.7 | 0.4 | 0.41 |
| **$P_2O_5$** | 0.29 | 1.09 | 1.07 | 0.07 | 0.53 | 0.151 | 0.163 |
| **Volume sum** | 95.32 | 96.77 | | 97.36 | 97.69 | | |
| **Ba** | 571 | 653 | 654 | 1217 | 1049 | 178 | 201 |
| **La** | 15 | 37 | 39 | 48 | 37 | 8 | 6 |
| **Ce** | 37 | 89 | 80 | 77 | 59 | 10 | 9 |
| **Rb** | 32 | 42 | 41 | 74 | 42 | 6 | 5 |
| **Sr** | 512 | 431 | 425 | 71 | 512 | 295 | 297 |
| **Y** | 20 | 56 | 53 | 22 | 30 | 21 | 20 |
| **Zr** | 100 | 255 | 246 | 180 | 202 | 68 | 48 |
| **Nb** | 3.3 | 10.4 | 9.3 | 9 | 12.3 | 3.2 | 1 |
| **Co** | | | | | | | |
| **Cr** | 8 | 17 | 16 | 2 | 83 | 203 | 171 |
| **Ni** | 4 | 22 | 23 | 0 | 43 | 167 | 159 |
| **Sc** | 19 | 35 | 35 | 3 | 15 | 36 | 39 |
| **V** | 191 | 252 | 249 | 1 | 124 | 232 | 242 |
| **Cu** | 35 | 327 | 323 | 0 | 56 | 112 | 121 |
| **Mo** | | | | | | | |
| **Pb** | 7 | 17 | 18 | 14 | 9 | 0 | 1 |
| **Zn** | 66 | 139 | 136 | 42 | 81 | 62 | 63 |
| **Ga** | 16 | 20 | 19 | 16 | 17 | 14 | 15 |
| **Th** | 4 | 5 | 6 | 10 | 2 | 0 | 0 |
| **U** | | | 1 | | | 1 | 1 |
| **Nd** | 20 | 52 | 48 | 32 | 33 | 7 | 10 |

[1] Latitude and longitude in WGS 84 coordinates.
* Sample data from Victor Camp, personal communication, 2008. Location is approximate based on field notes.

## Table A1, cont.

| Sample | WR07AE103 | WR07AE104 | WR07AE105 | WR07AE106 | WR07AE110 | WR07AE111 | WR07AE112 |
|---|---|---|---|---|---|---|---|
| **Unit** | **Tlb** | **Tlb** | **Tlb** | **Trt** | **Tlb** | **Tlb** | |
| **Description** | basalt | basalt | basalt | rhyolite | basalt | basalt | dacite |
| **Latitude**[1] | 41.6332 | 41.63593 | 41.62844 | 41.90549 | 41.86497 | 41.86308 | 41.8785 |
| **Longitude**[1] | -119.91875 | -119.92752 | -119.94015 | -120.11652 | -120.23934 | -120.23661 | -120.22428 |
| **$SiO_2$** | 48.06 | 48.15 | 48.45 | 73.5 | 48.62 | 48.36 | 67.53 |
| **$TiO_2$** | 0.841 | 0.94 | 1.021 | 0.08 | 1.016 | 1.005 | 0.638 |
| **$Al_2O_3$** | 17.78 | 17.83 | 17.3 | 14.64 | 17.78 | 17.58 | 16.71 |
| **FeO** | 9.05 | 9.32 | 9.9 | 1.62 | 9.48 | 9.49 | 2.88 |
| **MnO** | 0.172 | 0.173 | 0.182 | 0.085 | 0.176 | 0.176 | 0.061 |
| **MgO** | 9.72 | 8.97 | 8.42 | 0.1 | 8.73 | 8.77 | 0.39 |
| **CaO** | 11.33 | 11.4 | 11.29 | 0.76 | 11.09 | 11.39 | 1.99 |
| **$Na_2O$** | 2.52 | 2.64 | 2.81 | 4.86 | 2.6 | 2.7 | 5.26 |
| **$K_2O$** | 0.37 | 0.4 | 0.45 | 4.3 | 0.34 | 0.36 | 4.34 |
| **$P_2O_5$** | 0.157 | 0.172 | 0.185 | 0.057 | 0.165 | 0.167 | 0.19 |
| **Volume sum** | | | | | | | |
| **Ba** | 210 | 240 | 241 | 973 | 306 | 204 | 1502 |
| **La** | 3 | 5 | 10 | 30 | 7 | 6 | 39 |
| **Ce** | 9 | 15 | 15 | 54 | 12 | 13 | 71 |
| **Rb** | 4 | 4 | 5 | 89 | 4 | 4 | 80 |
| **Sr** | 317 | 325 | 315 | 64 | 296 | 295 | 285 |
| **Y** | 19 | 22 | 24 | 23 | 26 | 23 | 28 |
| **Zr** | 46 | 51 | 56 | 141 | 56 | 56 | 323 |
| **Nb** | 1.9 | 1.9 | 1.4 | 12 | 1.9 | 0.9 | 16.4 |
| **Co** | | | | | | | |
| **Cr** | 216 | 177 | 178 | 1 | 201 | 177 | 2 |
| **Ni** | 183 | 169 | 142 | 0 | 155 | 145 | 0 |
| **Sc** | 38 | 38 | 39 | 3 | 40 | 41 | 7 |
| **V** | 228 | 250 | 269 | 3 | 247 | 251 | 19 |
| **Cu** | 64 | 110 | 148 | 2 | 109 | 125 | 2 |
| **Mo** | | | | | | | |
| **Pb** | 0 | 0 | 1 | 19 | 3 | 1 | 14 |
| **Zn** | 64 | 66 | 72 | 53 | 70 | 71 | 70 |
| **Ga** | 17 | 14 | 16 | 17 | 15 | 16 | 17 |
| **Th** | 0 | 0 | 0 | 9 | 0 | 0 | 6 |
| **U** | 1 | 0 | 0 | 4 | 0 | 0 | 3 |
| **Nd** | 9 | 12 | 12 | 22 | 11 | 10 | 33 |

[1] Latitude and longitude in WGS 84 coordinates.
* Sample data from Victor Camp, personal communication, 2008. Location is approximate based on field notes.

## Table A1, cont.

| Sample | WR07AE114 | WR07AE115 | WR07AE116 | WR07AE117 | WR07AE120 | WR07AE15 | WR07AE16 |
|---|---|---|---|---|---|---|---|
| **Unit** | **Tovu** | **Tmbl** | **Tmbl** | **Tmbl** | | **Tovl** | **Tovl** |
| **Description** | andesite | basalt | basalt | basalt | Basaltic andesite | basalt | andesite |
| **Latitude**[1] | 41.40038 | 41.38642 | 41.38725 | 41.38767 | 41.43918 | 41.72069 | 41.72078 |
| **Longitude**[1] | -120.21325 | -120.21345 | -120.21463 | -120.21648 | -120.21702 | -120.22229 | -120.22835 |
| **$SiO_2$** | 61.7 | 48.51 | 49.07 | 48.81 | 53.79 | 51.36 | 58.59 |
| **$TiO_2$** | 0.653 | 1.709 | 1.012 | 1.046 | 1.196 | 1.53 | 1.33 |
| **$Al_2O_3$** | 16.85 | 17.27 | 18.23 | 18.13 | 17.42 | 17.63 | 15.95 |
| **FeO** | 5.73 | 12.33 | 10.26 | 10.26 | 8.56 | 11.31 | 8.6 |
| **MnO** | 0.122 | 0.201 | 0.173 | 0.173 | 0.159 | 0.18 | 0.12 |
| **MgO** | 2.51 | 6.72 | 8.29 | 7.69 | 4.94 | 3.79 | 3.27 |
| **CaO** | 5.81 | 8.27 | 9.3 | 9.89 | 8.41 | 8.39 | 5.72 |
| **$Na_2O$** | 3.71 | 3.49 | 2.93 | 2.71 | 3.69 | 3.5 | 3.93 |
| **$K_2O$** | 2.74 | 0.92 | 0.52 | 1.06 | 1.45 | 1.63 | 2.28 |
| **$P_2O_5$** | 0.186 | 0.583 | 0.225 | 0.232 | 0.378 | 0.67 | 0.21 |
| **Volume sum** | | | | | | 97.27 | 97.7 |
| **Ba** | 828 | 553 | 285 | 311 | 550 | 613 | 648 |
| **La** | 14 | 22 | 9 | 10 | 16 | 32 | 20 |
| **Ce** | 36 | 40 | 15 | 19 | 41 | 66 | 35 |
| **Rb** | 67 | 9 | 6 | 19 | 30 | 49 | 52 |
| **Sr** | 517 | 508 | 395 | 410 | 526 | 502 | 455 |
| **Y** | 22 | 29 | 20 | 20 | 24 | 42 | 26 |
| **Zr** | 151 | 99 | 54 | 56 | 113 | 220 | 117 |
| **Nb** | 4 | 4.7 | 1.8 | 2.3 | 5.7 | 7.6 | 11.3 |
| **Co** | | | | | | | |
| **Cr** | 40 | 39 | 52 | 50 | 58 | 41 | 5 |
| **Ni** | 10 | 84 | 132 | 133 | 47 | 29 | 50 |
| **Sc** | 17 | 26 | 28 | 29 | 26 | 30 | 19 |
| **V** | 138 | 287 | 227 | 228 | 242 | 236 | 199 |
| **Cu** | 71 | 100 | 96 | 90 | 74 | 292 | 135 |
| **Mo** | | | | | | | |
| **Pb** | 7 | 6 | 2 | 2 | 7 | 14 | 10 |
| **Zn** | 64 | 119 | 86 | 87 | 88 | 126 | 73 |
| **Ga** | 17 | 19 | 18 | 16 | 19 | 20 | 17 |
| **Th** | 6 | 1 | 0 | 0 | 4 | 5 | 5 |
| **U** | 3 | 0 | 1 | 0 | 2 | | |
| **Nd** | 20 | 26 | 12 | 13 | 24 | 39 | 22 |

[1] Latitude and longitude in WGS 84 coordinates.
* Sample data from Victor Camp, personal communication, 2008. Location is approximate based on field notes.

## Table A1, cont.

| Sample | WR07AE19 | WR07AE21 | WR07AE24 | WR07AE27 | WR07AE33 | WR07AE35 | WR07AE38 |
|---|---|---|---|---|---|---|---|
| Unit | Tovl | Tovl | Tovl | Tovl | Tovl | Tovl | Tovl |
| Description | basalt | Basaltic andesite | basalt | basalt | basalt | basalt | basalt |
| Latitude[1] | 41.70136 | 41.70138 | 41.70141 | 41.70167 | 41.70403 | 41.70403 | 41.70415 |
| Longitude[1] | -120.23794 | -120.23925 | -120.23982 | -120.24244 | -120.2482 | -120.2482 | -120.24854 |
| $SiO_2$ | 52.32 | 53.38 | 51.3 | 49.84 | 52.29 | 51.9 | 51.82 |
| $TiO_2$ | 1.17 | 1.256 | 0.948 | 1.177 | 1.24 | 1.22 | 1.24 |
| $Al_2O_3$ | 19.43 | 17.1 | 20.64 | 18.72 | 19.18 | 19.12 | 19.15 |
| FeO | 9.5 | 10.87 | 8.9 | 10.93 | 10.1 | 9.93 | 9.95 |
| MnO | 0.18 | 0.154 | 0.125 | 0.17 | 0.16 | 0.18 | 0.17 |
| MgO | 3.48 | 3.99 | 3.99 | 5.85 | 3.12 | 3.6 | 3.57 |
| CaO | 9.08 | 8.05 | 9.85 | 9.04 | 8.58 | 8.94 | 9 |
| $Na_2O$ | 3.71 | 4 | 3.36 | 3.24 | 3.78 | 3.52 | 3.48 |
| $K_2O$ | 0.89 | 0.98 | 0.73 | 0.71 | 1.18 | 1.2 | 1.23 |
| $P_2O_5$ | 0.23 | 0.225 | 0.164 | 0.316 | 0.38 | 0.39 | 0.4 |
| Volume sum | 97.72 | | | | 97.52 | 97.79 | 98.03 |
| Ba | 364 | 398 | 294 | 291 | 530 | 505 | 502 |
| La | 11 | 11 | 9 | 13 | 15 | 14 | 17 |
| Ce | 26 | 22 | 20 | 27 | 34 | 34 | 38 |
| Rb | 15 | 17 | 12 | 10 | 22 | 27 | 27 |
| Sr | 516 | 468 | 560 | 537 | 558 | 557 | 557 |
| Y | 25 | 24 | 18 | 23 | 30 | 28 | 31 |
| Zr | 76 | 74 | 53 | 69 | 101 | 104 | 107 |
| Nb | 1.2 | 2.5 | 1.2 | 2.9 | 3 | 3 | 3 |
| Co | | | | | | | |
| Cr | 7 | 1 | 25 | 33 | 12 | 17 | 16 |
| Ni | 3 | 4 | 11 | 30 | 8 | 12 | 10 |
| Sc | 31 | 37 | 27 | 31 | 30 | 30 | 29 |
| V | 274 | 325 | 259 | 262 | 257 | 248 | 249 |
| Cu | 115 | 127 | 46 | 131 | 144 | 149 | 156 |
| Mo | | | | | | | |
| Pb | 4 | 6 | 4 | 4 | 7 | 9 | 8 |
| Zn | 90 | 94 | 73 | 86 | 100 | 98 | 99 |
| Ga | 19 | 18 | 18 | 18 | 20 | 19 | 21 |
| Th | 1 | 3 | 1 | 0 | 3 | 2 | 2 |
| U | | 2 | 0 | 1 | | | |
| Nd | 15 | 15 | 9 | 16 | 23 | 23 | 25 |

[1] Latitude and longitude in WGS 84 coordinates.
* Sample data from Victor Camp, personal communication, 2008. Location is approximate based on field notes.

## Table A1, cont.

| Sample | WR07AE40 | WR07AE42 | WR07AE43 | WR07AE47 | WR07AE48 | WR07AE56 | WR07AE65 |
|---|---|---|---|---|---|---|---|
| Unit | Tovl | Tlb | Tlb | Tovu | Tovu | Tovc | Tovl |
| Description | basalt | andesite | andesite | basalt feeder | basalt feeder | andesite | basalt |
| Latitude[1] | 41.70427 | 41.73907 | 41.74688 | 41.4811 | 41.48347 | 41.57455 | 41.644 |
| Longitude[1] | -120.24906 | -120.23653 | -120.23281 | -120.22469 | -120.2258 | -120.27159 | -120.29832 |
| $SiO_2$ | 51.92 | 58.78 | 57.97 | 55.23 | 51.87 | 57.91 | 53.32 |
| $TiO_2$ | 1.26 | 0.91 | 0.94 | 1.06 | 1.63 | 0.66 | 1.34 |
| $Al_2O_3$ | 19.29 | 16.93 | 17.4 | 18.18 | 17.48 | 18.67 | 19.46 |
| FeO | 10.03 | 6.49 | 6.95 | 8 | 10.79 | 7.19 | 9.78 |
| MnO | 0.17 | 0.12 | 0.13 | 0.15 | 0.23 | 0.14 | 0.17 |
| MgO | 3.32 | 3.59 | 3.49 | 4.08 | 3.95 | 3.31 | 2.59 |
| CaO | 8.85 | 5.93 | 6.11 | 7.37 | 7.71 | 6.95 | 7.45 |
| $Na_2O$ | 3.54 | 4.11 | 4.06 | 3.79 | 3.96 | 3.67 | 4.23 |
| $K_2O$ | 1.23 | 2.61 | 2.45 | 1.79 | 1.72 | 1.21 | 1.25 |
| $P_2O_5$ | 0.4 | 0.51 | 0.51 | 0.35 | 0.67 | 0.29 | 0.42 |
| Volume sum | 98.09 | 98.44 | 98 | 97.57 | 96.54 | 97.44 | 97.24 |
| Ba | 526 | 969 | 1045 | 784 | 627 | 578 | 724 |
| La | 20 | 31 | 36 | 20 | 26 | 16 | 20 |
| Ce | 34 | 62 | 59 | 45 | 66 | 32 | 47 |
| Rb | 25 | 42 | 30 | 58 | 43 | 26 | 19 |
| Sr | 555 | 504 | 524 | 574 | 479 | 688 | 833 |
| Y | 32 | 25 | 27 | 25 | 40 | 17 | 22 |
| Zr | 107 | 201 | 203 | 174 | 197 | 91 | 122 |
| Nb | 3.4 | 11.9 | 12.2 | 5.6 | 6.9 | 2.6 | 8.6 |
| Co | | | | | | | |
| Cr | 16 | 82 | 85 | 37 | 10 | 26 | 3 |
| Ni | 10 | 45 | 44 | 16 | 16 | 7 | 0 |
| Sc | 30 | 17 | 16 | 20 | 30 | 16 | 15 |
| V | 250 | 129 | 105 | 191 | 259 | 147 | 185 |
| Cu | 177 | 65 | 48 | 52 | 292 | 46 | 33 |
| Mo | | | | | | | |
| Pb | 8 | 9 | 9 | 12 | 14 | 8 | 6 |
| Zn | 103 | 78 | 75 | 87 | 121 | 80 | 92 |
| Ga | 20 | 17 | 17 | 19 | 23 | 19 | 20 |
| Th | 2 | 3 | 3 | 8 | 5 | 4 | 2 |
| U | | | | | | | |
| Nd | 24 | 28 | 29 | 25 | 35 | 19 | 24 |

[1] Latitude and longitude in WGS 84 coordinates.
* Sample data from Victor Camp, personal communication, 2008. Location is approximate based on field notes.

## Table A1, cont.

| Sample | WR07AE66 | WR07AE67 | WR07AE71 | WR07AE80 | WR07AE83 | WR07AE84 |
|---|---|---|---|---|---|---|
| Unit | Tovu | Tovu | Tovl | Tlb | Tlb | Tlb |
| Description | basaltic andesite? | basaltic andesite | basalt | basalt | basalt | basalt |
| Latitude[1] | 41.64155 | 41.63912 | 41.63402 | 41.70842 | 41.69359 | 41.71077 |
| Longitude[1] | -120.30493 | -120.30339 | -120.27082 | -120.01483 | -120.06051 | -120.06071 |
| $SiO_2$ | 55.14 | 54.34 | 50.42 | 48.64 | 48.54 | 48.49 |
| $TiO_2$ | 0.85 | 0.86 | 1.49 | 1.068 | 1.068 | 1.048 |
| $Al_2O_3$ | 18.15 | 18.22 | 17.19 | 17.6 | 17.67 | 17.6 |
| FeO | 7.9 | 7.92 | 9.67 | 9.84 | 9.97 | 9.69 |
| MnO | 0.15 | 0.15 | 0.16 | 0.177 | 0.164 | 0.173 |
| MgO | 4.3 | 4.46 | 6.34 | 8.02 | 7.98 | 8.52 |
| CaO | 8.26 | 8.83 | 9.94 | 11.39 | 11.41 | 11.34 |
| $Na_2O$ | 3.55 | 3.56 | 3.14 | 2.67 | 2.7 | 2.67 |
| $K_2O$ | 1.48 | 1.43 | 1.31 | 0.41 | 0.33 | 0.32 |
| $P_2O_5$ | 0.22 | 0.22 | 0.34 | 0.178 | 0.165 | 0.139 |
| Volume sum | 98.08 | 98.87 | 98.41 | | | |
| Ba | 526 | 512 | 436 | 263 | 206 | 196 |
| La | 15 | 18 | 19 | 12 | 7 | 6 |
| Ce | 34 | 34 | 36 | 17 | 7 | 6 |
| Rb | 26 | 22 | 32 | 5 | 4 | 4 |
| Sr | 812 | 858 | 615 | 330 | 332 | 327 |
| Y | 18 | 19 | 22 | 23 | 23 | 20 |
| Zr | 85 | 85 | 127 | 70 | 61 | 60 |
| Nb | 2.1 | 1.3 | 7.6 | 3.2 | 1.6 | 1.8 |
| Co | | | | | | |
| Cr | 40 | 45 | 65 | 197 | 204 | 206 |
| Ni | 10 | 12 | 59 | 140 | 152 | 172 |
| Sc | 27 | 28 | 31 | 37 | 37 | 36 |
| V | 255 | 256 | 263 | 242 | 288 | 255 |
| Cu | 155 | 61 | 109 | 110 | 102 | 102 |
| Mo | | | | | | |
| Pb | 9 | 6 | 5 | 1 | 2 | 2 |
| Zn | 80 | 77 | 90 | 65 | 63 | 62 |
| Ga | 19 | 19 | 18 | 15 | 16 | 15 |
| Th | 3 | 3 | 4 | 0 | 2 | 4 |
| U | | | | 2 | 0 | 1 |
| Nd | 22 | 20 | 24 | 13 | 8 | 8 |

[1] Latitude and longitude in WGS 84 coordinates.
* Sample data from Victor Camp, personal communication, 2008. Location is approximate based on field notes.

## Table A1, cont.

| Sample | WR07AE85 | WR07AE86 | WR07AE87 | WR07AE88 | WR07AE89 | WR07AE94 |
|---|---|---|---|---|---|---|
| Unit | Tmr | Tlb | Tlb | Tlb | | Tlb |
| Description | rhyolite | basalt | andesite | basalt | dacite | basalt |
| Latitude[1] | 41.61695 | 41.65003 | 41.63766 | 41.65368 | 41.8658 | 41.60726 |
| Longitude[1] | -120.09774 | -120.07344 | -120.09799 | -120.09048 | -120.07027 | -120.07304 |
| $SiO_2$ | 72.93 | 47.8 | 57.64 | 48.3 | 65.82 | 47.99 |
| $TiO_2$ | 0.154 | 1.05 | 0.951 | 0.977 | 0.511 | 1.303 |
| $Al_2O_3$ | 14.99 | 17.33 | 17.03 | 17.66 | 17.14 | 17.5 |
| FeO | 1.35 | 9.92 | 6.82 | 8.97 | 3.69 | 10.05 |
| MnO | 0.062 | 0.179 | 0.147 | 0.171 | 0.138 | 0.176 |
| MgO | 0.14 | 10.4 | 4.05 | 9.26 | 1.01 | 8.88 |
| CaO | 0.75 | 10.41 | 6.82 | 10.55 | 2.96 | 10.67 |
| $Na_2O$ | 5.23 | 2.25 | 3.94 | 3.45 | 5.48 | 2.91 |
| $K_2O$ | 4.35 | 0.47 | 2.08 | 0.5 | 3.01 | 0.33 |
| $P_2O_5$ | 0.067 | 0.193 | 0.53 | 0.155 | 0.256 | 0.188 |
| Volume sum | | | | | | |
| Ba | 1162 | 234 | 894 | 156 | 1065 | 193 |
| La | 38 | 6 | 24 | 9 | 24 | 9 |
| Ce | 66 | 9 | 53 | 14 | 46 | 13 |
| Rb | 77 | 3 | 37 | 6 | 55 | 5 |
| Sr | 81 | 237 | 513 | 274 | 335 | 329 |
| Y | 24 | 22 | 22 | 21 | 26 | 24 |
| Zr | 168 | 53 | 186 | 72 | 209 | 80 |
| Nb | 8.5 | 1.7 | 11.5 | 3.6 | 9.7 | 2.8 |
| Co | | | | | | |
| Cr | 3 | 261 | 72 | 211 | 4 | 151 |
| Ni | 0 | 188 | 46 | 151 | 0 | 160 |
| Sc | 5 | 41 | 19 | 37 | 5 | 32 |
| V | 4 | 245 | 136 | 215 | 19 | 250 |
| Cu | 0 | 108 | 57 | 103 | 2 | 110 |
| Mo | | | | | | |
| Pb | 14 | 0 | 9 | 2 | 13 | 1 |
| Zn | 49 | 66 | 76 | 56 | 78 | 72 |
| Ga | 16 | 14 | 17 | 13 | 19 | 15 |
| Th | 9 | 1 | 3 | 1 | 4 | 3 |
| U | 4 | 0 | 3 | 1 | 2 | 2 |
| Nd | 27 | 11 | 25 | 9 | 22 | 12 |

[1] Latitude and longitude in WGS 84 coordinates.
* Sample data from Victor Camp, personal communication, 2008. Location is approximate based on field notes.

## Table A1, cont.

| Sample | WR07AE95 | WR07AE96 | WR07AE97 | WR07AE98 | WR07AE99 | WR08AE01 |
|---|---|---|---|---|---|---|
| **Unit** | **Tlb** | **Tlb** | **Tlb** | **Tlb** | | **Trt** |
| **Description** | basalt | basalt | andesite | basalt | Basaltic andesite | basalt |
| **Latitude**[1] | 41.59908 | 41.60447 | 41.59541 | 41.59501 | 41.61038 | 41.46002 |
| **Longitude**[1] | -120.06781 | -120.00702 | -120.00851 | -119.99276 | -119.99927 | -120.25315 |
| **$SiO_2$** | 48.16 | 48.23 | 57.44 | 47.1 | 56.89 | 50.28 |
| **$TiO_2$** | 1.268 | 1.199 | 0.632 | 1.247 | 0.63 | 1.239 |
| **$Al_2O_3$** | 17.42 | 17.51 | 16.09 | 17.18 | 16.1 | 18.49 |
| **FeO** | 9.72 | 9.63 | 6.67 | 9.63 | 6.58 | 8.79 |
| **MnO** | 0.169 | 0.167 | 0.129 | 0.173 | 0.129 | 0.148 |
| **MgO** | 8.35 | 8.9 | 6.16 | 8.43 | 6.14 | 4.97 |
| **CaO** | 11.39 | 11 | 7.85 | 12.82 | 8.63 | 9.73 |
| **$Na_2O$** | 2.89 | 2.73 | 2.9 | 2.78 | 2.88 | 3.49 |
| **$K_2O$** | 0.44 | 0.39 | 2 | 0.4 | 1.89 | 0.88 |
| **$P_2O_5$** | 0.204 | 0.241 | 0.12 | 0.238 | 0.12 | 0.267 |
| **Volume sum** | | | | | | 98.3 |
| **Ba** | 199 | 261 | 423 | 201 | 437 | 414 |
| **La** | 9 | 8 | 14 | 10 | 15 | 12 |
| **Ce** | 15 | 15 | 26 | 13 | 25 | 23 |
| **Rb** | 6 | 6 | 56 | 4 | 45 | 13 |
| **Sr** | 346 | 394 | 226 | 381 | 244 | 644 |
| **Y** | 22 | 22 | 22 | 23 | 19 | 21 |
| **Zr** | 88 | 80 | 83 | 83 | 84 | 74 |
| **Nb** | 5.5 | 4.3 | 3.8 | 4.5 | 3.6 | 3.5 |
| **Co** | | | | | | |
| **Cr** | 192 | 205 | 140 | 193 | 135 | 97 |
| **Ni** | 147 | 177 | 112 | 180 | 103 | 51 |
| **Sc** | 36 | 37 | 27 | 35 | 24 | 29 |
| **V** | 226 | 243 | 162 | 233 | 151 | 280 |
| **Cu** | 103 | 96 | 85 | 128 | 85 | 99 |
| **Mo** | | | | | | |
| **Pb** | 2 | 2 | 8 | 1 | 7 | 4 |
| **Zn** | 63 | 63 | 49 | 63 | 49 | 86 |
| **Ga** | 16 | 15 | 15 | 15 | 14 | |
| **Th** | 1 | 1 | 6 | 1 | 5 | 2 |
| **U** | 0 | 1 | 1 | 0 | 1 | 0 |
| **Nd** | 12 | 9 | 13 | 11 | 12 | 17 |

[1] Latitude and longitude in WGS 84 coordinates.
* Sample data from Victor Camp, personal communication, 2008. Location is approximate based on field notes.

## Table A1, cont.

| Sample | WR08AE02 | WR08AE03 | WR08AE04 | WR08AE07 | WR08AE08 | WR08AE14 |
|---|---|---|---|---|---|---|
| **Unit** | **Trt** | | **Tovu** | **Tmvu** | **Tmvu** | **Tmvu** |
| **Description** | basalt | andesitic tuff | basalt | basalt | basalt | welded tuff |
| **Latitude**[1] | 41.45899 | 41.43837 | 41.47734 | 41.31076 | 41.31553 | 41.34763 |
| **Longitude**[1] | -120.27962 | -120.28921 | -120.27922 | -120.30493 | -120.28399 | -120.32976 |
| **$SiO_2$** | 49.5 | 64.53 | 55.19 | 50.25 | 53.04 | 64.74 |
| **$TiO_2$** | 1.163 | 0.481 | 0.635 | 1.068 | 1.475 | 0.851 |
| **$Al_2O_3$** | 18.39 | 15.82 | 18.85 | 17.48 | 17.49 | 14.8 |
| **FeO** | 9.08 | 2.01 | 7.62 | 8.92 | 8.9 | 3.32 |
| **MnO** | 0.155 | 0.028 | 0.177 | 0.156 | 0.142 | 0.113 |
| **MgO** | 5.92 | 0.66 | 3.39 | 7.13 | 3.36 | 0.83 |
| **CaO** | 9.76 | 2.21 | 7.99 | 8.98 | 7.44 | 2.15 |
| **$Na_2O$** | 3.37 | 2 | 3.47 | 3.31 | 4.42 | 3.71 |
| **$K_2O$** | 0.76 | 6.32 | 1.16 | 1 | 1.34 | 3.67 |
| **$P_2O_5$** | 0.265 | 0.078 | 0.227 | 0.442 | 0.617 | 0.192 |
| **Volume sum** | 98.35 | 94.14 | 98.72 | 98.74 | 98.21 | 94.37 |
| **Ba** | 389 | 1232 | 553 | 597 | 821 | 1209 |
| **La** | 15 | 29 | 15 | 22 | 20 | 34 |
| **Ce** | 21 | 60 | 24 | 43 | 49 | 70 |
| **Rb** | 11 | 185 | 23 | 16 | 19 | 72 |
| **Sr** | 621 | 318 | 754 | 659 | 665 | 300 |
| **Y** | 20 | 24 | 15 | 20 | 33 | 37 |
| **Zr** | 71 | 347 | 70 | 111 | 132 | 240 |
| **Nb** | 3.2 | 9.3 | 1.7 | 5.6 | 5.5 | 9.9 |
| **Co** | | | | | | |
| **Cr** | 121 | 9 | 11 | 172 | 24 | 3 |
| **Ni** | 58 | 3 | 4 | 126 | 10 | 0 |
| **Sc** | 30 | 7 | 18 | 26 | 27 | 13 |
| **V** | 258 | 69 | 185 | 237 | 231 | 30 |
| **Cu** | 100 | 17 | 162 | 74 | 44 | 1 |
| **Mo** | | | | | | |
| **Pb** | 3 | 23 | 13 | 7 | 7 | 17 |
| **Zn** | 83 | 49 | 94 | 99 | 109 | 90 |
| **Ga** | | | | | | |
| **Th** | 2 | 20 | 2 | 1 | 1 | 7 |
| **U** | 2 | 5 | 3 | 1 | 2 | 2 |
| **Nd** | 14 | 29 | 16 | 25 | 32 | 35 |

[1] Latitude and longitude in WGS 84 coordinates.
* Sample data from Victor Camp, personal communication, 2008. Location is approximate based on field notes.

## Table A1, cont.

| Sample | WR08AE16 | WR08AE17 | WR08AE18 | WR08AE19 | WR08AE20 |
|---|---|---|---|---|---|
| **Unit** | **Tmvu** | **Tmvu** | **Tmvu** | **Tmvu** | **Tovl** |
| **Description** | basalt | basalt | basalt | basalt | andesite |
| **Latitude**[1] | 41.33617 | 41.31171 | 41.28352 | 41.28649 | 41.71543 |
| **Longitude**[1] | -120.29749 | -120.33548 | -120.33652 | -120.34728 | -120.30203 |
| **$SiO_2$** | 50.65 | 51.53 | 52.18 | 53.33 | 56.41 |
| **$TiO_2$** | 1.122 | 1.059 | 1.107 | 1.059 | 0.555 |
| **$Al_2O_3$** | 17.89 | 17.64 | 17.88 | 17.59 | 18.94 |
| **FeO** | 8.75 | 8.5 | 8.27 | 8.09 | 6.63 |
| **MnO** | 0.136 | 0.146 | 0.139 | 0.157 | 0.155 |
| **MgO** | 5.51 | 5.78 | 4.51 | 5.35 | 1.83 |
| **CaO** | 9.1 | 9.02 | 8.89 | 8.56 | 7.32 |
| **$Na_2O$** | 3.47 | 3.34 | 3.33 | 3.4 | 3.88 |
| **$K_2O$** | 1.02 | 1.03 | 1.29 | 1.31 | 1.39 |
| **$P_2O_5$** | 0.473 | 0.267 | 0.366 | 0.343 | 0.433 |
| **Volume sum** | 98.12 | 98.32 | 97.97 | 99.18 | 97.54 |
| **Ba** | 613 | 517 | 869 | 1410 | 559 |
| **La** | 23 | 16 | 21 | 25 | 19 |
| **Ce** | 42 | 26 | 39 | 40 | 43 |
| **Rb** | 16 | 19 | 21 | 23 | 23 |
| **Sr** | 677 | 575 | 664 | 605 | 948 |
| **Y** | 22 | 18 | 24 | 31 | 19 |
| **Zr** | 114 | 98 | 120 | 123 | 109 |
| **Nb** | 5.4 | 4.2 | 5.5 | 5 | 3.3 |
| **Co** | | | | | |
| **Cr** | 134 | 154 | 102 | 108 | 1 |
| **Ni** | 84 | 99 | 53 | 66 | 1 |
| **Sc** | 27 | 26 | 25 | 25 | 10 |
| **V** | 228 | 222 | 220 | 221 | 119 |
| **Cu** | 79 | 83 | 64 | 66 | 62 |
| **Mo** | | | | | |
| **Pb** | 6 | 5 | 6 | 7 | 6 |
| **Zn** | 95 | 83 | 88 | 88 | 96 |
| **Ga** | | | | | |
| **Th** | 0 | 1 | 2 | 2 | 1 |
| **U** | 2 | 2 | 0 | 1 | 0 |
| **Nd** | 23 | 15 | 23 | 26 | 23 |

[1] Latitude and longitude in WGS 84 coordinates.
* Sample data from Victor Camp, personal communication, 2008. Location is approximate based on field notes.

## Table A2.

**WR07AE40 Plagioclase IRR266-44 J = 0.002439847**

| Step (°C) | % $^{39}Ar_K$ Rel | % $^{40}Ar^*$ | $^{40}Ar/^{39}Ar$ | $^{37}Ar/^{39}Ar$ | $^{36}Ar/^{39}Ar$ | K/Ca | Cl/K | Age **(Ma)** |
|---|---|---|---|---|---|---|---|---|
| 550 | 10.0750 | 6.953 | 55.94744 | 69.84314 | 0.19535 | 0.00717 | 0.16247 | 17.863 ± 1.221 |
| 625 | 19.9716 | 24.338 | 21.74895 | 72.27020 | 0.07554 | 0.00691 | 0.05958 | 24.305 ± 0.545 |
| 700 | 22.1514 | 15.047 | 34.21411 | 70.52274 | 0.11773 | 0.00709 | 0.00887 | 23.615 ± 0.716 |
| 775 | 16.9910 | 4.279 | 91.35055 | 66.56444 | 0.31419 | 0.00754 | 0.00277 | 17.911 ± 1.672 |
| 820 | 9.9378 | 3.941 | 95.54307 | 62.22192 | 0.32767 | 0.00809 | 0.00550 | 17.204 ± 1.863 |
| 875 | 7.8526 | 0.780 | 261.76782 | 55.31123 | 0.89410 | 0.00914 | 0.01112 | 9.305 ± 5.205 |
| 925 | 5.7056 | 0.792 | 304.35182 | 53.77897 | 1.03656 | 0.00941 | 0.04560 | 10.962 ± 7.952 |
| 975 | 3.6981 | 1.685 | 376.86279 | 52.91219 | 1.26838 | 0.00957 | 0.22811 | 28.737 ± 11.276 |
| 1025 | 3.6170 | 3.079 | 330.28443 | 55.11492 | 1.09840 | 0.00917 | 0.59223 | 45.875 ± 8.987 |

| | | | | | |
|---|---|---|---|---|---|
| | | | Wtd Mean Plateau age **(Ma)** | | none |
| | Intercept = | 290.9±1.2 | Isochron age **(Ma)** | MSWD = 1.11 | 25.40 ± 0.94 |
| | | | Integrated age **(Ma)** | | 20.729 ± 0.679 |

## Table A3.

**WR07AE49 Plagioclase IRR266-50 J = 0.002284517**

| Step (°C) | % $^{39}Ar_K$ Rel | % $^{40}Ar^*$ | $^{40}Ar/^{39}Ar$ | $^{37}Ar/^{39}Ar$ | $^{36}Ar/^{39}Ar$ | K/Ca | Cl/K | Age **(Ma)** |
|---|---|---|---|---|---|---|---|---|
| 550 | 0.8775 | 36.688 | 17.47286 | 13.84662 | 0.04119 | 0.03754 | -0.00004 | 26.471 ± 6.670 |
| 625 | 2.1047 | 60.080 | 10.99838 | 13.96394 | 0.01869 | 0.03723 | 0.00047 | 27.280 ± 0.797 |
| 700 | 6.4858 | 77.692 | 8.23487 | 14.41359 | 0.01014 | 0.03606 | 0.00017 | 26.428 ± 0.179 |
| 775 | 5.8394 | 88.559 | 7.21550 | 14.93880 | 0.00688 | 0.03478 | 0.00012 | 26.405 ± 0.414 |
| 850 | 8.2472 | 92.317 | 6.95964 | 14.42862 | 0.00575 | 0.03602 | 0.00007 | 26.539 ± 0.174 |
| 925 | 13.3539 | 92.257 | 6.97018 | 14.81898 | 0.00587 | 0.03506 | 0.00012 | 26.569 ± 0.125 |
| 1000 | 14.2586 | 87.774 | 7.35616 | 14.46968 | 0.00699 | 0.03591 | -0.00010 | 26.671 ± 0.249 |
| 1075 | 16.8916 | 95.331 | 6.74250 | 14.67075 | 0.00507 | 0.03542 | -0.00002 | 26.555 ± 0.126 |
| 1150 | 12.4807 | 96.646 | 6.66326 | 14.38482 | 0.00468 | 0.03613 | 0.00006 | 26.599 ± 0.130 |
| 1225 | 7.5982 | 93.619 | 6.80873 | 14.52931 | 0.00544 | 0.03577 | 0.00026 | 26.333 ± 0.194 |
| 1400 | 11.8624 | 92.565 | 6.93284 | 13.84240 | 0.00552 | 0.03756 | 0.00027 | 26.498 ± 0.275 |

| | | | | | |
|---|---|---|---|---|---|
| | | | Wtd Mean Plateau age **(Ma)** | MSWD = | 26.54 ± 0.08 |
| | Intercept = | 295±14 | Isochron age **(Ma)** | MSWD = | 26.53 ± 0.09 |
| | | | Integrated age **(Ma)** | | 26.551 ± 0.151 |
| | | | Low Cl/K age **(Ma)** | MSWD = | ± |

## Table A4.

**AE05WR03 Plagioclase IRR266-38 J = 0.002626108**

| Step (°C) | % $^{39}Ar_K$ Rel | % $^{40}Ar^*$ | $^{40}Ar/^{39}Ar$ | $^{37}Ar/^{39}Ar$ | $^{36}Ar/^{39}Ar$ | K/Ca | Cl/K | Age **(Ma)** |
|---|---|---|---|---|---|---|---|---|
| 550 | 3.8209 | 2.069 | 163.25409 | 78.24913 | 0.56249 | 0.00636 | 0.22975 | 16.800 ± 34.037 |
| 600 | 7.2916 | 7.556 | 71.70566 | 106.83624 | 0.25366 | 0.00456 | 0.12916 | 27.414 ± 4.633 |
| 675 | 17.8692 | 21.360 | 24.83480 | 118.38713 | 0.09862 | 0.00408 | 0.02190 | 27.065 ± 1.353 |
| 750 | 22.7133 | 70.635 | 7.67623 | 116.72118 | 0.03970 | 0.00415 | 0.00249 | 27.627 ± 0.513 |
| 825 | 20.8421 | 65.968 | 8.09148 | 116.12173 | 0.04123 | 0.00417 | 0.00921 | 27.189 ± 0.551 |
| 900 | 12.2632 | 28.556 | 18.61155 | 110.95241 | 0.07549 | 0.00438 | 0.04051 | 26.973 ± 0.904 |
| 985 | 5.9499 | 17.630 | 25.95670 | 97.94622 | 0.09929 | 0.00501 | 1.42026 | 23.036 ± 1.693 |
| 1085 | 2.1914 | 13.713 | 39.32596 | 86.99650 | 0.13869 | 0.00568 | 0.59056 | 26.910 ± 3.818 |
| 1200 | 1.7169 | 1.707 | 98.29517 | 70.91038 | 0.34635 | 0.00705 | 0.08023 | 8.323 ± 7.790 |
| 1400 | 5.3414 | 0.102 | 267.90479 | 105.05444 | 0.93453 | 0.00465 | 0.04336 | 1.392 ± 8.230 |

| | | | | | |
|---|---|---|---|---|---|
| | | | Wtd Mean Plateau age **(Ma)** | MSWD = 0.99 | 27.17 ± 0.33 |
| | Intercept = | 293.7±7.5 | Isochron age **(Ma)** | MSWD = 0.16 | 27.48 ± 0.48 |
| | | | Integrated age **(Ma)** | | 24.92 ± 0.59 |
| | | | Low Cl/K age **(Ma)** | MSWD = | 27.6 ± 0.5 |

## Table A5.

**07-C-6 Plagioclase IRR266-42 J = 0.002506046**

| Step (°C) | % $^{39}Ar_K$ Rel | % $^{40}Ar^*$ | $^{40}Ar/^{39}Ar$ | $^{37}Ar/^{39}Ar$ | $^{36}Ar/^{39}Ar$ | K/Ca | Cl/K | Age **(Ma)** |
|---|---|---|---|---|---|---|---|---|
| 550 | 1.6336 | 60.632 | 10.05269 | 16.42473 | 0.01786 | 0.03160 | 0.02099 | 27.647 ± 2.355 |
| 625 | 4.9166 | 80.859 | 7.51154 | 16.72784 | 0.00943 | 0.03102 | 0.00793 | 27.556 ± 0.756 |
| 700 | 10.2258 | 87.022 | 6.72620 | 17.10845 | 0.00763 | 0.03032 | 0.00137 | 26.570 ± 0.212 |
| 775 | 17.1761 | 90.190 | 6.52065 | 17.16298 | 0.00685 | 0.03022 | 0.00061 | 26.696 ± 0.147 |
| 850 | 17.7963 | 89.985 | 6.57178 | 17.27796 | 0.00695 | 0.03002 | 0.00240 | 26.845 ± 0.157 |
| 925 | 11.6229 | 84.078 | 7.06368 | 17.25008 | 0.00852 | 0.03007 | 0.00811 | 26.959 ± 0.192 |
| 1000 | 6.3171 | 70.100 | 8.31372 | 16.30165 | 0.01287 | 0.03184 | 0.24577 | 26.441 ± 0.280 |
| 1075 | 2.4023 | 74.297 | 8.06667 | 15.75030 | 0.01131 | 0.03297 | 0.02144 | 27.177 ± 0.607 |
| 1150 | 3.9203 | 84.756 | 7.02928 | 15.45012 | 0.00784 | 0.03361 | 0.01952 | 27.010 ± 0.537 |
| 1400 | 23.9889 | 92.071 | 6.45840 | 15.99159 | 0.00610 | 0.03246 | 0.00240 | 26.969 ± 0.131 |

| | | | | | |
|---|---|---|---|---|---|
| | | | Wtd Mean Plateau age **(Ma)** | MSWD = 0.81 | 26.821 ± 0.083 |
| | Intercept = | 288±17 | Isochron age **(Ma)** | MSWD = 0.88 | 26.90 ± 0.13 |
| | | | Integrated age **(Ma)** | | 26.871 ± 0.161 |
| | | | Low Cl/K age **(Ma)** | MSWD = | 26.70 ± 0.15 |

## Table A6.

**07-C-19 Plagioclase IRR266-40 J = 0.002561241**

| Step (°C) | % $^{39}Ar_K$ Rel | % $^{40}Ar^*$ | $^{40}Ar/^{39}Ar$ | $^{37}Ar/^{39}Ar$ | $^{36}Ar/^{39}Ar$ | K/Ca | Cl/K | Age **(Ma)** |
|---|---|---|---|---|---|---|---|---|
| 550 | 0.4424 | 51.760 | 11.22553 | 19.94881 | 0.02373 | 0.02596 | 0.00220 | 27.003 ± 2.956 |
| 625 | 1.8866 | 62.462 | 8.67826 | 21.50875 | 0.01690 | 0.02405 | 0.00015 | 25.232 ± 1.093 |
| 700 | 4.8044 | 81.111 | 6.77415 | 22.19006 | 0.01040 | 0.02330 | 0.00026 | 25.585 ± 0.667 |
| 775 | 9.0968 | 87.715 | 6.23086 | 22.31545 | 0.00869 | 0.02317 | 0.00214 | 25.452 ± 0.224 |
| 850 | 13.8489 | 88.679 | 6.12627 | 22.59742 | 0.00853 | 0.02287 | 0.00026 | 25.306 ± 0.172 |
| 925 | 17.3422 | 93.034 | 5.83461 | 22.81220 | 0.00762 | 0.02265 | 0.00045 | 25.288 ± 0.154 |
| 1000 | 13.2893 | 80.198 | 6.82465 | 23.00961 | 0.01087 | 0.02246 | 0.00055 | 25.500 ± 0.198 |
| 1075 | 11.2411 | 94.603 | 5.79041 | 22.98090 | 0.00735 | 0.02248 | 0.00101 | 25.521 ± 0.198 |
| 1150 | 7.3812 | 88.149 | 6.25748 | 22.17908 | 0.00858 | 0.02331 | 0.00296 | 25.683 ± 0.254 |
| 1250 | 13.6456 | 90.927 | 6.25712 | 21.00064 | 0.00767 | 0.02464 | 0.00970 | 26.465 ± 0.176 |
| 1350 | 7.0215 | 89.013 | 6.55638 | 23.71221 | 0.00892 | 0.02178 | 0.00363 | 27.191 ± 0.243 |

| | | | | |
|---|---|---|---|---|
| | | Wtd Mean Plateau age **(Ma)** | MSWD = 0.38 | 25.42 ± 0.05 |
| Intercept = | 304±24 | Isochron age **(Ma)** | MSWD = 0.37 | 25.31 ± 0.16 |
| | | Integrated age **(Ma)** | | 25.704 ± 0.140 |
| | | Low Cl/K age **(Ma)** | | none |

## Table A7.

**07-C-10 Groundmass IRR266-36 J = 0.002673929**

| Step (°C) | % $^{39}Ar_K$ Rel | % $^{40}Ar^*$ | $^{40}Ar/^{39}Ar$ | $^{37}Ar/^{39}Ar$ | $^{36}Ar/^{39}Ar$ | K/Ca | Cl/K | Age **(Ma)** |
|---|---|---|---|---|---|---|---|---|
| 550 | 3.2430 | 95.253 | 5.34789 | 0.51109 | 0.00097 | 1.02628 | 0.00051 | 24.416 ± 0.107 |
| 625 | 18.4908 | 98.437 | 5.15439 | 0.35387 | 0.00034 | 1.48240 | 0.00017 | 24.317 ± 0.081 |
| 650 | 13.5939 | 98.713 | 5.09163 | 0.35571 | 0.00029 | 1.47474 | 0.00008 | 24.090 ± 0.080 |
| 675 | 9.6789 | 98.540 | 5.09637 | 0.44362 | 0.00034 | 1.18241 | 0.00010 | 24.072 ± 0.080 |
| 725 | 6.4058 | 97.978 | 5.14908 | 0.65575 | 0.00050 | 0.79981 | 0.00017 | 24.185 ± 0.083 |
| 775 | 5.1043 | 97.397 | 5.16709 | 0.73495 | 0.00063 | 0.71358 | 0.00033 | 24.127 ± 0.084 |
| 840 | 7.7527 | 97.792 | 5.10596 | 0.65833 | 0.00053 | 0.79667 | 0.00047 | 23.938 ± 0.082 |
| 800 | 1.7458 | 99.835 | 5.06708 | 0.60456 | 0.00016 | 0.86755 | 0.00053 | 24.249 ± 0.101 |
| 900 | 8.4479 | 97.946 | 5.07872 | 0.65409 | 0.00050 | 0.80184 | 0.00075 | 23.849 ± 0.081 |
| 950 | 7.7645 | 96.426 | 5.11421 | 0.74151 | 0.00079 | 0.70726 | 0.00107 | 23.645 ± 0.083 |
| 1000 | 10.3963 | 95.233 | 5.13722 | 1.29327 | 0.00116 | 0.40537 | 0.01174 | 23.467 ± 0.083 |
| 1050 | 6.5585 | 94.658 | 5.16354 | 6.67332 | 0.00274 | 0.07828 | 0.00149 | 23.529 ± 0.089 |
| 1125 | 0.8175 | 92.831 | 5.38338 | 15.03452 | 0.00542 | 0.03455 | 0.00238 | 24.187 ± 0.190 |

| | | | | |
|---|---|---|---|---|
| | | Wtd Mean Plateau age **(Ma)** | | none |
| Intercept = | 183 ± 130 | Isochron age **(Ma)** | MSWD = 11.1 | 24.2 ± 0.3 |
| | | Integrated age **(Ma)** | | 23.98 ± 0.11 |
| | | Low Cl/K age **(Ma)** | | **24.1 ± 0.1** |

## Table A8.

**JC08-WR405 Groundmass IRR266-48 J = 0.002344283**

| Step (°C) | % $^{39}Ar_K$ Rel | % $^{40}Ar^*$ | $^{40}Ar/^{39}Ar$ | $^{37}Ar/^{39}Ar$ | $^{36}Ar/^{39}Ar$ | K/Ca | Cl/K | Age **(Ma)** |
|---|---|---|---|---|---|---|---|---|
| 550 | 5.5866 | 78.324 | 9.52682 | 1.73351 | 0.00744 | 0.30233 | 0.00145 | 31.321 ± 0.714 |
| 625 | 15.0842 | 56.557 | 12.56579 | 2.59557 | 0.01916 | 0.20180 | 0.00103 | 29.860 ± 0.583 |
| 630 | 6.1304 | 80.431 | 8.36867 | 2.33084 | 0.00615 | 0.22476 | 0.00036 | 28.288 ± 0.292 |
| 675 | 9.5608 | 85.116 | 7.74587 | 2.10048 | 0.00445 | 0.24945 | 0.00056 | 27.709 ± 0.140 |
| 725 | 14.5490 | 88.393 | 7.49387 | 1.77963 | 0.00340 | 0.29449 | 0.00089 | 27.832 ± 0.149 |
| 775 | 12.4805 | 87.941 | 7.44417 | 1.92384 | 0.00354 | 0.27239 | 0.00151 | 27.511 ± 0.128 |
| 825 | 8.2313 | 86.060 | 7.57651 | 2.11855 | 0.00413 | 0.24732 | 0.00254 | 27.406 ± 0.135 |
| 875 | 6.7535 | 88.282 | 7.31887 | 1.68067 | 0.00333 | 0.31185 | 0.00497 | 27.152 ± 0.121 |
| 925 | 8.2794 | 85.092 | 7.69408 | 1.93784 | 0.00438 | 0.27042 | 0.00815 | 27.514 ± 0.124 |
| 975 | 7.9472 | 77.377 | 8.38911 | 5.93968 | 0.00803 | 0.08799 | 0.05453 | 27.353 ± 0.133 |
| 1025 | 4.7824 | 70.481 | 9.03032 | 14.83917 | 0.01307 | 0.03501 | 0.00599 | 26.982 ± 0.173 |
| 1075 | 0.4734 | 59.955 | 11.25541 | 14.31843 | 0.01915 | 0.03630 | 0.00484 | 28.585 ± 1.791 |
| 1150 | 0.1413 | 35.761 | 18.72379 | 13.79688 | 0.04452 | 0.03768 | 0.00265 | 28.355 ± 7.095 |

| | | | | | |
|---|---|---|---|---|---|
| | | | Wtd Mean Plateau age **(Ma)** | MSWD = | none |
| | Intercept | ± | Isochron age **(Ma)** | MSWD = | **27.50 ± 0.21** |
| | | | Integrated age **(Ma)** | | 28.128 ± 0.156 |
| | | | Low Cl/K age **(Ma)** | MSWD = | 28.3 ± 0.3 |

## Table A9.

**JC07-WR303 Sanidine IRR253-88 07L0305 J = 0.002071645**

| Run # | $^{40}Ar^*$ (mol/g ) | % $^{40}Ar^*$ | $^{40}Ar/^{39}Ar$ | $^{37}Ar/^{39}Ar$ | $^{36}Ar/^{39}Ar$ | K/Ca | Cl/K | Age (Ma) |
|---|---|---|---|---|---|---|---|---|
| 07L0305A | 3.6460E-14 | 98.251 | 7.11870 | 0.31584 | 0.00048 | 1.66094 | 0.00071 | 25.958 ± 0.112 |
| 07L0305B | 3.0870E-14 | 97.804 | 7.14536 | 0.30923 | 0.00058 | 1.69646 | 0.00084 | 25.937 ± 0.120 |
| 07L0305C | 3.3157E-14 | 98.861 | 7.12637 | 0.29048 | 0.00032 | 1.80596 | 0.00045 | 26.145 ± 0.116 |
| 07L0305D | 2.6224E-14 | 97.200 | 7.01449 | 0.28143 | 0.00071 | 1.86406 | 0.00043 | ~~25.308 ± 0.127~~ |
| 07L0305E | 2.7700E-14 | 97.639 | 7.16840 | 0.39514 | 0.00065 | 1.32754 | 0.00028 | 25.978 ± 0.127 |
| 07L0305F | 2.8506E-14 | 98.851 | 7.13443 | 0.29685 | 0.00033 | 1.76725 | 0.00035 | 26.172 ± 0.128 |

| | | | |
|---|---|---|---|
| n = 5 | Weighted Mean Age (Ma) | (MSWD = 0.83) | 26.04 ± 0.05 |
| | Isochron age (Ma) | | N/A |
| | Total gas age (Ma) | | 25.929 ± 0.045 |

**Figure A1.**

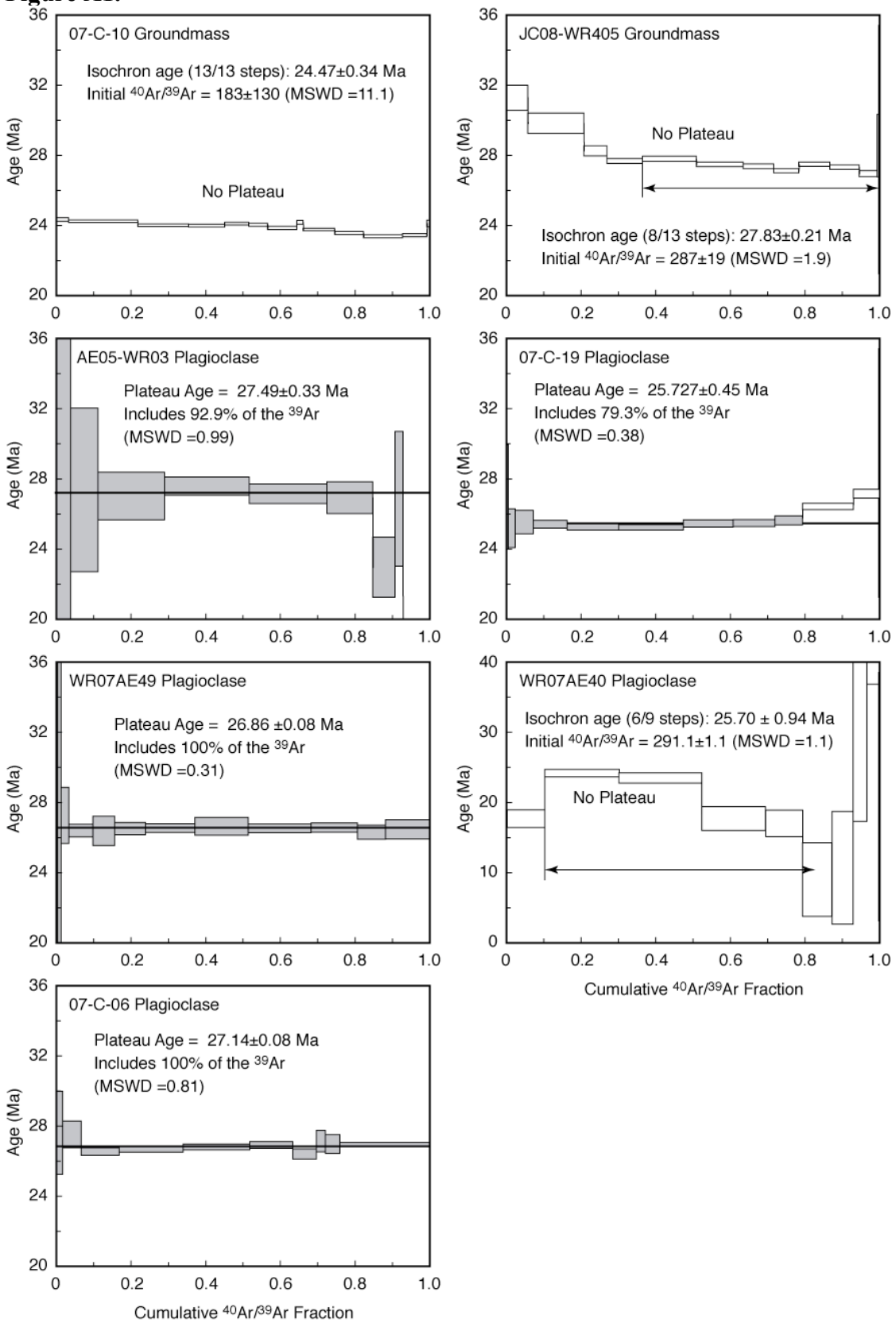
07-C-10 Groundmass
Isochron age (13/13 steps): 24.47±0.34 Ma
Initial 40Ar/39Ar = 183±130 (MSWD =11.1)
No Plateau
JC08-WR405 Groundmass
No Plateau
Isochron age (8/13 steps): 27.83±0.21 Ma
Initial 40Ar/39Ar = 287±19 (MSWD =1.9)
AE05-WR03 Plagioclase
Plateau Age = 27.49±0.33 Ma
Includes 92.9% of the 39Ar
(MSWD =0.99)
07-C-19 Plagioclase
Plateau Age = 25.727±0.45 Ma
Includes 79.3% of the 39Ar
(MSWD =0.38)
WR07AE49 Plagioclase
Plateau Age = 26.86 ±0.08 Ma
Includes 100% of the 39Ar
(MSWD =0.31)
WR07AE40 Plagioclase
Isochron age (6/9 steps): 25.70 ± 0.94 Ma
Initial 40Ar/39Ar = 291.1±1.1 (MSWD =1.1)
No Plateau
07-C-06 Plagioclase
Plateau Age = 27.14±0.08 Ma
Includes 100% of the 39Ar
(MSWD =0.81)
Age (Ma)
Cumulative 40Ar/39Ar Fraction

## Notes for Tables A10-A13:

These data were obtained at the New Mexico Geochronology Research Laboratory.
Isotopic ratios corrected for blank, radioactive decay, and mass discrimination, not corrected for interfering reactions.
Errors quoted for individual analyses include analytical error only, without interfering reaction or J uncertainties.
Mean age is weighted mean age of Taylor (1982). Mean age error is weighted error of the mean (Taylor, 1982), multiplied by the root of the MSWD where MSWD>1, and also incorporates uncertainty in J factors and irradiation correction uncertainties.
Decay constants and isotopic abundances after Steiger and Jäger (1977).
# symbol preceding sample ID denotes analyses excluded from mean age calculations.
Ages calculated relative to FC-2 Fish Canyon Tuff sanidine interlaboratory standard at 27.84 Ma
Decay Constant (LambdaK (total)) = 5.543e-10/a
Correction factors:
(39Ar/37Ar)Ca = 0.00068 ± 5e-05
(36Ar/37Ar)Ca = 0.00028 ± 2e-05
(38Ar/39Ar)K = 0.0125
(40Ar/39Ar)K = 0 ± 0.0004
*analysis in lines in italics not used in final age calculation*

## Table A10.

| ID | Power (watts) | $^{40}Ar/^{39}Ar$ | $^{38}Ar/^{39}Ar$ | $^{37}Ar/^{39}Ar$ | $^{36}Ar/^{39}Ar$ (x $10^{-3}$) | $^{39}ArK$ (x $10^{-15}$ mol) | K/Ca | Cl/K | $^{40}Ar^{*}$ (%) | Age (Ma) | ±1s (Ma) |
|---|---|---|---|---|---|---|---|---|---|---|---|
| **H08-57, anorthoclase, J=0.0008649±0.05%, D=1.004±0.001, NM-221A, Lab#=58640** | | | | | | | | | | | |
| *08A* | *3.2* | *17.14* | *0.0170628* | *3.4557* | *2.1492* | *0.657* | *0.1* | *0.001213838* | *98.0* | *26.071* | *0.358* |
| 10A | 3.2 | 17.33 | 0.0137873 | 0.1915 | 1.1867 | 1.862 | 2.7 | 0.000298402 | 98.1 | 26.322 | 0.139 |
| 14A | 3.2 | 17.35 | 0.0128373 | 0.1474 | 1.1256 | 1.939 | 3.5 | 3.76358E-05 | 98.2 | 26.375 | 0.129 |
| 09A | 3.2 | 17.40 | 0.0129299 | 0.1434 | 1.1501 | 4.594 | 3.6 | 6.19526E-05 | 98.1 | 26.449 | 0.082 |
| 07A | 3.2 | 17.20 | 0.0124395 | 0.1411 | 0.3206 | 4.874 | 3.6 | -3.09849E-05 | 99.5 | 26.522 | 0.074 |
| 11A | 3.2 | 17.39 | 0.0132398 | 0.1429 | 0.8971 | 2.224 | 3.6 | 0.000160896 | 98.5 | 26.551 | 0.126 |
| 06A | 3.2 | 17.41 | 0.0133579 | 0.1633 | 0.8759 | 2.628 | 3.1 | 0.000195058 | 98.6 | 26.588 | 0.114 |
| 05A | 3.2 | 17.30 | 0.0133166 | 0.1146 | 0.4594 | 3.669 | 4.5 | 0.000204357 | 99.3 | 26.604 | 0.080 |
| 12A | 3.2 | 17.24 | 0.0129486 | 0.1405 | 0.2021 | 5.632 | 3.6 | 0.000116176 | 99.7 | 26.635 | 0.066 |
| 02A | 3.2 | 17.56 | 0.011968 | 0.1411 | 1.2012 | 6.221 | 3.6 | -0.000207205 | 98.0 | 26.672 | 0.061 |
| 13A | 3.2 | 17.18 | 0.0130391 | 0.1521 | -0.1272 | 1.651 | 3.4 | 0.000158497 | 100.3 | 26.694 | 0.138 |
| 03A | 3.2 | 17.41 | 0.0125145 | 0.1894 | 0.5801 | 3.927 | 2.7 | -2.28307E-05 | 99.1 | 26.727 | 0.077 |
| 04A | 3.2 | 17.22 | 0.0129799 | 0.1539 | -0.1469 | 2.532 | 3.3 | 0.000143147 | 100.3 | 26.767 | 0.093 |
| 01A | 3.2 | 17.32 | 0.0120527 | 0.1306 | 0.1385 | 8.726 | 3.9 | -0.000128884 | 99.8 | 26.788 | 0.054 |
| 15A | 3.2 | 17.61 | 0.0154218 | 0.1858 | 0.8192 | 1.352 | 2.7 | 0.000770149 | 98.7 | 26.923 | 0.155 |
| **Mean age ± 2s** | | | | **n=14** | **MSWD=2.52** | | **3.4** | **±1.0** | | **26.642** | **0.077** |

## Table A11.

| ID | Power (watts) | $^{40}Ar/^{39}Ar$ | $^{38}Ar/^{39}Ar$ | $^{37}Ar/^{39}Ar$ | $^{36}Ar/^{39}Ar$ ($x\ 10^{-3}$) | $^{39}ArK$ ($x\ 10^{-15}$ mol) | K/Ca | Cl/K | $^{40}Ar^*$ (%) | Age (Ma) | ±1s (Ma) |
|---|---|---|---|---|---|---|---|---|---|---|---|
| **JC08-WR410, plag, J=0.0008571±0.06%, D=1.004±0.001, NM-221D, Lab#=58674** | | | | | | | | | | | |
| 01 | 0.65 | 20.45 | 0.0272614 | 4.0463 | 31.3362 | 0.250 | 0.13 | 0.002545656 | 56.4 | 17.784 | 1.291 |
| 14 | 3.2 | 14.94 | 0.0156973 | 4.8037 | 11.5929 | 1.083 | 0.11 | 0.000369212 | 79.7 | 18.388 | 0.281 |
| 12 | 3.2 | 15.27 | 0.0144712 | 5.6012 | 12.2883 | 0.747 | 0.09 | 6.21188E-06 | 79.3 | 18.690 | 0.449 |
| 03 | 3.2 | 18.64 | 0.0202985 | 3.7165 | 22.6609 | 1.143 | 0.14 | 0.001054815 | 65.7 | 18.891 | 0.362 |
| 02 | 3.2 | 13.32 | 0.0166483 | 4.7696 | 4.5699 | 0.620 | 0.11 | 0.000996589 | 92.8 | 19.079 | 0.519 |
| 16 | 3.2 | 18.94 | 0.020484 | 4.6378 | 23.0957 | 1.237 | 0.11 | 0.001100747 | 66.0 | 19.288 | 0.320 |
| 11 | 3.2 | 21.09 | 0.0223018 | 5.2670 | 30.5658 | 0.250 | 0.10 | 0.001230813 | 59.2 | 19.291 | 1.272 |
| 07 | 3.2 | 14.30 | 0.0152881 | 5.8282 | 7.5523 | 1.028 | 0.09 | 0.000482563 | 87.8 | 19.382 | 0.306 |
| 13 | 3.2 | 14.89 | 0.0148313 | 4.6121 | 8.9638 | 1.343 | 0.11 | 0.000261376 | 84.8 | 19.473 | 0.240 |
| 05 | 3.2 | 14.16 | 0.0111561 | 4.7172 | 6.476 | 0.616 | 0.11 | -0.000629279 | 89.2 | 19.489 | 0.511 |
| 04 | 3.2 | 15.67 | 0.0139484 | 6.6472 | 12.159 | 0.678 | 0.08 | -0.000114524 | 80.6 | 19.508 | 0.496 |
| 08 | 3.2 | 15.69 | 0.0170562 | 5.2745 | 11.7531 | 0.684 | 0.10 | 0.000746915 | 80.6 | 19.526 | 0.475 |
| 15 | 3.2 | 16.18 | 0.0184513 | 5.8688 | 13.44 | 0.936 | 0.09 | 0.001058091 | 78.5 | 19.594 | 0.408 |
| 10 | 3.2 | 21.48 | 0.015118 | 5.3539 | 29.5395 | 0.346 | 0.10 | -0.000711595 | 61.4 | 20.357 | 0.798 |
| 09 | 3.2 | 14.54 | 0.0124484 | 4.5372 | 3.3207 | 0.265 | 0.11 | -0.000109797 | 95.8 | 21.490 | 1.055 |
| 06 | 3.2 | 20.66 | 0.0122313 | 6.8319 | 24.5358 | 0.165 | 0.07 | -0.001230151 | 67.6 | 21.573 | 1.819 |
| **Mean age ± 2s** | | | | **n=16** | **MSWD=1.60** | | **0.10 ±0.03** | | | **19.22** | **0.27** |

## Table A12.

| ID | Power (watts) | $^{40}Ar/^{39}Ar$ | $^{38}Ar/^{39}Ar$ | $^{37}Ar/^{39}Ar$ | $^{36}Ar/^{39}Ar$ ($x\ 10^{-3}$) | $^{39}ArK$ ($x\ 10^{-15}$ mol) | K/Ca | Cl/K | $^{40}Ar^*$ (%) | Age (Ma) | ±1s (Ma) |
|---|---|---|---|---|---|---|---|---|---|---|---|
| **JC08-WR412, san, J=0.000852±0.05%, D=1.004±0.001, NM-221G, Lab#=58695** | | | | | | | | | | | |
| *09* | *3.2* | *16.83* | *0.0113308* | *0.0105* | *0.5564* | *2.604* | *48.6* | *-0.000352507* | *99.0* | *25.443* | *0.096* |
| 04 | 3.2 | 16.87 | 0.013197 | 0.0112 | 0.2315 | 2.500 | 45.7 | 0.00018127 | 99.6 | 25.648 | 0.106 |
| 03 | 3.2 | 16.90 | 0.0127999 | 0.0083 | 0.2556 | 10.944 | 61.2 | 6.99768E-05 | 99.6 | 25.674 | 0.049 |
| 08 | 3.2 | 17.42 | 0.0126102 | 0.0110 | 1.9095 | 4.214 | 46.6 | -6.8174E-05 | 96.8 | 25.726 | 0.080 |
| 05 | 3.2 | 16.92 | 0.0122261 | 0.0095 | 0.2165 | 4.278 | 53.5 | -8.69216E-05 | 99.6 | 25.727 | 0.075 |
| 02 | 3.2 | 17.07 | 0.0123734 | 0.0087 | 0.6748 | 4.027 | 58.6 | -6.98664E-05 | 98.8 | 25.747 | 0.081 |
| 06 | 3.2 | 16.98 | 0.01154 | 0.0077 | 0.2355 | 5.478 | 66.4 | -0.000277987 | 99.6 | 25.807 | 0.063 |
| 07 | 3.2 | 17.00 | 0.0117052 | 0.0101 | 0.2978 | 3.609 | 50.6 | -0.000235413 | 99.5 | 25.815 | 0.082 |
| 13 | 3.2 | 16.99 | 0.0125361 | 0.0082 | 0.2482 | 5.011 | 62.2 | -2.71502E-06 | 99.6 | 25.824 | 0.071 |
| 11 | 3.2 | 17.07 | 0.0127138 | 0.0092 | 0.3285 | 2.083 | 55.7 | 4.23658E-05 | 99.4 | 25.900 | 0.131 |
| 10 | 3.2 | 17.04 | 0.0117796 | 0.0102 | 0.1707 | 2.361 | 50.0 | -0.00020822 | 99.7 | 25.934 | 0.108 |
| 12 | 3.2 | 17.22 | 0.0125727 | 0.0080 | 0.4508 | 1.629 | 63.5 | -3.07143E-06 | 99.2 | 26.077 | 0.164 |
| *01* | *3.2* | *17.41* | *0.011945* | *0.0097* | *0.168* | *13.722* | *52.7* | *-0.000162273* | *99.7* | *26.494* | *0.052* |
| **Mean age ± 2s** | | | | **n=11** | **MSWD=1.38** | | **55.8 ±14.2** | | | **25.765** | **0.061** |

## Table A13.

| ID | Power (watts) | $^{40}Ar/^{39}Ar$ | $^{38}Ar/^{39}Ar$ | $^{37}Ar/^{39}Ar$ | $^{36}Ar/^{39}Ar$ (x $10^{-3}$) | $^{39}ArK$ (x $10^{-15}$ mol) | K/Ca | Cl/K | $^{40}Ar^{*}$ (%) | Age (Ma) | ±1s (Ma) |
|---|---|---|---|---|---|---|---|---|---|---|---|
| **JC08-WR411, san, J=0.0008306±0.05%, D=1.004±0.001, NM-221M, Lab#=58734** | | | | | | | | | | | |
| 06A | 3.2 | 17.90 | 0.0121843 | 0.0103 | 0.5625 | 12.790 | 49.7 | -0.000116406 | 99.1 | 26.382 | 0.050 |
| 07A | 3.2 | 17.91 | 0.0118818 | 0.0100 | 0.4886 | 18.232 | 51.2 | -0.000196377 | 99.2 | 26.425 | 0.050 |
| 10A | 3.2 | 17.87 | 0.0125958 | 0.0098 | 0.3501 | 17.293 | 51.9 | 8.57227E-06 | 99.4 | 26.436 | 0.049 |
| 09A | 3.2 | 17.97 | 0.0122719 | 0.0106 | 0.6462 | 16.709 | 48.3 | -9.64699E-05 | 98.9 | 26.451 | 0.049 |
| 04A | 3.2 | 17.86 | 0.0123285 | 0.0103 | 0.1943 | 17.596 | 49.4 | -5.73937E-05 | 99.7 | 26.481 | 0.049 |
| 15A | 3.2 | 18.03 | 0.0129255 | 0.0110 | 0.7347 | 10.300 | 46.4 | 8.0003E-05 | 98.8 | 26.491 | 0.050 |
| 02A | 3.2 | 17.88 | 0.01215 | 0.0102 | 0.2155 | 19.283 | 49.9 | -0.000107938 | 99.6 | 26.500 | 0.045 |
| 01A | 3.2 | 17.97 | 0.0122005 | 0.0298 | 0.4833 | 29.704 | 17.1 | -0.000107489 | 99.2 | 26.519 | 0.039 |
| 05A | 3.2 | 17.90 | 0.0119761 | 0.0124 | 0.1809 | 10.596 | 41.2 | -0.000154281 | 99.7 | 26.546 | 0.052 |
| 03A | 3.2 | 17.97 | 0.0118132 | 0.0171 | 0.368 | 13.736 | 29.9 | -0.000209015 | 99.4 | 26.573 | 0.053 |
| 14A | 3.2 | 17.92 | 0.0125249 | 0.0105 | 0.1428 | 7.301 | 48.4 | -3.20001E-07 | 99.8 | 26.596 | 0.055 |
| 12A | 3.2 | 17.93 | 0.0129579 | 0.0109 | 0.1615 | 8.050 | 46.9 | 0.000118659 | 99.7 | 26.599 | 0.051 |
| 08A | 3.2 | 17.97 | 0.0121555 | 0.0115 | 0.1111 | 12.902 | 44.5 | -0.000100988 | 99.8 | 26.682 | 0.048 |
| 11A | 3.2 | 18.01 | 0.0126522 | 0.0307 | 0.1512 | 10.810 | 16.6 | 3.48472E-05 | 99.8 | 26.720 | 0.053 |
| *13A* | *3.2* | *18.07* | *0.0128226* | *1.3048* | *0.661* | *0.931* | *0.39* | *7.7204E-05* | *99.5* | *26.766* | *0.274* |
| **Mean age ± 2s** | | | | **n=14** | **MSWD=3.72** | | **42.3** | **±24.2** | | **26.526** | **0.058** |

**Table A14.**

| Map unit | Age | Short desription | Thickness | Long description |
|---|---|---|---|---|
| **Qal** | Holocene | Alluvium | | Unconsolidated sedimentary deposits associated with modern fluvial systems. |
| **Qf** | Holocene | Fan deposits | | Unconsolidated coarse gravel deposits in alluvial fans. |
| **Qc** | Holocene | Colluvium | | Unconsolidated soil and sediments deposited at the base of slopes by sheetwash. |
| **Ql** | Holocene | Modern lakes | | Perennial lakes. |
| **Qp** | Holocene | Playa deposits | | Evaporite and clay deposits in ephemeral lakes. |
| **Qhs** | Holocene | Hot spring deposits | | Siliceous and calcareous sinter, where sufficiently abundant to be mapped separately. |
| **Qls** | Holocene | Landslides and slumps | | Undifferentiated landslides, including debris flows and slump blocks. |
| **Qe** | Holocene | Eolian deposits | | Eolian sand dunes, mostly stabilized as indicated by vegetation growth. |
| **Qoa** | Pleistocene (?) | Older alluvium | | Older fluvial deposits, possibly Pleistocene, currently being dissected by modern streams. |
| **Qof** | Pleistocene (?) | Older fan deposits | | Older alluvial fan deposits, possibly Pleistocene, currently being dissected by modern streams. |
| **Qols** | Pleistocene (?) | Older landslides | | Stratigraphically and geomorphically older landslides and debris flows, possibly Pleistocene. |
| **Qpd** | Pleistocene | Delta deposits | | Gilbert-type fan delta deposits from Pleistocene Lake Surprise. Remnants of deltas on the floor of Surprise Valley are flat-topped with steep foreset beds of coarse gravel and horizontal topsets. |
| **Qpb** | Pleistocene | Beach deposits | | Beach berm deposits from Pleistocene Lake Surprise, mostly fine gravel. Silicified near Leonards Hot Springs. |
| **Qpl** | Pleistocene | Lake deposits | | Lake sediments deposited in Pleistocene Lake Surprise. Primarily fine-grained sediments, often tuffaceous, but also includes minor gravels and waterlain tuffs. |
| **Tlb** | late Miocene-Pliocene | LKOT basalts | 1-30 m | Low-potassium, high-alumina olivine tholeiites, generally holocrystalline and diktytaxitic, with a very restricted range of compositions and ranging in age from ~3-8 Ma. Includes the Vya Group, Devil's Garden, and Alturas Plateau basalts of Carmichael et al (2006). Individual flows are 1-10 m thick and interbedded with Tts, though occasionally multiple flows are ponded to 25-30 m. |

**Table A14, cont.**

| Map unit | Age | Short desription | Thickness | Long description |
|---|---|---|---|---|
| **Tts** | late Miocene to Pliocene | Tuffs and tuffaceous sediments | up to 100 m | Generally silicic volcaniclastic sediments consisting of conglomerate, sandstone, and siltstone interbedded with rhyolite ash and silicic ash-flow tuff. North of Leonards Hot Springs, Tts consists of graded 10-30 cm thick beds of pebble conglomerate (most basalt pebbles) interlayered with coarse-grained, 2-3 cm thick sandstone beds of similar composition. In places, the conglomerate and sandstone interfinger with ash-rich, greenish gray siltstone and rhyolite tuff and ash-flow tuff. The siltstone is poorly bedded, normally graded and includes reworked tuff and lithic fragments. Rhyolite tuff beds are unwelded and contain abundant glass shards, lapilli, and phenocrysts of plagioclase and quartz. The entire sequence is interbedded with Tlb throughout the map area; on the west side of the Warner Range, it may include the Alturas Tuff of Carmichael et al (2006) and Collins (1999). |
| **Tmr** | Mid- to late-Miocene | rhyolite flows and domes | | Rhyolite domes and flows, often including obsidian carapaces, that range in age from 7-15 Ma. Rhyolites are generally light gray and phenocryst-poor. In the northern portion of the Warner Range, these directly overlie the 27 Ma Solider Creek volcanics (Tsc). |
| **Tmt** | Mid-Miocene | Tuff and tuffaceous sediments | 90-200 m | Graded, cross-bedded coarse sandstones with abundant plagioclase crystal fragments and dark lava chips, and massive, inversely graded deposits of angular mafic lava blocks in a sandy matrix. Below the summit of Warren Peak, this unit includes a layer of tuff with a fine-grained gray ashy matrix supporting a mixture of <1 cm white pumice lapilli and angular black fragments of what appears to be glassy lava. Mapped as Tvt by Duffield and Weldin (1976). |
| **Tmbl & Tmbu** | Mid-Miocene | Basalt and andesite flows | up to 1000 m, separated by Tmt | A stack of ~100 basaltic to andesitic lava flows. Individual flows are 2–5 m thick, occasionally up to 20 m, with scoriacious tops and massive interiors. The interiors of some units exhibit coarse, gabbro-like textures in hand specimen and thin section, suggesting that they are sills. Flows often have prominent columnar jointing, but are locally glassy and flow-banded. Phenocrysts are variably abundant and include plagioclase, pyroxene, and olivine. Duffield and McKee (1986) divided these flows into two units ("Tvm" and "Tvb") separated by a layer of tuff, but they are indistinguishable in outcrop and have a small age range from 14-16 Ma, so here they are considered upper (Tmbu) and lower (Tmbl) divisions of one unit. |

**Table A14, cont.**

| Map unit | Age | Short desription | Thickness | Long description |
|---|---|---|---|---|
| **Trt** | Early middle Miocene | Rhyolitic tuffs and tuffaceous sediments | 0-250 m | A poorly exposed unit consisting of biotite- and sanidine-bearing tuffaceous sandstone and siltstone and densely welded tuffs. The presence of biotite marks them as distinctly different from locally-derived pyroclastic flows. Included in Tvc mapped by Duffield and Weldin (1976), but 17-19 Ma ages suggest a significant hiatus in deposition after the underlying Oligocene layers. |
| **Tmvu** | Mid-Miocene | | | Undifferentiated Miocene volcanic rocks, primarily mid-Miocene, and including Tmr, Tmt, Tmbu, and Tmbl. |
| **Tovu** | Oligocene | undivided volcanic rocks | | Consists primarily of several densely welded ash-flow tuffs and less common (mostly andesitic) lava flows of Oligocene age. Includes the "Fortynine Tuff" of Carmichael et al. (2006) and most of Tvc of Duffield and Weldin (1976). |
| **Tovh** | Oligocene | Hays Volcano | | Volcanic edifice in the Hays Canyon Range composed of basaltic andesite flows, agglutinate lavas, and scoriaceous tuffs. Two dates from flows within the volcanic sequence suggest rapid accumulation of flows: a flow near the more eroded core was dated at 23.91 ± 0.13 Ma, and a flow on the top flank was dated at 24.55 ± 0.16 Ma (Carmichael et al, 2006). |
| **Tovp** | Oligocene | Payne Peak andesite | | Dark-gray-weathering, phenocryst-poor lava flows with a fine-grained groundmass of plagioclase and pyroxene. Flows cap Payne Peak and surrounding high points. |
| **Tovb** | Oligocene | Bald Mountain basalt | 10-20 m | Thin but continuous basalt flow capping Bald Mountain and dated at 24.47 ± 0.34 Ma (Colgan et al., in prep). |
| **Tovc** | Oligocene | Cedar Pass volcanic complex | up to 1200 m | Pyroclastic deposits and lesser lava flows exposed in the vicinity of Cedar Pass. Mostly massive and unsorted to crudely stratified gravity flows and rock avalanches, though occasionally bedding is well-developed. Lava blocks range in size from a few cm to >2 m, and range in texture from dark, phenocryst-poor lavas to lighter gray-green lavas with abundant phenocrysts of plagioclase and hornblende. In places, porphyritic lava flows with phenocrysts of plagioclase, hornblende, and lesser pyroxene are interbedded with the pyroclastic deposits. |
| **Tovi** | Oligocene | Hypabyssal intrusions | | Phenocryst-rich hypabyssal intrusive rocks within the Cedar Pass volcanic complex. Phenocrysts consist almost entirely of hornblende and plagioclase crystals, 2-5 mm in size. Rarely hornblende crystals reach 2-3 cm. |

**Table A14, cont.**

| Map unit | Age | Short desription | Thickness | Long description |
|---|---|---|---|---|
| **Tovl** | Oligocene | Lake City series | up to 2000 m | A series of mafic lava flows, tuffs, and tuff breccias that ranges in thickness from a few tens of meters near Cedar Pass to over two kilometers below Buck Mountain. Individual flows are a few meters thick, vesicular with massive interiors, dark when fresh but often reddish-weathering. Flows vary from aphanitic to moderately porphyritic with phenocrysts of plagioclase, olivine, and pyroxene; the olivine is most often altered and the plagioclase is usually partly altered to white mica. Some flows contain abundant (>50%) large (>1cm) plagioclase phenocrysts. Tuffs are poorly exposed, particularly on the east side of the Warner Range, but vent-proximal tuff breccias reach their thickest extent on the west side of the range. |
| **Tlw** | Oligocene | Lost Woods Formation | 300-1000 m | Andesitic and basaltic lahars, sedimentary rocks (sandstone, shale and conglomerate) and interbedded flows. The entire unit is conspicuously red-weathering. Lahars comprise beds ~ 2-3 m thick, with a sandy to pebbly matrix and poorly sorted subangular to angular clasts averaging ~ 10 cm but reaching 40 cm. Andesite and basalt flows are less than 4 m thick and include porphyritic plagioclase basalt and hornblende andesite. Sedimentary successions have conglomerate lenses, sandstones and shales, and contain abundant fossil wood. |
| **Tdc** | Oligocene | Deep Creek Formation | up to 380 m | Poorly-exposed, slope-forming unit consisting mostly of fine-grained tuffs. Includes highly altered and silicified breccia with a green matrix. |
| **Tscc** | Oligocene | Steamboat - Cougar Cliffs | 250-350 m | Massive, cliff-forming andesitic lahars and debris flows with mostly subangular clasts up to 1 m in size. Poorly sorted, and generally matrix supported. Matrix consists mostly of mud, minor ash, and abundant mm-sized hornblende and plagioclase crystals. Clasts are predominantly andesite with purple-grey, aphanitic groundmass, 1-2 mm plagioclase and larger hornblende phenocrysts. The unit forms prominent cliffs south of Simpsons Canyon, but the unit becomes thinner and less resistant to the north. Locally, thinly-bedded conglomerates, sandstones and siltstones are interlayered with the lahars |
| **Tsbn** | Late Eocene - Oligocene | Steamboat - Badger's Nose | 250-500 | Primarily fine-grained volcaniclastic sediments, including a lacustrine shale with abundant leaf fossils of late Eocene-early Oligocene age (Myers, 2006). |

**Table A14, cont.**

| Map unit | Age | Short desription | Thickness | Long description |
|---|---|---|---|---|
| **Tsu** | Late Eocene - Oligocene | Steamboat - undifferentiated | 200-1600+ m | Undifferentiated sedimentary unit that includes both sub-units of the Steamboat formation. |
| **Tmrv** | Eocene | McCulley Ranch Formation | 650+ m | Fractured and deeply weathered andesitic debris flows interbedded with andesite flows. Near the top of the unit, Axelrod (1966) reports a K-Ar age of 40.8 ± 3.0 Ma (corrected) on plagioclase from an andesite flow, suggesting an Eocene age for the entire sequence. |

# Appendix B

## Analytical methods and data from Chapter 2

**Detrital zircon analysis methods**

Zircon concentrates were prepared at Stanford University and handpicked under a binocular microscope to ensure purity and freedom from cracks, inclusions, or obvious alteration. At the Stanford - U.S.G.S. Micro Analytical Center (SUMAC), the selected grains were mounted in epoxy with the laboratory standard R33 (419 Ma; Black et al., 2004) and polished with diamond compound to expose the mid points of the crystals. Polished grain mounts were imaged in reflected light with an optical microscope, gold-coated, and imaged in cathodoluminescence (CL) mode with a JEOL 5600 scanning electron microscope.

Most samples were analyzed at SUMAC. The SHRIMP-RG ion microprobe at SUMAC was operated with an $O^{2-}$ primary ion beam varying from 4 to 6 nA, which produced a spot with a diameter of ~20–30 μm and a depth of 1–2 μm on the target zircons. Eleven peaks were measured sequentially for 10 min with an ETP electron multiplier ($Zr^2O$, $^{204}Pb$, $^{206}Pb$, $^{207}Pb$, $^{208}Pb$, $^{238}U$, ThO, UO, ErO, YbO, and HfO). Data was reduced following the methods described by Ireland and Williams (2003), using the SQUID and IsoPlot programs of Ludwig (2001, 2003). Analytical data are presented in Tables A1 and A2.

One sample was analyzed by laser ablation multicollector inductively coupled plasma mass spectrometry (LA-MC-ICPMS) at the Arizona LaserChron Center . The analyses involve ablation of zircon with a New Wave/Lambda Physik DUV193 Excimer laser (operating at a wavelength of 193 nm) using a spot diameter of 10 microns. The ablated material is carried in helium into the plasma source of a GVI Isoprobe, which is equipped with a flight tube of sufficient width that U, Th, and Pb isotopes are measured simultaneously. All measurements are made in static mode, using 10e11

ohm Faraday detectors for $^{238}U$, $^{232}Th$, $^{208}Pb$, and $^{206}Pb$, a 10e12 ohm faraday collector for $^{207}Pb$, and an ion-counting channel for $^{204}Pb$. Ion yields are ~1.0 mv per ppm. Each analysis consists of one 20-second integration on peaks with the laser off (for backgrounds), 20 one-second integrations with the laser firing, and a 30 second delay to purge the previous sample and prepare for the next analysis. The ablation pit is ~15 microns in depth. The analytical data are reported in Table A3. Uncertainties shown in these tables are at the 1-sigma level, and include only measurement errors.

**On the following pages:**

**Table B1.** U-Pb (zircon) geochronologic data from samples analyzed on the SHRIMP-RG. Errors are 1 sigma unless otherwise indicated.

**Table B2.** Trace element data from samples analyzed on the SHRIMP-RG.

**Table B3.** U-Pb (zircon) geochronologic analyses by Laser-Ablation Multicollector ICP Mass Spectrometry

## Table B1.

| Spot Name | Pb/U const #rej | 204 cts /sec | 204 /206 | % err | 1.005 | %err | 1.010 | %err | Obs 206 /238 | % err | 248 /254 | % err |
|---|---|---|---|---|---|---|---|---|---|---|---|---|
| **3755.1** | 0 | 0.05 | 7.7E-4 | 50 | .051 | 6.3 | .109 | 10.3 | .011 | 2.4 | .321 | 0.7 |
| **3755.1** | 0 | 0.00 | --- | 0 | .068 | 4.2 | .223 | 5.5 | .035 | 3.1 | .685 | 4.5 |
| **3755.11** | 0 | 0.09 | 7.2E-4 | 65 | .050 | 4.4 | .161 | 5.7 | .012 | 3.4 | .508 | 1.2 |
| **3755.12** | 1 | 0.00 | --- | 0 | .049 | 2.7 | .041 | 11.1 | .012 | 3.0 | .119 | 3.5 |
| **3755.13** | 1 | 0.40 | 2.1E-4 | 25 | .049 | 1.1 | .076 | 9.7 | .024 | 6.0 | .188 | 25.3 |
| **3755.14** | 0 | 0.00 | --- | 0 | .050 | 3.6 | .220 | 5.1 | .035 | 3.6 | .560 | 0.5 |
| **3755.15** | 0 | 0.05 | 1.0E-3 | 50 | .050 | 7.3 | .327 | 7.1 | .013 | 2.7 | .953 | 0.7 |
| **3755.16** | 0 | 0.00 | --- | 0 | .050 | 5.7 | .042 | 14.2 | .010 | 4.6 | .141 | 0.5 |
| **3755.17** | 0 | 0.04 | 1.2E-3 | 71 | .049 | 8.6 | .196 | 10.3 | .037 | 6.2 | .557 | 0.9 |
| **3755.2** | 0 | 0.09 | 5.3E-4 | 64 | .051 | 3.6 | .172 | 4.7 | .049 | 3.0 | .500 | 0.4 |
| **3755.3** | 0 | 0.11 | 3.8E-4 | 45 | .050 | 2.9 | .406 | 2.5 | .015 | 2.2 | 1.128 | 0.4 |
| **3755.4** | 0 | 0.00 | --- | 0 | .051 | 4.9 | .120 | 7.6 | .047 | 3.2 | .367 | 1.5 |
| **3755.5** | 0 | 0.08 | 1.7E-5 | 50 | .182 | 0.6 | .090 | 1.4 | .859 | 3.1 | .331 | 1.4 |
| **3755.6** | 0 | 0.08 | 1.2E-4 | 50 | .051 | 2.0 | .210 | 6.2 | .042 | 5.0 | .575 | 4.5 |
| **3755.7** | 0 | 0.13 | 5.0E-3 | 50 | .061 | 9.0 | .287 | 9.8 | .011 | 3.6 | .536 | 1.0 |
| **3755.8** | 0 | 0.12 | 2.0E-3 | 45 | .053 | 6.1 | .134 | 9.0 | .011 | 2.3 | .340 | 0.5 |
| **3755.9** | 0 | 0.08 | 4.3E-5 | 50 | .077 | 2.6 | .075 | 3.8 | .097 | 7.3 | .103 | 7.4 |
| **3763.1** | 0 | 0.04 | 4.5E-5 | 50 | .053 | 1.5 | .149 | 2.1 | .069 | 3.0 | .456 | 0.6 |
| **3763.2** | 0 | -0.08 | -1.3E-3 | 50 | .054 | 7.3 | .239 | 8.0 | .031 | 5.0 | .645 | 0.7 |
| **3763.3** | 0 | 0.08 | 2.6E-3 | 50 | .049 | 9.3 | .241 | 10.1 | .012 | 3.3 | .519 | 0.5 |
| **3763.4** | 0 | -0.01 | -2.5E-4 | 50 | .046 | 12.2 | .195 | 8.8 | .012 | 2.6 | .585 | 0.4 |
| **3763.5** | 0 | 0.00 | --- | 0 | .053 | 4.5 | .154 | 6.3 | .048 | 4.5 | .464 | 1.0 |
| **4147.1** | 0 | 0.00 | --- | 0 | .050 | 3.0 | .225 | 3.4 | .032 | 3.5 | .671 | 0.3 |
| **4147.11** | 0 | 0.12 | 1.2E-3 | 38 | .064 | 5.2 | .229 | 5.5 | .012 | 3.0 | .538 | 0.3 |
| **4147.9** | 0 | 0.00 | --- | 0 | .051 | 5.6 | .236 | 6.3 | .030 | 3.2 | .681 | 0.5 |
| **07AE58-1.1** | 0 | 0.00 | --- | 0 | .050 | 5.6 | .075 | 10.8 | .009 | 4.4 | .223 | 0.4 |
| **07AE58-2.1** | 0 | 0.03 | 2.4E-5 | 64 | .052 | 1.3 | .107 | 2.2 | .069 | 2.2 | .292 | 0.5 |
| **07AE58-3.1** | 0 | -0.07 | -5.4E-4 | 50 | .049 | 4.2 | .105 | 6.8 | .029 | 3.6 | .344 | 1.5 |
| **07AE58-4.1** | 0 | 0.04 | 6.0E-4 | 50 | .050 | 5.6 | .161 | 7.5 | .026 | 5.2 | .483 | 1.2 |
| **07AE59-1.2** | 0 | 0.00 | --- | 0 | .050 | 8.2 | .200 | 6.1 | .033 | 2.2 | .551 | 0.7 |
| **07AE59-10.2** | 0 | 0.00 | --- | 0 | .055 | 8.2 | .157 | 7.1 | .036 | 3.9 | .439 | 1.8 |
| **07AE59-11.2** | 0 | 0.00 | --- | 0 | .055 | 6.6 | .112 | 6.6 | .034 | 1.8 | .324 | 0.7 |
| **07AE59-12.2** | 0 | 0.00 | --- | 0 | .047 | 4.5 | .232 | 3.0 | .033 | 2.3 | .672 | 0.3 |
| **07AE59-13.1** | 0 | 0.05 | 6.6E-4 | 66 | .054 | 5.3 | .109 | 8.9 | .029 | 3.7 | .341 | 0.6 |
| **07AE59-14.1** | 1 | 2.65 | 2.6E-2 | 10 | .389 | 11.1 | .991 | 7.5 | .047 | 9.9 | .449 | 0.7 |
| **07AE59-15.1** | 0 | 0.03 | 8.3E-4 | 65 | .060 | 7.3 | .141 | 10.9 | .028 | 2.9 | .341 | 0.8 |
| **07AE59-2.2** | 0 | 0.00 | --- | 0 | .046 | 8.8 | .303 | 5.7 | .010 | 2.2 | .887 | 0.5 |
| **07AE59-3.2** | 0 | 0.00 | --- | 0 | .051 | 7.6 | .205 | 5.6 | .033 | 2.0 | .498 | 0.6 |
| **07AE59-4.2** | 0 | 0.07 | 1.7E-3 | 58 | .052 | 10.2 | .104 | 10.4 | .032 | 2.8 | .337 | 1.0 |
| **07AE59-5.2** | 0 | 0.00 | --- | 0 | .052 | 9.5 | .170 | 7.7 | .032 | 2.5 | .469 | 0.8 |
| **07AE59-6.2** | 0 | 0.00 | --- | 0 | .048 | 11.1 | .108 | 9.5 | .032 | 2.6 | .346 | 0.9 |
| **07AE59-7.2** | 0 | 0.00 | --- | 0 | .049 | 6.7 | .191 | 5.0 | .032 | 3.0 | .566 | 0.5 |
| **07AE59-8.2** | 0 | 0.00 | --- | 0 | .049 | 5.5 | .159 | 4.4 | .035 | 1.5 | .474 | 0.5 |
| **07AE59-9.2** | 0 | 0.00 | --- | 0 | .047 | 7.7 | .158 | 5.9 | .036 | 2.0 | .481 | 0.6 |
| **08AE26-1.1** | 0 | 0.00 | --- | 0 | .075 | 0.9 | .085 | 2.0 | .311 | 4.3 | .256 | 0.4 |
| **08AE26-2.1** | 0 | 0.00 | --- | 0 | .087 | 1.2 | .337 | 1.1 | .362 | 21.0 | 1.048 | 0.3 |
| **08AE26-2.2** | 0 | 0.03 | 2.9E-5 | 64 | .087 | 1.2 | .231 | 1.9 | .391 | 3.1 | .734 | 0.9 |
| **08AE26-3.1** | 0 | 0.00 | --- | 0 | .048 | 3.8 | .263 | 3.9 | .008 | 3.4 | .788 | 0.2 |
| **08AE26-4.1** | 0 | -0.08 | -1.2E-3 | 50 | .044 | 6.6 | .152 | 8.4 | .028 | 3.6 | .379 | 0.6 |
| **08AE26-5.1** | 0 | 0.03 | 1.5E-4 | 64 | .047 | 3.9 | .156 | 4.6 | .031 | 2.9 | .457 | 0.3 |
| **08AE26-6.1** | 0 | 0.08 | 3.3E-5 | 50 | .057 | 0.9 | .200 | 1.2 | .122 | 3.1 | .609 | 1.0 |
| **08AE26-7.1** | 0 | 0.04 | 4.3E-5 | 72 | .054 | 1.5 | .120 | 2.6 | .113 | 3.5 | .354 | 0.3 |
| **08AE26-8.1** | 0 | 0.07 | 4.8E-4 | 50 | .049 | 4.1 | .152 | 5.6 | .027 | 4.2 | .420 | 1.1 |
| **08AE26-9.1** | 0 | 0.09 | 5.0E-3 | 50 | .084 | 9.0 | .223 | 12.8 | .008 | 4.1 | .517 | 0.9 |
| **3763-6.1** | 0 | 0.10 | 1.4E-3 | 45 | .049 | 5.8 | .221 | 6.6 | .038 | 4.9 | .604 | 0.6 |
| **3763-7.1** | 0 | 3.44 | 3.8E-2 | 9 | .550 | 3.2 | 1.336 | 4.5 | .029 | 9.7 | .491 | 0.8 |
| **3990-1** | 0 | 0.00 | --- | 0 | .047 | 4.5 | .220 | 6.8 | .037 | 3.5 | .601 | 0.4 |
| **3990-10.1** | 0 | 0.05 | 2.1E-4 | 50 | .049 | 3.2 | .130 | 4.6 | .034 | 4.3 | .388 | 0.5 |
| **3990-11.1** | 0 | 0.03 | 9.0E-5 | 64 | .047 | 2.7 | .035 | 7.2 | .013 | 2.9 | .097 | 0.3 |

## Table B1, cont.

| Spot Name | 254 /238 | % err | 238 /196 | Pb/U: UO/U^2 | % err | % comm 206 | ppm U | ppm Th | 232Th /238U | Ln UO/U | Ln Pb/U | Corr 206 /238 |
|---|---|---|---|---|---|---|---|---|---|---|---|---|
| **3755.1** | 5.23 | 1.3 | .250 | .00040 | 2.4 | 1.40 | | | 0.34 | 1.654 | -4.533 | .006 |
| **3755.1** | 4.99 | 1.1 | .137 | .00139 | 1.9 | 0.00 | | | 0.72 | 1.608 | -3.346 | .023 |
| **3755.11** | 5.49 | 0.9 | .481 | .00040 | 1.6 | 1.31 | | | 0.53 | 1.703 | -4.415 | .007 |
| **3755.12** | 5.41 | 1.5 | 1.402 | .00039 | 1.1 | 0.00 | | | 0.12 | 1.688 | -4.461 | .006 |
| **3755.13** | 5.40 | 1.1 | 3.508 | .00078 | 0.5 | 0.39 | | | 0.20 | 1.687 | -3.753 | .013 |
| **3755.14** | 5.54 | 1.4 | .267 | .00113 | 1.4 | 0.00 | | | 0.59 | 1.713 | -3.355 | .018 |
| **3755.15** | 5.36 | 1.3 | .160 | .00045 | 2.7 | 1.85 | | | 1.00 | 1.679 | -4.354 | .007 |
| **3755.16** | 5.13 | 1.1 | .368 | .00038 | 2.1 | 0.00 | | | 0.15 | 1.634 | -4.602 | .006 |
| **3755.17** | 5.40 | 1.3 | .041 | .00124 | 3.3 | 2.25 | | | 0.58 | 1.687 | -3.328 | .020 |
| **3755.2** | 5.37 | 1.3 | .154 | .00168 | 1.5 | 0.95 | | | 0.53 | 1.681 | -3.032 | .027 |
| **3755.3** | 5.78 | 0.9 | .842 | .00044 | 1.1 | 0.68 | | | 1.18 | 1.754 | -4.227 | .007 |
| **3755.4** | 5.25 | 1.9 | .087 | .00169 | 2.0 | 0.00 | | | 0.39 | 1.658 | -3.058 | .027 |
| **3755.5** | 5.36 | 1.7 | .234 | .02957 | 0.6 | 0.03 | | | 0.35 | 1.679 | -0.152 | .478 |
| **3755.6** | 5.13 | 2.2 | .651 | .00159 | 0.8 | 0.22 | | | 0.60 | 1.636 | -3.162 | .026 |
| **3755.7** | 5.32 | 1.6 | .100 | .00040 | 3.6 | 9.09 | | | 0.56 | 1.671 | -4.587 | .007 |
| **3755.8** | 5.41 | 1.2 | .236 | .00040 | 2.3 | 3.67 | | | 0.36 | 1.688 | -4.513 | .006 |
| **3755.9** | 5.73 | 0.9 | .885 | .00297 | 0.5 | 0.08 | | | 0.11 | 1.745 | -2.339 | .048 |
| **3763.1** | 5.42 | 1.2 | .718 | .00232 | 0.6 | 0.08 | | | 0.48 | 1.690 | -2.678 | .038 |
| **3763.2** | 5.35 | 1.2 | .096 | .00106 | 2.4 | -2.27 | | | 0.68 | 1.677 | -3.460 | .017 |
| **3763.3** | 5.54 | 1.0 | .116 | .00040 | 3.4 | 4.72 | | | 0.55 | 1.711 | -4.452 | .006 |
| **3763.4** | 5.26 | 1.1 | .187 | .00042 | 2.7 | -0.45 | | | 0.61 | 1.660 | -4.431 | .007 |
| **3763.5** | 5.29 | 1.7 | .114 | .00169 | 1.9 | 0.00 | | | 0.49 | 1.666 | -3.038 | .027 |
| **4147.1** | 5.36 | 1.1 | .359 | .00110 | 1.2 | 0.00 | | | 0.71 | 1.680 | -3.445 | .018 |
| **4147.11** | 5.24 | 1.1 | .405 | .00043 | 1.8 | 2.15 | | | 0.57 | 1.656 | -4.452 | .007 |
| **4147.9** | 5.33 | 1.5 | .104 | .00106 | 2.2 | 0.00 | | | 0.71 | 1.673 | -3.493 | .017 |
| **07AE58-1.1** | 5.21 | 1.6 | .368 | .00032 | 2.1 | 0.00 | | | 0.23 | 1.650 | -4.733 | .005 |
| **07AE58-2.1** | 5.57 | 0.5 | .808 | .00221 | 0.6 | 0.04 | | | 0.31 | 1.718 | -2.677 | .036 |
| **07AE58-3.1** | 5.32 | 1.9 | .204 | .00101 | 1.6 | -0.97 | | | 0.36 | 1.672 | -3.532 | .016 |
| **07AE58-4.1** | 5.06 | 2.0 | .128 | .00099 | 2.2 | 1.08 | | | 0.51 | 1.621 | -3.673 | .016 |
| **07AE59-1.2** | 5.49 | 0.8 | .163 | .00111 | 2.3 | 0.00 | 238 | 133 | 0.58 | 1.703 | -3.399 | .017 |
| **07AE59-10.2** | 5.63 | 0.9 | .147 | .00113 | 2.4 | 0.00 | 218 | 97 | 0.46 | 1.728 | -3.328 | .017 |
| **07AE59-11.2** | 5.57 | 0.8 | .233 | .00109 | 2.0 | 0.00 | 344 | 113 | 0.34 | 1.717 | -3.381 | .017 |
| **07AE59-12.2** | 5.53 | 0.4 | .632 | .00109 | 1.2 | 0.00 | 926 | 633 | 0.71 | 1.711 | -3.398 | .017 |
| **07AE59-13.1** | 5.46 | 1.0 | .110 | .00098 | 2.1 | 1.20 | | | 0.36 | 1.697 | -3.536 | .016 |
| **07AE59-14.1** | 4.64 | 2.1 | .102 | .00202 | 2.3 | 47.49 | | | 0.47 | 1.535 | -3.708 | .033 |
| **07AE59-15.1** | 5.08 | 1.7 | .056 | .00109 | 3.1 | 1.50 | | | 0.36 | 1.625 | -3.580 | .018 |
| **07AE59-2.2** | 5.48 | 1.1 | .531 | .00033 | 2.2 | 0.00 | 773 | 696 | 0.93 | 1.701 | -4.612 | .005 |
| **07AE59-3.2** | 5.54 | 0.7 | .201 | .00106 | 2.2 | 0.00 | 295 | 149 | 0.52 | 1.712 | -3.420 | .016 |
| **07AE59-4.2** | 5.44 | 1.0 | .107 | .00107 | 3.0 | 3.11 | 155 | 53 | 0.35 | 1.695 | -3.472 | .016 |
| **07AE59-5.2** | 5.59 | 0.9 | .130 | .00103 | 2.7 | 0.00 | 191 | 91 | 0.49 | 1.720 | -3.432 | .016 |
| **07AE59-6.2** | 5.49 | 0.9 | .125 | .00105 | 2.8 | 0.00 | 183 | 64 | 0.36 | 1.703 | -3.443 | .016 |
| **07AE59-7.2** | 5.41 | 0.6 | .273 | .00110 | 1.9 | 0.00 | 395 | 227 | 0.59 | 1.688 | -3.430 | .017 |
| **07AE59-8.2** | 5.63 | 0.5 | .391 | .00109 | 1.6 | 0.00 | 580 | 279 | 0.50 | 1.728 | -3.357 | .017 |
| **07AE59-9.2** | 5.69 | 0.8 | .207 | .00111 | 2.1 | 0.00 | 309 | 151 | 0.50 | 1.738 | -3.323 | .017 |
| **08AE26-1.1** | 5.35 | 1.3 | .300 | .01073 | 0.7 | 0.00 | | | 0.27 | 1.677 | -1.169 | .173 |
| **08AE26-2.1** | 5.54 | 3.1 | .191 | .01490 | 0.9 | 0.00 | | | 1.10 | 1.711 | -1.016 | .241 |
| **08AE26-2.2** | 5.15 | 1.0 | .112 | .01466 | 0.9 | 0.05 | | | 0.77 | 1.638 | -0.940 | .237 |
| **08AE26-3.1** | 5.14 | 1.5 | .917 | .00030 | 1.4 | 0.00 | | | 0.83 | 1.637 | -4.827 | .005 |
| **08AE26-4.1** | 5.16 | 1.9 | .100 | .00103 | 2.3 | -2.24 | | | 0.40 | 1.642 | -3.557 | .017 |
| **08AE26-5.1** | 5.25 | 1.3 | .254 | .00113 | 1.3 | 0.28 | | | 0.48 | 1.659 | -3.464 | .018 |
| **08AE26-6.1** | 5.35 | 0.9 | .833 | .00425 | 0.5 | 0.06 | | | 0.64 | 1.677 | -2.101 | .069 |
| **08AE26-7.1** | 5.41 | 1.3 | .356 | .00381 | 0.7 | 0.08 | | | 0.37 | 1.688 | -2.185 | .062 |
| **08AE26-8.1** | 5.11 | 1.7 | .206 | .00101 | 1.6 | 0.87 | | | 0.44 | 1.631 | -3.635 | .016 |
| **08AE26-9.1** | 4.50 | 1.5 | .118 | .00040 | 4.2 | 8.99 | | | 0.54 | 1.504 | -4.900 | .006 |
| **3763-6.1** | 5.56 | 1.1 | .102 | .00123 | 2.3 | 2.57 | | | 0.63 | 1.716 | -3.287 | .020 |
| **3763-7.1** | 5.04 | 2.0 | .156 | .00112 | 2.0 | 68.94 | | | 0.52 | 1.617 | -4.708 | .018 |
| **3990-1** | 5.52 | 0.9 | .199 | .00121 | 1.7 | 0.00 | | | 0.63 | 1.709 | -3.295 | .019 |
| **3990-10.1** | 5.47 | 1.5 | .406 | .00114 | 1.2 | 0.38 | | | 0.41 | 1.699 | -3.372 | .018 |
| **3990-11.1** | 5.61 | 0.9 | 1.593 | .00041 | 1.0 | 0.16 | | | 0.10 | 1.725 | -4.345 | .007 |

## Table B1, cont.

| Spot Name | % err | ppm Rad 206Pb | Total 208Pb /232Th | % err | 204corr 206Pb /238U Age | 1s err | 207corr 206Pb /238U Age | 1s err | 208corr 206Pb /238U Age | 1s err | 204corr 207Pb /206Pb Age |
|---|---|---|---|---|---|---|---|---|---|---|---|
| **3755.1** | 2.8 | | .0021 | 10.7 | **40.6** | **1.2** | **40.9** | **1.2** | **41.1** | **1.2** | **-355** |
| **3755.1** | 2.4 | | .0070 | 7.5 | **143.7** | **3.4** | **140.3** | **3.4** | **144.1** | **4.0** | **875** |
| **3755.11** | 2.2 | | .0020 | 6.2 | **41.4** | **1.0** | **41.8** | **0.9** | **42.1** | **1.0** | **-408** |
| **3755.12** | 1.9 | | .0021 | 11.8 | **40.1** | **0.7** | **40.0** | **0.7** | **40.1** | **0.8** | **169** |
| **3755.13** | 1.6 | | .0048 | 27.2 | **80.8** | **1.3** | **81.0** | **1.3** | **80.6** | **1.5** | **2** |
| **3755.14** | 2.0 | | .0068 | 5.5 | **116.2** | **2.3** | **116.0** | **2.4** | **114.2** | **2.7** | **172** |
| **3755.15** | 3.1 | | .0024 | 7.7 | **46.2** | **1.5** | **46.9** | **1.5** | **46.8** | **1.8** | **-704** |
| **3755.16** | 2.5 | | .0017 | 14.4 | **39.1** | **1.0** | **39.0** | **1.0** | **39.2** | **1.0** | **173** |
| **3755.17** | 3.7 | | .0067 | 11.0 | **124.6** | **4.9** | **127.4** | **4.7** | **126.7** | **5.3** | **-1136** |
| **3755.2** | 2.1 | | .0089 | 5.1 | **170.7** | **3.7** | **172.0** | **3.6** | **171.7** | **3.9** | **-166** |
| **3755.3** | 1.8 | | .0024 | 3.1 | **45.2** | **0.8** | **45.3** | **0.8** | **44.8** | **1.1** | **-93** |
| **3755.4** | 2.5 | | .0085 | 8.1 | **173.4** | **4.2** | **173.0** | **4.3** | **173.6** | **4.6** | **259** |
| **3755.5** | 1.6 | | .1236 | 2.6 | **2517.1** | **33.1** | **2449.3** | **44.8** | **2524.6** | **34.5** | **2673** |
| **3755.6** | 1.7 | | .0089 | 7.9 | **162.7** | **2.7** | **162.7** | **2.7** | **161.4** | **3.3** | **159** |
| **3755.7** | 3.9 | | .0033 | 10.6 | **38.1** | **2.4** | **41.2** | **1.6** | **39.6** | **1.9** | |
| **3755.8** | 2.8 | | .0024 | 9.5 | **39.6** | **1.3** | **40.8** | **1.1** | **40.6** | **1.2** | |
| **3755.9** | 1.6 | | .0333 | 8.5 | **301.7** | **4.6** | **292.8** | **4.6** | **296.1** | **4.8** | **1114** |
| **3763.1** | 1.6 | | .0117 | 2.7 | **237.4** | **3.8** | **237.1** | **3.8** | **237.8** | **4.1** | **282** |
| **3763.2** | 2.8 | | .0060 | 8.5 | **111.9** | **3.3** | **108.7** | **3.1** | **108.1** | **3.6** | **987** |
| **3763.3** | 3.7 | | .0028 | 10.8 | **39.2** | **1.7** | **41.1** | **1.5** | **39.7** | **1.7** | |
| **3763.4** | 3.1 | | .0021 | 9.4 | **43.6** | **1.3** | **43.5** | **1.4** | **43.4** | **1.5** | **159** |
| **3763.5** | 2.4 | | .0086 | 6.8 | **173.6** | **4.1** | **172.8** | **4.1** | **173.6** | **4.5** | **350** |
| **4147.1** | 1.9 | | .0057 | 3.9 | **113.5** | **2.1** | **113.2** | **2.1** | **113.4** | **2.4** | **207** |
| **4147.11** | 2.3 | | .0028 | 6.0 | **43.6** | **1.1** | **43.7** | **1.0** | **43.4** | **1.2** | **10** |
| **4147.9** | 2.6 | | .0057 | 6.8 | **109.7** | **2.9** | **109.3** | **2.9** | **109.1** | **3.4** | **221** |
| **07AE58-1.1** | 2.5 | | .0017 | 11.1 | **33.3** | **0.8** | **33.2** | **0.8** | **33.3** | **0.9** | **205** |
| **07AE58-2.1** | 1.6 | | .0124 | 2.7 | **226.1** | **3.5** | **225.9** | **3.5** | **225.1** | **3.7** | **254** |
| **07AE58-3.1** | 2.2 | | .0047 | 7.3 | **105.4** | **2.3** | **104.2** | **2.3** | **104.9** | **2.4** | **496** |
| **07AE58-4.1** | 2.6 | | .0051 | 8.1 | **101.1** | **2.7** | **101.9** | **2.7** | **102.2** | **3.0** | **-260** |
| **07AE59-1.2** | 2.3 | 3.5 | .0058 | 6.6 | **108.2** | **2.5** | **107.9** | **2.5** | **107.3** | **2.8** | **217** |
| **07AE59-10.2** | 2.4 | 3.2 | .0059 | 7.7 | **110.2** | **2.6** | **109.3** | **2.7** | **109.6** | **2.9** | **401** |
| **07AE59-11.2** | 2.0 | 4.9 | .0055 | 6.9 | **106.6** | **2.1** | **105.7** | **2.1** | **106.4** | **2.2** | **415** |
| **07AE59-12.2** | 1.2 | 13.2 | .0055 | 3.2 | **106.2** | **1.3** | **106.4** | **1.3** | **105.8** | **1.5** | **33** |
| **07AE59-13.1** | 2.6 | | .0049 | 9.3 | **100.5** | **2.7** | **100.9** | **2.6** | **101.9** | **2.8** | **-83** |
| **07AE59-14.1** | 2.7 | | .0687 | 8.0 | **109.6** | **10.7** | **121.6** | **11.5** | **118.5** | **11.3** | |
| **07AE59-15.1** | 3.4 | | .0069 | 11.5 | **110.9** | **3.9** | **111.0** | **3.8** | **111.1** | **4.1** | **86** |
| **07AE59-2.2** | 2.2 | 3.3 | .0016 | 6.1 | **32.4** | **0.7** | **32.4** | **0.7** | **32.2** | **0.9** | **-16** |
| **07AE59-3.2** | 2.2 | 4.1 | .0064 | 6.0 | **104.1** | **2.2** | **103.7** | **2.3** | **102.0** | **2.5** | **229** |
| **07AE59-4.2** | 3.0 | 2.2 | .0048 | 10.9 | **101.6** | **3.5** | **104.4** | **3.1** | **105.2** | **3.3** | |
| **07AE59-5.2** | 2.7 | 2.6 | .0055 | 8.2 | **100.9** | **2.7** | **100.5** | **2.8** | **100.2** | **3.0** | **268** |
| **07AE59-6.2** | 2.8 | 2.5 | .0048 | 10.0 | **103.2** | **2.8** | **103.2** | **2.9** | **103.6** | **3.1** | **95** |
| **07AE59-7.2** | 1.9 | 5.7 | .0054 | 5.3 | **107.5** | **2.0** | **107.4** | **2.0** | **107.4** | **2.3** | **141** |
| **07AE59-8.2** | 1.6 | 8.3 | .0053 | 4.7 | **107.0** | **1.7** | **106.8** | **1.7** | **106.9** | **1.8** | **161** |
| **07AE59-9.2** | 2.1 | 4.5 | .0053 | 6.3 | **108.3** | **2.3** | **108.5** | **2.3** | **108.4** | **2.5** | **69** |
| **08AE26-1.1** | 1.6 | | .0550 | 2.6 | **1031.1** | **15.4** | **1029.1** | **16.1** | **1029.2** | **16.0** | **1076** |
| **08AE26-2.1** | 1.7 | | .0738 | 2.0 | **1390.4** | **21.4** | **1393.0** | **23.2** | **1382.2** | **25.5** | **1357** |
| **08AE26-2.2** | 1.7 | | .0709 | 2.8 | **1370.3** | **21.5** | **1372.3** | **23.3** | **1369.3** | **24.3** | **1344** |
| **08AE26-3.1** | 2.0 | | .0015 | 4.4 | **31.2** | **0.6** | **31.2** | **0.6** | **31.2** | **0.7** | **75** |
| **08AE26-4.1** | 2.7 | | .0064 | 8.8 | **108.8** | **3.2** | **107.0** | **2.9** | **105.1** | **3.2** | **664** |
| **08AE26-5.1** | 2.0 | | .0059 | 5.0 | **116.2** | **2.3** | **116.7** | **2.3** | **116.3** | **2.5** | **-50** |
| **08AE26-6.1** | 1.5 | | .0215 | 2.2 | **428.1** | **6.4** | **427.7** | **6.5** | **428.2** | **7.1** | **460** |
| **08AE26-7.1** | 1.6 | | .0199 | 3.1 | **384.9** | **6.1** | **385.3** | **6.2** | **384.5** | **6.5** | **352** |
| **08AE26-8.1** | 2.2 | | .0056 | 6.1 | **103.3** | **2.3** | **104.0** | **2.2** | **103.6** | **2.4** | **-209** |
| **08AE26-9.1** | 4.4 | | .0027 | 13.6 | **37.8** | **2.5** | **39.6** | **1.8** | **40.5** | **2.1** | |
| **3763-6.1** | 2.7 | | .0069 | 7.1 | **123.3** | **3.6** | **126.4** | **3.4** | **125.2** | **3.9** | |
| **3763-7.1** | 2.5 | | .0468 | 5.2 | **36.0** | **7.6** | **44.6** | **3.0** | **45.6** | **6.4** | |
| **3990-1** | 2.3 | | .0068 | 7.2 | **124.4** | **2.8** | **124.7** | **2.8** | **123.1** | **3.2** | **38** |
| **3990-10.1** | 1.9 | | .0059 | 5.0 | **117.1** | **2.2** | **117.5** | **2.2** | **117.5** | **2.4** | **-20** |
| **3990-11.1** | 1.8 | | .0023 | 7.4 | **42.5** | **0.8** | **42.5** | **0.8** | **42.5** | **0.8** | **-4** |

**Table B1, cont.**

| Spot Name | 1s err | 204corr 208Pb /232Th Age | 1s err | % Dis-cor-dant | 4corr 208r /232 | % err | Total 238 /206 | % err | Total 207 /206 | % err | 4corr 238/ 206r | % err |
|---|---|---|---|---|---|---|---|---|---|---|---|---|
| **3755.1** | **434** | **30** | **7** | -976 | .0015 | 21.4 | 156.24 | 2.8 | .0515 | 6.3 | 158.45 | 2.9 |
| **3755.1** | **87** | **141** | **8** | 509 | .0070 | 6.0 | 44.36 | 2.4 | .0682 | 4.2 | 44.36 | 2.4 |
| **3755.11** | **494** | **33** | **5** | -1086 | .0016 | 14.7 | 153.25 | 2.2 | .0499 | 4.4 | 155.28 | 2.4 |
| **3755.12** | **62** | **42** | **5** | 321 | .0021 | 11.3 | 160.27 | 1.9 | .0494 | 2.7 | 160.27 | 1.9 |
| **3755.13** | **51** | **87** | **9** | -97 | .0043 | 10.3 | 78.98 | 1.6 | .0492 | 1.1 | 79.28 | 1.6 |
| **3755.14** | **84** | **137** | **7** | 48 | .0068 | 5.5 | 55.00 | 2.0 | .0495 | 3.6 | 55.00 | 2.0 |
| **3755.15** | **688** | **43** | **4** | -1625 | .0021 | 10.3 | 136.48 | 3.1 | .0504 | 7.3 | 139.05 | 3.3 |
| **3755.16** | **132** | **35** | **5** | 342 | .0017 | 14.4 | 164.35 | 2.5 | .0495 | 5.7 | 164.35 | 2.5 |
| **3755.17** | **1443** | **102** | **26** | -1012 | .0051 | 25.0 | 50.10 | 3.7 | .0489 | 8.6 | 51.25 | 4.0 |
| **3755.2** | **312** | **158** | **16** | -197 | .0079 | 9.9 | 36.92 | 2.1 | .0509 | 3.6 | 37.28 | 2.2 |
| **3755.3** | **161** | **47** | **2** | -306 | .0023 | 3.5 | 141.14 | 1.8 | .0499 | 2.9 | 142.12 | 1.8 |
| **3755.4** | **112** | **170** | **14** | 49 | .0085 | 8.0 | 36.68 | 2.5 | .0514 | 4.9 | 36.68 | 2.5 |
| **3755.5** | **11** | **2340** | **51** | 6 | .1227 | 2.2 | 2.09 | 1.6 | .1824 | 0.6 | 2.09 | 1.6 |
| **3755.6** | **64** | **175** | **11** | -2 | .0087 | 6.5 | 39.04 | 1.7 | .0510 | 2.0 | 39.13 | 1.7 |
| **3755.7** | | **23** | **23** | | .0011 | 99.7 | 153.18 | 3.9 | .0613 | 9.0 | 168.49 | 6.4 |
| **3755.8** | | **20** | **13** | | .0010 | 61.8 | 156.51 | 2.8 | .0526 | 6.1 | 162.47 | 3.2 |
| **3755.9** | **52** | **649** | **27** | 269 | .0326 | 4.2 | 20.85 | 1.6 | .0773 | 2.6 | 20.87 | 1.6 |
| **3763.1** | **38** | **232** | **6** | 19 | .0115 | 2.7 | 26.64 | 1.6 | .0526 | 1.5 | 26.66 | 1.6 |
| **3763.2** | **272** | **146** | **17** | 782 | .0072 | 11.9 | 58.39 | 2.8 | .0541 | 7.3 | 57.09 | 3.0 |
| **3763.3** | | **34** | **12** | | .0017 | 36.8 | 156.04 | 3.7 | .0486 | 9.3 | 163.77 | 4.4 |
| **3763.4** | **278** | **45** | **4** | 266 | .0022 | 9.6 | 148.06 | 3.1 | .0456 | 12.2 | 147.40 | 3.1 |
| **3763.5** | **101** | **174** | **12** | 101 | .0086 | 6.7 | 36.63 | 2.4 | .0535 | 4.5 | 36.63 | 2.4 |
| **4147.1** | **70** | **114** | **4** | 83 | .0057 | 3.9 | 56.31 | 1.9 | .0503 | 3.0 | 56.31 | 1.9 |
| **4147.11** | **395** | **46** | **5** | -78 | .0023 | 11.1 | 144.09 | 2.3 | .0638 | 5.2 | 147.26 | 2.5 |
| **4147.9** | **131** | **114** | **8** | 101 | .0057 | 6.8 | 58.29 | 2.6 | .0506 | 5.6 | 58.29 | 2.6 |
| **07AE58-1.1** | **129** | **34** | **4** | 514 | .0017 | 11.1 | 192.94 | 2.5 | .0502 | 5.6 | 192.94 | 2.5 |
| **07AE58-2.1** | **32** | **247** | **7** | 12 | .0123 | 2.7 | 28.00 | 1.6 | .0516 | 1.3 | 28.01 | 1.6 |
| **07AE58-3.1** | **170** | **114** | **12** | 371 | .0056 | 10.9 | 61.28 | 2.2 | .0493 | 4.2 | 60.69 | 2.2 |
| **07AE58-4.1** | **326** | **88** | **10** | -358 | .0043 | 11.5 | 62.58 | 2.6 | .0503 | 5.6 | 63.27 | 2.7 |
| **07AE59-1.2** | **189** | **118** | **8** | 100 | .0058 | 6.5 | 59.06 | 2.3 | .0505 | 8.2 | 59.06 | 2.3 |
| **07AE59-10.2** | **184** | **119** | **9** | 264 | .0059 | 7.5 | 57.99 | 2.4 | .0547 | 8.2 | 57.99 | 2.4 |
| **07AE59-11.2** | **148** | **111** | **8** | 290 | .0055 | 6.9 | 59.97 | 2.0 | .0551 | 6.6 | 59.97 | 2.0 |
| **07AE59-12.2** | **108** | **110** | **4** | -69 | .0055 | 3.2 | 60.18 | 1.2 | .0467 | 4.5 | 60.18 | 1.2 |
| **07AE59-13.1** | **393** | **75** | **16** | -183 | .0037 | 21.7 | 62.89 | 2.6 | .0543 | 5.3 | 63.65 | 2.7 |
| **07AE59-14.1** | | | | | | | 30.61 | 2.7 | .3887 | 11.1 | 58.30 | 9.8 |
| **07AE59-15.1** | **458** | **108** | **24** | -23 | .0054 | 22.0 | 56.76 | 3.4 | .0600 | 7.3 | 57.63 | 3.5 |
| **07AE59-2.2** | **213** | **33** | **2** | -149 | .0016 | 6.1 | 198.66 | 2.2 | .0457 | 8.8 | 198.66 | 2.2 |
| **07AE59-3.2** | **175** | **129** | **8** | 120 | .0064 | 6.0 | 61.44 | 2.2 | .0507 | 7.6 | 61.44 | 2.2 |
| **07AE59-4.2** | | **36** | **36** | | .0018 | 98.5 | 61.00 | 3.0 | .0516 | 10.2 | 62.96 | 3.5 |
| **07AE59-5.2** | **218** | **110** | **9** | 165 | .0055 | 8.1 | 63.37 | 2.7 | .0516 | 9.5 | 63.37 | 2.7 |
| **07AE59-6.2** | **262** | **96** | **10** | -8 | .0048 | 9.9 | 61.99 | 2.8 | .0479 | 11.1 | 61.99 | 2.8 |
| **07AE59-7.2** | **158** | **109** | **6** | 31 | .0054 | 5.3 | 59.48 | 1.9 | .0489 | 6.7 | 59.48 | 1.9 |
| **07AE59-8.2** | **129** | **108** | **5** | 50 | .0053 | 4.7 | 59.76 | 1.6 | .0493 | 5.5 | 59.76 | 1.6 |
| **07AE59-9.2** | **184** | **107** | **7** | -36 | .0053 | 6.3 | 59.00 | 2.1 | .0474 | 7.7 | 59.00 | 2.1 |
| **08AE26-1.1** | **19** | **1083** | **28** | 4 | .0550 | 2.6 | 5.77 | 1.6 | .0753 | 0.9 | 5.77 | 1.6 |
| **08AE26-2.1** | **22** | **1438** | **29** | -2 | .0738 | 2.0 | 4.15 | 1.7 | .0868 | 1.2 | 4.15 | 1.7 |
| **08AE26-2.2** | **24** | **1378** | **36** | -2 | .0706 | 2.6 | 4.22 | 1.7 | .0867 | 1.2 | 4.22 | 1.7 |
| **08AE26-3.1** | **90** | **31** | **1** | 140 | .0015 | 4.4 | 205.86 | 2.0 | .0475 | 3.8 | 205.86 | 2.0 |
| **08AE26-4.1** | **321** | **168** | **25** | 510 | .0083 | 14.8 | 60.06 | 2.7 | .0437 | 6.6 | 58.75 | 2.9 |
| **08AE26-5.1** | **128** | **115** | **6** | -143 | .0057 | 5.6 | 54.81 | 2.0 | .0474 | 3.9 | 54.96 | 2.0 |
| **08AE26-6.1** | **23** | **427** | **8** | 7 | .0213 | 2.0 | 14.55 | 1.5 | .0567 | 0.9 | 14.56 | 1.5 |
| **08AE26-7.1** | **39** | **393** | **13** | -8 | .0196 | 3.3 | 16.24 | 1.6 | .0542 | 1.5 | 16.25 | 1.6 |
| **08AE26-8.1** | **246** | **100** | **9** | -303 | .0049 | 9.1 | 61.35 | 2.2 | .0494 | 4.1 | 61.89 | 2.2 |
| **08AE26-9.1** | | | | | | | 154.70 | 4.4 | .0845 | 9.0 | 169.97 | 6.6 |
| **3763-6.1** | | **105** | **17** | | .0052 | 16.2 | 50.45 | 2.7 | .0493 | 5.8 | 51.79 | 2.9 |
| **3763-7.1** | | | | | | | 55.41 | 2.5 | .5498 | 3.2 | 178.37 | 21.1 |
| **3990-1** | **107** | **137** | **10** | -70 | .0068 | 7.2 | 51.31 | 2.3 | .0468 | 4.5 | 51.31 | 2.3 |
| **3990-10.1** | **117** | **111** | **7** | -117 | .0055 | 5.9 | 54.33 | 1.9 | .0488 | 3.2 | 54.54 | 1.9 |
| **3990-11.1** | **81** | **41** | **4** | -110 | .0020 | 10.2 | 150.96 | 1.8 | .0473 | 2.7 | 151.21 | 1.8 |

## Table B1, cont.

| Spot Name | 4corr 207r /206r | % err | 4corr 207r /235 | % err | 4corr 206r /238 | % err | err corr |
|---|---|---|---|---|---|---|---|
| **3755.1** | .0399 | 16.8 | 0.03 | 17.0 | .0063 | 2.9 | .169 |
| **3755.1** | .0682 | 4.2 | 0.21 | 4.8 | .0225 | 2.4 | .495 |
| **3755.11** | .0391 | 18.9 | 0.03 | 19.1 | .0064 | 2.4 | .124 |
| **3755.12** | .0494 | 2.7 | 0.04 | 3.2 | .0062 | 1.9 | .574 |
| **3755.13** | .0461 | 2.1 | 0.08 | 2.6 | .0126 | 1.6 | .595 |
| **3755.14** | .0495 | 3.6 | 0.12 | 4.1 | .0182 | 2.0 | .491 |
| **3755.15** | .0351 | 24.8 | 0.03 | 25.0 | .0072 | 3.3 | .130 |
| **3755.16** | .0495 | 5.7 | 0.04 | 6.2 | .0061 | 2.5 | .410 |
| **3755.17** | .0302 | 47.2 | 0.08 | 47.4 | .0195 | 4.0 | .085 |
| **3755.2** | .0430 | 12.6 | 0.16 | 12.7 | .0268 | 2.2 | .170 |
| **3755.3** | .0443 | 6.6 | 0.04 | 6.8 | .0070 | 1.8 | .271 |
| **3755.4** | .0514 | 4.9 | 0.19 | 5.5 | .0273 | 2.5 | .454 |
| **3755.5** | .1822 | 0.6 | 12.00 | 1.7 | .4777 | 1.6 | .926 |
| **3755.6** | .0492 | 2.7 | 0.17 | 3.2 | .0256 | 1.7 | .522 |
| **3755.7** | | | | | .0059 | 6.4 | |
| **3755.8** | .0217 | 68.0 | 0.02 | 68.1 | .0062 | 3.2 | .048 |
| **3755.9** | .0767 | 2.6 | 0.51 | 3.0 | .0479 | 1.6 | .514 |
| **3763.1** | .0519 | 1.7 | 0.27 | 2.3 | .0375 | 1.6 | .696 |
| **3763.2** | .0720 | 13.3 | 0.17 | 13.7 | .0175 | 3.0 | .219 |
| **3763.3** | | | | | .0061 | 4.4 | |
| **3763.4** | .0492 | 11.9 | 0.05 | 12.3 | .0068 | 3.1 | .251 |
| **3763.5** | .0535 | 4.5 | 0.20 | 5.1 | .0273 | 2.4 | .467 |
| **4147.1** | .0503 | 3.0 | 0.12 | 3.6 | .0178 | 1.9 | .529 |
| **4147.11** | .0462 | 16.4 | 0.04 | 16.6 | .0068 | 2.5 | .148 |
| **4147.9** | .0506 | 5.6 | 0.12 | 6.2 | .0172 | 2.6 | .425 |
| **07AE58-1.1** | .0502 | 5.6 | 0.04 | 6.1 | .0052 | 2.5 | .414 |
| **07AE58-2.1** | .0513 | 1.4 | 0.25 | 2.1 | .0357 | 1.6 | .749 |
| **07AE58-3.1** | .0571 | 7.7 | 0.13 | 8.0 | .0165 | 2.2 | .278 |
| **07AE58-4.1** | .0414 | 12.8 | 0.09 | 13.1 | .0158 | 2.7 | .205 |
| **07AE59-1.2** | .0505 | 8.2 | 0.12 | 8.5 | .0169 | 2.3 | .272 |
| **07AE59-10.2** | .0547 | 8.2 | 0.13 | 8.6 | .0172 | 2.4 | .283 |
| **07AE59-11.2** | .0551 | 6.6 | 0.13 | 6.9 | .0167 | 2.0 | .282 |
| **07AE59-12.2** | .0467 | 4.5 | 0.11 | 4.7 | .0166 | 1.2 | .260 |
| **07AE59-13.1** | .0445 | 16.0 | 0.10 | 16.3 | .0157 | 2.7 | .167 |
| **07AE59-14.1** | | | | | .0172 | 9.8 | |
| **07AE59-15.1** | .0477 | 19.3 | 0.11 | 19.6 | .0174 | 3.5 | .180 |
| **07AE59-2.2** | .0457 | 8.8 | 0.03 | 9.1 | .0050 | 2.2 | .245 |
| **07AE59-3.2** | .0507 | 7.6 | 0.11 | 7.9 | .0163 | 2.2 | .274 |
| **07AE59-4.2** | .0255 | 64.7 | 0.06 | 64.8 | .0159 | 3.5 | .054 |
| **07AE59-5.2** | .0516 | 9.5 | 0.11 | 9.9 | .0158 | 2.7 | .274 |
| **07AE59-6.2** | .0479 | 11.1 | 0.11 | 11.4 | .0161 | 2.8 | .244 |
| **07AE59-7.2** | .0489 | 6.7 | 0.11 | 7.0 | .0168 | 1.9 | .267 |
| **07AE59-8.2** | .0493 | 5.5 | 0.11 | 5.7 | .0167 | 1.6 | .272 |
| **07AE59-9.2** | .0474 | 7.7 | 0.11 | 8.0 | .0169 | 2.1 | .263 |
| **08AE26-1.1** | .0753 | 0.9 | 1.80 | 1.9 | .1735 | 1.6 | .862 |
| **08AE26-2.1** | .0868 | 1.2 | 2.88 | 2.1 | .2407 | 1.7 | .827 |
| **08AE26-2.2** | .0863 | 1.2 | 2.82 | 2.1 | .2368 | 1.7 | .819 |
| **08AE26-3.1** | .0475 | 3.8 | 0.03 | 4.3 | .0049 | 2.0 | .470 |
| **08AE26-4.1** | .0617 | 15.0 | 0.14 | 15.3 | .0170 | 2.9 | .193 |
| **08AE26-5.1** | .0451 | 5.2 | 0.11 | 5.6 | .0182 | 2.0 | .355 |
| **08AE26-6.1** | .0562 | 1.0 | 0.53 | 1.9 | .0687 | 1.5 | .827 |
| **08AE26-7.1** | .0536 | 1.7 | 0.45 | 2.4 | .0615 | 1.6 | .686 |
| **08AE26-8.1** | .0423 | 9.8 | 0.09 | 10.1 | .0162 | 2.2 | .219 |
| **08AE26-9.1** | | | | | .0059 | 6.6 | |
| **3763-6.1** | .0278 | 37.1 | 0.07 | 37.2 | .0193 | 2.9 | .079 |
| **3763-7.1** | | | | | .0056 | 21.1 | |
| **3990-1** | .0468 | 4.5 | 0.13 | 5.0 | .0195 | 2.3 | .452 |
| **3990-10.1** | .0457 | 4.8 | 0.12 | 5.2 | .0183 | 1.9 | .370 |
| **3990-11.1** | .0460 | 3.3 | 0.04 | 3.8 | .0066 | 1.8 | .469 |

**Table B1, cont.**

| Spot Name | Pb/U const #rej | 204 cts /sec | 204 /206 | % err | 1.005 | %err | 1.010 | %err | Obs 206 /238 | % err | 248 /254 | % err |
|---|---|---|---|---|---|---|---|---|---|---|---|---|
| **3990-12.1** | 1 | 0.05 | 8.9E-5 | 72 | .112 | 4.1 | .437 | 4.5 | .675 | 3.5 | 1.336 | 1.2 |
| **3990-13.1** | 0 | 0.00 | --- | 0 | .049 | 2.1 | .077 | 6.9 | .031 | 1.8 | .077 | 2.4 |
| **3990-14.1** | 0 | -0.04 | -3.5E-4 | 55 | .046 | 5.5 | .140 | 9.3 | .037 | 6.1 | .435 | 0.5 |
| **3990-15.1** | 0 | 0.00 | --- | 0 | .051 | 2.7 | .147 | 3.8 | .052 | 3.7 | .426 | 0.4 |
| **3990-16.1** | 1 | 0.00 | --- | 0 | .049 | 3.2 | .153 | 4.3 | .038 | 3.1 | .421 | 0.4 |
| **3990-17.1** | 0 | 0.03 | 1.1E-4 | 64 | .049 | 2.9 | .127 | 4.2 | .038 | 2.6 | .387 | 1.5 |
| **3990-18.1** | 0 | 0.21 | 4.4E-4 | 38 | .044 | 17.5 | .161 | 3.2 | .060 | 8.4 | .468 | 1.3 |
| **3990-19.1** | 0 | 0.11 | 7.8E-4 | 50 | .049 | 4.2 | .054 | 9.5 | .029 | 1.7 | .158 | 0.9 |
| **3990-2.1** | 0 | 0.00 | --- | 0 | .052 | 3.4 | .141 | 5.4 | .031 | 3.1 | .396 | 0.4 |
| **3990-20.1** | 1 | 0.03 | 2.9E-4 | 71 | .057 | 9.0 | .196 | 17.5 | .033 | 16.1 | .437 | 1.5 |
| **3990-21.1** | 0 | 0.04 | 1.6E-4 | 72 | .048 | 3.3 | .109 | 4.9 | .031 | 4.1 | .342 | 0.5 |
| **3990-22.1** | 0 | 0.00 | --- | 0 | .057 | 7.9 | .066 | 16.5 | .024 | 6.6 | .201 | 6.3 |
| **3990-23.1** | 0 | 0.00 | --- | 0 | .048 | 1.7 | .168 | 2.2 | .039 | 4.2 | .525 | 1.1 |
| **3990-24.1** | 0 | 0.00 | --- | 0 | .048 | 8.3 | .208 | 5.8 | .014 | 2.1 | .592 | 0.9 |
| **3990-24.1** | 1 | 0.00 | --- | 0 | .056 | 8.4 | .172 | 13.5 | .018 | 14.4 | .477 | 2.5 |
| **3990-25.1** | 0 | 0.00 | --- | 0 | .044 | 9.8 | .138 | 8.4 | .016 | 2.6 | .410 | 0.6 |
| **3990-3.1** | 0 | 0.05 | 9.8E-4 | 50 | .045 | 7.3 | .160 | 9.0 | .037 | 4.0 | .445 | 0.7 |
| **3990-4.1** | 0 | 0.09 | 1.3E-4 | 45 | .052 | 1.9 | .204 | 2.5 | .061 | 3.1 | .590 | 0.3 |
| **3990-5.1** | 0 | 0.10 | 8.5E-4 | 50 | .050 | 4.5 | .091 | 10.0 | .025 | 3.1 | .257 | 0.5 |
| **3990-6.1** | 0 | 0.26 | 4.9E-4 | 35 | .057 | 2.9 | .317 | 6.1 | .035 | 5.1 | 1.353 | 2.3 |
| **3990-7.1** | 0 | 0.07 | 1.5E-3 | 68 | .060 | 6.6 | .219 | 8.2 | .026 | 6.5 | .601 | 0.6 |
| **3990-8.1** | 0 | 0.00 | --- | 0 | .050 | 3.3 | .039 | 7.8 | .012 | 2.5 | .095 | 0.3 |
| **3990-9.1** | 0 | 0.07 | 2.6E-4 | 50 | .049 | 3.0 | .032 | 8.5 | .013 | 3.6 | .084 | 0.4 |
| **4145-1.1** | 0 | 0.00 | --- | 0 | .050 | 2.7 | .158 | 3.6 | .048 | 2.3 | .462 | 0.3 |
| **4145-10.1** | 0 | 0.10 | 2.9E-4 | 67 | .049 | 2.6 | .208 | 3.0 | .034 | 3.6 | .592 | 0.2 |
| **4145-11.1** | 0 | 0.07 | 1.3E-3 | 50 | .056 | 6.4 | .224 | 7.8 | .031 | 4.6 | .637 | 0.6 |
| **4145-12.1** | 0 | 0.00 | --- | 0 | .048 | 6.0 | .263 | 5.6 | .034 | 1.9 | .695 | 0.5 |
| **4145-13.1** | 0 | 0.04 | 1.5E-4 | 72 | .050 | 2.9 | .170 | 3.8 | .033 | 3.4 | .473 | 0.6 |
| **4145-14.1** | 0 | 0.08 | 5.0E-4 | 88 | .060 | 8.5 | .250 | 7.4 | .045 | 3.6 | .710 | 1.3 |
| **4145-15.1** | 0 | 0.04 | 4.1E-4 | 71 | .047 | 5.0 | .128 | 7.3 | .033 | 4.6 | .380 | 0.6 |
| **4145-16.1** | 0 | 0.07 | 8.6E-4 | 50 | .052 | 5.2 | .216 | 6.7 | .012 | 5.2 | .567 | 0.8 |
| **4145-17.1** | 0 | 0.12 | 1.7E-4 | 41 | .050 | 1.8 | .287 | 1.8 | .051 | 2.6 | .863 | 0.2 |
| **4145-18.1** | 0 | 0.06 | 5.3E-4 | 50 | .050 | 5.3 | .185 | 5.6 | .033 | 5.2 | .565 | 0.4 |
| **4145-19.1** | 0 | -0.13 | -7.3E-4 | 50 | .050 | 3.8 | .219 | 4.3 | .048 | 4.8 | .640 | 0.4 |
| **4145-2.1** | 0 | 0.00 | --- | 0 | .054 | 6.0 | .144 | 8.6 | .033 | 3.2 | .361 | 0.7 |
| **4145-20.1** | 0 | 0.07 | 4.3E-4 | 50 | .046 | 3.9 | .225 | 4.4 | .034 | 4.5 | .678 | 0.3 |
| **4145-21.1** | 1 | 0.03 | 1.3E-4 | 64 | .048 | 3.3 | .203 | 3.9 | .032 | 3.7 | .626 | 0.3 |
| **4145-22.1** | 0 | 0.16 | 3.2E-4 | 41 | .048 | 2.2 | .237 | 2.5 | .034 | 3.4 | .706 | 0.7 |
| **4145-23.1** | 0 | 0.00 | --- | 0 | .050 | 4.6 | .239 | 7.4 | .031 | 1.7 | .669 | 0.4 |
| **4145-24.1** | 0 | 0.08 | 2.4E-3 | 50 | .056 | 8.0 | .214 | 9.9 | .012 | 3.2 | .633 | 0.5 |
| **4145-25.1** | 0 | 0.07 | 2.0E-4 | 50 | .051 | 2.5 | .223 | 2.9 | .052 | 3.3 | .642 | 0.3 |
| **4145-26** | 0 | 0.11 | 1.6E-3 | 50 | .051 | 6.1 | .192 | 7.3 | .036 | 2.3 | .479 | 0.9 |
| **4145-27** | 0 | 0.05 | 4.9E-4 | 50 | .045 | 5.3 | .250 | 5.5 | .035 | 2.7 | .630 | 1.1 |
| **4145-28** | 0 | 0.03 | 2.6E-4 | 64 | .049 | 4.6 | .202 | 5.5 | .039 | 3.0 | .581 | 0.6 |
| **4145-29** | 0 | 0.05 | 6.5E-4 | 74 | .052 | 5.7 | .176 | 7.3 | .034 | 2.1 | .506 | 0.8 |
| **4145-3.1** | 0 | 0.06 | 5.3E-4 | 64 | .046 | 4.7 | .197 | 5.5 | .036 | 3.4 | .622 | 0.4 |
| **4145-4.1** | 0 | 0.04 | 2.8E-4 | 72 | .051 | 3.9 | .235 | 4.5 | .034 | 3.5 | .662 | 0.4 |
| **4145-5.1** | 0 | 0.05 | 2.4E-4 | 67 | .048 | 3.8 | .179 | 4.2 | .049 | 3.0 | .522 | 0.4 |
| **4145-6.1** | 0 | 0.03 | 2.7E-4 | 65 | .052 | 4.5 | .129 | 6.8 | .034 | 2.0 | .371 | 0.6 |
| **4145-7.1** | 0 | 0.08 | 6.8E-4 | 50 | .050 | 4.5 | .393 | 4.0 | .011 | 7.4 | 1.205 | 1.1 |
| **4145-8.1** | 0 | 0.08 | 3.5E-4 | 50 | .051 | 3.2 | .183 | 4.0 | .032 | 4.5 | .549 | 0.3 |
| **4145-9.1** | 0 | 0.00 | --- | 0 | .051 | 3.7 | .169 | 4.9 | .034 | 2.8 | .513 | 0.4 |
| **4147-1.1** | 0 | 0.08 | 7.5E-4 | 46 | .049 | 4.8 | .176 | 6.1 | .028 | 4.7 | .544 | 0.4 |
| **4147-2.1** | 0 | 0.03 | 2.6E-4 | 64 | .050 | 4.4 | .138 | 6.4 | .032 | 3.3 | .384 | 0.5 |
| **4147-3.1** | 0 | 0.03 | 1.0E-3 | 64 | .063 | 8.2 | .175 | 11.9 | .028 | 4.3 | .336 | 1.0 |
| **4147-4.1** | 0 | 0.05 | 7.1E-4 | 66 | .052 | 5.8 | .210 | 6.8 | .012 | 2.9 | .559 | 0.3 |
| **4147-5.1** | 0 | 0.06 | 4.4E-4 | 50 | .047 | 4.2 | .180 | 5.1 | .011 | 2.7 | .520 | 0.6 |
| **4147-6.1** | 0 | 0.00 | --- | 0 | .050 | 4.8 | .213 | 4.9 | .049 | 1.5 | .608 | 0.6 |
| **4147-7.1** | 0 | 0.06 | 1.1E-4 | 50 | .050 | 2.0 | .214 | 2.3 | .032 | 2.7 | .634 | 1.9 |
| **4147-8.1** | 0 | 0.13 | 8.0E-4 | 50 | .052 | 4.1 | .193 | 4.6 | .047 | 3.7 | .534 | 1.3 |

## Table B1, cont.

| Spot Name | 254 /238 | % err | 238 /196 | Pb/U: UO/U^2 | % err | % comm 206 | ppm U | ppm Th | 232Th /238U | Ln UO/U | Ln Pb/U | Corr 206 /238 |
|---|---|---|---|---|---|---|---|---|---|---|---|---|
| **3990-12.1** | 5.57 | 1.1 | .048 | .02071 | 1.9 | 0.16 | | | 1.40 | 1.718 | -0.395 | .335 |
| **3990-13.1** | 5.50 | 1.1 | 1.032 | .00103 | 0.8 | 0.00 | | | 0.08 | 1.704 | -3.463 | .017 |
| **3990-14.1** | 5.43 | 1.7 | .193 | .00124 | 1.7 | -0.63 | | | 0.46 | 1.692 | -3.290 | .020 |
| **3990-15.1** | 5.29 | 1.8 | .377 | .00184 | 1.1 | 0.00 | | | 0.45 | 1.666 | -2.954 | .030 |
| **3990-16.1** | 5.59 | 1.7 | .374 | .00120 | 1.5 | 0.00 | | | 0.44 | 1.720 | -3.263 | .019 |
| **3990-17.1** | 5.56 | 1.2 | .446 | .00124 | 1.1 | 0.20 | | | 0.41 | 1.715 | -3.261 | .020 |
| **3990-18.1** | 5.40 | 2.6 | .476 | .00199 | 0.9 | 0.79 | | | 0.49 | 1.686 | -2.825 | .032 |
| **3990-19.1** | 5.35 | 0.9 | .256 | .00100 | 1.6 | 1.41 | | | 0.17 | 1.676 | -3.566 | .016 |
| **3990-2.1** | 5.70 | 0.6 | .368 | .00096 | 1.3 | 0.00 | | | 0.42 | 1.741 | -3.461 | .015 |
| **3990-20.1** | 6.04 | 2.1 | .199 | .00108 | 3.6 | 0.52 | | | 0.46 | 1.798 | -3.415 | .018 |
| **3990-21.1** | 5.54 | 0.3 | .443 | .00098 | 1.2 | 0.29 | | | 0.36 | 1.711 | -3.476 | .016 |
| **3990-22.1** | 5.15 | 2.4 | .070 | .00090 | 3.2 | 0.00 | | | 0.21 | 1.639 | -3.709 | .015 |
| **3990-23.1** | 5.57 | 1.6 | 1.224 | .00124 | 0.7 | 0.00 | | | 0.55 | 1.718 | -3.249 | .020 |
| **3990-24.1** | 5.70 | 0.9 | .457 | .00044 | 2.1 | 0.00 | 684 | 411 | 0.62 | 1.740 | -4.247 | .007 |
| **3990-24.1** | 5.67 | 2.1 | .449 | .00057 | 3.9 | 0.00 | | | 0.50 | 1.736 | -4.026 | .009 |
| **3990-25.1** | 5.62 | 0.8 | .260 | .00051 | 2.5 | 0.00 | 385 | 160 | 0.43 | 1.727 | -4.111 | .008 |
| **3990-3.1** | 5.35 | 1.3 | .079 | .00128 | 2.6 | 1.77 | | | 0.47 | 1.677 | -3.309 | .021 |
| **3990-4.1** | 5.61 | 0.9 | .691 | .00194 | 0.8 | 0.24 | | | 0.62 | 1.724 | -2.791 | .031 |
| **3990-5.1** | 5.32 | 1.1 | .273 | .00088 | 1.7 | 1.53 | | | 0.27 | 1.671 | -3.696 | .014 |
| **3990-6.1** | 5.27 | 1.3 | .796 | .00125 | 0.8 | 0.88 | | | 1.42 | 1.662 | -3.368 | .020 |
| **3990-7.1** | 5.34 | 1.8 | .106 | .00089 | 2.7 | 2.67 | | | 0.63 | 1.676 | -3.682 | .014 |
| **3990-8.1** | 5.50 | 1.4 | 1.311 | .00041 | 1.1 | 0.00 | | | 0.10 | 1.704 | -4.389 | .007 |
| **3990-9.1** | 5.57 | 0.9 | 1.273 | .00042 | 1.1 | 0.47 | | | 0.09 | 1.717 | -4.345 | .007 |
| **4145-1.1** | 5.39 | 1.3 | .364 | .00166 | 1.1 | 0.00 | | | 0.48 | 1.684 | -3.029 | .027 |
| **4145-10.1** | 5.31 | 1.0 | .520 | .00119 | 1.0 | 0.51 | | | 0.62 | 1.670 | -3.394 | .019 |
| **4145-11.1** | 5.32 | 0.7 | .082 | .00108 | 2.7 | 2.39 | | | 0.67 | 1.671 | -3.507 | .017 |
| **4145-12.1** | 5.46 | 1.1 | .133 | .00111 | 2.0 | 0.00 | | | 0.73 | 1.697 | -3.389 | .018 |
| **4145-13.1** | 5.56 | 1.3 | .471 | .00107 | 1.1 | 0.27 | | | 0.50 | 1.715 | -3.406 | .017 |
| **4145-14.1** | 5.25 | 1.1 | .150 | .00163 | 1.6 | 0.90 | | | 0.75 | 1.659 | -3.104 | .026 |
| **4145-15.1** | 5.37 | 1.4 | .158 | .00114 | 1.9 | 0.74 | | | 0.40 | 1.681 | -3.408 | .018 |
| **4145-16.1** | 5.41 | 1.6 | .362 | .00041 | 2.0 | 1.55 | | | 0.60 | 1.689 | -4.434 | .007 |
| **4145-17.1** | 5.52 | 0.8 | .775 | .00168 | 0.7 | 0.30 | | | 0.91 | 1.709 | -2.970 | .027 |
| **4145-18.1** | 5.24 | 1.4 | .184 | .00117 | 1.7 | 0.95 | | | 0.59 | 1.655 | -3.434 | .019 |
| **4145-19.1** | 5.34 | 1.0 | .181 | .00168 | 1.5 | -1.32 | | | 0.67 | 1.674 | -3.017 | .027 |
| **4145-2.1** | 5.35 | 0.8 | .096 | .00113 | 2.4 | 0.00 | | | 0.38 | 1.678 | -3.425 | .018 |
| **4145-20.1** | 5.43 | 1.3 | .266 | .00115 | 1.5 | 0.78 | | | 0.71 | 1.691 | -3.384 | .019 |
| **4145-21.1** | 5.20 | 3.1 | .363 | .00115 | 1.4 | 0.23 | | | 0.66 | 1.648 | -3.436 | .019 |
| **4145-22.1** | 5.35 | 1.0 | .731 | .00118 | 0.9 | 0.58 | | | 0.74 | 1.678 | -3.381 | .019 |
| **4145-23.1** | 5.35 | 1.5 | .175 | .00112 | 1.8 | 0.00 | | | 0.70 | 1.676 | -3.464 | .018 |
| **4145-24.1** | 5.34 | 1.7 | .140 | .00041 | 3.2 | 4.41 | | | 0.66 | 1.675 | -4.471 | .007 |
| **4145-25.1** | 5.51 | 1.5 | .391 | .00170 | 1.0 | 0.36 | | | 0.67 | 1.707 | -2.959 | .027 |
| **4145-26** | 5.62 | 1.6 | .105 | .00113 | 2.3 | 2.94 | | | 0.50 | 1.726 | -3.353 | .018 |
| **4145-27** | 5.39 | 1.7 | .142 | .00119 | 2.0 | 0.89 | | | 0.66 | 1.685 | -3.364 | .019 |
| **4145-28** | 5.53 | 2.1 | .171 | .00126 | 1.8 | 0.47 | | | 0.61 | 1.710 | -3.257 | .020 |
| **4145-29** | 5.45 | 0.7 | .122 | .00113 | 2.2 | 1.18 | | | 0.53 | 1.696 | -3.395 | .018 |
| **4145-3.1** | 5.47 | 1.0 | .163 | .00121 | 2.1 | 0.95 | | | 0.65 | 1.700 | -3.340 | .020 |
| **4145-4.1** | 5.31 | 1.9 | .224 | .00120 | 1.6 | 0.50 | | | 0.69 | 1.670 | -3.381 | .019 |
| **4145-5.1** | 5.36 | 1.3 | .211 | .00169 | 1.4 | 0.44 | | | 0.55 | 1.679 | -3.023 | .027 |
| **4145-6.1** | 5.52 | 1.6 | .173 | .00110 | 1.8 | 0.49 | | | 0.39 | 1.708 | -3.395 | .018 |
| **4145-7.1** | 4.98 | 2.5 | .490 | .00045 | 1.6 | 1.23 | | | 1.27 | 1.605 | -4.479 | .007 |
| **4145-8.1** | 5.29 | 1.4 | .339 | .00113 | 1.3 | 0.63 | | | 0.58 | 1.667 | -3.448 | .018 |
| **4145-9.1** | 5.44 | 1.0 | .238 | .00115 | 1.5 | 0.00 | | | 0.54 | 1.693 | -3.377 | .019 |
| **4147-1.1** | 5.12 | 1.5 | .165 | .00107 | 1.8 | 1.35 | | | 0.57 | 1.633 | -3.580 | .017 |
| **4147-2.1** | 5.25 | 1.4 | .158 | .00113 | 1.7 | 0.47 | | | 0.40 | 1.659 | -3.461 | .018 |
| **4147-3.1** | 5.12 | 1.4 | .043 | .00104 | 3.5 | 1.84 | | | 0.35 | 1.633 | -3.612 | .017 |
| **4147-4.1** | 5.32 | 1.2 | .248 | .00041 | 2.2 | 1.29 | | | 0.59 | 1.671 | -4.461 | .007 |
| **4147-5.1** | 5.28 | 1.1 | .483 | .00041 | 1.5 | 0.80 | | | 0.55 | 1.663 | -4.484 | .007 |
| **4147-6.1** | 5.44 | 0.7 | .130 | .00167 | 1.6 | 0.00 | | | 0.64 | 1.694 | -3.007 | .027 |
| **4147-7.1** | 5.22 | 0.3 | .760 | .00115 | 0.8 | 0.19 | | | 0.67 | 1.653 | -3.436 | .019 |
| **4147-8.1** | 5.33 | 1.3 | .145 | .00164 | 1.5 | 1.44 | | | 0.56 | 1.674 | -3.071 | .027 |

**Table B1, cont.**

| Spot Name | % err | ppm Rad $^{206}Pb$ | Total $^{208}Pb/^{232}Th$ | % err | 204corr $^{206}Pb/^{238}U$ Age | 1s err | 207corr $^{206}Pb/^{238}U$ Age | 1s err | 208corr $^{206}Pb/^{238}U$ Age | 1s err | 204corr $^{207}Pb/^{206}Pb$ Age |
|---|---|---|---|---|---|---|---|---|---|---|---|
| **3990-12.1** | 2.4 | | .1043 | 5.2 | **1858.1** | **38.3** | **1865.1** | **45.9** | **1829.7** | **51.4** | **1812** |
| **3990-13.1** | 1.7 | | .0160 | 7.5 | **106.6** | **1.8** | **106.4** | **1.8** | **103.9** | **1.8** | **166** |
| **3990-14.1** | 2.3 | | .0061 | 9.6 | **128.6** | **2.9** | **128.1** | **2.9** | **128.1** | **3.2** | **257** |
| **3990-15.1** | 1.9 | | .0098 | 4.3 | **189.0** | **3.5** | **188.7** | **3.5** | **188.4** | **3.7** | **236** |
| **3990-16.1** | 2.1 | | .0067 | 4.8 | **124.2** | **2.6** | **124.1** | **2.6** | **123.4** | **2.8** | **157** |
| **3990-17.1** | 1.9 | | .0062 | 4.9 | **127.3** | **2.3** | **127.5** | **2.4** | **127.6** | **2.5** | **51** |
| **3990-18.1** | 1.7 | | .0105 | 3.8 | **202.5** | **3.5** | **205.7** | **4.0** | **203.5** | **3.8** | **-556** |
| **3990-19.1** | 2.2 | | .0053 | 9.8 | **101.8** | **2.3** | **103.1** | **2.2** | **103.2** | **2.3** | **-495** |
| **3990-2.1** | 2.0 | | .0052 | 5.8 | **99.0** | **2.0** | **98.5** | **2.0** | **98.6** | **2.1** | **276** |
| **3990-20.1** | 3.9 | | .0075 | 18.0 | **111.4** | **4.3** | **110.8** | **4.3** | **109.1** | **5.0** | **312** |
| **3990-21.1** | 1.9 | | .0048 | 5.2 | **101.2** | **1.9** | **101.5** | **1.9** | **101.7** | **2.0** | **-38** |
| **3990-22.1** | 3.6 | | .0046 | 18.0 | **93.5** | **3.3** | **92.4** | **3.3** | **93.5** | **3.5** | **489** |
| **3990-23.1** | 1.6 | | .0061 | 2.9 | **127.7** | **2.0** | **127.7** | **2.1** | **128.1** | **2.3** | **106** |
| **3990-24.1** | 2.1 | 3.9 | .0022 | 6.3 | **42.9** | **0.9** | **42.9** | **0.9** | **42.7** | **1.0** | **91** |
| **3990-24.1** | 4.2 | | .0031 | 14.3 | **58.6** | **2.4** | **58.0** | **2.4** | **58.3** | **2.7** | **470** |
| **3990-25.1** | 2.5 | 2.6 | .0025 | 8.8 | **50.5** | **1.3** | **50.7** | **1.3** | **50.5** | **1.4** | **-83** |
| **3990-3.1** | 3.0 | | .0071 | 9.5 | **130.1** | **4.0** | **133.0** | **4.0** | **131.6** | **4.4** | **-1101** |
| **3990-4.1** | 1.7 | | .0103 | 3.1 | **198.9** | **3.3** | **199.0** | **3.3** | **198.5** | **3.7** | **188** |
| **3990-5.1** | 2.3 | | .0048 | 10.3 | **90.1** | **2.1** | **91.2** | **2.1** | **91.2** | **2.2** | **-549** |
| **3990-6.1** | 1.7 | | .0045 | 6.7 | **128.2** | **2.2** | **128.0** | **2.2** | **139.6** | **3.3** | **183** |
| **3990-7.1** | 3.1 | | .0050 | 8.8 | **89.8** | **3.2** | **90.8** | **2.8** | **91.3** | **3.3** | **-471** |
| **3990-8.1** | 1.8 | | .0025 | 8.0 | **42.3** | **0.8** | **42.2** | **0.8** | **42.2** | **0.8** | **181** |
| **3990-9.1** | 1.8 | | .0025 | 8.7 | **43.0** | **0.8** | **43.0** | **0.8** | **43.1** | **0.8** | **-43** |
| **4145-1.1** | 1.8 | | .0087 | 4.0 | **170.2** | **3.1** | **170.2** | **3.1** | **169.8** | **3.3** | **184** |
| **4145-10.1** | 1.8 | | .0064 | 3.5 | **121.8** | **2.2** | **122.3** | **2.2** | **121.8** | **2.4** | **-48** |
| **4145-11.1** | 3.1 | | .0058 | 8.4 | **109.0** | **3.6** | **110.5** | **3.4** | **110.9** | **3.9** | **-587** |
| **4145-12.1** | 2.5 | | .0064 | 6.1 | **114.2** | **2.8** | **114.3** | **2.9** | **112.3** | **3.3** | **91** |
| **4145-13.1** | 1.9 | | .0059 | 4.3 | **109.9** | **2.0** | **110.0** | **2.1** | **109.6** | **2.2** | **105** |
| **4145-14.1** | 2.2 | | .0088 | 7.9 | **165.8** | **3.8** | **165.1** | **3.7** | **165.9** | **4.4** | **326** |
| **4145-15.1** | 2.4 | | .0059 | 7.8 | **117.0** | **2.9** | **118.1** | **2.8** | **117.8** | **3.0** | **-319** |
| **4145-16.1** | 2.5 | | .0024 | 7.2 | **41.5** | **1.1** | **41.8** | **1.0** | **41.5** | **1.2** | **-380** |
| **4145-17.1** | 1.6 | | .0086 | 2.5 | **171.7** | **2.8** | **172.2** | **2.8** | **172.2** | **3.3** | **67** |
| **4145-18.1** | 2.3 | | .0059 | 6.0 | **119.8** | **2.8** | **120.8** | **2.8** | **121.2** | **3.1** | **-220** |
| **4145-19.1** | 2.1 | | .0089 | 4.8 | **174.6** | **3.8** | **172.4** | **3.6** | **171.8** | **4.1** | **611** |
| **4145-2.1** | 2.8 | | .0069 | 9.1 | **116.2** | **3.2** | **115.3** | **3.3** | **114.8** | **3.5** | **390** |
| **4145-20.1** | 2.1 | | .0059 | 4.8 | **117.6** | **2.5** | **118.8** | **2.5** | **118.5** | **2.8** | **-365** |
| **4145-21.1** | 2.1 | | .0057 | 4.4 | **118.1** | **2.4** | **118.5** | **2.4** | **118.7** | **2.7** | **-22** |
| **4145-22.1** | 1.7 | | .0061 | 3.1 | **121.3** | **2.1** | **122.1** | **2.1** | **121.9** | **2.4** | **-147** |
| **4145-23.1** | 2.3 | | .0062 | 7.8 | **115.8** | **2.7** | **115.5** | **2.7** | **114.7** | **3.2** | **205** |
| **4145-24.1** | 3.5 | | .0022 | 10.5 | **41.2** | **1.7** | **42.6** | **1.5** | **43.0** | **1.7** | |
| **4145-25.1** | 1.8 | | .0091 | 3.4 | **174.0** | **3.1** | **174.4** | **3.1** | **173.7** | **3.5** | **86** |
| **4145-26** | 2.7 | | .0070 | 7.8 | **113.7** | **3.5** | **116.8** | **3.2** | **115.2** | **3.6** | |
| **4145-27** | 2.5 | | .0073 | 6.1 | **121.6** | **3.0** | **123.2** | **3.1** | **120.1** | **3.5** | **-505** |
| **4145-28** | 2.3 | | .0067 | 6.0 | **129.0** | **3.0** | **129.5** | **3.0** | **129.0** | **3.4** | **-31** |
| **4145-29** | 2.7 | | .0061 | 7.8 | **115.5** | **3.2** | **116.3** | **3.1** | **116.4** | **3.5** | **-197** |
| **4145-3.1** | 2.5 | | .0059 | 6.1 | **124.0** | **3.2** | **125.5** | **3.2** | **125.8** | **3.6** | **-446** |
| **4145-4.1** | 2.1 | | .0066 | 5.0 | **123.2** | **2.7** | **123.4** | **2.6** | **122.8** | **3.0** | **69** |
| **4145-5.1** | 2.0 | | .0089 | 4.7 | **172.5** | **3.5** | **173.5** | **3.5** | **172.7** | **3.8** | **-86** |
| **4145-6.1** | 2.3 | | .0059 | 7.2 | **113.0** | **2.6** | **113.1** | **2.6** | **113.2** | **2.8** | **76** |
| **4145-7.1** | 2.2 | | .0023 | 4.7 | **46.5** | **1.1** | **46.9** | **1.0** | **47.3** | **1.4** | **-392** |
| **4145-8.1** | 1.9 | | .0058 | 4.5 | **115.7** | **2.3** | **116.1** | **2.3** | **116.4** | **2.5** | **-24** |
| **4145-9.1** | 2.1 | | .0058 | 5.4 | **118.4** | **2.4** | **118.0** | **2.5** | **118.6** | **2.7** | **245** |
| **4147-1.1** | 2.4 | | .0053 | 6.5 | **108.6** | **2.6** | **109.9** | **2.6** | **110.4** | **2.9** | **-483** |
| **4147-2.1** | 2.3 | | .0063 | 6.8 | **116.6** | **2.6** | **116.9** | **2.7** | **116.6** | **2.9** | **4** |
| **4147-3.1** | 3.8 | | .0084 | 12.6 | **105.6** | **4.2** | **105.7** | **4.0** | **104.2** | **4.4** | **77** |
| **4147-4.1** | 2.6 | | .0024 | 7.3 | **42.0** | **1.2** | **42.3** | **1.1** | **42.1** | **1.3** | **-287** |
| **4147-5.1** | 2.1 | | .0022 | 5.6 | **41.8** | **0.9** | **42.1** | **0.9** | **42.0** | **1.0** | **-326** |
| **4147-6.1** | 2.2 | | .0090 | 5.4 | **171.3** | **3.7** | **171.1** | **3.7** | **170.2** | **4.2** | **210** |
| **4147-7.1** | 1.7 | | .0060 | 3.4 | **118.6** | **2.0** | **118.5** | **2.0** | **118.6** | **2.2** | **129** |
| **4147-8.1** | 2.1 | | .0091 | 5.2 | **166.2** | **3.7** | **168.2** | **3.6** | **167.3** | **4.0** | **-369** |

## Table B1, cont.

| Spot Name | 1s err | 204corr $^{208}Pb/^{232}Th$ Age | 1s err | % Dis cor-dant | 4corr 208r /232 | % err | Total 238 /206 | % err | Total 207 /206 | % err | 4corr 238/ 206r | % err |
|---|---|---|---|---|---|---|---|---|---|---|---|---|
| **3990-12.1** | **76** | **1990** | **101** | -2 | .1035 | 5.1 | 2.99 | 2.4 | .1120 | 4.1 | 2.99 | 2.4 |
| **3990-13.1** | **49** | **320** | **23** | 56 | .0160 | 7.1 | 59.99 | 1.7 | .0494 | 2.1 | 59.99 | 1.7 |
| **3990-14.1** | **168** | **135** | **14** | 100 | .0067 | 10.7 | 49.96 | 2.3 | .0462 | 5.5 | 49.65 | 2.3 |
| **3990-15.1** | **63** | **197** | **8** | 25 | .0098 | 4.3 | 33.61 | 1.9 | .0509 | 2.7 | 33.61 | 1.9 |
| **3990-16.1** | **76** | **135** | **7** | 27 | .0067 | 4.8 | 51.39 | 2.1 | .0492 | 3.2 | 51.39 | 2.1 |
| **3990-17.1** | **88** | **121** | **6** | -60 | .0060 | 5.1 | 50.06 | 1.9 | .0486 | 2.9 | 50.16 | 1.9 |
| **3990-18.1** | **587** | **190** | **11** | -374 | .0094 | 5.7 | 31.09 | 1.7 | .0435 | 17.5 | 31.34 | 1.8 |
| **3990-19.1** | **440** | **48** | **30** | -586 | .0024 | 61.1 | 61.93 | 2.2 | .0495 | 4.2 | 62.81 | 2.3 |
| **3990-2.1** | **79** | **106** | **6** | 179 | .0052 | 5.8 | 64.61 | 2.0 | .0518 | 3.4 | 64.61 | 2.0 |
| **3990-20.1** | **257** | **143** | **26** | 180 | .0071 | 18.4 | 57.06 | 3.9 | .0568 | 9.0 | 57.36 | 3.9 |
| **3990-21.1** | **124** | **92** | **6** | -138 | .0045 | 6.7 | 63.02 | 1.9 | .0477 | 3.3 | 63.20 | 1.9 |
| **3990-22.1** | **174** | **92** | **16** | 423 | .0046 | 16.9 | 68.48 | 3.6 | .0569 | 7.9 | 68.48 | 3.6 |
| **3990-23.1** | **41** | **123** | **3** | -17 | .0061 | 2.7 | 50.00 | 1.6 | .0481 | 1.7 | 50.00 | 1.6 |
| **3990-24.1** | **197** | **45** | **3** | 113 | .0022 | 6.2 | 149.75 | 2.1 | .0478 | 8.3 | 149.75 | 2.1 |
| **3990-24.1** | **186** | **63** | **9** | 702 | .0031 | 14.1 | 109.44 | 4.2 | .0565 | 8.4 | 109.44 | 4.2 |
| **3990-25.1** | **240** | **51** | **4** | -265 | .0025 | 8.8 | 127.14 | 2.5 | .0445 | 9.8 | 127.14 | 2.5 |
| **3990-3.1** | **818** | **110** | **20** | -946 | .0055 | 17.9 | 48.16 | 3.0 | .0453 | 7.3 | 49.03 | 3.1 |
| **3990-4.1** | **61** | **203** | **7** | -5 | .0101 | 3.3 | 31.83 | 1.7 | .0518 | 1.9 | 31.91 | 1.7 |
| **3990-5.1** | **495** | **63** | **18** | -710 | .0031 | 29.3 | 69.98 | 2.3 | .0498 | 4.5 | 71.07 | 2.4 |
| **3990-6.1** | **143** | **86** | **6** | 42 | .0043 | 6.7 | 49.36 | 1.7 | .0569 | 2.9 | 49.80 | 1.7 |
| **3990-7.1** | **1097** | **75** | **19** | -624 | .0037 | 24.8 | 69.42 | 3.1 | .0603 | 6.6 | 71.32 | 3.6 |
| **3990-8.1** | **76** | **51** | **4** | 329 | .0025 | 8.0 | 151.88 | 1.8 | .0497 | 3.3 | 151.88 | 1.8 |
| **3990-9.1** | **130** | **35** | **8** | -201 | .0017 | 23.7 | 148.86 | 1.8 | .0491 | 3.0 | 149.57 | 1.8 |
| **4145-1.1** | **62** | **176** | **7** | 8 | .0087 | 4.0 | 37.37 | 1.8 | .0498 | 2.7 | 37.37 | 1.8 |
| **4145-10.1** | **167** | **122** | **6** | -139 | .0061 | 5.1 | 52.14 | 1.8 | .0494 | 2.6 | 52.41 | 1.8 |
| **4145-11.1** | **801** | **92** | **15** | -639 | .0045 | 16.7 | 57.27 | 3.1 | .0564 | 6.4 | 58.67 | 3.3 |
| **4145-12.1** | **142** | **130** | **8** | -20 | .0064 | 6.1 | 55.94 | 2.5 | .0478 | 6.0 | 55.94 | 2.5 |
| **4145-13.1** | **106** | **115** | **6** | -5 | .0057 | 4.9 | 57.98 | 1.9 | .0503 | 2.9 | 58.13 | 1.9 |
| **4145-14.1** | **353** | **164** | **17** | 97 | .0082 | 10.5 | 38.04 | 2.2 | .0602 | 8.5 | 38.39 | 2.3 |
| **4145-15.1** | **316** | **105** | **13** | -372 | .0052 | 12.6 | 54.20 | 2.4 | .0466 | 5.0 | 54.61 | 2.5 |
| **4145-16.1** | **464** | **41** | **5** | -1016 | .0020 | 11.5 | 152.54 | 2.5 | .0524 | 5.2 | 154.95 | 2.6 |
| **4145-17.1** | **67** | **169** | **4** | -61 | .0084 | 2.6 | 36.93 | 1.6 | .0498 | 1.8 | 37.04 | 1.6 |
| **4145-18.1** | **285** | **106** | **9** | -283 | .0053 | 8.6 | 52.79 | 2.3 | .0499 | 5.3 | 53.29 | 2.3 |
| **4145-19.1** | **200** | **201** | **15** | 250 | .0100 | 7.4 | 36.89 | 2.1 | .0496 | 3.8 | 36.41 | 2.2 |
| **4145-2.1** | **135** | **139** | **13** | 235 | .0069 | 9.1 | 55.00 | 2.8 | .0544 | 6.0 | 55.00 | 2.8 |
| **4145-20.1** | **242** | **110** | **7** | -410 | .0055 | 6.2 | 53.90 | 2.1 | .0462 | 3.9 | 54.32 | 2.1 |
| **4145-21.1** | **105** | **112** | **5** | -118 | .0056 | 4.7 | 53.95 | 2.1 | .0475 | 3.3 | 54.08 | 2.1 |
| **4145-22.1** | **128** | **117** | **4** | -221 | .0058 | 3.7 | 52.34 | 1.7 | .0481 | 2.2 | 52.64 | 1.7 |
| **4145-23.1** | **107** | **124** | **10** | 77 | .0062 | 7.7 | 55.19 | 2.3 | .0502 | 4.6 | 55.19 | 2.3 |
| **4145-24.1** | | **25** | **10** | | .0012 | 39.6 | 149.23 | 3.5 | .0560 | 8.0 | 156.11 | 4.2 |
| **4145-25.1** | **97** | **177** | **7** | -50 | .0088 | 3.8 | 36.41 | 1.8 | .0507 | 2.5 | 36.54 | 1.8 |
| **4145-26** | | **96** | **24** | | .0048 | 24.9 | 54.53 | 2.7 | .0507 | 6.1 | 56.18 | 3.1 |
| **4145-27** | **312** | **135** | **10** | -515 | .0067 | 7.2 | 52.05 | 2.5 | .0450 | 5.3 | 52.52 | 2.5 |
| **4145-28** | **178** | **129** | **9** | -124 | .0064 | 6.8 | 49.24 | 2.3 | .0493 | 4.6 | 49.47 | 2.3 |
| **4145-29** | **463** | **105** | **15** | -270 | .0052 | 14.4 | 54.66 | 2.7 | .0522 | 5.7 | 55.32 | 2.8 |
| **4145-3.1** | **376** | **107** | **10** | -460 | .0053 | 9.4 | 51.00 | 2.5 | .0464 | 4.7 | 51.49 | 2.6 |
| **4145-4.1** | **180** | **126** | **8** | -44 | .0063 | 6.0 | 51.57 | 2.1 | .0515 | 3.9 | 51.83 | 2.2 |
| **4145-5.1** | **166** | **170** | **10** | -150 | .0085 | 5.9 | 36.72 | 2.0 | .0481 | 3.8 | 36.88 | 2.0 |
| **4145-6.1** | **175** | **109** | **10** | -33 | .0054 | 9.1 | 56.28 | 2.3 | .0515 | 4.5 | 56.56 | 2.3 |
| **4145-7.1** | **372** | **43** | **2** | -943 | .0021 | 5.8 | 136.51 | 2.2 | .0495 | 4.5 | 138.21 | 2.3 |
| **4145-8.1** | **164** | **108** | **6** | -121 | .0054 | 6.0 | 54.87 | 1.9 | .0508 | 3.2 | 55.22 | 2.0 |
| **4145-9.1** | **86** | **117** | **6** | 107 | .0058 | 5.3 | 53.93 | 2.1 | .0511 | 3.7 | 53.93 | 2.1 |
| **4147-1.1** | **399** | **90** | **10** | -544 | .0044 | 11.0 | 58.07 | 2.4 | .0492 | 4.8 | 58.86 | 2.4 |
| **4147-2.1** | **175** | **117** | **10** | -96 | .0058 | 8.5 | 54.54 | 2.3 | .0500 | 4.4 | 54.80 | 2.3 |
| **4147-3.1** | **557** | **131** | **29** | -27 | .0065 | 22.1 | 59.41 | 3.8 | .0625 | 8.2 | 60.52 | 4.0 |
| **4147-4.1** | **482** | **42** | **5** | -783 | .0021 | 12.3 | 150.89 | 2.6 | .0516 | 5.8 | 152.86 | 2.8 |
| **4147-5.1** | **247** | **40** | **3** | -881 | .0020 | 7.6 | 152.66 | 2.1 | .0470 | 4.2 | 153.89 | 2.2 |
| **4147-6.1** | **111** | **181** | **10** | 23 | .0090 | 5.4 | 37.14 | 2.2 | .0503 | 4.8 | 37.14 | 2.2 |
| **4147-7.1** | **62** | **118** | **4** | 9 | .0059 | 3.0 | 53.77 | 1.7 | .0502 | 2.0 | 53.88 | 1.7 |
| **4147-8.1** | **421** | **155** | **17** | -322 | .0077 | 10.7 | 37.73 | 2.1 | .0516 | 4.1 | 38.29 | 2.2 |

## Table B1, cont.

| Spot Name | 4corr 207r /206r | % err | 4corr 207r /235 | % err | 4corr 206r /238 | % err | err corr |
|---|---|---|---|---|---|---|---|
| **3990-12.1** | .1108 | 4.2 | 5.10 | 4.8 | .3341 | 2.4 | .494 |
| **3990-13.1** | .0494 | 2.1 | 0.11 | 2.7 | .0167 | 1.7 | .625 |
| **3990-14.1** | .0514 | 7.3 | 0.14 | 7.7 | .0201 | 2.3 | .299 |
| **3990-15.1** | .0509 | 2.7 | 0.21 | 3.3 | .0298 | 1.9 | .559 |
| **3990-16.1** | .0492 | 3.2 | 0.13 | 3.8 | .0195 | 2.1 | .542 |
| **3990-17.1** | .0470 | 3.7 | 0.13 | 4.1 | .0199 | 1.9 | .449 |
| **3990-18.1** | .0370 | 21.8 | 0.16 | 21.9 | .0319 | 1.8 | .081 |
| **3990-19.1** | .0379 | 16.6 | 0.08 | 16.7 | .0159 | 2.3 | .137 |
| **3990-2.1** | .0518 | 3.4 | 0.11 | 4.0 | .0155 | 2.0 | .502 |
| **3990-20.1** | .0526 | 11.3 | 0.13 | 11.9 | .0174 | 3.9 | .325 |
| **3990-21.1** | .0453 | 5.1 | 0.10 | 5.5 | .0158 | 1.9 | .348 |
| **3990-22.1** | .0569 | 7.9 | 0.11 | 8.7 | .0146 | 3.6 | .412 |
| **3990-23.1** | .0481 | 1.7 | 0.13 | 2.4 | .0200 | 1.6 | .683 |
| **3990-24.1** | .0478 | 8.3 | 0.04 | 8.6 | .0067 | 2.1 | .248 |
| **3990-24.1** | .0565 | 8.4 | 0.07 | 9.4 | .0091 | 4.2 | .444 |
| **3990-25.1** | .0445 | 9.8 | 0.05 | 10.1 | .0079 | 2.5 | .249 |
| **3990-3.1** | .0306 | 27.0 | 0.09 | 27.2 | .0204 | 3.1 | .115 |
| **3990-4.1** | .0499 | 2.6 | 0.22 | 3.1 | .0313 | 1.7 | .536 |
| **3990-5.1** | .0371 | 18.4 | 0.07 | 18.6 | .0141 | 2.4 | .129 |
| **3990-6.1** | .0497 | 6.1 | 0.14 | 6.4 | .0201 | 1.7 | .271 |
| **3990-7.1** | .0382 | 41.5 | 0.07 | 41.6 | .0140 | 3.6 | .087 |
| **3990-8.1** | .0497 | 3.3 | 0.05 | 3.7 | .0066 | 1.8 | .491 |
| **3990-9.1** | .0452 | 5.4 | 0.04 | 5.7 | .0067 | 1.8 | .325 |
| **4145-1.1** | .0498 | 2.7 | 0.18 | 3.2 | .0268 | 1.8 | .565 |
| **4145-10.1** | .0451 | 6.9 | 0.12 | 7.1 | .0191 | 1.8 | .256 |
| **4145-11.1** | .0366 | 29.5 | 0.09 | 29.7 | .0170 | 3.3 | .111 |
| **4145-12.1** | .0478 | 6.0 | 0.12 | 6.5 | .0179 | 2.5 | .386 |
| **4145-13.1** | .0481 | 4.5 | 0.11 | 4.9 | .0172 | 1.9 | .385 |
| **4145-14.1** | .0529 | 15.6 | 0.19 | 15.7 | .0261 | 2.3 | .146 |
| **4145-15.1** | .0405 | 12.3 | 0.10 | 12.6 | .0183 | 2.5 | .196 |
| **4145-16.1** | .0396 | 17.9 | 0.04 | 18.1 | .0065 | 2.6 | .143 |
| **4145-17.1** | .0473 | 2.8 | 0.18 | 3.3 | .0270 | 1.6 | .502 |
| **4145-18.1** | .0421 | 11.3 | 0.11 | 11.6 | .0188 | 2.3 | .202 |
| **4145-19.1** | .0602 | 9.2 | 0.23 | 9.5 | .0275 | 2.2 | .232 |
| **4145-2.1** | .0544 | 6.0 | 0.14 | 6.6 | .0182 | 2.8 | .424 |
| **4145-20.1** | .0398 | 9.3 | 0.10 | 9.6 | .0184 | 2.1 | .223 |
| **4145-21.1** | .0456 | 4.3 | 0.12 | 4.8 | .0185 | 2.1 | .429 |
| **4145-22.1** | .0434 | 5.1 | 0.11 | 5.4 | .0190 | 1.7 | .318 |
| **4145-23.1** | .0502 | 4.6 | 0.13 | 5.2 | .0181 | 2.3 | .449 |
| **4145-24.1** | | | | | .0064 | 4.2 | |
| **4145-25.1** | .0477 | 4.1 | 0.18 | 4.5 | .0274 | 1.8 | .404 |
| **4145-26** | .0261 | 50.2 | 0.06 | 50.3 | .0178 | 3.1 | .062 |
| **4145-27** | .0377 | 11.7 | 0.10 | 12.0 | .0190 | 2.5 | .210 |
| **4145-28** | .0455 | 7.3 | 0.13 | 7.7 | .0202 | 2.3 | .304 |
| **4145-29** | .0425 | 18.5 | 0.11 | 18.7 | .0181 | 2.8 | .151 |
| **4145-3.1** | .0386 | 14.3 | 0.10 | 14.5 | .0194 | 2.6 | .179 |
| **4145-4.1** | .0474 | 7.6 | 0.13 | 7.9 | .0193 | 2.2 | .276 |
| **4145-5.1** | .0445 | 6.8 | 0.17 | 7.1 | .0271 | 2.0 | .286 |
| **4145-6.1** | .0475 | 7.4 | 0.12 | 7.7 | .0177 | 2.3 | .302 |
| **4145-7.1** | .0394 | 14.3 | 0.04 | 14.5 | .0072 | 2.3 | .159 |
| **4145-8.1** | .0456 | 6.8 | 0.11 | 7.1 | .0181 | 2.0 | .279 |
| **4145-9.1** | .0511 | 3.7 | 0.13 | 4.3 | .0185 | 2.1 | .488 |
| **4147-1.1** | .0380 | 15.1 | 0.09 | 15.3 | .0170 | 2.4 | .160 |
| **4147-2.1** | .0461 | 7.3 | 0.12 | 7.6 | .0182 | 2.3 | .301 |
| **4147-3.1** | .0476 | 23.4 | 0.11 | 23.8 | .0165 | 4.0 | .167 |
| **4147-4.1** | .0410 | 18.9 | 0.04 | 19.1 | .0065 | 2.8 | .145 |
| **4147-5.1** | .0404 | 9.6 | 0.04 | 9.8 | .0065 | 2.2 | .219 |
| **4147-6.1** | .0503 | 4.8 | 0.19 | 5.2 | .0269 | 2.2 | .413 |
| **4147-7.1** | .0486 | 2.6 | 0.12 | 3.1 | .0186 | 1.7 | .537 |
| **4147-8.1** | .0397 | 16.3 | 0.14 | 16.4 | .0261 | 2.2 | .137 |

## Table B2.

| | Pb7/6 | Pb8/6 | 206/238 | 208/248 | 254/238 | U238/Zr | ThO248/Zr | UO254/Zr |
|---|---|---|---|---|---|---|---|---|
| **07AE59-2.1** | 0.049928 | 0.238961 | 0.010090 | 0.000794 | 5.516503 | 0.325106 | 0.986833 | 1.793449 |
| **07AE59-15.1** | 0.059180 | 0.132999 | 0.028753 | 0.002199 | 5.095927 | 0.057319 | 0.099688 | 0.292096 |
| **07AE59-13.1** | 0.053770 | 0.108177 | 0.030047 | 0.001750 | 5.466014 | 0.111505 | 0.207083 | 0.609486 |
| **07AE59-11.1** | 0.059053 | 0.203733 | 0.030816 | 0.002147 | 5.408010 | 0.277656 | 0.811767 | 1.501565 |
| **07AE59-12.1** | 0.051999 | 0.237615 | 0.031005 | 0.001988 | 5.396280 | 0.626304 | 2.321540 | 3.379711 |
| **07AE59-4.1** | 0.050783 | 0.135166 | 0.031050 | 0.002294 | 5.421682 | 0.092926 | 0.170027 | 0.503814 |
| **07AE59-3.1** | 0.052915 | 0.176806 | 0.031972 | 0.002055 | 5.471858 | 0.191225 | 0.525949 | 1.046353 |
| **07AE59-1.1** | 0.046536 | 0.179172 | 0.032286 | 0.001782 | 5.362326 | 0.196384 | 0.637679 | 1.053077 |
| **07AE59-6.1** | 0.049218 | 0.196602 | 0.033368 | 0.002115 | 5.359898 | 0.280826 | 0.870978 | 1.505201 |
| **07AE59-9.1** | 0.057014 | 0.177376 | 0.033570 | 0.002322 | 5.539555 | 0.179304 | 0.459820 | 0.993267 |
| **07AE59-5.1** | 0.044831 | 0.151899 | 0.034146 | 0.002049 | 5.528986 | 0.132818 | 0.336175 | 0.734349 |
| **07AE59-8.1** | 0.046082 | 0.214964 | 0.035702 | 0.002140 | 5.686129 | 0.404615 | 1.450865 | 2.300693 |
| **07AE59-10.1** | 0.055879 | 0.207364 | 0.036828 | 0.002453 | 5.840697 | 0.191580 | 0.596521 | 1.118960 |
| **07AE59-7.1** | 0.046914 | 0.255503 | 0.037328 | 0.002387 | 5.788992 | 0.378498 | 1.512155 | 2.191120 |
| **07AE59-14.1** | 0.397614 | 0.996024 | 0.046760 | 0.022228 | 4.661988 | 0.104810 | 0.219607 | 0.488622 |
| **07AE58-1.1** | 0.050233 | 0.072101 | 0.009015 | 0.000560 | 5.211243 | 0.372966 | 0.432564 | 1.943615 |
| **07AE58-4.1** | 0.050554 | 0.160665 | 0.026031 | 0.001710 | 5.077028 | 0.128023 | 0.313155 | 0.649975 |
| **07AE58-3.1** | 0.050070 | 0.106589 | 0.029271 | 0.001698 | 5.331325 | 0.206096 | 0.378601 | 1.098764 |
| **07AE58-2.1** | 0.051426 | 0.106957 | 0.068792 | 0.004521 | 5.581383 | 0.815080 | 1.326596 | 4.549274 |
| **08AE26-3.1** | 0.047544 | 0.264824 | 0.008028 | 0.000523 | 5.160306 | 0.933060 | 3.789599 | 4.814873 |
| **08AE26-9.1** | 0.083443 | 0.218709 | 0.008189 | 0.000766 | 4.520154 | 0.119437 | 0.279263 | 0.539871 |
| **08AE26-8.1** | 0.050107 | 0.151363 | 0.026772 | 0.001892 | 5.117553 | 0.210706 | 0.451355 | 1.078298 |
| **08AE26-4.1** | 0.043407 | 0.158073 | 0.028054 | 0.002260 | 5.180488 | 0.101777 | 0.199676 | 0.527252 |
| **08AE26-5.1** | 0.048408 | 0.160575 | 0.031577 | 0.002107 | 5.272467 | 0.257742 | 0.620296 | 1.358937 |
| **08AE26-7.1** | 0.054041 | 0.118776 | 0.112858 | 0.006994 | 5.425483 | 0.362610 | 0.694996 | 1.967333 |
| **08AE26-6.1** | 0.056770 | 0.200364 | 0.120820 | 0.007436 | 5.353126 | 0.847889 | 2.760473 | 4.538855 |
| **08AE26-1.1** | 0.074728 | 0.083939 | 0.312205 | 0.019134 | 5.343689 | 0.302114 | 0.413782 | 1.614402 |
| **08AE26-2.2** | 0.086845 | 0.231400 | 0.388822 | 0.023781 | 5.166732 | 0.115270 | 0.436110 | 0.595569 |
| **08AE26-2.1** | 0.086559 | 0.334788 | 0.436920 | 0.025891 | 5.385223 | 0.204280 | 1.154124 | 1.100091 |
| **4147-5.1** | 0.047703 | 0.180250 | 0.011451 | 0.000751 | 5.294759 | 0.488113 | 1.342289 | 2.584441 |
| **4147-4.1** | 0.051954 | 0.212540 | 0.011705 | 0.000836 | 5.329259 | 0.253444 | 0.753917 | 1.350667 |
| **4147.11** | 0.062698 | 0.225421 | 0.012091 | 0.000965 | 5.238341 | 0.409852 | 1.157505 | 2.146944 |
| **4147-3.1** | 0.062035 | 0.171527 | 0.027450 | 0.002733 | 5.133481 | 0.043581 | 0.075072 | 0.223722 |
| **4147-1.1** | 0.048727 | 0.174061 | 0.028188 | 0.001767 | 5.119585 | 0.166541 | 0.462415 | 0.852623 |
| **4147.9** | 0.050600 | 0.230226 | 0.030875 | 0.001953 | 5.334941 | 0.105248 | 0.383105 | 0.561493 |
| **4147-2.1** | 0.048955 | 0.133663 | 0.031710 | 0.002091 | 5.264131 | 0.160063 | 0.324444 | 0.842594 |
| **4147.1** | 0.049544 | 0.223335 | 0.032256 | 0.001998 | 5.375713 | 0.364376 | 1.313791 | 1.958779 |
| **4147-7.1** | 0.049463 | 0.211492 | 0.032645 | 0.002067 | 5.298448 | 0.756692 | 2.527143 | 4.009291 |
| **4147-8.1** | 0.049220 | 0.190156 | 0.047934 | 0.003203 | 5.344959 | 0.145420 | 0.413824 | 0.777263 |
| **4147-6.1** | 0.051101 | 0.213402 | 0.049268 | 0.003162 | 5.452545 | 0.132108 | 0.439322 | 0.720322 |
| **3755.16** | 0.048808 | 0.043927 | 0.010112 | 0.000615 | 5.137640 | 0.373045 | 0.269557 | 1.916570 |
| **3755.1** | 0.051403 | 0.105670 | 0.010988 | 0.000692 | 5.232958 | 0.251587 | 0.422079 | 1.316542 |
| **3755.12** | 0.049738 | 0.042999 | 0.011542 | 0.000767 | 5.413621 | 1.447585 | 0.936198 | 7.836678 |
| **3755.7** | 0.060245 | 0.278054 | 0.011695 | 0.001139 | 5.331723 | 0.101553 | 0.290050 | 0.541455 |
| **3755.8** | 0.052037 | 0.134859 | 0.011772 | 0.000861 | 5.415107 | 0.239019 | 0.440632 | 1.294314 |
| **3755.11** | 0.050183 | 0.160924 | 0.012053 | 0.000696 | 5.510840 | 0.495371 | 1.379588 | 2.729911 |
| **3755.15** | 0.050631 | 0.328628 | 0.013225 | 0.000848 | 5.371638 | 0.161852 | 0.829723 | 0.869411 |
| **3755.3** | 0.048827 | 0.405706 | 0.014608 | 0.000910 | 5.791445 | 0.854933 | 5.568843 | 4.951296 |
| **3755.13** | 0.050316 | 0.083473 | 0.022645 | 0.001594 | 5.432833 | 3.752781 | 4.450799 | 20.388231 |
| **3755.14** | 0.050636 | 0.217658 | 0.034646 | 0.002431 | 5.549524 | 0.272693 | 0.845900 | 1.513316 |
| **3755.1** | 0.066823 | 0.219415 | 0.035015 | 0.002226 | 5.015349 | 0.143089 | 0.493894 | 0.717642 |
| **3755.17** | 0.049020 | 0.199690 | 0.036836 | 0.002445 | 5.397160 | 0.041773 | 0.125674 | 0.225455 |
| **3755.6** | 0.050954 | 0.212869 | 0.041865 | 0.002978 | 5.156328 | 0.676527 | 2.024580 | 3.488394 |
| **3755.4** | 0.050928 | 0.119571 | 0.046897 | 0.002894 | 5.264127 | 0.089321 | 0.173077 | 0.470196 |
| **3755.2** | 0.050390 | 0.171214 | 0.048802 | 0.003108 | 5.378267 | 0.155803 | 0.418855 | 0.837952 |
| **3755.9** | 0.077613 | 0.076018 | 0.094580 | 0.012512 | 5.689346 | 0.878438 | 0.504766 | 4.997737 |
| **3755.5** | 0.181438 | 0.089959 | 0.867284 | 0.043927 | 5.372695 | 0.235865 | 0.418930 | 1.267230 |
| **3763.4** | 0.047515 | 0.196272 | 0.011539 | 0.000735 | 5.270753 | 0.190753 | 0.587654 | 1.005411 |
| **3763.3** | 0.049138 | 0.234483 | 0.012352 | 0.001005 | 5.545660 | 0.117249 | 0.337903 | 0.650221 |
| **3763-7.1** | 0.544679 | 1.329255 | 0.028768 | 0.015448 | 5.045169 | 0.161510 | 0.399797 | 0.814847 |
| **3763.2** | 0.055108 | 0.231684 | 0.031016 | 0.002084 | 5.333048 | 0.097968 | 0.337727 | 0.522469 |

**Table B2, cont.**

| | Y89/Zr | La139/Zr | Ce140/Zr | Sm147/Zr | Eu153/Zr | Gd155/Zr | HoO181/Zr |
|---|---|---|---|---|---|---|---|
| **07AE59-2.1** | 18.661357 | 0.000250 | 0.125537 | 0.011111 | 0.015201 | 0.023744 | 0.236691 |
| **07AE59-15.1** | 9.837978 | 0.000033 | 0.052458 | 0.003871 | 0.004036 | 0.012639 | 0.135719 |
| **07AE59-13.1** | 10.565375 | 0.000128 | 0.071413 | 0.004349 | 0.004852 | 0.013124 | 0.147021 |
| **07AE59-11.1** | 30.945983 | 0.000043 | 0.181964 | 0.020182 | 0.015808 | 0.046168 | 0.416505 |
| **07AE59-12.1** | 54.665241 | 0.000882 | 0.266731 | 0.030078 | 0.030916 | 0.078458 | 0.744162 |
| **07AE59-4.1** | 9.820547 | 0.000079 | 0.077947 | 0.003146 | 0.003860 | 0.011264 | 0.135165 |
| **07AE59-3.1** | 27.183123 | 0.000093 | 0.109490 | 0.017109 | 0.016551 | 0.041239 | 0.382077 |
| **07AE59-1.1** | 29.740753 | 0.000138 | 0.128943 | 0.018453 | 0.018107 | 0.048555 | 0.413194 |
| **07AE59-6.1** | 39.462047 | 0.000409 | 0.128825 | 0.023230 | 0.021622 | 0.054769 | 0.550478 |
| **07AE59-9.1** | 24.955419 | 0.000065 | 0.106158 | 0.016429 | 0.015601 | 0.039787 | 0.358173 |
| **07AE59-5.1** | 20.108844 | 0.000086 | 0.094434 | 0.012859 | 0.014036 | 0.032665 | 0.277936 |
| **07AE59-8.1** | 63.498069 | 0.000439 | 0.271506 | 0.041125 | 0.039501 | 0.113106 | 0.933901 |
| **07AE59-10.1** | 29.253206 | 0.000246 | 0.136899 | 0.015588 | 0.018924 | 0.044248 | 0.411190 |
| **07AE59-7.1** | 55.995228 | 0.000326 | 0.242535 | 0.037853 | 0.039607 | 0.095448 | 0.815753 |
| **07AE59-14.1** | 12.448265 | 0.001120 | 0.093127 | 0.007239 | 0.005096 | 0.016954 | 0.162004 |
| **07AE58-1.1** | 7.391348 | 0.000214 | 0.090765 | 0.001939 | 0.004272 | 0.005993 | 0.083558 |
| **07AE58-4.1** | 15.569219 | 0.000069 | 0.098471 | 0.008114 | 0.007810 | 0.021648 | 0.208804 |
| **07AE58-3.1** | 7.523177 | 0.000062 | 0.112879 | 0.003779 | 0.007566 | 0.010561 | 0.094205 |
| **07AE58-2.1** | 18.390371 | 0.000063 | 0.090092 | 0.003731 | 0.001600 | 0.015102 | 0.248435 |
| **08AE26-3.1** | 65.442975 | 0.000310 | 0.274920 | 0.027236 | 0.029297 | 0.105097 | 0.994110 |
| **08AE26-9.1** | 9.309823 | 0.017128 | 0.224688 | 0.019782 | 0.034153 | 0.022236 | 0.085645 |
| **08AE26-8.1** | 9.127120 | 0.000086 | 0.139371 | 0.004966 | 0.010152 | 0.014163 | 0.119099 |
| **08AE26-4.1** | 7.322100 | 0.000976 | 0.076788 | 0.003817 | 0.007153 | 0.009998 | 0.091866 |
| **08AE26-5.1** | 13.267451 | 0.000083 | 0.078206 | 0.003895 | 0.008210 | 0.010288 | 0.161323 |
| **08AE26-7.1** | 10.619846 | 0.000079 | 0.132054 | 0.003531 | 0.006855 | 0.009264 | 0.131705 |
| **08AE26-6.1** | 29.018179 | 0.020165 | 0.348152 | 0.042029 | 0.039070 | 0.073850 | 0.402210 |
| **08AE26-1.1** | 12.897530 | 0.000116 | 0.051697 | 0.004008 | 0.000793 | 0.013389 | 0.180834 |
| **08AE26-2.2** | 35.838071 | 0.000151 | 0.150486 | 0.022936 | 0.023695 | 0.054317 | 0.516671 |
| **08AE26-2.1** | 69.987187 | 0.000514 | 0.237175 | 0.043303 | 0.051725 | 0.117063 | 1.015877 |
| **4147-5.1** | 22.142408 | 0.006981 | 0.152892 | 0.011389 | 0.014766 | 0.028800 | 0.297126 |
| **4147-4.1** | 20.225570 | 0.000214 | 0.079001 | 0.019639 | 0.024002 | 0.041834 | 0.290775 |
| **4147.11** | 6.590329 | 0.690217 | 0.976755 | 0.017496 | 0.012999 | 0.013047 | 0.085593 |
| **4147-3.1** | 4.376004 | 0.000029 | 0.053958 | 0.002060 | 0.002979 | 0.005688 | 0.054828 |
| **4147-1.1** | 14.752084 | 0.000036 | 0.085590 | 0.006746 | 0.003824 | 0.021168 | 0.193367 |
| **4147.9** | 19.675905 | 0.000105 | 0.109096 | 0.018235 | 0.016695 | 0.041432 | 0.277177 |
| **4147-2.1** | 12.985410 | 0.000034 | 0.059249 | 0.004824 | 0.002856 | 0.014992 | 0.177294 |
| **4147.1** | 46.717491 | 0.000217 | 0.136344 | 0.024647 | 0.021488 | 0.065370 | 0.658982 |
| **4147-7.1** | 48.463430 | 0.000238 | 0.343172 | 0.027273 | 0.036100 | 0.065977 | 0.650755 |
| **4147-8.1** | 7.777702 | 0.000068 | 0.096449 | 0.005566 | 0.006052 | 0.012223 | 0.105144 |
| **4147-6.1** | 11.742378 | 0.000121 | 0.052806 | 0.008133 | 0.005330 | 0.018718 | 0.162510 |
| **3755.16** | 6.611482 | 0.000020 | 0.049229 | 0.001858 | 0.003384 | 0.006437 | 0.082963 |
| **3755.1** | 18.376056 | 0.000166 | 0.149999 | 0.009063 | 0.009025 | 0.025423 | 0.250881 |
| **3755.12** | 21.561671 | 0.002921 | 0.100533 | 0.004786 | 0.007422 | 0.016519 | 0.267428 |
| **3755.7** | 9.695146 | 0.000165 | 0.109502 | 0.006888 | 0.010303 | 0.015247 | 0.128674 |
| **3755.8** | 16.048514 | 0.056562 | 0.238805 | 0.011894 | 0.009199 | 0.024441 | 0.227381 |
| **3755.11** | 38.277939 | 0.001117 | 0.318337 | 0.027727 | 0.025473 | 0.063579 | 0.558665 |
| **3755.15** | 16.268623 | 0.000106 | 0.162899 | 0.012667 | 0.012618 | 0.029395 | 0.223641 |
| **3755.3** | 30.273588 | 0.031177 | 0.520629 | 0.030737 | 0.060467 | 0.053043 | 0.409619 |
| **3755.13** | 18.669046 | 0.007646 | 0.141427 | 0.005131 | 0.004948 | 0.009758 | 0.189775 |
| **3755.14** | 29.669069 | 0.000106 | 0.097052 | 0.012640 | 0.010493 | 0.036883 | 0.416481 |
| **3755.1** | 11.508005 | 0.001092 | 0.085396 | 0.008438 | 0.007435 | 0.020036 | 0.152678 |
| **3755.17** | 14.861192 | 0.000043 | 0.060359 | 0.009433 | 0.016140 | 0.021876 | 0.202869 |
| **3755.6** | 12.605866 | 0.000119 | 0.176109 | 0.004428 | 0.005136 | 0.013230 | 0.167923 |
| **3755.4** | 5.257325 | 0.000047 | 0.059265 | 0.001798 | 0.001438 | 0.005856 | 0.069761 |
| **3755.2** | 9.766350 | 0.000080 | 0.115610 | 0.005394 | 0.004615 | 0.012726 | 0.130952 |
| **3755.9** | 16.008167 | 0.002983 | 0.077370 | 0.006746 | 0.009748 | 0.019053 | 0.223304 |
| **3755.5** | 12.054769 | 0.000613 | 0.052229 | 0.005534 | 0.006271 | 0.014765 | 0.166211 |
| **3763.4** | 18.239364 | 0.000111 | 0.179093 | 0.011817 | 0.014008 | 0.028760 | 0.245957 |
| **3763.3** | 11.648683 | 0.000110 | 0.171134 | 0.007421 | 0.010018 | 0.018288 | 0.160706 |
| **3763-7.1** | 14.029429 | 0.240579 | 0.501843 | 0.017521 | 0.013841 | 0.024963 | 0.192472 |
| **3763.2** | 16.040477 | 0.000121 | 0.104069 | 0.015124 | 0.012383 | 0.031143 | 0.228380 |

## Table B2, cont.

| | YbO188/Zr | HfO196/Zr | 204/206 | 207/206 no 204cr | Age Est. 206/238 | Age Est. 208/232 | Th ppm | U ppm |
|---|---|---|---|---|---|---|---|---|
| **07AE59-2.1** | 0.348231 | 9.540888 | 0.001732 | 0.050 | 34 | 42 | 156 | 266 |
| **07AE59-15.1** | 0.159119 | 9.150963 | 0.000627 | 0.059 | 96 | 117 | 16 | 43 |
| **07AE59-13.1** | 0.192066 | 9.389956 | 0.000636 | 0.054 | 100 | 93 | 33 | 90 |
| **07AE59-11.1** | 0.486904 | 11.868253 | 0.000633 | 0.059 | 102 | 114 | 128 | 222 |
| **07AE59-12.1** | 0.818342 | 10.070365 | 0.000142 | 0.052 | 103 | 106 | 367 | 501 |
| **07AE59-4.1** | 0.175645 | 11.026718 | 0.002291 | 0.051 | 103 | 122 | 27 | 75 |
| **07AE59-3.1** | 0.416133 | 10.151566 | 0.000951 | 0.053 | 106 | 109 | 83 | 155 |
| **07AE59-1.1** | 0.427057 | 10.420599 | 0.000455 | 0.047 | 107 | 95 | 101 | 156 |
| **07AE59-6.1** | 0.605368 | 10.008370 | 0.001214 | 0.049 | 111 | 113 | 138 | 223 |
| **07AE59-9.1** | 0.392382 | 11.168475 | 0.000000 | 0.057 | 112 | 124 | 73 | 147 |
| **07AE59-5.1** | 0.309309 | 10.733661 | 0.000000 | 0.045 | 113 | 109 | 53 | 109 |
| **07AE59-8.1** | 0.893829 | 10.816362 | 0.000380 | 0.046 | 119 | 114 | 229 | 341 |
| **07AE59-10.1** | 0.484754 | 10.416004 | 0.002907 | 0.056 | 122 | 130 | 94 | 166 |
| **07AE59-7.1** | 0.853524 | 10.092307 | 0.000000 | 0.047 | 124 | 127 | 239 | 325 |
| **07AE59-14.1** | 0.184472 | 7.907632 | 0.027833 | 0.398 | 155 | 1182 | 35 | 72 |
| **07AE58-1.1** | 0.200942 | 9.676957 | 0.000325 | 0.050 | 30 | 30 | 68 | 288 |
| **07AE58-4.1** | 0.240283 | 9.842162 | 0.000693 | 0.051 | 87 | 91 | 49 | 96 |
| **07AE58-3.1** | 0.128664 | 9.571147 | 0.000365 | 0.050 | 97 | 90 | 60 | 163 |
| **07AE58-2.1** | 0.416364 | 10.621009 | 0.000019 | 0.051 | 229 | 240 | 209 | 674 |
| **08AE26-3.1** | 0.877922 | 8.362639 | 0.000000 | 0.048 | 27 | 28 | 598 | 713 |
| **08AE26-9.1** | 0.120138 | 7.999526 | 0.003953 | 0.083 | 27 | 41 | 44 | 80 |
| **08AE26-8.1** | 0.144737 | 9.212112 | 0.000521 | 0.050 | 89 | 101 | 71 | 160 |
| **08AE26-4.1** | 0.136484 | 9.194299 | 0.000753 | 0.043 | 93 | 120 | 32 | 78 |
| **08AE26-5.1** | 0.316490 | 7.348426 | 0.000122 | 0.048 | 105 | 112 | 98 | 201 |
| **08AE26-7.1** | 0.278756 | 8.749274 | 0.000051 | 0.054 | 375 | 372 | 110 | 291 |
| **08AE26-6.1** | 0.384734 | 11.296102 | 0.000031 | 0.057 | 402 | 395 | 436 | 672 |
| **08AE26-1.1** | 0.261046 | 13.419291 | 0.000013 | 0.075 | 1038 | 1018 | 65 | 239 |
| **08AE26-2.2** | 0.555730 | 8.214866 | 0.000046 | 0.087 | 1292 | 1265 | 69 | 88 |
| **08AE26-2.1** | 1.032991 | 6.217882 | 0.000032 | 0.087 | 1452 | 1377 | 182 | 163 |
| **4147-5.1** | 0.354473 | 7.396232 | 0.000528 | 0.048 | 38 | 40 | 212 | 383 |
| **4147-4.1** | 0.291070 | 8.134622 | 0.000708 | 0.052 | 39 | 44 | 119 | 200 |
| **4147.11** | 0.143341 | 10.176495 | 0.001464 | 0.063 | 40 | 51 | 183 | 318 |
| **4147-3.1** | 0.078958 | 9.845892 | 0.000858 | 0.062 | 91 | 145 | 12 | 33 |
| **4147-1.1** | 0.215263 | 9.607802 | 0.000727 | 0.049 | 94 | 94 | 73 | 126 |
| **4147.9** | 0.276547 | 9.490255 | 0.000337 | 0.051 | 103 | 104 | 60 | 83 |
| **4147-2.1** | 0.222782 | 10.417915 | 0.000206 | 0.049 | 105 | 111 | 51 | 125 |
| **4147.1** | 0.716695 | 9.292112 | 0.000000 | 0.050 | 107 | 106 | 207 | 290 |
| **4147-7.1** | 0.873336 | 8.881823 | 0.000086 | 0.049 | 109 | 110 | 399 | 594 |
| **4147-8.1** | 0.123573 | 8.978720 | 0.000764 | 0.049 | 159 | 170 | 65 | 115 |
| **4147-6.1** | 0.199285 | 8.406058 | 0.000161 | 0.051 | 164 | 168 | 69 | 107 |
| **3755.16** | 0.151575 | 11.059970 | 0.000333 | 0.049 | 34 | 33 | 43 | 284 |
| **3755.1** | 0.318513 | 9.967357 | 0.000859 | 0.051 | 37 | 37 | 67 | 195 |
| **3755.12** | 0.497212 | 11.234247 | 0.000071 | 0.050 | 38 | 41 | 148 | 1161 |
| **3755.7** | 0.171424 | 9.504191 | 0.003972 | 0.060 | 39 | 61 | 46 | 80 |
| **3755.8** | 0.263136 | 9.818824 | 0.002043 | 0.052 | 39 | 46 | 70 | 192 |
| **3755.11** | 0.597455 | 10.029550 | 0.000587 | 0.050 | 40 | 37 | 218 | 404 |
| **3755.15** | 0.247003 | 9.824715 | 0.001129 | 0.051 | 44 | 45 | 131 | 129 |
| **3755.3** | 0.636777 | 6.404166 | 0.000342 | 0.049 | 49 | 48 | 879 | 733 |
| **3755.13** | 0.585927 | 11.493554 | 0.000229 | 0.050 | 75 | 85 | 703 | 3020 |
| **3755.14** | 0.506809 | 10.355153 | 0.000000 | 0.051 | 115 | 129 | 134 | 224 |
| **3755.1** | 0.188270 | 9.736244 | 0.000234 | 0.067 | 116 | 118 | 78 | 106 |
| **3755.17** | 0.286934 | 8.737815 | 0.001548 | 0.049 | 122 | 130 | 20 | 33 |
| **3755.6** | 0.274751 | 11.781437 | 0.000122 | 0.051 | 139 | 158 | 320 | 517 |
| **3755.4** | 0.105567 | 10.493596 | 0.000255 | 0.051 | 156 | 154 | 27 | 70 |
| **3755.2** | 0.195252 | 9.377151 | 0.000418 | 0.050 | 162 | 165 | 66 | 124 |
| **3755.9** | 0.405886 | 12.624674 | 0.000042 | 0.078 | 314 | 666 | 80 | 740 |
| **3755.5** | 0.224275 | 9.491698 | 0.000021 | 0.181 | 2883 | 2336 | 66 | 188 |
| **3763.4** | 0.296989 | 9.260352 | 0.002741 | 0.048 | 38 | 39 | 93 | 149 |
| **3763.3** | 0.212494 | 10.604721 | 0.002586 | 0.049 | 41 | 53 | 53 | 96 |
| **3763-7.1** | 0.220185 | 8.834523 | 0.037542 | 0.545 | 96 | 822 | 63 | 121 |
| **3763.2** | 0.231607 | 9.406992 | 0.000767 | 0.055 | 103 | 111 | 53 | 77 |

**Table B2, cont.**

| | Y ppm | La ppm | Ce ppm | Sm ppm | Eu ppm | Gd ppm | Dy ppm | Yb ppm | Hf ppm | Th/U | Yb /Gd |
|---|---|---|---|---|---|---|---|---|---|---|---|
| **07AE59-2.1** | 842 | 0.03 | 16 | 2.8 | 1.22 | 19 | 29 | 303 | 8937 | 0.59 | 16.2 |
| **07AE59-15.1** | 444 | 0.00 | 7 | 1.0 | 0.33 | 10 | 17 | 139 | 8572 | 0.36 | 13.9 |
| **07AE59-13.1** | 476 | 0.01 | 9 | 1.1 | 0.39 | 10 | 18 | 167 | 8796 | 0.36 | 16.1 |
| **07AE59-11.1** | 1396 | 0.00 | 23 | 5.1 | 1.27 | 36 | 51 | 424 | 11117 | 0.58 | 11.6 |
| **07AE59-12.1** | 2465 | 0.09 | 34 | 7.6 | 2.49 | 62 | 92 | 713 | 9433 | 0.73 | 11.5 |
| **07AE59-4.1** | 443 | 0.01 | 10 | 0.8 | 0.31 | 9 | 17 | 153 | 10329 | 0.36 | 17.2 |
| **07AE59-3.1** | 1226 | 0.01 | 14 | 4.3 | 1.33 | 33 | 47 | 362 | 9509 | 0.54 | 11.1 |
| **07AE59-1.1** | 1341 | 0.01 | 16 | 4.7 | 1.46 | 38 | 51 | 372 | 9761 | 0.65 | 9.7 |
| **07AE59-6.1** | 1780 | 0.04 | 16 | 5.9 | 1.74 | 43 | 68 | 527 | 9375 | 0.62 | 12.2 |
| **07AE59-9.1** | 1125 | 0.01 | 14 | 4.1 | 1.26 | 31 | 44 | 342 | 10462 | 0.49 | 10.9 |
| **07AE59-5.1** | 907 | 0.01 | 12 | 3.2 | 1.13 | 26 | 34 | 269 | 10054 | 0.49 | 10.4 |
| **07AE59-8.1** | 2864 | 0.05 | 35 | 10.4 | 3.18 | 89 | 115 | 778 | 10132 | 0.67 | 8.7 |
| **07AE59-10.1** | 1319 | 0.03 | 17 | 3.9 | 1.52 | 35 | 51 | 422 | 9757 | 0.57 | 12.1 |
| **07AE59-7.1** | 2525 | 0.03 | 31 | 9.6 | 3.19 | 75 | 100 | 743 | 9454 | 0.74 | 9.9 |
| **07AE59-14.1** | 561 | 0.12 | 12 | 1.8 | 0.41 | 13 | 20 | 161 | 7407 | 0.48 | 12.0 |
| **07AE58-1.1** | 333 | 0.02 | 12 | 0.5 | 0.34 | 5 | 10 | 175 | 9065 | 0.24 | 37.0 |
| **07AE58-4.1** | 702 | 0.01 | 13 | 2.0 | 0.63 | 17 | 26 | 209 | 9219 | 0.51 | 12.2 |
| **07AE58-3.1** | 339 | 0.01 | 14 | 1.0 | 0.61 | 8 | 12 | 112 | 8966 | 0.37 | 13.4 |
| **07AE58-2.1** | 829 | 0.01 | 12 | 0.9 | 0.13 | 12 | 31 | 363 | 9949 | 0.31 | 30.4 |
| **08AE26-3.1** | 2951 | 0.03 | 35 | 6.9 | 2.36 | 83 | 122 | 764 | 7833 | 0.84 | 9.2 |
| **08AE26-9.1** | 420 | 1.84 | 29 | 5.0 | 2.75 | 18 | 11 | 105 | 7493 | 0.55 | 6.0 |
| **08AE26-8.1** | 412 | 0.01 | 18 | 1.3 | 0.82 | 11 | 15 | 126 | 8629 | 0.45 | 11.3 |
| **08AE26-4.1** | 330 | 0.10 | 10 | 1.0 | 0.58 | 8 | 11 | 119 | 8613 | 0.40 | 15.0 |
| **08AE26-5.1** | 598 | 0.01 | 10 | 1.0 | 0.66 | 8 | 20 | 276 | 6883 | 0.49 | 33.9 |
| **08AE26-7.1** | 479 | 0.01 | 17 | 0.9 | 0.55 | 7 | 16 | 243 | 8196 | 0.38 | 33.2 |
| **08AE26-6.1** | 1309 | 2.16 | 44 | 10.6 | 3.15 | 58 | 50 | 335 | 10581 | 0.65 | 5.7 |
| **08AE26-1.1** | 582 | 0.01 | 7 | 1.0 | 0.06 | 11 | 22 | 227 | 12570 | 0.27 | 21.5 |
| **08AE26-2.2** | 1616 | 0.02 | 19 | 5.8 | 1.91 | 43 | 64 | 484 | 7695 | 0.78 | 11.3 |
| **08AE26-2.1** | 3156 | 0.06 | 30 | 10.9 | 4.17 | 93 | 125 | 900 | 5824 | 1.12 | 9.7 |
| **4147-5.1** | 999 | 0.75 | 20 | 2.9 | 1.19 | 23 | 37 | 309 | 6928 | 0.55 | 13.6 |
| **4147-4.1** | 912 | 0.02 | 10 | 5.0 | 1.93 | 33 | 36 | 253 | 7620 | 0.59 | 7.7 |
| **4147.11** | 297 | 74.03 | 125 | 4.4 | 1.05 | 10 | 11 | 125 | 9533 | 0.57 | 12.1 |
| **4147-3.1** | 197 | 0.00 | 7 | 0.5 | 0.24 | 4 | 7 | 69 | 9223 | 0.36 | 15.3 |
| **4147-1.1** | 665 | 0.00 | 11 | 1.7 | 0.31 | 17 | 24 | 187 | 9000 | 0.58 | 11.2 |
| **4147.9** | 887 | 0.01 | 14 | 4.6 | 1.34 | 33 | 34 | 241 | 8890 | 0.73 | 7.4 |
| **4147-2.1** | 586 | 0.00 | 8 | 1.2 | 0.23 | 12 | 22 | 194 | 9759 | 0.41 | 16.4 |
| **4147.1** | 2107 | 0.02 | 17 | 6.2 | 1.73 | 52 | 81 | 624 | 8704 | 0.71 | 12.1 |
| **4147-7.1** | 2186 | 0.03 | 44 | 6.9 | 2.91 | 52 | 80 | 760 | 8320 | 0.67 | 14.6 |
| **4147-8.1** | 351 | 0.01 | 12 | 1.4 | 0.49 | 10 | 13 | 108 | 8411 | 0.57 | 11.1 |
| **4147-6.1** | 530 | 0.01 | 7 | 2.1 | 0.43 | 15 | 20 | 174 | 7874 | 0.65 | 11.7 |
| **3755.16** | 298 | 0.00 | 6 | 0.5 | 0.27 | 5 | 10 | 132 | 10360 | 0.15 | 25.9 |
| **3755.1** | 829 | 0.02 | 19 | 2.3 | 0.73 | 20 | 31 | 277 | 9337 | 0.34 | 13.8 |
| **3755.12** | 972 | 0.31 | 13 | 1.2 | 0.60 | 13 | 33 | 433 | 10523 | 0.13 | 33.2 |
| **3755.7** | 437 | 0.02 | 14 | 1.7 | 0.83 | 12 | 16 | 149 | 8903 | 0.57 | 12.4 |
| **3755.8** | 724 | 6.07 | 31 | 3.0 | 0.74 | 19 | 28 | 229 | 9198 | 0.36 | 11.9 |
| **3755.11** | 1726 | 0.12 | 41 | 7.0 | 2.05 | 50 | 69 | 520 | 9395 | 0.54 | 10.4 |
| **3755.15** | 734 | 0.01 | 21 | 3.2 | 1.02 | 23 | 28 | 215 | 9203 | 1.02 | 9.3 |
| **3755.3** | 1365 | 3.34 | 67 | 7.8 | 4.87 | 42 | 50 | 554 | 5999 | 1.20 | 13.2 |
| **3755.13** | 842 | 0.82 | 18 | 1.3 | 0.40 | 8 | 23 | 510 | 10766 | 0.23 | 66.2 |
| **3755.14** | 1338 | 0.01 | 12 | 3.2 | 0.85 | 29 | 51 | 441 | 9700 | 0.60 | 15.1 |
| **3755.1** | 519 | 0.12 | 11 | 2.1 | 0.60 | 16 | 19 | 164 | 9120 | 0.73 | 10.4 |
| **3755.17** | 670 | 0.00 | 8 | 2.4 | 1.30 | 17 | 25 | 250 | 8185 | 0.59 | 14.5 |
| **3755.6** | 569 | 0.01 | 22 | 1.1 | 0.41 | 10 | 21 | 239 | 11036 | 0.62 | 22.9 |
| **3755.4** | 237 | 0.01 | 8 | 0.5 | 0.12 | 5 | 9 | 92 | 9830 | 0.39 | 19.9 |
| **3755.2** | 440 | 0.01 | 15 | 1.4 | 0.37 | 10 | 16 | 170 | 8784 | 0.53 | 16.9 |
| **3755.9** | 722 | 0.32 | 10 | 1.7 | 0.79 | 15 | 27 | 353 | 11826 | 0.11 | 23.5 |
| **3755.5** | 544 | 0.07 | 7 | 1.4 | 0.51 | 12 | 20 | 195 | 8891 | 0.35 | 16.7 |
| **3763.4** | 823 | 0.01 | 23 | 3.0 | 1.13 | 23 | 30 | 259 | 8674 | 0.62 | 11.4 |
| **3763.3** | 525 | 0.01 | 22 | 1.9 | 0.81 | 14 | 20 | 185 | 9934 | 0.55 | 12.8 |
| **3763-7.1** | 633 | 25.80 | 64 | 4.4 | 1.11 | 20 | 24 | 192 | 8276 | 0.52 | 9.7 |
| **3763.2** | 723 | 0.01 | 13 | 3.8 | 1.00 | 25 | 28 | 202 | 8812 | 0.69 | 8.2 |

**Table B2, cont.**

| | U /Yb | Th /Yb | Ce /Sm | Yb /Ce | U /Ce | Y /Yb | Th /Ce | Yb /La | Ce /Eu | Gd /Eu | LaCh 0.319 | CeCh 0.82 |
|---|---|---|---|---|---|---|---|---|---|---|---|---|
| **07AE59-2.1** | 0.9 | 0.51 | 6 | 19 | 17 | 2.8 | 10 | 11311 | 13 | 15 | 0.08 | 20 |
| **07AE59-15.1** | 0.3 | 0.11 | 7 | 21 | 6 | 3.2 | 2 | 39045 | 21 | 31 | 0.01 | 8 |
| **07AE59-13.1** | 0.5 | 0.20 | 8 | 18 | 10 | 2.8 | 4 | 12190 | 23 | 27 | 0.04 | 11 |
| **07AE59-11.1** | 0.5 | 0.30 | 5 | 18 | 10 | 3.3 | 6 | 91274 | 18 | 29 | 0.01 | 28 |
| **07AE59-12.1** | 0.7 | 0.51 | 4 | 21 | 15 | 3.5 | 11 | 7532 | 14 | 25 | 0.30 | 42 |
| **07AE59-4.1** | 0.5 | 0.18 | 13 | 15 | 7 | 2.9 | 3 | 17977 | 32 | 29 | 0.03 | 12 |
| **07AE59-3.1** | 0.4 | 0.23 | 3 | 26 | 11 | 3.4 | 6 | 36333 | 10 | 24 | 0.03 | 17 |
| **07AE59-1.1** | 0.4 | 0.27 | 4 | 23 | 9 | 3.6 | 6 | 25051 | 11 | 26 | 0.05 | 20 |
| **07AE59-6.1** | 0.4 | 0.26 | 3 | 32 | 14 | 3.4 | 8 | 12005 | 9 | 25 | 0.14 | 20 |
| **07AE59-9.1** | 0.4 | 0.21 | 3 | 25 | 11 | 3.3 | 5 | 48734 | 11 | 25 | 0.02 | 17 |
| **07AE59-5.1** | 0.4 | 0.20 | 4 | 22 | 9 | 3.4 | 4 | 29162 | 11 | 23 | 0.03 | 15 |
| **07AE59-8.1** | 0.4 | 0.29 | 3 | 22 | 10 | 3.7 | 7 | 16534 | 11 | 28 | 0.15 | 42 |
| **07AE59-10.1** | 0.4 | 0.22 | 4 | 24 | 9 | 3.1 | 5 | 15990 | 11 | 23 | 0.08 | 21 |
| **07AE59-7.1** | 0.4 | 0.32 | 3 | 24 | 10 | 3.4 | 8 | 21235 | 10 | 24 | 0.11 | 38 |
| **07AE59-14.1** | 0.5 | 0.22 | 7 | 14 | 6 | 3.5 | 3 | 1337 | 29 | 33 | 0.38 | 15 |
| **07AE58-1.1** | 1.6 | 0.39 | 24 | 15 | 25 | 1.9 | 6 | 7622 | 34 | 14 | 0.07 | 14 |
| **07AE58-4.1** | 0.5 | 0.24 | 6 | 17 | 8 | 3.4 | 4 | 28176 | 20 | 27 | 0.02 | 15 |
| **07AE58-3.1** | 1.5 | 0.53 | 15 | 8 | 11 | 3.0 | 4 | 16941 | 24 | 14 | 0.02 | 18 |
| **07AE58-2.1** | 1.9 | 0.58 | 12 | 31 | 59 | 2.3 | 18 | 53509 | 89 | 93 | 0.02 | 14 |
| **08AE26-3.1** | 0.9 | 0.78 | 5 | 22 | 20 | 3.9 | 17 | 22957 | 15 | 35 | 0.10 | 43 |
| **08AE26-9.1** | 0.8 | 0.42 | 6 | 4 | 3 | 4.0 | 2 | 57 | 10 | 6 | 5.76 | 35 |
| **08AE26-8.1** | 1.3 | 0.57 | 14 | 7 | 9 | 3.3 | 4 | 13637 | 22 | 14 | 0.03 | 22 |
| **08AE26-4.1** | 0.7 | 0.27 | 10 | 12 | 8 | 2.8 | 3 | 1136 | 17 | 14 | 0.33 | 12 |
| **08AE26-5.1** | 0.7 | 0.36 | 10 | 28 | 20 | 2.2 | 10 | 30849 | 15 | 12 | 0.03 | 12 |
| **08AE26-7.1** | 1.2 | 0.45 | 19 | 14 | 17 | 2.0 | 7 | 28671 | 31 | 13 | 0.03 | 21 |
| **08AE26-6.1** | 2.0 | 1.30 | 4 | 8 | 15 | 3.9 | 10 | 155 | 14 | 19 | 6.78 | 54 |
| **08AE26-1.1** | 1.1 | 0.29 | 7 | 34 | 36 | 2.6 | 10 | 18348 | 103 | 166 | 0.04 | 8 |
| **08AE26-2.2** | 0.2 | 0.14 | 3 | 25 | 5 | 3.3 | 4 | 29858 | 10 | 22 | 0.05 | 23 |
| **08AE26-2.1** | 0.2 | 0.20 | 3 | 30 | 5 | 3.5 | 6 | 16328 | 7 | 22 | 0.17 | 37 |
| **4147-5.1** | 1.2 | 0.69 | 7 | 16 | 20 | 3.2 | 11 | 412 | 16 | 19 | 2.35 | 24 |
| **4147-4.1** | 0.8 | 0.47 | 2 | 25 | 20 | 3.6 | 12 | 11023 | 5 | 17 | 0.07 | 12 |
| **4147.11** | 2.5 | 1.46 | 28 | 1 | 3 | 2.4 | 1 | 2 | 119 | 10 | 232.1 | 152 |
| **4147-3.1** | 0.5 | 0.17 | 13 | 10 | 5 | 2.9 | 2 | 22315 | 29 | 19 | 0.01 | 8 |
| **4147-1.1** | 0.7 | 0.39 | 6 | 17 | 12 | 3.5 | 7 | 47989 | 36 | 54 | 0.01 | 13 |
| **4147.9** | 0.3 | 0.25 | 3 | 17 | 6 | 3.7 | 4 | 21382 | 10 | 24 | 0.04 | 17 |
| **4147-2.1** | 0.6 | 0.26 | 6 | 26 | 16 | 3.0 | 7 | 53987 | 33 | 51 | 0.01 | 9 |
| **4147.1** | 0.5 | 0.33 | 3 | 36 | 17 | 3.4 | 12 | 26784 | 10 | 30 | 0.07 | 21 |
| **4147-7.1** | 0.8 | 0.52 | 6 | 17 | 14 | 2.9 | 9 | 29749 | 15 | 18 | 0.08 | 53 |
| **4147-8.1** | 1.1 | 0.61 | 9 | 9 | 9 | 3.3 | 5 | 14712 | 25 | 20 | 0.02 | 15 |
| **4147-6.1** | 0.6 | 0.40 | 3 | 26 | 16 | 3.1 | 10 | 13335 | 16 | 34 | 0.04 | 8 |
| **3755.16** | 2.2 | 0.32 | 13 | 21 | 45 | 2.3 | 7 | 61267 | 23 | 19 | 0.01 | 8 |
| **3755.1** | 0.7 | 0.24 | 8 | 14 | 10 | 3.0 | 3 | 15554 | 26 | 28 | 0.06 | 23 |
| **3755.12** | 2.7 | 0.34 | 11 | 34 | 90 | 2.2 | 12 | 1382 | 21 | 22 | 0.98 | 16 |
| **3755.7** | 0.5 | 0.31 | 8 | 11 | 6 | 2.9 | 3 | 8429 | 17 | 15 | 0.06 | 17 |
| **3755.8** | 0.8 | 0.30 | 10 | 8 | 6 | 3.2 | 2 | 38 | 41 | 26 | 19.02 | 37 |
| **3755.11** | 0.8 | 0.42 | 6 | 13 | 10 | 3.3 | 5 | 4341 | 20 | 24 | 0.38 | 50 |
| **3755.15** | 0.6 | 0.61 | 7 | 10 | 6 | 3.4 | 6 | 18854 | 20 | 23 | 0.04 | 25 |
| **3755.3** | 1.3 | 1.59 | 9 | 8 | 11 | 2.5 | 13 | 166 | 14 | 9 | 10.48 | 81 |
| **3755.13** | 5.9 | 1.38 | 14 | 28 | 167 | 1.7 | 39 | 622 | 45 | 19 | 2.57 | 22 |
| **3755.14** | 0.5 | 0.30 | 4 | 36 | 18 | 3.0 | 11 | 38875 | 15 | 34 | 0.04 | 15 |
| **3755.1** | 0.6 | 0.48 | 5 | 15 | 10 | 3.2 | 7 | 1399 | 18 | 26 | 0.37 | 13 |
| **3755.17** | 0.1 | 0.08 | 3 | 32 | 4 | 2.7 | 3 | 54332 | 6 | 13 | 0.01 | 9 |
| **3755.6** | 2.2 | 1.34 | 20 | 11 | 23 | 2.4 | 14 | 18677 | 54 | 25 | 0.04 | 27 |
| **3755.4** | 0.8 | 0.30 | 17 | 12 | 9 | 2.6 | 4 | 18201 | 65 | 40 | 0.02 | 9 |
| **3755.2** | 0.7 | 0.39 | 11 | 12 | 8 | 2.6 | 4 | 19707 | 40 | 27 | 0.03 | 18 |
| **3755.9** | 2.1 | 0.23 | 6 | 36 | 75 | 2.0 | 8 | 1105 | 13 | 19 | 1.00 | 12 |
| **3755.5** | 1.0 | 0.34 | 5 | 29 | 28 | 2.8 | 10 | 2968 | 13 | 23 | 0.21 | 8 |
| **3763.4** | 0.6 | 0.36 | 8 | 11 | 7 | 3.2 | 4 | 21718 | 20 | 20 | 0.04 | 28 |
| **3763.3** | 0.5 | 0.29 | 12 | 8 | 4 | 2.8 | 2 | 15702 | 27 | 18 | 0.04 | 27 |
| **3763-7.1** | 0.6 | 0.33 | 14 | 3 | 2 | 3.3 | 1 | 7 | 58 | 18 | 80.89 | 78 |
| **3763.2** | 0.4 | 0.26 | 3 | 15 | 6 | 3.6 | 4 | 15512 | 13 | 25 | 0.04 | 16 |

## Table B2, cont.

| | Pr Calc Ch 0.121 | SmCh 0.2 | EuCh 0.0761 | GdCh 0.267 | Ho Ch 0.0755 | YbCh 0.221 | Yb/Dy Chon | Ce /Ce* | Hf ppm | Eu/Eu* |
|---|---|---|---|---|---|---|---|---|---|---|
| **07AE59-2.1** | 0.7 | 14 | 16 | 70 | 386 | 1372 | 3.56 | 84 | 8937 | 0.51 |
| **07AE59-15.1** | 0.1 | 5 | 4 | 37 | 221 | 627 | 2.83 | 218 | 8572 | 0.32 |
| **07AE59-13.1** | 0.3 | 5 | 5 | 39 | 240 | 757 | 3.16 | 98 | 8796 | 0.35 |
| **07AE59-11.1** | 0.3 | 25 | 17 | 137 | 679 | 1918 | 2.83 | 437 | 11117 | 0.28 |
| **07AE59-12.1** | 2.1 | 38 | 33 | 232 | 1213 | 3224 | 2.66 | 53 | 9433 | 0.35 |
| **07AE59-4.1** | 0.2 | 4 | 4 | 33 | 220 | 692 | 3.14 | 167 | 10329 | 0.36 |
| **07AE59-3.1** | 0.4 | 22 | 18 | 122 | 623 | 1640 | 2.63 | 148 | 9509 | 0.34 |
| **07AE59-1.1** | 0.6 | 23 | 19 | 144 | 674 | 1683 | 2.50 | 125 | 9761 | 0.33 |
| **07AE59-6.1** | 1.2 | 29 | 23 | 162 | 897 | 2385 | 2.66 | 50 | 9375 | 0.33 |
| **07AE59-9.1** | 0.3 | 21 | 17 | 118 | 584 | 1546 | 2.65 | 191 | 10462 | 0.33 |
| **07AE59-5.1** | 0.4 | 16 | 15 | 97 | 453 | 1219 | 2.69 | 143 | 10054 | 0.37 |
| **07AE59-8.1** | 1.5 | 52 | 42 | 335 | 1522 | 3522 | 2.31 | 89 | 10132 | 0.32 |
| **07AE59-10.1** | 0.7 | 20 | 20 | 131 | 670 | 1910 | 2.85 | 86 | 9757 | 0.39 |
| **07AE59-7.1** | 1.2 | 48 | 42 | 282 | 1330 | 3363 | 2.53 | 102 | 9454 | 0.36 |
| **07AE59-14.1** | 1.3 | 9 | 5 | 50 | 264 | 727 | 2.75 | 20 | 7407 | 0.25 |
| **07AE58-1.1** | 0.3 | 2 | 5 | 18 | 136 | 792 | 5.81 | 97 | 9065 | 0.69 |
| **07AE58-4.1** | 0.3 | 10 | 8 | 64 | 340 | 947 | 2.78 | 195 | 9219 | 0.32 |
| **07AE58-3.1** | 0.2 | 5 | 8 | 31 | 154 | 507 | 3.30 | 286 | 8966 | 0.66 |
| **07AE58-2.1** | 0.2 | 5 | 2 | 45 | 405 | 1641 | 4.05 | 224 | 9949 | 0.12 |
| **08AE26-3.1** | 1.1 | 34 | 31 | 311 | 1620 | 3459 | 2.13 | 129 | 7833 | 0.30 |
| **08AE26-9.1** | 10.4 | 25 | 36 | 66 | 140 | 473 | 3.39 | 5 | 7493 | 0.89 |
| **08AE26-8.1** | 0.2 | 6 | 11 | 42 | 194 | 570 | 2.94 | 256 | 8629 | 0.66 |
| **08AE26-4.1** | 1.0 | 5 | 8 | 30 | 150 | 538 | 3.59 | 21 | 8613 | 0.63 |
| **08AE26-5.1** | 0.2 | 5 | 9 | 30 | 263 | 1247 | 4.74 | 155 | 6883 | 0.71 |
| **08AE26-7.1** | 0.2 | 4 | 7 | 27 | 215 | 1098 | 5.12 | 278 | 8196 | 0.66 |
| **08AE26-6.1** | 15.4 | 53 | 41 | 219 | 656 | 1516 | 2.31 | 5 | 10581 | 0.38 |
| **08AE26-1.1** | 0.3 | 5 | 1 | 40 | 295 | 1029 | 3.49 | 78 | 12570 | 0.06 |
| **08AE26-2.2** | 0.6 | 29 | 25 | 161 | 842 | 2190 | 2.60 | 130 | 7695 | 0.37 |
| **08AE26-2.1** | 1.7 | 55 | 55 | 346 | 1656 | 4070 | 2.46 | 68 | 5824 | 0.40 |
| **4147-5.1** | 4.8 | 14 | 16 | 85 | 484 | 1397 | 2.88 | 7 | 6928 | 0.45 |
| **4147-4.1** | 0.7 | 25 | 25 | 124 | 474 | 1147 | 2.42 | 53 | 7620 | 0.46 |
| **4147.11** | 90.6 | 22 | 14 | 39 | 140 | 565 | 4.05 | 1 | 9533 | 0.47 |
| **4147-3.1** | 0.1 | 3 | 3 | 17 | 89 | 311 | 3.48 | 284 | 9223 | 0.48 |
| **4147-1.1** | 0.2 | 9 | 4 | 63 | 315 | 848 | 2.69 | 294 | 9000 | 0.18 |
| **4147.9** | 0.5 | 23 | 18 | 123 | 452 | 1090 | 2.41 | 132 | 8890 | 0.33 |
| **4147-2.1** | 0.1 | 6 | 3 | 44 | 289 | 878 | 3.04 | 233 | 9759 | 0.18 |
| **4147.1** | 0.8 | 31 | 23 | 193 | 1074 | 2824 | 2.63 | 87 | 8704 | 0.29 |
| **4147-7.1** | 0.9 | 34 | 38 | 195 | 1061 | 3441 | 3.24 | 198 | 8320 | 0.47 |
| **4147-8.1** | 0.2 | 7 | 6 | 36 | 171 | 487 | 2.84 | 209 | 8411 | 0.40 |
| **4147-6.1** | 0.4 | 10 | 6 | 55 | 265 | 785 | 2.96 | 67 | 7874 | 0.24 |
| **3755.16** | 0.1 | 2 | 4 | 19 | 135 | 597 | 4.42 | 352 | 10360 | 0.54 |
| **3755.1** | 0.5 | 11 | 10 | 75 | 409 | 1255 | 3.07 | 144 | 9337 | 0.33 |
| **3755.12** | 2.0 | 6 | 8 | 49 | 436 | 1959 | 4.49 | 11 | 10523 | 0.46 |
| **3755.7** | 0.4 | 9 | 11 | 45 | 210 | 675 | 3.22 | 112 | 8903 | 0.55 |
| **3755.8** | 17.3 | 15 | 10 | 72 | 371 | 1037 | 2.80 | 2 | 9198 | 0.30 |
| **3755.11** | 2.3 | 35 | 27 | 188 | 911 | 2354 | 2.58 | 53 | 9395 | 0.33 |
| **3755.15** | 0.4 | 16 | 13 | 87 | 365 | 973 | 2.67 | 209 | 9203 | 0.36 |
| **3755.3** | 17.7 | 39 | 64 | 157 | 668 | 2509 | 3.76 | 6 | 5999 | 0.82 |
| **3755.13** | 3.7 | 6 | 5 | 29 | 309 | 2309 | 7.46 | 7 | 10766 | 0.38 |
| **3755.14** | 0.4 | 16 | 11 | 109 | 679 | 1997 | 2.94 | 125 | 9700 | 0.27 |
| **3755.1** | 1.4 | 11 | 8 | 59 | 249 | 742 | 2.98 | 18 | 9120 | 0.31 |
| **3755.17** | 0.2 | 12 | 17 | 65 | 331 | 1131 | 3.42 | 170 | 8185 | 0.62 |
| **3755.6** | 0.3 | 6 | 5 | 39 | 274 | 1083 | 3.95 | 255 | 11036 | 0.37 |
| **3755.4** | 0.1 | 2 | 2 | 17 | 114 | 416 | 3.66 | 216 | 9830 | 0.24 |
| **3755.2** | 0.2 | 7 | 5 | 38 | 213 | 769 | 3.60 | 220 | 8784 | 0.30 |
| **3755.9** | 2.4 | 9 | 10 | 56 | 364 | 1599 | 4.39 | 8 | 11826 | 0.47 |
| **3755.5** | 0.8 | 7 | 7 | 44 | 271 | 884 | 3.26 | 20 | 8891 | 0.38 |
| **3763.4** | 0.4 | 15 | 15 | 85 | 401 | 1170 | 2.92 | 226 | 8674 | 0.42 |
| **3763.3** | 0.3 | 9 | 11 | 54 | 262 | 837 | 3.20 | 239 | 9934 | 0.47 |
| **3763-7.1** | 48.2 | 22 | 15 | 74 | 314 | 868 | 2.77 | 1 | 8276 | 0.36 |
| **3763.2** | 0.5 | 19 | 13 | 92 | 372 | 913 | 2.45 | 116 | 8812 | 0.31 |

**Table B2, cont.**

| | Pb7/6 | Pb8/6 | 206/238 | 208/248 | 254/238 | U238/Zr | ThO248/Zr | UO254/Zr |
|---|---|---|---|---|---|---|---|---|
| **3763-6.1** | 0.049275 | 0.216348 | 0.038633 | 0.002493 | 5.571125 | 0.102624 | 0.344022 | 0.571731 |
| **3763.5** | 0.053559 | 0.156215 | 0.047803 | 0.003040 | 5.294246 | 0.116243 | 0.285512 | 0.615420 |
| **3763.1** | 0.052051 | 0.145806 | 0.069150 | 0.004072 | 5.426460 | 0.729810 | 1.807252 | 3.960285 |
| **4145-7.1** | 0.049997 | 0.390602 | 0.011399 | 0.000742 | 4.993386 | 0.505556 | 3.035117 | 2.524437 |
| **4145-16.1** | 0.052826 | 0.218694 | 0.012009 | 0.000860 | 5.415903 | 0.365043 | 1.114695 | 1.977038 |
| **4145-24.1** | 0.056061 | 0.218182 | 0.012130 | 0.000784 | 5.362973 | 0.141621 | 0.477985 | 0.759508 |
| **4145-11.1** | 0.055501 | 0.226285 | 0.030349 | 0.002023 | 5.352527 | 0.084033 | 0.285327 | 0.449789 |
| **4145-8.1** | 0.051344 | 0.185711 | 0.031494 | 0.002017 | 5.291446 | 0.350942 | 1.017421 | 1.856988 |
| **4145-18.1** | 0.050054 | 0.180451 | 0.032346 | 0.001969 | 5.240407 | 0.187201 | 0.554883 | 0.981009 |
| **4145-21.1** | 0.047994 | 0.203564 | 0.032448 | 0.002006 | 5.134214 | 0.366275 | 1.206179 | 1.880534 |
| **4145-23.1** | 0.049456 | 0.235009 | 0.032512 | 0.002134 | 5.359567 | 0.178616 | 0.639428 | 0.957307 |
| **4145-12.1** | 0.049045 | 0.265184 | 0.033212 | 0.002326 | 5.457734 | 0.135122 | 0.511568 | 0.737460 |
| **4145-2.1** | 0.052902 | 0.138966 | 0.033304 | 0.002395 | 5.354318 | 0.096664 | 0.186770 | 0.517570 |
| **4145-13.1** | 0.049760 | 0.162286 | 0.033377 | 0.002068 | 5.528361 | 0.474264 | 1.242285 | 2.621905 |
| **4145-15.1** | 0.046851 | 0.132494 | 0.033508 | 0.002171 | 5.377741 | 0.160094 | 0.327382 | 0.860945 |
| **4145-29** | 0.053333 | 0.177778 | 0.033603 | 0.002167 | 5.456058 | 0.124011 | 0.341794 | 0.676613 |
| **4145-10.1** | 0.050029 | 0.204538 | 0.033690 | 0.002191 | 5.311744 | 0.526068 | 1.654321 | 2.794339 |
| **4145-22.1** | 0.048265 | 0.233571 | 0.034122 | 0.002106 | 5.369210 | 0.743831 | 2.814810 | 3.993784 |
| **4145-6.1** | 0.051226 | 0.133041 | 0.034209 | 0.002232 | 5.517731 | 0.172972 | 0.352725 | 0.954414 |
| **4145-9.1** | 0.050766 | 0.165457 | 0.034212 | 0.002028 | 5.439405 | 0.240770 | 0.671982 | 1.309645 |
| **4145-20.1** | 0.046683 | 0.220823 | 0.034354 | 0.002068 | 5.432765 | 0.268104 | 0.983548 | 1.456545 |
| **4145-4.1** | 0.051304 | 0.233810 | 0.034503 | 0.002291 | 5.315265 | 0.224585 | 0.790652 | 1.193728 |
| **4145-27** | 0.045709 | 0.247154 | 0.035431 | 0.002568 | 5.400457 | 0.142047 | 0.484454 | 0.767119 |
| **4145-3.1** | 0.046139 | 0.198175 | 0.035838 | 0.002650 | 4.318480 | 0.165246 | 0.442892 | 0.713611 |
| **4145-26** | 0.050310 | 0.188115 | 0.036064 | 0.002519 | 5.603313 | 0.106015 | 0.285519 | 0.594037 |
| **4145-28** | 0.048661 | 0.197531 | 0.038705 | 0.002394 | 5.492413 | 0.174191 | 0.556262 | 0.956729 |
| **4145-14.1** | 0.060900 | 0.255003 | 0.045353 | 0.003110 | 5.247760 | 0.153584 | 0.571198 | 0.805972 |
| **4145-1.1** | 0.049877 | 0.161029 | 0.048037 | 0.003114 | 5.387724 | 0.369724 | 0.918526 | 1.991971 |
| **4145-19.1** | 0.049710 | 0.216889 | 0.048421 | 0.003076 | 5.339210 | 0.183214 | 0.625584 | 0.978219 |
| **4145-5.1** | 0.048428 | 0.174678 | 0.048949 | 0.003058 | 5.364539 | 0.212997 | 0.595488 | 1.142631 |
| **4145-17.1** | 0.049778 | 0.286209 | 0.051651 | 0.003102 | 5.530891 | 0.782811 | 3.731124 | 4.329641 |
| **4145-25.1** | 0.050089 | 0.218901 | 0.052481 | 0.003250 | 5.515006 | 0.395116 | 1.396617 | 2.179065 |
| **3990-8.1** | 0.048858 | 0.038354 | 0.012495 | 0.000918 | 5.496150 | 1.333539 | 0.696315 | 7.329333 |
| **3990-11.1** | 0.047626 | 0.034637 | 0.012953 | 0.000821 | 5.616376 | 1.579415 | 0.863119 | 8.870590 |
| **3990-9.1** | 0.049428 | 0.031999 | 0.013013 | 0.000888 | 5.569850 | 1.284445 | 0.602081 | 7.154167 |
| **3990-24.1** | 0.059226 | 0.202733 | 0.013995 | 0.001034 | 5.593669 | 0.566178 | 1.552812 | 3.167010 |
| **3990-22.1** | 0.059367 | 0.069300 | 0.022571 | 0.001538 | 5.171808 | 0.078435 | 0.079755 | 0.405648 |
| **3990-5.1** | 0.049661 | 0.091318 | 0.025080 | 0.001678 | 5.325283 | 0.276991 | 0.378094 | 1.475056 |
| **3990-7.1** | 0.059726 | 0.219178 | 0.026174 | 0.001784 | 5.360181 | 0.104378 | 0.335609 | 0.559484 |
| **3990-19.1** | 0.049271 | 0.050118 | 0.029581 | 0.001758 | 5.334293 | 0.254132 | 0.214318 | 1.355615 |
| **3990-21.1** | 0.047177 | 0.105438 | 0.031182 | 0.001715 | 5.620197 | 0.445517 | 0.853983 | 2.503891 |
| **3990-13.1** | 0.049435 | 0.076361 | 0.031295 | 0.005693 | 5.495689 | 1.056354 | 0.443402 | 5.805391 |
| **3990-2.1** | 0.051955 | 0.137346 | 0.031428 | 0.001909 | 5.702727 | 0.372269 | 0.841813 | 2.122949 |
| **3990-10.1** | 0.048605 | 0.129592 | 0.034517 | 0.002114 | 5.476067 | 0.414591 | 0.877265 | 2.270329 |
| **3990-6.1** | 0.056560 | 0.319909 | 0.035666 | 0.001589 | 5.255814 | 0.791061 | 5.678876 | 4.157671 |
| **3990-1** | 0.047296 | 0.211240 | 0.036984 | 0.002363 | 5.517755 | 0.202977 | 0.671059 | 1.119977 |
| **3990-14.1** | 0.047600 | 0.146045 | 0.036995 | 0.002286 | 5.428074 | 0.196891 | 0.465256 | 1.068738 |
| **3990-3.1** | 0.044475 | 0.157136 | 0.037927 | 0.002507 | 5.358254 | 0.079526 | 0.189076 | 0.426120 |
| **3990-17.1** | 0.049071 | 0.129071 | 0.038140 | 0.002287 | 5.560684 | 0.452643 | 0.974108 | 2.517006 |
| **3990-20.1** | 0.051384 | 0.159142 | 0.038285 | 0.002256 | 5.977157 | 0.225940 | 0.610072 | 1.350477 |
| **3990-16.1** | 0.047963 | 0.149283 | 0.038326 | 0.002443 | 5.558653 | 0.380027 | 0.890191 | 2.112436 |
| **3990-23.1** | 0.048085 | 0.167062 | 0.038715 | 0.002214 | 5.583891 | 1.242416 | 3.629439 | 6.937514 |
| **3990-15.1** | 0.050900 | 0.148490 | 0.052274 | 0.003436 | 5.300473 | 0.380665 | 0.859904 | 2.017703 |
| **3990-18.1** | 0.039722 | 0.144492 | 0.058775 | 0.003374 | 5.398400 | 0.489785 | 1.232843 | 2.644053 |
| **3990-4.1** | 0.051457 | 0.200990 | 0.062369 | 0.003799 | 5.604082 | 0.685696 | 2.262556 | 3.842697 |
| **3990-12.1** | 0.114073 | 0.431173 | 0.668886 | 0.038671 | 5.591296 | 0.048393 | 0.360910 | 0.270580 |

**Table B2, cont.**

| | Y89/Zr | La139/Zr | Ce140/Zr | Sm147/Zr | Eu153/Zr | Gd155/Zr | HoO181/Zr | YbO188/Zr |
|---|---|---|---|---|---|---|---|---|
| **3763-6.1** | 16.610697 | 0.000138 | 0.133026 | 0.010481 | 0.013206 | 0.024602 | 0.233529 | 0.314991 |
| **3763.5** | 8.582027 | 0.000084 | 0.070377 | 0.003631 | 0.003750 | 0.010000 | 0.114564 | 0.164277 |
| **3763.1** | 35.025079 | 0.000142 | 0.109379 | 0.009922 | 0.007808 | 0.031183 | 0.482565 | 0.696902 |
| **4145-7.1** | 24.677879 | 0.000469 | 0.449701 | 0.027883 | 0.019236 | 0.055514 | 0.331410 | 0.324631 |
| **4145-16.1** | 25.270581 | 0.000315 | 0.153102 | 0.020099 | 0.012681 | 0.046250 | 0.358064 | 0.368728 |
| **4145-24.1** | 13.929597 | 0.000161 | 0.065343 | 0.012983 | 0.018897 | 0.025821 | 0.195050 | 0.218310 |
| **4145-11.1** | 14.326707 | 0.000111 | 0.097216 | 0.012258 | 0.012732 | 0.026945 | 0.202435 | 0.214260 |
| **4145-8.1** | 27.824770 | 0.000266 | 0.093725 | 0.020874 | 0.010451 | 0.045921 | 0.380878 | 0.389910 |
| **4145-18.1** | 11.385947 | 0.000068 | 0.101367 | 0.007357 | 0.004849 | 0.017639 | 0.154013 | 0.167947 |
| **4145-21.1** | 25.555295 | 0.000088 | 0.130661 | 0.020093 | 0.010052 | 0.046662 | 0.361070 | 0.346486 |
| **4145-23.1** | 22.682286 | 0.000174 | 0.127696 | 0.023946 | 0.013581 | 0.045740 | 0.319957 | 0.314908 |
| **4145-12.1** | 14.802701 | 0.000164 | 0.117911 | 0.010421 | 0.007872 | 0.024405 | 0.206206 | 0.210945 |
| **4145-2.1** | 7.698722 | 0.000102 | 0.048713 | 0.003213 | 0.002135 | 0.009527 | 0.103995 | 0.132780 |
| **4145-13.1** | 16.673335 | 0.000035 | 0.159749 | 0.005544 | 0.002702 | 0.020087 | 0.223258 | 0.280238 |
| **4145-15.1** | 15.187830 | 0.000135 | 0.099755 | 0.010043 | 0.008497 | 0.023134 | 0.203597 | 0.275105 |
| **4145-29** | 12.287839 | 0.000068 | 0.084830 | 0.006189 | 0.003829 | 0.017187 | 0.168954 | 0.197356 |
| **4145-10.1** | 27.324171 | 0.000144 | 0.133036 | 0.014085 | 0.009096 | 0.035770 | 0.369414 | 0.435877 |
| **4145-22.1** | 45.341063 | 0.000592 | 0.119665 | 0.024614 | 0.015187 | 0.055449 | 0.619199 | 0.691490 |
| **4145-6.1** | 12.059496 | 0.000016 | 0.072268 | 0.005134 | 0.003087 | 0.014227 | 0.167929 | 0.216991 |
| **4145-9.1** | 13.442541 | 0.000060 | 0.100042 | 0.005761 | 0.003737 | 0.017202 | 0.185534 | 0.219649 |
| **4145-20.1** | 26.579187 | 0.000074 | 0.096776 | 0.015252 | 0.010636 | 0.042476 | 0.377443 | 0.400785 |
| **4145-4.1** | 38.069925 | 0.000109 | 0.102688 | 0.020458 | 0.014848 | 0.051219 | 0.528902 | 0.585657 |
| **4145-27** | 16.955553 | 0.000044 | 0.086942 | 0.007529 | 0.005379 | 0.023841 | 0.229226 | 0.251387 |
| **4145-3.1** | 21.212183 | 0.000041 | 0.076975 | 0.010079 | 0.007567 | 0.029670 | 0.301363 | 0.334430 |
| **4145-26** | 9.305557 | 0.000045 | 0.076104 | 0.003735 | 0.002319 | 0.011418 | 0.125791 | 0.153746 |
| **4145-28** | 25.485526 | 0.000093 | 0.083879 | 0.013388 | 0.008026 | 0.035549 | 0.358972 | 0.395245 |
| **4145-14.1** | 16.132242 | 0.000283 | 0.114848 | 0.012339 | 0.013041 | 0.026216 | 0.220784 | 0.284792 |
| **4145-1.1** | 10.260484 | 0.000099 | 0.161506 | 0.005945 | 0.003918 | 0.014041 | 0.135022 | 0.174147 |
| **4145-19.1** | 17.829213 | 0.000042 | 0.065114 | 0.005713 | 0.005453 | 0.019818 | 0.239255 | 0.320914 |
| **4145-5.1** | 10.459484 | 0.000075 | 0.127027 | 0.006602 | 0.009244 | 0.016539 | 0.138471 | 0.179809 |
| **4145-17.1** | 33.407447 | 0.000981 | 0.246357 | 0.032195 | 0.039889 | 0.068248 | 0.468211 | 0.487251 |
| **4145-25.1** | 22.248011 | 0.000773 | 0.079220 | 0.022082 | 0.008261 | 0.043763 | 0.319693 | 0.331767 |
| **3990-8.1** | 20.538190 | 0.000456 | 0.109506 | 0.003949 | 0.006961 | 0.014642 | 0.250228 | 0.523440 |
| **3990-11.1** | 24.922140 | 0.000054 | 0.141871 | 0.004504 | 0.007723 | 0.018172 | 0.307800 | 0.652618 |
| **3990-9.1** | 15.897824 | 0.000054 | 0.071042 | 0.003191 | 0.005307 | 0.011139 | 0.197851 | 0.420108 |
| **3990-24.1** | 12.722258 | 0.000072 | 0.239080 | 0.004801 | 0.007220 | 0.014800 | 0.157678 | 0.280738 |
| **3990-22.1** | 1.802841 | 0.000069 | 0.020640 | 0.002022 | 0.002365 | 0.004397 | 0.022594 | 0.018854 |
| **3990-5.1** | 5.580507 | 0.000071 | 0.049500 | 0.007803 | 0.006302 | 0.016202 | 0.075364 | 0.058387 |
| **3990-7.1** | 3.772736 | 0.000096 | 0.127446 | 0.005772 | 0.012730 | 0.012107 | 0.047664 | 0.027556 |
| **3990-19.1** | 3.717701 | 0.000038 | 0.043268 | 0.003178 | 0.005297 | 0.009152 | 0.047341 | 0.062040 |
| **3990-21.1** | 17.819427 | 0.000049 | 0.274001 | 0.005848 | 0.011077 | 0.018186 | 0.229282 | 0.384397 |
| **3990-13.1** | 13.898797 | 0.000060 | 0.034573 | 0.004757 | 0.005210 | 0.018669 | 0.190818 | 0.184261 |
| **3990-2.1** | 10.031320 | 0.000072 | 0.236642 | 0.003755 | 0.007752 | 0.011339 | 0.130129 | 0.211016 |
| **3990-10.1** | 16.268192 | 0.000047 | 0.119272 | 0.005152 | 0.004170 | 0.017067 | 0.215974 | 0.327290 |
| **3990-6.1** | 5.920811 | 0.021757 | 0.118601 | 0.005964 | 0.011499 | 0.007880 | 0.077636 | 0.108087 |
| **3990-1** | 30.340771 | 0.000054 | 0.120480 | 0.014397 | 0.011573 | 0.042964 | 0.431380 | 0.481058 |
| **3990-14.1** | 16.961196 | 0.000053 | 0.128930 | 0.004976 | 0.003759 | 0.017340 | 0.228819 | 0.304607 |
| **3990-3.1** | 9.529290 | 0.000050 | 0.089698 | 0.004027 | 0.005183 | 0.009928 | 0.125314 | 0.203009 |
| **3990-17.1** | 18.408302 | 0.000042 | 0.084751 | 0.006825 | 0.007075 | 0.017444 | 0.235854 | 0.449371 |
| **3990-20.1** | 13.396401 | 0.000518 | 0.162845 | 0.009580 | 0.014085 | 0.021818 | 0.181435 | 0.245337 |
| **3990-16.1** | 18.999328 | 0.000019 | 0.113001 | 0.005342 | 0.005467 | 0.017596 | 0.251051 | 0.394065 |
| **3990-23.1** | 44.433266 | 0.000231 | 0.211463 | 0.013821 | 0.009155 | 0.046023 | 0.603467 | 0.864163 |
| **3990-15.1** | 10.892133 | 0.000052 | 0.130462 | 0.003918 | 0.003119 | 0.011961 | 0.142835 | 0.209290 |
| **3990-18.1** | 9.957147 | 0.000048 | 0.154370 | 0.003220 | 0.006309 | 0.009267 | 0.120987 | 0.252695 |
| **3990-4.1** | 29.221956 | 0.000414 | 0.129483 | 0.023040 | 0.007179 | 0.051923 | 0.412253 | 0.395336 |
| **3990-12.1** | 9.998127 | 0.000930 | 0.438684 | 0.023261 | 0.029246 | 0.034729 | 0.154292 | 0.118319 |

## Table B2, cont.

| | HfO196/Zr | 204/206 | 207/206 no 204cr | Age Est. 206/238 | Age Est. 208/232 | Th ppm | U ppm | Y ppm | La ppm | Ce ppm |
|---|---|---|---|---|---|---|---|---|---|---|
| **3763-6.1** | 10.887119 | 0.001391 | 0.049 | 128 | 133 | 54 | 85 | 749 | 0.01 | 17 |
| **3763.5** | 9.867142 | 0.000223 | 0.054 | 159 | 162 | 45 | 91 | 387 | 0.01 | 9 |
| **3763.1** | 8.040691 | 0.000050 | 0.052 | 230 | 217 | 285 | 587 | 1580 | 0.02 | 14 |
| **4145-7.1** | 12.257221 | 0.000839 | 0.050 | 38 | 39 | 479 | 374 | 1113 | 0.05 | 57 |
| **4145-16.1** | 10.236020 | 0.000899 | 0.053 | 40 | 46 | 176 | 293 | 1140 | 0.03 | 20 |
| **4145-24.1** | 8.016169 | 0.002273 | 0.056 | 40 | 42 | 75 | 113 | 628 | 0.02 | 8 |
| **4145-11.1** | 9.693444 | 0.001482 | 0.056 | 101 | 108 | 45 | 67 | 646 | 0.01 | 12 |
| **4145-8.1** | 9.900682 | 0.000328 | 0.051 | 105 | 107 | 161 | 275 | 1255 | 0.03 | 12 |
| **4145-18.1** | 10.043654 | 0.000430 | 0.050 | 108 | 105 | 88 | 145 | 513 | 0.01 | 13 |
| **4145-21.1** | 11.180244 | 0.000109 | 0.048 | 108 | 107 | 190 | 279 | 1153 | 0.01 | 17 |
| **4145-23.1** | 10.049632 | 0.000000 | 0.049 | 108 | 114 | 101 | 142 | 1023 | 0.02 | 16 |
| **4145-12.1** | 9.641692 | 0.000285 | 0.049 | 110 | 124 | 81 | 109 | 668 | 0.02 | 15 |
| **4145-2.1** | 10.870098 | 0.000000 | 0.053 | 111 | 127 | 29 | 77 | 347 | 0.01 | 6 |
| **4145-13.1** | 14.362455 | 0.000183 | 0.050 | 111 | 110 | 196 | 388 | 752 | 0.00 | 20 |
| **4145-15.1** | 9.299152 | 0.000504 | 0.047 | 111 | 115 | 52 | 128 | 685 | 0.01 | 13 |
| **4145-29** | 11.665398 | 0.001026 | 0.053 | 112 | 115 | 54 | 100 | 554 | 0.01 | 11 |
| **4145-10.1** | 10.392763 | 0.000279 | 0.050 | 112 | 117 | 261 | 414 | 1232 | 0.02 | 17 |
| **4145-22.1** | 9.489531 | 0.000258 | 0.048 | 113 | 112 | 444 | 592 | 2045 | 0.06 | 15 |
| **4145-6.1** | 11.135609 | 0.000220 | 0.051 | 114 | 119 | 56 | 141 | 544 | 0.00 | 9 |
| **4145-9.1** | 10.784373 | 0.000151 | 0.051 | 114 | 108 | 106 | 194 | 606 | 0.01 | 13 |
| **4145-20.1** | 10.835187 | 0.000461 | 0.047 | 114 | 110 | 155 | 216 | 1199 | 0.01 | 12 |
| **4145-4.1** | 9.279174 | 0.000336 | 0.051 | 115 | 122 | 125 | 177 | 1717 | 0.01 | 13 |
| **4145-27** | 10.911111 | 0.000542 | 0.046 | 118 | 137 | 76 | 114 | 765 | 0.00 | 11 |
| **4145-3.1** | 8.488863 | 0.000435 | 0.046 | 119 | 141 | 70 | 106 | 957 | 0.00 | 10 |
| **4145-26** | 11.822949 | 0.001823 | 0.050 | 120 | 134 | 45 | 88 | 420 | 0.00 | 10 |
| **4145-28** | 11.390806 | 0.000217 | 0.049 | 129 | 127 | 88 | 142 | 1149 | 0.01 | 11 |
| **4145-14.1** | 8.578775 | 0.000807 | 0.061 | 151 | 165 | 90 | 119 | 728 | 0.03 | 15 |
| **4145-1.1** | 10.813483 | 0.000000 | 0.050 | 160 | 166 | 145 | 295 | 463 | 0.01 | 21 |
| **4145-19.1** | 10.141995 | 0.000000 | 0.050 | 161 | 164 | 99 | 145 | 804 | 0.00 | 8 |
| **4145-5.1** | 9.765822 | 0.000241 | 0.048 | 163 | 163 | 94 | 169 | 472 | 0.01 | 16 |
| **4145-17.1** | 9.669901 | 0.000133 | 0.050 | 172 | 165 | 589 | 641 | 1507 | 0.11 | 31 |
| **4145-25.1** | 11.533664 | 0.000201 | 0.050 | 174 | 173 | 221 | 323 | 1003 | 0.08 | 10 |
| **3990-8.1** | 13.134001 | 0.000000 | 0.049 | 42 | 49 | 110 | 1086 | 926 | 0.05 | 14 |
| **3990-11.1** | 13.115550 | 0.000073 | 0.048 | 43 | 44 | 136 | 1314 | 1124 | 0.01 | 18 |
| **3990-9.1** | 12.717733 | 0.000268 | 0.049 | 43 | 47 | 95 | 1060 | 717 | 0.01 | 9 |
| **3990-24.1** | 13.866941 | 0.000000 | 0.059 | 47 | 55 | 245 | 469 | 574 | 0.01 | 31 |
| **3990-22.1** | 9.792840 | 0.000000 | 0.059 | 75 | 82 | 13 | 60 | 81 | 0.01 | 3 |
| **3990-5.1** | 10.738913 | 0.000857 | 0.050 | 83 | 89 | 60 | 219 | 252 | 0.01 | 6 |
| **3990-7.1** | 10.051484 | 0.001644 | 0.060 | 87 | 95 | 53 | 83 | 170 | 0.01 | 16 |
| **3990-19.1** | 8.788516 | 0.000726 | 0.049 | 98 | 94 | 34 | 201 | 168 | 0.00 | 6 |
| **3990-21.1** | 10.989923 | 0.000196 | 0.047 | 104 | 91 | 135 | 371 | 804 | 0.01 | 35 |
| **3990-13.1** | 13.793732 | 0.000000 | 0.049 | 104 | 303 | 70 | 860 | 627 | 0.01 | 4 |
| **3990-2.1** | 11.931679 | 0.000000 | 0.052 | 104 | 102 | 133 | 314 | 452 | 0.01 | 30 |
| **3990-10.1** | 12.066820 | 0.000204 | 0.049 | 115 | 112 | 139 | 336 | 734 | 0.01 | 15 |
| **3990-6.1** | 10.654871 | 0.000474 | 0.057 | 119 | 85 | 897 | 616 | 267 | 2.33 | 15 |
| **3990-1** | 11.216468 | 0.000199 | 0.047 | 123 | 126 | 106 | 166 | 1368 | 0.01 | 15 |
| **3990-14.1** | 11.933006 | 0.000609 | 0.048 | 123 | 122 | 73 | 158 | 765 | 0.01 | 16 |
| **3990-3.1** | 10.694584 | 0.000930 | 0.044 | 126 | 133 | 30 | 63 | 430 | 0.01 | 11 |
| **3990-17.1** | 11.035216 | 0.000086 | 0.049 | 127 | 122 | 154 | 373 | 830 | 0.00 | 11 |
| **3990-20.1** | 11.116127 | 0.000499 | 0.051 | 127 | 120 | 96 | 200 | 604 | 0.06 | 21 |
| **3990-16.1** | 11.103606 | 0.000108 | 0.048 | 127 | 130 | 141 | 313 | 857 | 0.00 | 14 |
| **3990-23.1** | 11.222732 | 0.000000 | 0.048 | 129 | 118 | 573 | 1028 | 2004 | 0.02 | 27 |
| **3990-15.1** | 12.135553 | 0.000000 | 0.051 | 174 | 183 | 136 | 299 | 491 | 0.01 | 17 |
| **3990-18.1** | 10.663745 | 0.000466 | 0.040 | 195 | 179 | 195 | 392 | 449 | 0.01 | 20 |
| **3990-4.1** | 12.074276 | 0.000149 | 0.051 | 207 | 202 | 357 | 569 | 1318 | 0.04 | 17 |
| **3990-12.1** | 9.380933 | 0.000097 | 0.114 | 2223 | 2057 | 57 | 40 | 451 | 0.10 | 56 |

**Table B2, cont.**

| | Sm ppm | Eu ppm | Gd ppm | Dy ppm | Yb ppm | Hf ppm | Th/U | Yb/Gd | U/Yb | Th/Yb | Ce/Sm |
|---|---|---|---|---|---|---|---|---|---|---|---|
| **3763-6.1** | 2.6 | 1.06 | 19 | 29 | 274 | 10198 | 0.64 | 14.1 | 0.3 | 0.20 | 6 |
| **3763.5** | 0.9 | 0.30 | 8 | 14 | 143 | 9243 | 0.49 | 18.1 | 0.6 | 0.32 | 10 |
| **3763.1** | 2.5 | 0.63 | 25 | 59 | 607 | 7532 | 0.49 | 24.6 | 1.0 | 0.47 | 6 |
| **4145-7.1** | 7.0 | 1.55 | 44 | 41 | 283 | 11482 | 1.28 | 6.4 | 1.3 | 1.70 | 8 |
| **4145-16.1** | 5.1 | 1.02 | 37 | 44 | 321 | 9588 | 0.60 | 8.8 | 0.9 | 0.55 | 4 |
| **4145-24.1** | 3.3 | 1.52 | 20 | 24 | 190 | 7509 | 0.67 | 9.3 | 0.6 | 0.40 | 3 |
| **4145-11.1** | 3.1 | 1.03 | 21 | 25 | 187 | 9080 | 0.68 | 8.8 | 0.4 | 0.24 | 4 |
| **4145-8.1** | 5.3 | 0.84 | 36 | 47 | 340 | 9274 | 0.58 | 9.4 | 0.8 | 0.47 | 2 |
| **4145-18.1** | 1.9 | 0.39 | 14 | 19 | 146 | 9408 | 0.60 | 10.5 | 1.0 | 0.60 | 7 |
| **4145-21.1** | 5.1 | 0.81 | 37 | 44 | 302 | 10473 | 0.68 | 8.2 | 0.9 | 0.63 | 3 |
| **4145-23.1** | 6.0 | 1.09 | 36 | 39 | 274 | 9414 | 0.71 | 7.6 | 0.5 | 0.37 | 3 |
| **4145-12.1** | 2.6 | 0.63 | 19 | 25 | 184 | 9032 | 0.74 | 9.5 | 0.6 | 0.44 | 6 |
| **4145-2.1** | 0.8 | 0.17 | 8 | 13 | 116 | 10182 | 0.38 | 15.4 | 0.7 | 0.26 | 8 |
| **4145-13.1** | 1.4 | 0.22 | 16 | 27 | 244 | 13454 | 0.51 | 15.4 | 1.6 | 0.80 | 15 |
| **4145-15.1** | 2.5 | 0.68 | 18 | 25 | 240 | 8711 | 0.41 | 13.1 | 0.5 | 0.22 | 5 |
| **4145-29** | 1.6 | 0.31 | 14 | 21 | 172 | 10927 | 0.54 | 12.7 | 0.6 | 0.31 | 7 |
| **4145-10.1** | 3.6 | 0.73 | 28 | 45 | 380 | 9735 | 0.63 | 13.4 | 1.1 | 0.69 | 5 |
| **4145-22.1** | 6.2 | 1.22 | 44 | 76 | 602 | 8889 | 0.75 | 13.7 | 1.0 | 0.74 | 2 |
| **4145-6.1** | 1.3 | 0.25 | 11 | 21 | 189 | 10431 | 0.39 | 16.8 | 0.7 | 0.29 | 7 |
| **4145-9.1** | 1.5 | 0.30 | 14 | 23 | 191 | 10102 | 0.55 | 14.1 | 1.0 | 0.55 | 9 |
| **4145-20.1** | 3.9 | 0.86 | 34 | 46 | 349 | 10150 | 0.72 | 10.4 | 0.6 | 0.45 | 3 |
| **4145-4.1** | 5.2 | 1.20 | 40 | 65 | 510 | 8692 | 0.71 | 12.6 | 0.3 | 0.24 | 3 |
| **4145-27** | 1.9 | 0.43 | 19 | 28 | 219 | 10221 | 0.67 | 11.6 | 0.5 | 0.35 | 6 |
| **4145-3.1** | 2.5 | 0.61 | 23 | 37 | 291 | 7952 | 0.66 | 12.4 | 0.4 | 0.24 | 4 |
| **4145-26** | 0.9 | 0.19 | 9 | 15 | 134 | 11075 | 0.51 | 14.8 | 0.7 | 0.34 | 10 |
| **4145-28** | 3.4 | 0.65 | 28 | 44 | 344 | 10670 | 0.62 | 12.3 | 0.4 | 0.26 | 3 |
| **4145-14.1** | 3.1 | 1.05 | 21 | 27 | 248 | 8036 | 0.76 | 12.0 | 0.5 | 0.36 | 5 |
| **4145-1.1** | 1.5 | 0.32 | 11 | 17 | 152 | 10129 | 0.49 | 13.7 | 1.9 | 0.96 | 14 |
| **4145-19.1** | 1.4 | 0.44 | 16 | 29 | 279 | 9500 | 0.68 | 17.8 | 0.5 | 0.35 | 6 |
| **4145-5.1** | 1.7 | 0.74 | 13 | 17 | 157 | 9148 | 0.56 | 12.0 | 1.1 | 0.60 | 10 |
| **4145-17.1** | 8.1 | 3.21 | 54 | 58 | 424 | 9058 | 0.92 | 7.9 | 1.5 | 1.39 | 4 |
| **4145-25.1** | 5.6 | 0.67 | 35 | 39 | 289 | 10804 | 0.68 | 8.4 | 1.1 | 0.76 | 2 |
| **3990-8.1** | 1.0 | 0.56 | 12 | 31 | 456 | 12303 | 0.10 | 39.4 | 2.4 | 0.24 | 14 |
| **3990-11.1** | 1.1 | 0.62 | 14 | 38 | 568 | 12286 | 0.10 | 39.6 | 2.3 | 0.24 | 16 |
| **3990-9.1** | 0.8 | 0.43 | 9 | 24 | 366 | 11913 | 0.09 | 41.6 | 2.9 | 0.26 | 11 |
| **3990-24.1** | 1.2 | 0.58 | 12 | 19 | 244 | 12990 | 0.52 | 20.9 | 1.9 | 1.00 | 25 |
| **3990-22.1** | 0.5 | 0.19 | 3 | 3 | 16 | 9173 | 0.21 | 4.7 | 3.7 | 0.77 | 5 |
| **3990-5.1** | 2.0 | 0.51 | 13 | 9 | 51 | 10059 | 0.27 | 4.0 | 4.3 | 1.17 | 3 |
| **3990-7.1** | 1.5 | 1.03 | 10 | 6 | 24 | 9415 | 0.64 | 2.5 | 3.5 | 2.21 | 11 |
| **3990-19.1** | 0.8 | 0.43 | 7 | 6 | 54 | 8232 | 0.17 | 7.5 | 3.7 | 0.63 | 7 |
| **3990-21.1** | 1.5 | 0.89 | 14 | 28 | 335 | 10295 | 0.36 | 23.3 | 1.1 | 0.40 | 24 |
| **3990-13.1** | 1.2 | 0.42 | 15 | 23 | 160 | 12921 | 0.08 | 10.9 | 5.4 | 0.44 | 4 |
| **3990-2.1** | 0.9 | 0.62 | 9 | 16 | 184 | 11177 | 0.42 | 20.5 | 1.7 | 0.72 | 32 |
| **3990-10.1** | 1.3 | 0.34 | 13 | 27 | 285 | 11303 | 0.41 | 21.1 | 1.2 | 0.49 | 12 |
| **3990-6.1** | 1.5 | 0.93 | 6 | 10 | 94 | 9981 | 1.46 | 15.1 | 6.5 | 9.53 | 10 |
| **3990-1** | 3.6 | 0.93 | 34 | 53 | 419 | 10507 | 0.64 | 12.3 | 0.4 | 0.25 | 4 |
| **3990-14.1** | 1.3 | 0.30 | 14 | 28 | 265 | 11178 | 0.46 | 19.4 | 0.6 | 0.28 | 13 |
| **3990-3.1** | 1.0 | 0.42 | 8 | 15 | 177 | 10018 | 0.47 | 22.5 | 0.4 | 0.17 | 11 |
| **3990-17.1** | 1.7 | 0.57 | 14 | 29 | 391 | 10337 | 0.41 | 28.4 | 1.0 | 0.39 | 6 |
| **3990-20.1** | 2.4 | 1.13 | 17 | 22 | 214 | 10413 | 0.48 | 12.4 | 0.9 | 0.45 | 9 |
| **3990-16.1** | 1.3 | 0.44 | 14 | 31 | 343 | 10401 | 0.45 | 24.7 | 0.9 | 0.41 | 11 |
| **3990-23.1** | 3.5 | 0.74 | 36 | 74 | 752 | 10513 | 0.56 | 20.7 | 1.4 | 0.76 | 8 |
| **3990-15.1** | 1.0 | 0.25 | 9 | 18 | 182 | 11368 | 0.45 | 19.3 | 1.6 | 0.75 | 17 |
| **3990-18.1** | 0.8 | 0.51 | 7 | 15 | 220 | 9989 | 0.50 | 30.0 | 1.8 | 0.88 | 24 |
| **3990-4.1** | 5.8 | 0.58 | 41 | 51 | 344 | 11310 | 0.63 | 8.4 | 1.7 | 1.04 | 3 |
| **3990-12.1** | 5.9 | 2.36 | 27 | 19 | 103 | 8787 | 1.42 | 3.8 | 0.4 | 0.55 | 10 |

## Table B2, cont.

| | Yb/Ce | U/Ce | Y/Yb | Th/Ce | Yb/La | Ce/Eu | Gd/Eu | La Ch 0.319 | Ce Ch 0.82 | Pr Calc Ch 0.121 | Sm Ch 0.2 |
|---|---|---|---|---|---|---|---|---|---|---|---|
| **3763-6.1** | 16 | 5 | 2.7 | 3 | 18544 | 16 | 18 | 0.05 | 21 | 0.4 | 13 |
| **3763.5** | 16 | 10 | 2.7 | 5 | 15816 | 30 | 26 | 0.03 | 11 | 0.2 | 5 |
| **3763.1** | 43 | 42 | 2.6 | 20 | 39956 | 22 | 39 | 0.05 | 17 | 0.4 | 13 |
| **4145-7.1** | 5 | 7 | 3.9 | 8 | 5619 | 37 | 28 | 0.16 | 70 | 1.4 | 35 |
| **4145-16.1** | 16 | 15 | 3.5 | 9 | 9497 | 19 | 36 | 0.11 | 24 | 0.9 | 25 |
| **4145-24.1** | 23 | 13 | 3.3 | 9 | 10983 | 5 | 13 | 0.05 | 10 | 0.5 | 16 |
| **4145-11.1** | 15 | 5 | 3.5 | 4 | 15687 | 12 | 21 | 0.04 | 15 | 0.4 | 15 |
| **4145-8.1** | 28 | 23 | 3.7 | 13 | 11917 | 14 | 43 | 0.09 | 15 | 0.9 | 26 |
| **4145-18.1** | 11 | 11 | 3.5 | 7 | 20158 | 33 | 36 | 0.02 | 16 | 0.3 | 9 |
| **4145-21.1** | 18 | 17 | 3.8 | 11 | 31838 | 21 | 46 | 0.03 | 20 | 0.4 | 25 |
| **4145-23.1** | 17 | 9 | 3.7 | 6 | 14684 | 15 | 33 | 0.06 | 20 | 0.7 | 30 |
| **4145-12.1** | 12 | 7 | 3.6 | 5 | 10456 | 24 | 30 | 0.06 | 18 | 0.5 | 13 |
| **4145-2.1** | 19 | 12 | 3.0 | 5 | 10602 | 36 | 44 | 0.03 | 8 | 0.2 | 4 |
| **4145-13.1** | 12 | 19 | 3.1 | 10 | 65390 | 94 | 73 | 0.01 | 25 | 0.2 | 7 |
| **4145-15.1** | 19 | 10 | 2.9 | 4 | 16529 | 19 | 27 | 0.05 | 16 | 0.4 | 13 |
| **4145-29** | 16 | 9 | 3.2 | 5 | 23430 | 35 | 44 | 0.02 | 13 | 0.2 | 8 |
| **4145-10.1** | 22 | 24 | 3.2 | 15 | 24657 | 23 | 39 | 0.05 | 21 | 0.5 | 18 |
| **4145-22.1** | 39 | 39 | 3.4 | 29 | 9487 | 12 | 36 | 0.20 | 19 | 1.5 | 31 |
| **4145-6.1** | 20 | 15 | 2.9 | 6 | 113012 | 37 | 45 | 0.01 | 11 | 0.1 | 6 |
| **4145-9.1** | 15 | 15 | 3.2 | 8 | 29821 | 42 | 45 | 0.02 | 16 | 0.2 | 7 |
| **4145-20.1** | 28 | 17 | 3.4 | 13 | 44242 | 14 | 39 | 0.02 | 15 | 0.4 | 19 |
| **4145-4.1** | 39 | 13 | 3.4 | 10 | 43428 | 11 | 34 | 0.04 | 16 | 0.5 | 26 |
| **4145-27** | 20 | 10 | 3.5 | 7 | 46761 | 26 | 43 | 0.01 | 14 | 0.2 | 10 |
| **4145-3.1** | 30 | 11 | 3.3 | 7 | 65934 | 16 | 38 | 0.01 | 12 | 0.2 | 13 |
| **4145-26** | 14 | 9 | 3.1 | 5 | 27985 | 52 | 48 | 0.01 | 12 | 0.1 | 5 |
| **4145-28** | 32 | 13 | 3.3 | 8 | 34335 | 17 | 43 | 0.03 | 13 | 0.4 | 17 |
| **4145-14.1** | 17 | 8 | 2.9 | 6 | 8161 | 14 | 20 | 0.10 | 18 | 0.7 | 16 |
| **4145-1.1** | 7 | 14 | 3.1 | 7 | 14245 | 65 | 35 | 0.03 | 25 | 0.3 | 8 |
| **4145-19.1** | 34 | 17 | 2.9 | 12 | 62710 | 19 | 36 | 0.01 | 10 | 0.2 | 7 |
| **4145-5.1** | 10 | 10 | 3.0 | 6 | 19371 | 22 | 18 | 0.03 | 20 | 0.3 | 8 |
| **4145-17.1** | 13 | 20 | 3.6 | 19 | 4034 | 10 | 17 | 0.33 | 38 | 2.3 | 41 |
| **4145-25.1** | 29 | 32 | 3.5 | 22 | 3486 | 15 | 52 | 0.26 | 12 | 1.7 | 28 |
| **3990-8.1** | 33 | 78 | 2.0 | 8 | 9318 | 25 | 21 | 0.15 | 17 | 0.6 | 5 |
| **3990-11.1** | 31 | 72 | 2.0 | 8 | 98030 | 29 | 23 | 0.02 | 22 | 0.2 | 6 |
| **3990-9.1** | 40 | 117 | 2.0 | 10 | 63416 | 21 | 21 | 0.02 | 11 | 0.2 | 4 |
| **3990-24.1** | 8 | 15 | 2.3 | 8 | 31569 | 53 | 20 | 0.02 | 37 | 0.2 | 6 |
| **3990-22.1** | 6 | 23 | 5.0 | 5 | 2228 | 14 | 18 | 0.02 | 3 | 0.2 | 3 |
| **3990-5.1** | 8 | 35 | 5.0 | 9 | 6632 | 12 | 25 | 0.02 | 8 | 0.3 | 10 |
| **3990-7.1** | 1 | 5 | 7.1 | 3 | 2335 | 16 | 9 | 0.03 | 20 | 0.3 | 7 |
| **3990-19.1** | 10 | 36 | 3.1 | 6 | 13178 | 13 | 17 | 0.01 | 7 | 0.1 | 4 |
| **3990-21.1** | 10 | 11 | 2.4 | 4 | 63800 | 39 | 16 | 0.02 | 43 | 0.2 | 7 |
| **3990-13.1** | 36 | 195 | 3.9 | 16 | 25096 | 11 | 35 | 0.02 | 5 | 0.2 | 6 |
| **3990-2.1** | 6 | 10 | 2.5 | 4 | 23721 | 48 | 14 | 0.02 | 37 | 0.2 | 5 |
| **3990-10.1** | 19 | 22 | 2.6 | 9 | 56865 | 45 | 40 | 0.02 | 19 | 0.2 | 7 |
| **3990-6.1** | 6 | 41 | 2.8 | 59 | 40 | 16 | 7 | 7.32 | 18 | 7.4 | 8 |
| **3990-1** | 27 | 11 | 3.3 | 7 | 72519 | 17 | 36 | 0.02 | 19 | 0.3 | 18 |
| **3990-14.1** | 16 | 10 | 2.9 | 4 | 46495 | 54 | 45 | 0.02 | 20 | 0.2 | 6 |
| **3990-3.1** | 15 | 6 | 2.4 | 3 | 32650 | 27 | 19 | 0.02 | 14 | 0.2 | 5 |
| **3990-17.1** | 36 | 34 | 2.1 | 14 | 87361 | 19 | 24 | 0.01 | 13 | 0.2 | 9 |
| **3990-20.1** | 10 | 10 | 2.8 | 5 | 3846 | 18 | 15 | 0.17 | 25 | 0.9 | 12 |
| **3990-16.1** | 24 | 22 | 2.5 | 10 | 169701 | 33 | 32 | 0.01 | 18 | 0.1 | 7 |
| **3990-23.1** | 28 | 38 | 2.7 | 21 | 30379 | 37 | 49 | 0.08 | 33 | 0.7 | 17 |
| **3990-15.1** | 11 | 18 | 2.7 | 8 | 32958 | 66 | 38 | 0.02 | 20 | 0.2 | 5 |
| **3990-18.1** | 11 | 20 | 2.0 | 10 | 43002 | 39 | 14 | 0.02 | 24 | 0.1 | 4 |
| **3990-4.1** | 21 | 34 | 3.8 | 22 | 7758 | 29 | 71 | 0.14 | 20 | 1.2 | 29 |
| **3990-12.1** | 2 | 1 | 4.4 | 1 | 1032 | 24 | 12 | 0.31 | 68 | 1.9 | 29 |

**Table B2, cont.**

| | Eu Ch 0.0761 | Gd Ch 0.267 | Ho Ch 0.0755 | Yb Ch 0.221 | Yb/Dy Chon | Ce/Ce* | Hf ppm | Eu/Eu* |
|---|---|---|---|---|---|---|---|---|
| **3763-6.1** | 14 | 73 | 381 | 1241 | 3.26 | 144 | 10198 | 0.45 |
| **3763.5** | 4 | 30 | 187 | 647 | 3.47 | 140 | 9243 | 0.34 |
| **3763.1** | 8 | 92 | 787 | 2746 | 3.49 | 117 | 7532 | 0.24 |
| **4145-7.1** | 20 | 164 | 540 | 1279 | 2.37 | 151 | 11482 | 0.27 |
| **4145-16.1** | 13 | 137 | 584 | 1453 | 2.49 | 75 | 9588 | 0.23 |
| **4145-24.1** | 20 | 76 | 318 | 860 | 2.71 | 60 | 7509 | 0.57 |
| **4145-11.1** | 13 | 80 | 330 | 844 | 2.56 | 122 | 9080 | 0.38 |
| **4145-8.1** | 11 | 136 | 621 | 1536 | 2.47 | 52 | 9274 | 0.18 |
| **4145-18.1** | 5 | 52 | 251 | 662 | 2.64 | 209 | 9408 | 0.23 |
| **4145-21.1** | 11 | 138 | 589 | 1365 | 2.32 | 178 | 10473 | 0.18 |
| **4145-23.1** | 14 | 135 | 522 | 1241 | 2.38 | 97 | 9414 | 0.22 |
| **4145-12.1** | 8 | 72 | 336 | 831 | 2.47 | 112 | 9032 | 0.27 |
| **4145-2.1** | 2 | 28 | 170 | 523 | 3.09 | 85 | 10182 | 0.21 |
| **4145-13.1** | 3 | 59 | 364 | 1104 | 3.03 | 592 | 13454 | 0.14 |
| **4145-15.1** | 9 | 68 | 332 | 1084 | 3.27 | 111 | 8711 | 0.31 |
| **4145-29** | 4 | 51 | 275 | 778 | 2.82 | 179 | 10927 | 0.20 |
| **4145-10.1** | 10 | 106 | 602 | 1717 | 2.85 | 132 | 9735 | 0.22 |
| **4145-22.1** | 16 | 164 | 1009 | 2725 | 2.70 | 34 | 8889 | 0.23 |
| **4145-6.1** | 3 | 42 | 274 | 855 | 3.12 | 517 | 10431 | 0.20 |
| **4145-9.1** | 4 | 51 | 302 | 865 | 2.86 | 239 | 10102 | 0.21 |
| **4145-20.1** | 11 | 126 | 615 | 1579 | 2.57 | 161 | 10150 | 0.23 |
| **4145-4.1** | 16 | 152 | 862 | 2308 | 2.68 | 117 | 8692 | 0.25 |
| **4145-27** | 6 | 71 | 374 | 991 | 2.65 | 253 | 10221 | 0.22 |
| **4145-3.1** | 8 | 88 | 491 | 1318 | 2.68 | 221 | 7952 | 0.24 |
| **4145-26** | 2 | 34 | 205 | 606 | 2.95 | 250 | 11075 | 0.19 |
| **4145-28** | 8 | 105 | 585 | 1557 | 2.66 | 118 | 10670 | 0.20 |
| **4145-14.1** | 14 | 78 | 360 | 1122 | 3.12 | 68 | 8036 | 0.40 |
| **4145-1.1** | 4 | 42 | 220 | 686 | 3.12 | 255 | 10129 | 0.23 |
| **4145-19.1** | 6 | 59 | 390 | 1264 | 3.24 | 208 | 9500 | 0.28 |
| **4145-5.1** | 10 | 49 | 226 | 708 | 3.14 | 245 | 9148 | 0.48 |
| **4145-17.1** | 42 | 202 | 763 | 1920 | 2.52 | 44 | 9058 | 0.47 |
| **4145-25.1** | 9 | 130 | 521 | 1307 | 2.51 | 19 | 10804 | 0.15 |
| **3990-8.1** | 7 | 43 | 408 | 2062 | 5.06 | 55 | 12303 | 0.50 |
| **3990-11.1** | 8 | 54 | 502 | 2571 | 5.13 | 385 | 12286 | 0.47 |
| **3990-9.1** | 6 | 33 | 323 | 1655 | 5.13 | 208 | 11913 | 0.49 |
| **3990-24.1** | 8 | 44 | 257 | 1106 | 4.30 | 509 | 12990 | 0.47 |
| **3990-22.1** | 3 | 13 | 37 | 74 | 2.02 | 54 | 9173 | 0.43 |
| **3990-5.1** | 7 | 48 | 123 | 230 | 1.87 | 96 | 10059 | 0.31 |
| **3990-7.1** | 13 | 36 | 78 | 109 | 1.40 | 208 | 9415 | 0.83 |
| **3990-19.1** | 6 | 27 | 77 | 244 | 3.17 | 166 | 8232 | 0.54 |
| **3990-21.1** | 12 | 54 | 374 | 1515 | 4.05 | 765 | 10295 | 0.59 |
| **3990-13.1** | 6 | 55 | 311 | 726 | 2.33 | 86 | 12921 | 0.30 |
| **3990-2.1** | 8 | 34 | 212 | 831 | 3.92 | 529 | 11177 | 0.65 |
| **3990-10.1** | 4 | 51 | 352 | 1290 | 3.66 | 354 | 11303 | 0.24 |
| **3990-6.1** | 12 | 23 | 127 | 426 | 3.37 | 3 | 9981 | 0.92 |
| **3990-1** | 12 | 127 | 703 | 1895 | 2.70 | 260 | 10507 | 0.25 |
| **3990-14.1** | 4 | 51 | 373 | 1200 | 3.22 | 348 | 11178 | 0.22 |
| **3990-3.1** | 5 | 29 | 204 | 800 | 3.92 | 263 | 10018 | 0.45 |
| **3990-17.1** | 7 | 52 | 384 | 1771 | 4.61 | 260 | 10337 | 0.36 |
| **3990-20.1** | 15 | 65 | 296 | 967 | 3.27 | 62 | 10413 | 0.53 |
| **3990-16.1** | 6 | 52 | 409 | 1553 | 3.79 | 689 | 10401 | 0.31 |
| **3990-23.1** | 10 | 136 | 984 | 3405 | 3.46 | 144 | 10513 | 0.20 |
| **3990-15.1** | 3 | 35 | 233 | 825 | 3.54 | 378 | 11368 | 0.25 |
| **3990-18.1** | 7 | 27 | 197 | 996 | 5.05 | 496 | 9989 | 0.63 |
| **3990-4.1** | 8 | 154 | 672 | 1558 | 2.32 | 50 | 11310 | 0.11 |
| **3990-12.1** | 31 | 103 | 252 | 466 | 1.85 | 88 | 8787 | 0.56 |

## Table B3.

| Analysis | U (ppm) | Isotopic ratios $^{206}Pb/^{204}Pb$ | U/Th | $^{207}Pb^*/^{235}U$ | ± (%) | $^{206}Pb^*/^{238}U$ | ± (%) | error corr. |
|---|---|---|---|---|---|---|---|---|
| WELL-17 | 127 | 27 | 1.1 | -0.03856 | 146.2 | 0.00270 | 13.4 | 0.09 |
| WELL-32 | 645 | 60 | 0.9 | -0.11335 | 244.1 | 0.00442 | 16.3 | 0.07 |
| WELL-33 | 274 | 76 | 1.0 | -0.05228 | 125.6 | 0.00534 | 6.1 | 0.05 |
| WELL-20 | 303 | 90 | 2.0 | -0.05152 | 134.9 | 0.00534 | 7.3 | 0.05 |
| WELL-18 | 170 | 453 | 1.2 | 0.05080 | 13.9 | 0.00549 | 2.9 | 0.21 |
| WELL-14 | 650 | 207 | 0.5 | -0.00399 | 120.8 | 0.00560 | 5.5 | 0.05 |
| WELL-26 | 269 | 132 | 1.1 | -0.00316 | 115.8 | 0.00567 | 6.1 | 0.05 |
| WELL-11 | 157 | 221 | 0.9 | 0.02856 | 43.4 | 0.00570 | 5.0 | 0.12 |
| WELL-12 | 197 | 563 | 1.0 | 0.04623 | 16.2 | 0.00587 | 3.5 | 0.22 |
| WELL-4 | 380 | 671 | 1.3 | 0.03310 | 15.4 | 0.00588 | 3.6 | 0.23 |
| WELL-6 | 617 | 413 | 0.8 | 0.02816 | 27.7 | 0.00589 | 3.9 | 0.14 |
| WELL-19 | 550 | 545 | 0.8 | 0.03240 | 17.0 | 0.00590 | 2.5 | 0.15 |
| WELL-9 | 285 | 735 | 0.8 | 0.04039 | 14.2 | 0.00591 | 4.3 | 0.30 |
| WELL-7 | 1194 | 1363 | 0.4 | 0.03619 | 7.8 | 0.00602 | 2.6 | 0.34 |
| WELL-23 | 1159 | 1717 | 4.2 | 0.03849 | 8.1 | 0.00604 | 1.8 | 0.22 |
| WELL-15 | 370 | 1153 | 1.6 | 0.04289 | 8.8 | 0.00604 | 2.3 | 0.26 |
| WELL-30 | 338 | 206 | 0.5 | 0.00365 | 94.0 | 0.00619 | 13.1 | 0.14 |
| WELL-3 | 1769 | 1470 | 2.5 | 0.04394 | 38.4 | 0.00635 | 3.7 | 0.10 |
| WELL-29 | 520 | 435 | 1.4 | 0.03924 | 13.4 | 0.00679 | 5.4 | 0.41 |
| WELL-27 | 1027 | 3265 | 4.5 | 0.08196 | 6.1 | 0.01213 | 3.7 | 0.61 |
| WELL-37 | 379 | 689 | 1.3 | 0.07944 | 18.0 | 0.01325 | 5.9 | 0.33 |
| WELL-1 | 280 | 1504 | 1.3 | 0.09821 | 7.3 | 0.01498 | 2.4 | 0.32 |
| WELL-35 | 720 | 2075 | 1.0 | 0.10121 | 7.6 | 0.01622 | 3.9 | 0.51 |
| WELL-34 | 119 | 509 | 0.9 | 0.09797 | 17.9 | 0.01684 | 2.6 | 0.15 |
| WELL-5 | 1188 | 5623 | 0.7 | 0.11263 | 9.2 | 0.01708 | 2.8 | 0.31 |
| WELL-16 | 1995 | 3555 | 0.7 | 0.11827 | 2.6 | 0.01793 | 1.0 | 0.39 |
| WELL-2 | 301 | 3960 | 1.1 | 0.17245 | 4.8 | 0.02447 | 2.1 | 0.45 |
| WELL-25 | 1886 | 4443 | 1.1 | 0.16834 | 4.0 | 0.02514 | 2.8 | 0.72 |
| WELL-21 | 547 | 4159 | 0.8 | 0.18806 | 2.9 | 0.02798 | 1.5 | 0.51 |
| WELL-8 | 256 | 4286 | 2.4 | 1.68106 | 5.0 | 0.16878 | 2.2 | 0.45 |
| WELL-13 | 212 | 33860 | 0.7 | 4.67352 | 2.1 | 0.30719 | 1.2 | 0.56 |
| WELL-31 | 41 | 4164 | 0.6 | 4.79007 | 2.2 | 0.31461 | 1.0 | 0.47 |
| WELL-24 | 282 | 12212 | 2.0 | 1.73326 | 5.6 | 0.11334 | 5.3 | 0.95 |

All uncertainties are reported at the 1-sigma level, and include only measurement errors. Systematic errors would increase age uncertainties by 1-2%.

U concentration and U/Th are calibrated relative to NIST SRM 610 and are accurate to ~20%. Common Pb correction is from 204Pb, with composition interpreted from Stacey and Kramers (1975) and uncertainties of 1.0 for 206Pb/ 204Pb, 0.3 for 207Pb/ 204Pb, and 2.0 for 208Pb/ 204Pb. U/Pb and 206Pb/207Pb fractionation is calibrated relative to fragments of a large Sri Lanka zircon of 564 ± 4 Ma (2-sigma).

U decay constants and composition as follows: 238U = 9.8485 x 10 -10, 235U = 1.55125 x 10 -10, 238U/ 235U = 137.88

**Table B3, cont.**

| | Apparent ages (Ma) | | | | | | | |
|---|---|---|---|---|---|---|---|---|
| **Analysis** | $^{206}Pb^*/^{238}U$ | ± (Ma) | $^{207}Pb^*/^{235}U$ | ± (Ma) | $^{206}Pb^*/^{207}Pb^*$ | ± (Ma) | **Best age (Ma)** | **± (Ma)** |
| WELL-17 | 17.4 | 2.3 | -39.9 | -59.6 | 0.0 | 1515.1 | 17.4 | 2.3 |
| WELL-32 | 28.4 | 4.6 | -122.2 | -327.8 | 0.0 | 1046.4 | 28.4 | 4.6 |
| WELL-33 | 34.3 | 2.1 | -54.5 | -70.4 | 0.0 | 1680.2 | 34.3 | 2.1 |
| WELL-20 | 34.4 | 2.5 | -53.7 | -74.5 | 0.0 | 1419.5 | 34.4 | 2.5 |
| WELL-18 | 35.3 | 1.0 | 50.3 | 6.8 | 841.0 | 284.5 | 35.3 | 1.0 |
| WELL-14 | 36.0 | 2.0 | -4.1 | -4.9 | 0.0 | 881.8 | 36.0 | 2.0 |
| WELL-26 | 36.4 | 2.2 | -3.2 | -3.7 | 0.0 | 820.9 | 36.4 | 2.2 |
| WELL-11 | 36.6 | 1.8 | 28.6 | 12.2 | -603.3 | 1219.7 | 36.6 | 1.8 |
| WELL-12 | 37.7 | 1.3 | 45.9 | 7.3 | 495.7 | 350.4 | 37.7 | 1.3 |
| WELL-4 | 37.8 | 1.3 | 33.1 | 5.0 | -297.4 | 384.7 | 37.8 | 1.3 |
| WELL-6 | 37.9 | 1.5 | 28.2 | 7.7 | -736.1 | 779.8 | 37.9 | 1.5 |
| WELL-19 | 37.9 | 0.9 | 32.4 | 5.4 | -361.4 | 438.5 | 37.9 | 0.9 |
| WELL-9 | 38.0 | 1.6 | 40.2 | 5.6 | 172.9 | 317.3 | 38.0 | 1.6 |
| WELL-7 | 38.7 | 1.0 | 36.1 | 2.8 | -134.2 | 183.0 | 38.7 | 1.0 |
| WELL-23 | 38.8 | 0.7 | 38.4 | 3.0 | 8.5 | 189.2 | 38.8 | 0.7 |
| WELL-15 | 38.8 | 0.9 | 42.6 | 3.7 | 261.9 | 195.5 | 38.8 | 0.9 |
| WELL-30 | 39.8 | 5.2 | 3.7 | 3.5 | 0.0 | 337.3 | 39.8 | 5.2 |
| WELL-3 | 40.8 | 1.5 | 43.7 | 16.4 | 204.0 | 916.9 | 40.8 | 1.5 |
| WELL-29 | 43.6 | 2.4 | 39.1 | 5.1 | -230.8 | 310.2 | 43.6 | 2.4 |
| WELL-27 | 77.7 | 2.9 | 80.0 | 4.7 | 148.5 | 112.6 | 77.7 | 2.9 |
| WELL-37 | 84.8 | 5.0 | 77.6 | 13.4 | -139.0 | 422.8 | 84.8 | 5.0 |
| WELL-1 | 95.8 | 2.2 | 95.1 | 6.7 | 77.4 | 164.9 | 95.8 | 2.2 |
| WELL-35 | 103.7 | 4.0 | 97.9 | 7.1 | -41.6 | 158.4 | 103.7 | 4.0 |
| WELL-34 | 107.7 | 2.8 | 94.9 | 16.3 | -215.6 | 448.9 | 107.7 | 2.8 |
| WELL-5 | 109.2 | 3.0 | 108.4 | 9.4 | 90.8 | 207.0 | 109.2 | 3.0 |
| WELL-16 | 114.5 | 1.1 | 113.5 | 2.8 | 91.6 | 56.0 | 114.5 | 1.1 |
| WELL-2 | 155.9 | 3.3 | 161.5 | 7.1 | 245.5 | 98.6 | 155.9 | 3.3 |
| WELL-25 | 160.0 | 4.5 | 158.0 | 5.8 | 127.1 | 64.9 | 160.0 | 4.5 |
| WELL-21 | 177.9 | 2.6 | 175.0 | 4.6 | 135.4 | 57.7 | 177.9 | 2.6 |
| WELL-8 | 1005.4 | 20.6 | 1001.4 | 31.5 | 992.6 | 90.1 | 1005.4 | 20.6 |
| WELL-13 | 1726.8 | 17.9 | 1762.5 | 17.6 | 1805.0 | 31.7 | 1805.0 | 31.7 |
| WELL-31 | 1763.3 | 15.6 | 1783.2 | 18.1 | 1806.4 | 34.5 | 1806.4 | 34.5 |
| WELL-24 | 692.1 | 34.7 | 1021.0 | 35.8 | 1814.4 | 31.2 | 1814.4 | 31.2 |